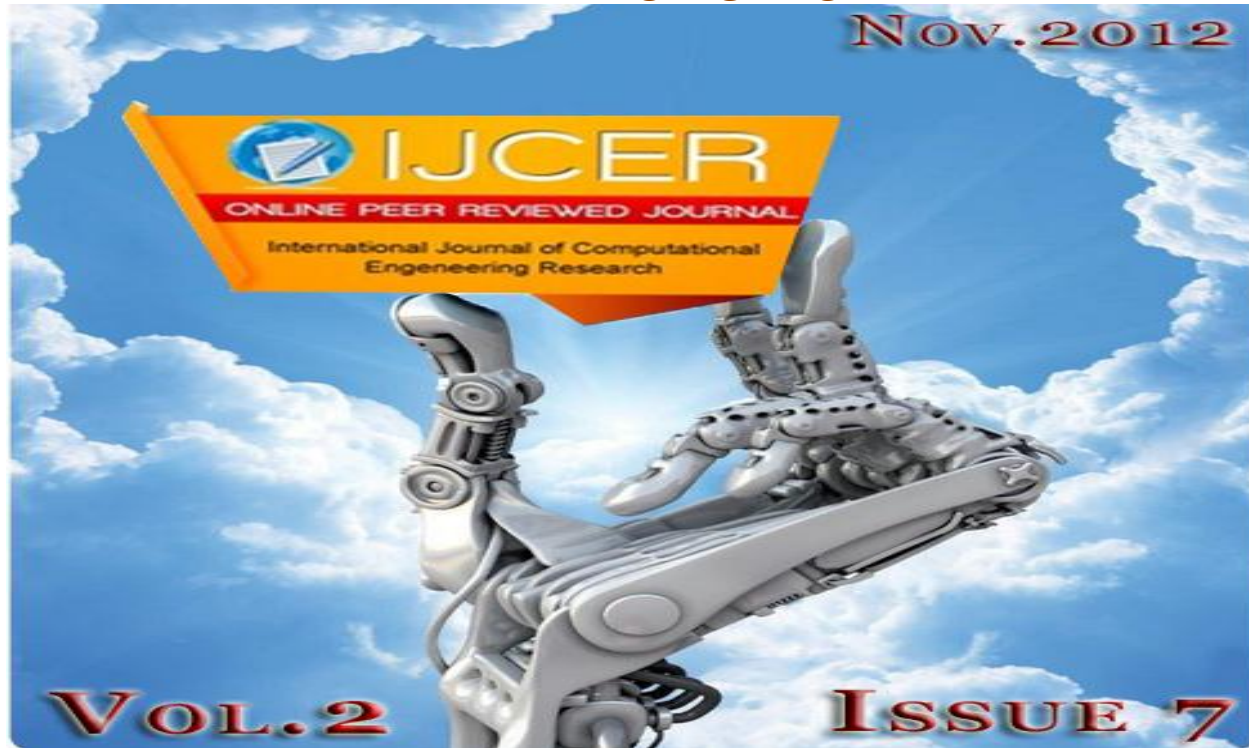


International Journal of computational Engineering Research (IJCER)

ISSN: 2250-3005



VOLUME 2

November 2012

ISSUE 7

Email: ijceronline@gmail.com

Url : www.ijceronline.com

International Journal of computational Engineering Research (IJCER)

Editorial Board

Editor-In-Chief

Prof. Chetan Sharma

Specialization: Electronics Engineering, India
Qualification: Ph.d, Nanotechnology, IIT Delhi, India

Editorial Committees

DR.Qais Faryadi

Qualification: PhD Computer Science
Affiliation: USIM(Islamic Science University of Malaysia)

Dr. Lingyan Cao

Qualification: Ph.D. Applied Mathematics in Finance
Affiliation: University of Maryland College Park, MD, US

Dr. A.V.L.N.S.H. HARIHARAN

Qualification: Phd Chemistry
Affiliation: GITAM UNIVERSITY, VISAKHAPATNAM, India

DR. MD. MUSTAFIZUR RAHMAN

Qualification: Phd Mechanical and Materials Engineering
Affiliation: University Kebangsaan Malaysia (UKM)

Dr. S. Morteza Bayareh

Qualificatio: Phd Mechanical Engineering, IUT
Affiliation: Islamic Azad University, Lamerd Branch
Daneshjoo Square, Lamerd, Fars, Iran

Dr. Zahéra Mekkioui

Qualification: Phd Electronics
Affiliation: University of Tlemcen, Algeria

Dr. Yilun Shang

Qualification: Postdoctoral Fellow Computer Science
Affiliation: University of Texas at San Antonio, TX 78249

Lugen M.Zake Sheet

Qualification: Phd, Department of Mathematics
Affiliation: University of Mosul, Iraq

Mohamed Abdellatif

Qualification: PhD Intelligence Technology
Affiliation: Graduate School of Natural Science and Technology

Meisam Mahdavi

Qualification: Phd Electrical and Computer Engineering

Affiliation: University of Tehran, North Kargar st. (across the ninth lane), Tehran, Iran

Dr. Ahmed Nabih Zaki Rashed

Qualification: Ph. D Electronic Engineering

Affiliation: Menoufia University, Egypt

Dr. José M. Merigó Lindahl

Qualification: Phd Business Administration

Affiliation: Department of Business Administration, University of Barcelona, Spain

Dr. Mohamed Shokry Nayle

Qualification: Phd, Engineering

Affiliation: faculty of engineering Tanta University Egypt

CONTENTS :

S.No.	Title Name	Page No.
1.	Harmonic Mitigation in AC–DC Converters for Induction Motor Drives by Vector Controlled Banoth Laxman Naik, Ch Hari Krishna	01-08
2.	A New Survivability Strategy With Congestion Control In WDM Optical Networks Salil Trived, ,Sachidanand, ,Geetanjali	09-10
3.	Multiparty Secure Communication by Using Quantum Key Distribution Protocols K.Gopinath , B.J.Job karuna sagar	10-15
4.	A Location-Based User Movement Prediction Approach For Geolife Project Zhiyuan Chen, Bahran Sanjabi, Dino Isa	16-19
5.	Hdl Implementation Of Amba-Ahb Compatible Memory Controller S.Ramakrishna ,K.Venugopal, B.Vijay Bhasker , R.Surya Prakash Rao	20-23
6.	IC TESTER USING 89s52 MICROCONTROLLER Miss.M.A.Tarkunde, Prof.Mrs.A.A.Shinde	24-27
7.	A Novel Approach To Automated Brain Tumor Classification Using Probabilistic Neural Network Varada S.Kolge , Prof.K.V.Kulhalli	28-30
8.	A New Analytical Method For The Sizing And Siting Of DG In Radial System To Minimize Real Power Losses Dr. A.Lakshmi Devi, A.Chaithanya	31-37
9.	Route To Chaos In An Area-Preserving System Dr. Nabajyoti Das	38-44
10.	Lp - convergence of Rees-Stanojevic sum Nawneet Hooda	45-47
11.	Wireless Electricity Transmission Based On Electromagnetic And Resonance Magnetic Coupling Prof. Burali Y. N, Prof. Patil C.B.	48-51
12.	Design of Bovine SemenTemperature ControllerUsing PID Tatag Lindu Bhakti, Adhi Susanto, Paulus Insap antosa, Diah Tri Widayati	52-58
13.	A Proposal for Implementation of Signature Based Intrusion Detection System Using Multithreading Technique Prof.D.P.Gaikwad, Pooja Pabshettiwar, Priyanka Musale , Pooja Paranjape, Ashwini S. Pawar	59-65
14.	An Efficient Vlsi Implementation Of Image Encryption With Minimal Operation S.Lakshmana Kiran, P.Sunitha	66-70
15.	Some Dynamical Behaviors In Lorenz Model Dr. Nabajyoti Das	71-76

16.	A Novel Parallel Domain Focused Crawler For Reduction In Load On The Network Rajender Nath, Naresh Kumar	77-84
17.	HBABC: A Hybrid Optimization Algorithm Combining Biogeography Based Optimization (BBO) And Artificial Bee Colony (ABC) Optimization For Obtaining Global Solution Of Discrete Design Problems Vimal Savsani	85-97
18.	Video Compression Using Spiht And Neural Network Sangeeta Mishra,2,Sudhir Sawarkar	98-103
19.	Matching Dominating Sets Of Euler Totient Cayley Graphs M.Manjuri, B.Maheswari	104-107
20.	Preparation and Characterization of Natural Degradable Microcapsules M. Geetha Devi, Susmita Dutta, Ashraf Talib Al-Hinaizand S.Feroz	108-111
21.	Water Marking Scheme With High Capacity Cdma Dr K Ramesh Babu, Vani.kasireddy	112-126
22.	FPGA Implementation Of Wavelet-Based Denoising Technique Toanalysis Of EEG Signal T.Chaitanya, G.S.Siva kumar	127-132
23.	Area Optimized And Pipelined FPGA Implementation Of AES Encryption And Decryption Mg Suresh, Dr.Nataraj.K.R	133-139
24.	Numerical Investigation For Exhaust Gas Emissions For A Dual Fuel Engine Configuration Using Hydrogen And Compressed Natural Gas (Cng) Premakumara. G, Akhil Thomas, Jayakrishnan .K, Anirudh Vuyyala4 ,L.M. Das	140-145
25.	An Affine Combination Of TVLMS Adaptive Filters For Echo Cancellation B. Srinivas, M.Tech, Dr. K. Manjunathachari	146-151
26.	Facts Placement For Maximum Power Transfer Capability And Stability In A Transmission Line C.Vasavi1, Dr. T.Gowri Manohar	152-160
27.	Hybridization Of Neighbourhood Search Metaheuristic With Data Mining Technique To Solve P-Median Problem D.Srinivas Reddy, A.Govardhan, Ssvn Sarma	161-165
28.	Key Infrastructure Elements For Cloud Computing S.J.Mohana, M.Saroja, M.Venkatachalam	166-169
29.	Control Of Unstable Periodic Orbits Coexisted With The Strange Attractor Dr. Nabajyoti Das	170-176
30.	A Distributed Canny Edge Detector And Its Implementation On FPGA Chandrashekar N.S. Dr. K.R. Nataraj	177-181

31.	Analytic Hierarchy Process For Evaluation Of Environmental Factors For Residential Land Use Suitability V.D.Patil, R.N.Sankhua, R.K.Jain	182-189
32.	Steganography With Data Integrity Deepali	190-193
33.	Estimation Of Word Recognition By Using Back-Propagation Neural Network Pin-Chang Chen¹, Hung-Teng Chang, Li-Chi Lai	194-198
34.	Perspective Of Watershed Management In Our Modern Society Biplab Das, Dr.AdityaBandyopadhyay	199-203
35.	Formation Of Knowledge Sharing System For Asia-Pacific Countries By Using Modern Information Techniques Nalin Warnajith, Sarkar Barbaq Quarmal, Masanori Itaba, Atsushi Minato ,Satoru Ozawa	204-211
36	Location Of The Zeros Of Polynomials M.H. Gulzar	212-214

Harmonic Mitigation in AC–DC Converters for Induction Motor Drives by Vector Controlled

¹BANOTH LAXMAN NAIK, ²CH HARI KRISHNA

¹.Student of Electrical and Electronics Engineering at Mother Teresa Institute of Science and Technology, India

². Associate Professor in the Department of Electrical and Electronics Engineering at Mother Teresa Institute of Science and Technology, India

Abstract

This paper deals with autotransformer-based multipulse ac–dc converters with reduced magnetics feeding vector controlled induction motor drives for improving the power quality at the point of common coupling. The proposed 12-pulse ac–dc converter-based harmonic mitigator consists of an autotransformer alongwith a passive shunt filter tuned for 11th harmonic frequency. This results in the elimination of 5th, 7th, and 11th harmonic currents. Similarly, the proposed 18-pulse ac–dc converterbased harmonic mitigator eliminates the 5th, 7th, 11th, 13th, and 17th harmonic currents, thereby improving the power quality at ac mains. The experimentation is carried out on the developed prototype of autotransformers-based ac–dc converters. Different power quality indexes of the proposed 12-pulse ac–dc converters are obtained from simulation and verified from experimental results.

1. Introduction

The use of induction motors has increased in industrial applications due to their advantages such as improved efficiency, ruggedness, reliability and low cost. For variable speed drives, dc motors have been used until now because of their flexible characteristics. To incorporate the flexible characteristics of a dc motor into an induction motor, vector control technique is adopted as a widely accepted choice. Normally ac–dc power converter feeding power to the VCIMD consists of a 6-pulse diode bridge rectifier, an energy storage element at dc link, a 3-phase voltage source inverter (VSI) and an induction motor. The diode bridge rectifier suffers from operating problems such as poor power factor, injection of harmonic currents into the ac mains etc. In order to prevent the harmonics from affecting the utility lines negatively, an Standard 519 has been reissued in 1992 giving clear limits for voltage and current distortions. Several methods based on the principle of increasing the number of rectification pulses in ac–dc converters have been reported in the literature. The conventional wye-delta transformer based 12-pulse rectification scheme is one such example. But the kVA rating of the transformer is 1.03 PO, where PO is the active power drawn by the converter. To reduce the transformer rating, autotransformer based multipulse ac–dc converters of reduced rating have been reported in the literature. For applications where the demand for harmonic current reduction is more stringent, an 18-pulse ac–dc converter is generally preferred. This converter is more economical than the 24-pulse ac–dc converter, while being more effective than the 12-pulse ac–dc converter. Autotransformer based 18-pulse ac–dc converters have been reported in for reducing the THD of ac mains current. However, the dc-link voltage is higher, making the scheme non applicable for retrofit applications. Hammond has proposed a new topology, but the transformer design is very complex to simplify the transformer design. Paice has reported a new topology for 18-pulse converters. But the THD of ac mains current with this topology is around 8% at full load. Kamath et.al. Have also reported an 18-pulse converter, but THD of ac mains current is high even at full load (6.9%) and as load decreases the THD increases further (13.1%THD at 50% load). In this paper, a novel autotransformer based 18-pulse ac–dc converter (Topology 'D'), which is suitable for retrofit applications, where presently 6-pulse converter is being used, referred as Topology 'A', shown in Fig. 1, have been proposed to feed VCIMD. The proposed ac–dc converter results in elimination of 5th, 7th, 11th and 13th harmonics. A set of tabulated results giving the comparison of the different power quality parameters is presented for a VCIMD fed from an existing 6-pulse ac–dc converter and different 18 pulse ac–dc converter. Moreover, the effect of load variation on various power quality indices is also studied. To demonstrate the effectiveness of proposed 18-pulse ac–dc converter feeding VCIMD. A laboratory prototype of the proposed autotransformer is designed and the developed and different tests have been carried out to validate the working of the proposed harmonic mitigator. The test results are found to be in close agreement with the simulated results under different operating and loading conditions.

2. Performance Of Harmonic Mitigation Alternatives

Variable frequency drives often have strict demands placed on them to mitigate harmonic distortion caused by non-linear loads. Many choices are available to them including line reactors, harmonic traps, 12-pulse rectifiers, 18-pulse rectifiers and low pass filters. Some of these solutions offer guaranteed results and have no adverse effect on the power system, while the performance of others is largely dependent on system conditions. Certain techniques require extensive system analysis to prevent resonance problems and capacitor failures, while others can be applied with virtually no analysis whatsoever. In some cases harmonic mitigation technique decisions were based on a technical misunderstanding, lack of information, theoretical data or on invalid assumptions. This Chapter explains the theory of operation of various passive harmonic mitigation techniques and demonstrates their typical real life performance. It takes the guesswork out of harmonic filtering by demonstrating the typical performance of various harmonic mitigation techniques and offering a quantitative analysis of alternatives for real life VFD operating conditions. Since power distribution transformers frequently have impedance ratings between 1.5% and 5.75%, one would expect that source impedance is often relatively high and that harmonics should therefore be quite low. However, transformer impedance ratings are based on transformer rated KVA, so when the transformer is partially loaded, the effective impedance of the transformer, relative to the actual load, is proportionately lower, [i.e.: 1.5% impedance at

Line Reactors:The use of AC line reactors is a common and economical means of increasing the source impedance relative to an individual load. Line reactors are connected in series with the six pulse rectifier diodes at the input to the VFD, as shown in Fig 2.1.

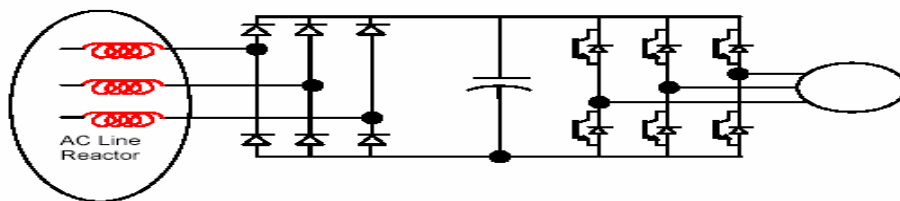


Fig AC line reactors connection at supply side

The typical harmonic spectrum data for a six pulse VFD load fed by a power supply with an

Effective source reactance of 3%, 5% and 8% looks as follows:

h	3 % reactance	5% reactance	8% impedance 3% dc choke & 5% ac reactor
5th	39%	32%	27%
7th	17%	12%	9%
11th	7%	5.8%	4.5%
13th	5%	3.9%	3.2%
17th	3%	2.2%	1.8%
19th	2.2%	1.7%	1.4%
23rd	1.5%	1%	0.8%
25th	1%	0.9%	0.75%
THID	44%	35%	29%

Table: 2.2. Typical harmonic spectrum data when effective reactance of 3%, 5% and 8%

These data represent the harmonics measured at the input to the six pulse rectifier and will reduce to lower percentages when measured further upstream, provided there are other linear loads operating on the system. If 20% of the system load is comprised of VFDs with 5% input impedance, and 80% has linear loads, the harmonic current distortion at the VFD input will be 35% THID, but only 7% at the supply transformer secondary. Typically costing less than 3% of the motor drive system, line reactors are the most economical means of reducing harmonics. Practical ratings can achieve 29% to 44% THID at the input to the six pulse

3. Reactor Performance at load

The harmonic mitigation performance of reactors varies with load because their effective impedance reduces proportionately as the current through them is decreased. At full load, a 5% effective impedance reactor achieves harmonic distortion of 35% THID, however, at 60% load it's effective impedance is only 3% $\{0.6 \times 5\% = 3\%$, and harmonics will be 44% THID. Although THID increased as a percentage, the total rms magnitude of harmonic current actually decreased by nearly 25% $\{1 - ((.6 \times 44\%) / 35\%) = 24.5\%$. Since voltage distortion at the transformer secondary is dependent upon the magnitude and frequency of current harmonics that cause harmonic voltage drops across the transformer's internal reactance, the voltage distortion (THVD), at the transformer secondary, actually decreases as this load is reduced.

Tuned Harmonic Trap Filters:

Harmonic Trap Performance:

Tuned harmonic filters (traps) involve the series connection of an inductance and capacitance to form a low impedance path for a specific (tuned) harmonic frequency. The filter is connected in parallel (shunt) with the power system to divert the tuned frequency currents away from the power source.

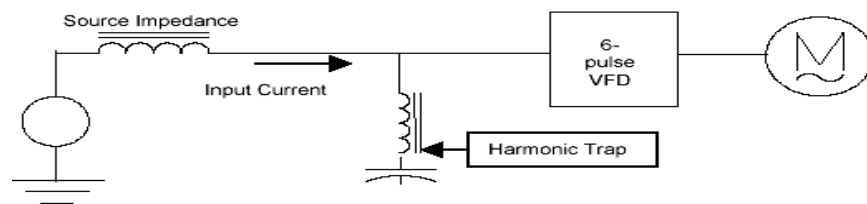


Fig : Harmonic Trap Performance with 0.25% source impedance

At that time we will give a non sinusoidal input to the as shown below:

Unlike line reactors, harmonic traps do not attenuate all harmonic frequencies. Most often they are tuned for 5th harmonic mitigation. If applied to a low impedance power source, as demonstrated in Fig. 2.4, the harmonic mitigation performance of this filter is quite limited and the benefit of this filter may be unrecognizable. To improve the performance of a trap filter, a 5% impedance line reactor may be connected in series with the input to the filter, as shown in

Fig. 2.6.

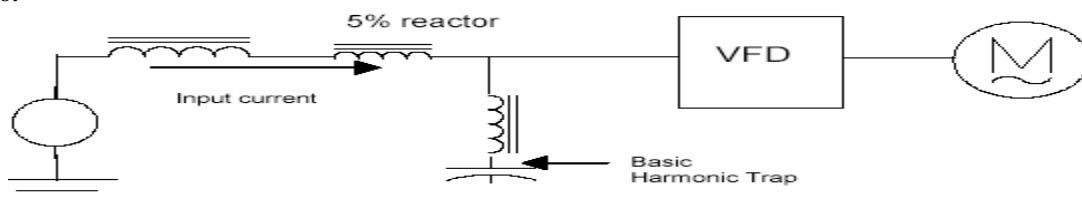


Fig.2.6. Line reactor performance with 0.25% source impedance

If the VFD has internal line reactance, then harmonic trap performance may improve slightly. The typical residual THID for a six pulse rectifier with a tuned 5th harmonic trap is between 20% to 30% at full load, provided there is significant source impedance. The watts loss of this type of filter can be 2-3% of the load and it can cost ten times the price of a line reactor. Tuned harmonic traps will alter the natural resonant frequency of the power system and may cause system resonance, increasing specific harmonic levels. They may attract harmonics from other non-linear loads sharing the same power source and must be increased in capacity to accommodate the addition of new loads. For best results, a power system study should be performed to determine the magnitude of harmonics to be filtered (from all loads), the power system resonant frequency and the impact of future addition of loads.

4. Harmonic Traps at Light Load onditions

Harmonic traps achieve their best attenuation of harmonics at full load conditions. At light load, the resultant THID can increase significantly and may be no better than the performance normally achieved with a line reactor. Fig.2.8. demonstrates the input current waveform of a six Pulse rectifier with a tuned 5th harmonic trap, operating at 50% load, when the line voltages were 3% unbalanced. Notice the similarity to a non-linear single phase load.

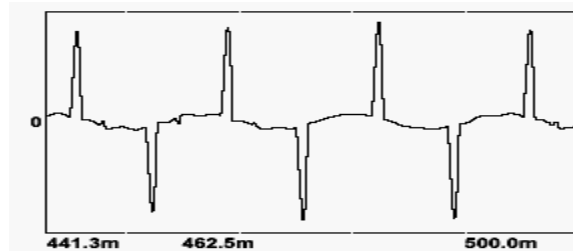


Fig.2.8. input current waveform with 3% line voltage unbalance and 0.25% source impedance.

Here the Harmonic current distortion = 139% THID.

2.4. Twelve Pulse Rectification

Twelve pulse rectifier configurations have been used for applications demanding lower harmonic levels than can be achieved using either traps or reactors. The theoretical benefits of 12-pulse rectification include cancellation of 5th, 7th, 17th, 19th, etc harmonics. However, real life harmonic mitigation resulting from the use of twelve pulse rectifiers can be quite different than one's theoretical expectations.

The most common method of twelve pulse rectification involves the parallel connection of two bridge rectifiers, each fed by a 30 degrees phase shifted transformer winding. Often the transformer has a single primary winding and dual secondary windings. One secondary winding is a delta and the other is connected in wye configuration to achieve 30 degrees of phase shift between secondary voltages.

"A major design goal in multipulse operation is to get the converters, or converter semiconductor devices, to share current equally. If this is achieved, then maximum power and minimum harmonic currents can be obtained." In order to achieve cancellation of harmonics, the two individual bridge rectifiers must share current equally. This can only be achieved if the output voltages of both transformer secondary windings are exactly equal. "Because of differences in the transformer secondary impedances and open circuit output voltages, this can be practically accomplished for a given load (typically rated load) but not over a range in loads." Typical losses of a twelve pulse transformer are 3% to 5% of the transformer KVA rating.

5. Twelve Pulse Performances with Balanced Line Voltages

Fig.2.9. illustrates actual measurements of input current harmonic distortion for a twelve pulse rectifier supplied from a balanced three phase voltage source while operating at full load conditions. For test purposes, the transformer had a delta primary with delta and wye secondary windings (each rated at one-half line voltage). To obtain "best case" results, the bridge rectifiers were series connected so equal DC current flowed in each converter. The data shows that when the current through both sets of rectifiers is equal, harmonics can be as low as 10% to 12% THID at full load. Current sharing reactors will help parallel connected bridge rectifiers to share current equally. While current sharing reactors are highly recommended for twelve pulse configurations, they are usually omitted in the interest of minimizing cost. Even with balanced. current however, harmonic distortion can increase appreciably at light load conditions.

6. Twelve Pulse Performances when Line voltages are not balanced:

Practical aspects of multipulse transformer winding configurations and circuit parameters make unlikely that perfect balance can be achieved between all six secondary voltages, especially when the load is varied from full load to no load conditions. Additionally, facility power system voltage unbalance is common

(according to ANSI C84.1, 34% of facilities surveyed in the USA experienced between 1% and 3% voltage unbalance at the service entrance point and even greater unbalance in the facility and closer to the loads). It is interesting to note that occasionally pulse drives are sold without the transformer, shifting responsibility for the transformer specification and system performance from the supplier to the user or installer. Fig. 2.10 demonstrates the impact of both line voltage unbalance and light loading conditions on the harmonic mitigation performance of twelve pulse rectifiers. Even with perfectly balanced

line voltages, the resultant %THID increases as the load is reduced (i.e.:23% THID at 20% load).

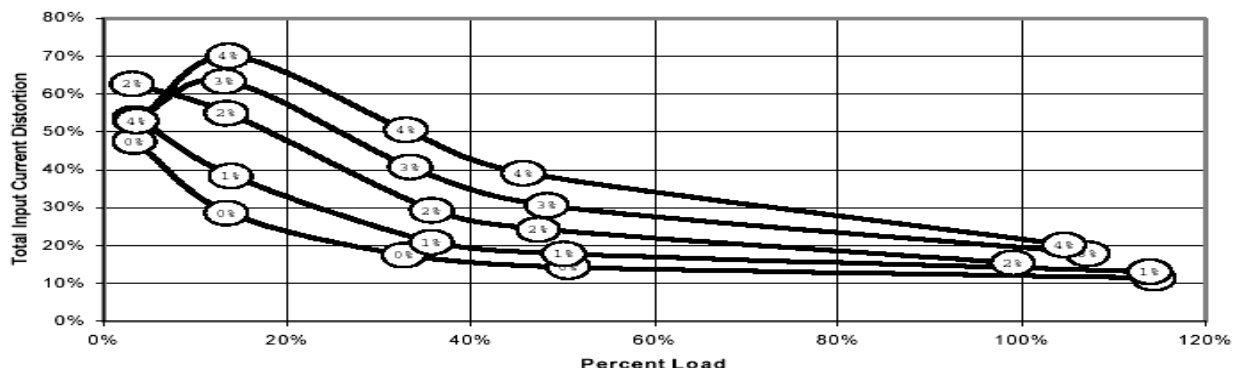


Fig12-pulse total input current harmonic distortion-varying with load

7. Multi - Pulse Converters Solutions For Harmonic Mitigation In Ac Drives

More and more ac drive installations are requiring manufacturer's to improve line side harmonics to ultimately meet IEEE Harmonic Std 519 Standard AC drive topologies utilize AC- DC-AC power conversion with a three phase rectifying bridge for the AC-DC function. A three- phase diode or SCR bridge generates 6 pulse types current that is ~ 32% rich in total harmonic current distortion. As ac drives proliferate, equipment system specifications limiting the amount of harmonic current injected into the grid are becoming more common and thus solicit cost effective harmonic mitigation solutions. System specifications are often written so measured total harmonic distortion at the *Point of Common Coupling (PCC)* in fig. 3.1 Complies with the maximum low voltage total harmonic Distortion levels (*THDV*) and system classification of IEEE 519 and current limits are shown in table 3.1.

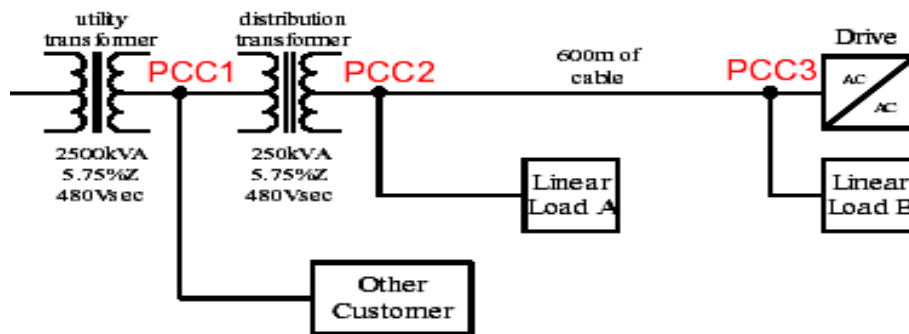


Fig point of common coupling

The PCC is usually at the power metering point (*PCC1*) where other customers connect to the common line voltage but may also be at (*PCC2*) or (*PCC3*) within a plant where linear and non- linear loads are connected. System classification and (*THDV*) options are *Special Application @3%*, *Dedicated System @ 10 %* and most specified option of *General System @ 5%*. Current harmonic distortion (*THDI*) of a single non-linear load is defined

as the square root of the sum of the squares of all harmonic currents divided by the fundamental component of the non-linear load. However, defines total harmonic current distortion limits in a system as *Total Demand Distortion (TDD)*. TDD limiting values are dependent on the ratio of short circuit current (*ISC*) at the *PCC* to the maximum demand load current (*IL*) supplied by the user. There are five classifications of (*ISC/IL*), but worst case TDD limit of 5% for an (*ISC/IL*) < 20 is often used.

8. Vector Control

Introduction

The various control strategies for the control of the inverter-fed induction motor have provided good steady state but poor dynamic response. From the traces of the dynamic responses, the cause of such poor dynamic response is found to be that their air gap flux linkages deviate from their set values. The deviation is not only in magnitude but also in phase. The variations in the flux linkages have to be controlled by the magnitude and frequency of the stator and rotor phase currents and instantaneous phases. The oscillations in the air gap flux linkages result in oscillations in electromagnetic torque and, if left unchecked, reflect as speed oscillations. This is undesirable in many high-performance applications. Air gap flux variations result in large excursions of stator currents, requiring large peak converter and inverter ratings to meet the dynamics. An enhancement of peak inverter rating increases cost and reduces the competitive edge of ac drives over dc drives.

Separately excited dc drives are simple in control because they independently control flux, which when maintained constant contributes to an independent control of torque. This is made possible with separate control of field and armature currents, which in turn control the field flux and the torque independently. Moreover, the dc motor control requires only the control of the field or armature current magnitudes.

As with the dc drives, independent control of the flux and torque is possible in ac drives. The stator current phasor can be resolved, say, along the rotor flux linkages, and the component along the rotor flux linkages is the field producing current, but this requires the position of the rotor flux linkages at every instant; note that this is dynamic, unlike in the dc machine. If this is available, then the control of ac machines is very similar to that of separately excited dc machines. The requirements of phase, frequency, and magnitude control of the currents and hence of the flux phasor are made possible by inverter control. The control is achieved in field

9. Principle of Vector Control

The fundamentals of vector control can be explained with the help of figure 3.5, where the machine model is represented in a synchronously rotating reference frame. The inverter is omitted from the figure, assuming that it has unity current gain, that is, it generates currents i_a , i_b ,

and i_c as dictated by the corresponding command currents i_a^* , i_b^* , and i_c^* from the controller. A

machine model with internal conversions is shown on the right. The machine terminal phase

currents i_a , i_b , i_c are converted to i_{ds} and i_{qs} components by $3\phi-2\phi$ transformation. These are then

converted to synchronously rotating frame by the unit vector components $\cos \theta_e$ and $\sin \theta_e$ before

applying them to the d^e-q^e machine model.

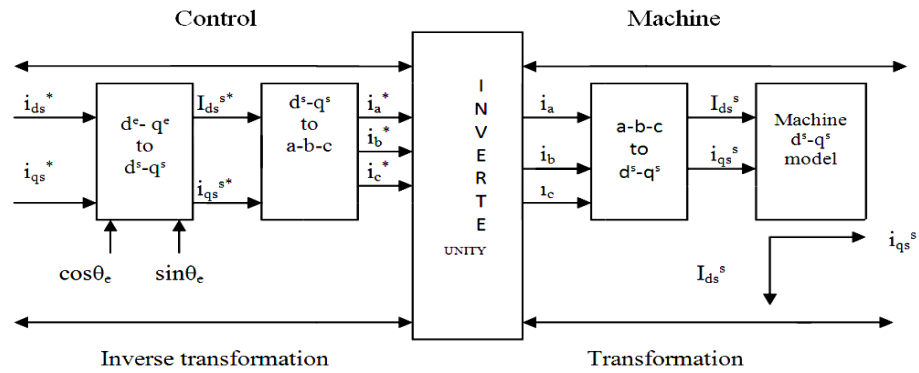


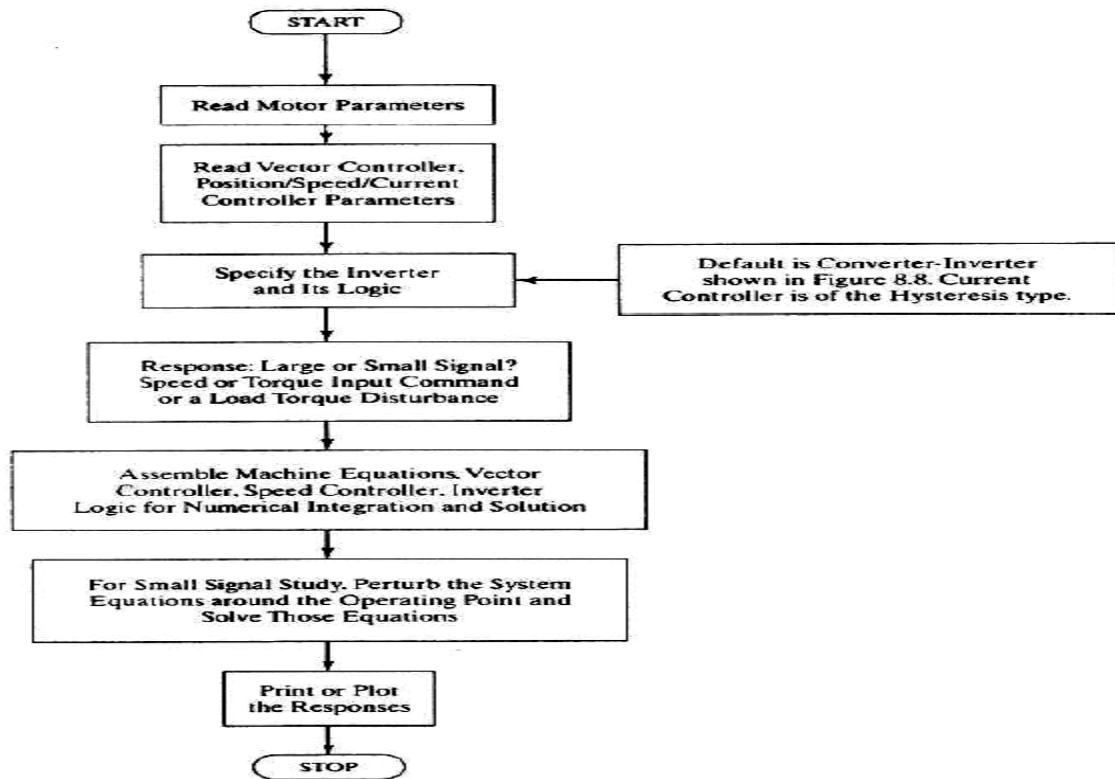
Fig 4.5 Basic block diagram of vector control

Vector control implementation principle with machine d^s-q^s model as shown. The controller makes two stages of inverse transformation, as shown, so that the control currents

i_{ds}^* and i_{qs}^* correspond to the machine currents i_{ds} and i_{qs} , respectively. In addition, the unit vector i_{ds}^* and

assures correct alignment of i_{ds} current with the flux vector Ψ_r and i_{qs} perpendicular to it, as shown. It can be noted that the transformation and inverse transformation including the inverter ideally do not incorporate any dynamics, and therefore, the response to i_{ds} and i_{qs} is instantaneous (neglecting computational and sampling delays).

Flow Chart for implementation of Vector control of induction motor



10. Conclusions and Future Scope Of Work

7.1. Conclusions:

1. A novel autotransformer based eighteen-pulse ac-dc converter has been designed and modeled with a VCIMD load
2. The proposed harmonic mitigator has been observed suitable for retrofit applications with variable frequency induction motor drives operating under varying load conditions.
3. The performance of the proposed harmonic mitigator fed VCIMD under varying load conditions is found to be satisfactory.
4. The proposed harmonic mitigator has resulted in reduction in rating of the magnetics leading to the saving in overall cost of the drive.
5. The observed performance of the proposed harmonic mitigator has demonstrated the capability of this converter to improve the power quality indices at ac mains in terms of THD of supply current, THD of supply voltage, power factor and crest factor. On the dc link side too, there is a remarkable improvement in ripple factor of dc link voltage.

7.2. Future Scope:

In this project simulated an 18-pulse ac-dc converter which is based on autotransformer based transformer. Extended this project in to 18-pulse to 36pulse and also Verify the power quality maintains or not and with the using of this project control the HVDC System & also implement in the traction systems.

References

1. P.Vas, Sensorless vector and direct torque control, Oxford University Press, 1998.
2. IEEE Guide for harmonic control and reactive compensation of Static Power Converters, IEEE Std. 519-1992.
3. D. A. Paice, Power Electronic Converter Harmonics: Multipulse Methods for Clean Power, New York, IEEE Press 1996.
4. S.Martinius, B.shalimi and P.A.Cahono, "A transformer connection for multipulse rectifier applications," Proc. Int. Conf. Powercon, Oct.2002,vol.22,pp.1021-1024

Author Name's



Mr.B.LAXMAN NAIK was born in 1989. He received B.Tech degree from Jawaharlal Nehru Technological University, Hyderabad in the year 2010. M.Tech Student of Power Electronics & Electrical Drives Engineering at Mother Teresa Institute of Science and Technology, Andhra Pradesh India.



Chalasan Hari Krishna was born in 1982. He graduated from Jawaharlal Nehru Technological University, Hyderabad in the year 2003. He received M.E degree from Satyabama University, Chennai in the year 2005. He presently Associate Professor in the Department of Electrical and Electronics Engineering at Mother Teresa Institute of Science and Technology, India. His research area includes DTC and Drives. He presented 11 research papers in various national and international conferences and journals. His research areas include PWM techniques, DC to AC converters and control of electrical drives conferences and journals. His research areas include PWM techniques, DC to AC converters and control of electrical drives

A New Survivability Strategy with Congestion Control In WDM Optical Networks

¹Salil Trivedi, ²Sachidanand, ³Geetanjali

^{1,2,3},Department of electronics and communicatin Lovely Professional University

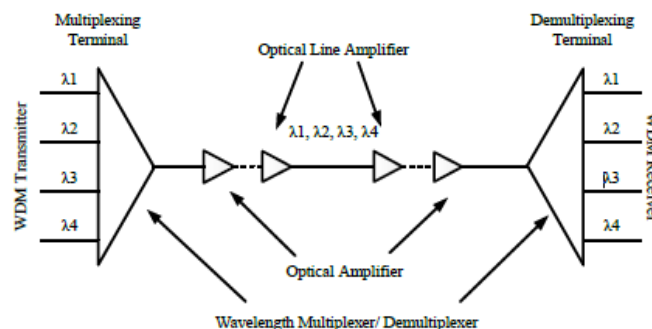
Abstract

Due to huge usage of internet and growing business, bandwidth required prove to be difficult resource to fulfill with normal structure of networks. Moreover to provide a good level of quality service is also a big concern. One big solution comes in form of Wavelength Division Multiplexing (WDM). Wavelength Division Multiplexing (WDM) is an important technique to exploit the huge bandwidth of the optical fiber. There has been a wide deployment of WDM transmission technology in today's optical networks. WDM is widely used technology in developed countries and is based on the transmission of several light beams of different wavelength simultaneously through an optical fiber. A wavelength typically operates in hundreds of Mbps or even Gbps needs to be utilized better if the connection request is less than 100 Mbps bandwidth, otherwise there is a tremendous wastage of bandwidth in a fiber for data transmission. Though the fiber bandwidth has been improved due to the advancements in fiber-optic technologies and the increase in number of wavelengths in a fiber, there has not been much research in the area of *fault tolerance, routing and wavelength assignment*. Due to huge transmission of data through optical fibers, congestion occurred regularly and it became big bottleneck to flow of data in process. To solve congestion issues we are proposing a survivability strategic algorithm with congestion control in WDM optical network which will improve congestion hit network and will provide us with good cost cutting as it can be implemented to developing countries due to low costing factor.

Keywords: WDM, congestion control.

1. Introduction

The rapid growth of Internet traffic has been the driving force for faster and more reliable data communication networks. Networking is a very promising technology to meet these ever increasing demands. The influence of networking on an organization of the computer systems has been tremendous, especially in the last 30 years. The old model of a single computer catering computation needs of an organization has been replaced by single network in which a number of separate but interconnected computers carry out the job.



Optical wavelength-division-multiplexing (WDM) networks are being increasingly deployed in the next generation wide area, metropolitan, and local area network infrastructures [1]. WDM is widely becoming accepted as a technology for meeting growing bandwidth. It establishes communication between pairs of network nodes by establishing paths and assigning wavelength to each path. No two paths going through the same fiber link use the same wavelength at the same time to observe wavelength continuity constraint [2, 3]. In our research we will propose a new algorithm for better congestion control which commonly used survivability strategy will be presented. We will provide our results with help of simulations to evaluate the performance in terms of congestion control and the results will be compared.

2. Problem Formulation

Due to huge transmission of data through optical fibers, congestion occurred regularly and it became big bottleneck to flow of data in process. Our focus will be on developing a better solution to this problem as to solve congestion issues we are proposing a survivability strategic algorithm with congestion control in WDM optical network which will improve congestion hit network and will provide us with good cost cutting as it can be implemented to developing countries due to low costing factor.

3. OBJECTIVES

- ✚ To analyze and developing a better algorithm for congestion control in Wavelength Division Multiplexing
- ✚ Test the proposed algorithm in Matlab or Opnet/ NS2.

4. Research Methodology

To achieve the set objectives, our proposal will focus on developing a better fast algorithm for Survivability Strategy with Congestion Control in Wavelength Division Multiplexing Optical Networks. We will propose the algorithm and will test it in MATLAB or OPNET/.NS2 for finding loopholes and will propose the better solutions by comparing it in these simulators.

5. Algorithm Functions

Length of route: It is the length of the route used by the signal to reach from source node to destination node. It is measured in miles and is the total sum of the distances between each node on that route.

Maximum possible cost (C_m): It is the maximum cost assumed for the link selected to transfer the signal.

Maximum route time (T_m): It is the maximum possible time may be taken by the signal to reach from source node to destination node through longest route.

Route time (T_R): It is the exact time consumed by the signal to reach from source node to destination node through route R. **Load per link (L_r):** It is the load of link r calculated by $L_r = \Lambda_r^m + \phi \Lambda_r^s$, where Λ_r^m is the number of wavelengths being used to carry the primary signals and Λ_r^s is the number of wavelengths which are being used to carry the backup signals on link r. ϕ is the parameter having value from 0 to 1 as per the weight of backup links on the routes. **Route hops (N_R):** This is the number of hops on route R. **Average load (L_A^R):** It is used to calculate the average load on route R equals to $1/N_R(\sum L_r)$ for all r belongs to R. **Variance of load (V_R):** This is difference of L_r and L_A^R for route R and is calculated by $1/N_R(\sum L_r^2 - L_A^R{}^2)$ for all link r on route R.

6. Scope Of Study

There is an ample scope of research in the stated area. Present study will reflect the importance of congestion control and will provide huge beneficial solution for developing countries as it will be very cost effective in term of implementation and working.

7. Conclusion

A brief review of existing studies show emergence of different technologies and WDM is one of the emerging technologies in it so we are proposing a new Survivability Strategy with Congestion Control in WDM Optical Networks. This work will provide us the big solution.

8. REFERENCES

- [1] K. Sivalingam and S. Subramaniam, Emerging Optical Network Technologies, Eds. Boston, MA: Springer-Verlag, 2004.
- [2] C. S. R. Murthy and M. Gurusamy, WDM Optical Networks-Concepts, Design, and Algorithms, Singapore: Pearson Education, 2003.
- [3] P. Singh, A.K. Sharma, and S. Rani, "An Efficient Wavelength Assignment Strategy for WDM Optical Networks," Int. J. of Optical Engineering, SPIE, 2007, Article in press.
- [4] S. Rani, A. K. Sharma, and P. Singh, "Resource allocation strategies for survivability in WDM optical networks," Int. Journal of Opt. Fiber Tech., vol. 13, issue 3, pp. 202-208, July 2007, Available at www.sciencedirect.com.
- [5] X. Yang, L. Shen, and B. Ramamurthy, "Survivable Lightpath Provisioning in WDM Mesh Networks under Shared Path Protection and Signal Quality Constraints", J. of Lightwave Technology, Vol. 23, 2005, pp. 1556-1567.
- [6] H V Madhyastha and N. Balakrishnan, "An Efficient Algorithm for Virtual-wavelength-path Routing Minimizing Average Number of Hops", IEEE J. on Selected Areas in Communications, Vol. 21, 2003, pp. 1433-1440.

Multiparty Secure Communication by Using Quantum Key Distribution Protocols

K.Gopinath¹, B.J.Job karuna sagar²

1. Associate Professor, Department of Computer Science and Engineering, K.S.R.M.College of Engineering (AP.), India

2. Assistant Professor, Department of Computer Science and Engineering, K.S.R.M.College of Engineering (AP.), India

Abstract

By using the order rearrangement of the single photon sequence and unitary transformations, a multiparty controlled quantum communication scheme for Carrier Sense Multiple Access with Collision Detection(CSMA/CD) is presented .In this scheme, messages can only be recovered by the receivers with the permission of all controllers .It is shown that the security of messages transformation can be ensured and the performance of the proposed scheme enhances significantly since the collision can be avoided. In the communication network, transmitting messages from source to destination may traverse several intermediate nodes. For a long period of time, multiple authentications and secure communications between the sender and the receiver are needed for us to transmit messages. In the classical field, authentication provides only conditional security and classical channel cannot provide secure communication for liar detection .In the quantum field , multiple quantum entanglement pairs can be used for liar detection, In this paper, we design quantum authentication protocol and secure communication protocol by only using quantum channel . these protocols previously share a quantum key distribution to detect the dishonest node. The quantum Key distribution can promote authentication and secure communication for achieving higher liar detection probability.

Index Terms—single photon sequence, CSMA/CD, multiparty control, quantum communication

1. Introduction

Quantum Communication is one of the most remarkable applications of quantum mechanics in quantum information, including quantum key distribution(QKD)[1],quantumsecret sharing(QSS)[2-5],quantum secure direct communication (QSDC)[6-8],quantum identity authentication(QIA)[9,10],quantum encryption[11] and so on .The works on quantum communication attract much attention, and a lot of schemes have been proposed for quantum communication in theoretic research recently. In 1993, Bennett et al.[12] proposed the first quantum teleportation scheme with an unknown single-particle state. Bouwmeester et al.[13] first realized quantum teleportation experimentally in 1997.By employing the non-locality of Einstein-Podolsky-Rosen(EPR)correlation pairs and quantum teleportation, a novel quantum synchronous communication protocol to resolve the two army problem effectively is proposed in reference[14].Based on quantum entanglement correlation, Zhou[15] presented a quantum communication protocol for data link layer, in which the maximum throughput enhanced significantly and the performance of the stop-and wait protocol improved effectively. However, there are few references about how to improve the performance of the classical CSMA/CD protocol with quantum method.In this paper, we will protocol with quantum controlled quantum CSMA/CD communication scheme utilizing the order rearrangement of single photon sequence and unitary transformations. In this scheme, the security of the messages transmission can be enhanced and the receivers can recover the messages only with the permission of all controllers.

Authentication is a process that can be used to verify personal identification. In the classical field, authentication is conditionally secure. Transmitting message in the classical channel cannot guarantee secure communication. In the quantum field , quantum channel is based on the laws of physics such as de-coherence time, no-cloning theorem, uncertainty principle and quantum teleportation. These physical properties make quantum channel more secure than the classical channel.In the wired communication network, the Byzantine general problem [1] was discussed on how to reach agreement and the Byzantine system [2] was focused on fault detection. To reach agreement and to detect fault component, we need more message exchange and routing path. Authentication and secure communication can be used to achieve these purposes quickly. In the quantum wireless environment, the quantum routing mechanism [5] can be established in the quantum wireless network. We can use this quantum routing path to do authentication and liar detection. To consider authentication, Barnum et al. [3] proposed a secure non-interactive quantum authentication scheme using multiple classical keys. Ju et al, [4] proposed an authenticating server to verify

transmitter and receiver using quantum channel and classical channel. To consider secure communication, the sharing quantum private keys [6] are able to avoid any Eve to steal entanglement pairs. In this paper, we propose a model to implement authentication and liar detection. The sender and receiver use flexible unitary operation to verify each other. Then they use a variety of measured basis tables defined in between, as a quantum key distribution for the communication. In order to prevent any Eavesdropper attacks, we can use more qubits for authentication and secure communication. The more qubits are used for the verification, the more reliable performance can be achieved. We transfer quantum information from sender to receiver by using quantum channel. This procedure needs three steps. The first step is authentication which is to verify sender and receiver themselves. The second step is secure communication which transmits messages safely from sender to receiver via several intermediate nodes. The third step is quantum data transfer which safely sends quantum information from source to destination. In order to describe this procedure, we employ three persons, Alice, Bob and Candy. Alice is the sending node and Bob is the receiver node. However Candy is the intermediate node which may be the dishonest node. Initially, Alice and Bob share N quantum pairs with entangled states as described in the following.

2. Multiparty Controlled CSMA/CD Communication Scheme

The structure of the multiparty controlled CSMA/CD communication scheme based on order rearrangement and unitary transformations is shown in Fig.1. Suppose Alice needs to send messages to Bob, Charlie and other receivers simultaneously, and the messages can only be recovered by the receivers with the agreement of all their relative controllers. Quantum controllers C_n , where n represents the number of the controllers. Eve on the channel can be detected by the validate communicators through the order rearrangement of single photon sequence and unitary transformations. If there exists Eve in the process of communication, Alice and Bob must terminate the communication and repeat the process from the beginning. Otherwise, quantum controllers n proclaim the order of the single photon sequence and corresponding operations carried out on each photon. Suppose quantum controllers n are believable, now let us describe the quantum communication scheme in detail as follows:

(S1) Each sending station, at leisure time, on the one hand, sets delay resend time t , quantum ACK measurement time γ [15] and sends a request frame to the bus for communication. On the other hand, each sending station prepares photon sequence M including Q photons. Suppose there are r receivers on the bus, and then the sending station divides the photon sequence M into r parts according to different messages. Each photon among M is in one of the following four states (0) , (1) and $(\pm = \frac{1}{\sqrt{2}}(0 \pm 1))$ randomly.

(S2) After hearing from Alice, the bus is to see whether it is currently available. If available, the bus feeds back the quantum ACK to the station and allows the station to send messages; if not, the bus defers the attempt until the end of the current carrier event. At the same time, quantum controllers C_n choose the appropriate value of n for each receiver and make unitary transformation I or U on each single photon.

$$I = |0\rangle\langle 0| + |1\rangle\langle 1| \dots \dots \dots (1)$$

$$U = |0\rangle\langle 1| - |1\rangle\langle 0|$$

It is easy to show that the states will evolve another under the operation U , i.e.,

$$U |-\rangle = -|+\rangle, U |+\rangle = |-\rangle,$$

$$U |0\rangle = -|1\rangle, U |1\rangle = |0\rangle,$$

It doesn't matter whichever controller receives M first. Suppose the controller C_l receives M first, then C_l carries out unitary transformation H on each single photon and disorders the sequence M .

$$H = \frac{1}{\sqrt{2}} \begin{bmatrix} 1 & 1 \\ 1 & 1 \end{bmatrix} \dots \dots \dots (2)$$

It is also easy to show that the states will evolve another under the operation H , i.e.,

$$H |+\rangle = |0\rangle, H |-\rangle = |1\rangle,$$

$$H|0\rangle = |+\rangle, H|1\rangle = |-\rangle,$$

Like C_1 , C_2 carries out quantum transformation on each photon and disorders the sequence received from C_n with the same procedures, and then sends the photon sequence to the next controller C_3 . Those procedures stop at C_n . Finally, a new photon sequence Q' is generated and then sent to receivers. (S3) After receiving the sequence Q' , each receiver chooses randomly a sufficiently large subset K_i ($i = 1, 2, L, r$) from Q' sequence for eavesdropping check. K_1, K_2, \dots, K_r correspond to Bob, Charlie and other receiver's checking sequence, respectively. Then each receiver announces the position of its checking sequence. For each checking photon, Alice chooses randomly a controller to inform each receiver of the quantum transformation H and then choose other controllers to announce their H operation in turn. Thus each receiver can choose the correct measurement basis to make measurement on his or her corresponding checking sequence and publish his or her measurement results in a classical channel.

(S4) On receiving the measurement results, quantum controllers C_n determine whether to announce the order of their relative sequence and operation information or not. If the error rate is lower than the error probability threshold set in advance, quantum controllers proclaim the relative photon sequence order and the operation information; if not, turns to (S1). (S5) Each receiver recovers the messages from the photon sequence Q' with the helps of the photon sequence order and quantum transformation information announced by their relative controllers.

3. Secure Communication Protocol

Based on the operation model, in Fig. 1, in each period time, we do secure communication before we transfer quantum qubit. The purpose of the secure communication protocol is focused on liar detection in the intermediate node. Fig.1 shows four negotiable steps which only use quantum channel to do secure communication. In the initial time, Alice and Bob previously share a quantum key distribution which includes two sequences in the measured basis. But Candy can not know these sequences. The first sequence is a measured bases table set, denoted $s = \{s_1, s_2, \dots, s_x\}$, where x is equal to $2n$ and n is the number of positive integers, where s_i denotes one basis table. Given an example, for $n=3$, the measured bases table set $s = \{s_1, s_2, s_3, s_4, s_5, s_6, s_7, s_8\}$ and three qubits represents one measured bases table set. We assume that qubits $|000\rangle$ represents s_1 . Table I denotes s . The procedure is shown as follows.
STEP1: Prepared T1-T3 Bases Alice prepares N entanglement pairs for verification. Each entanglement pairs has three particles as follows.

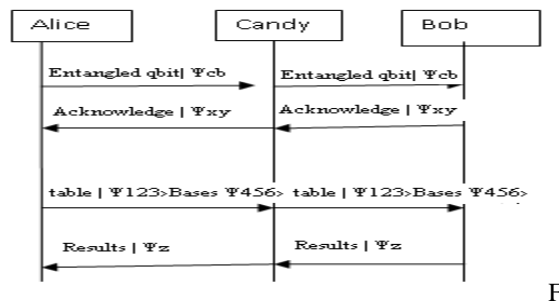


fig.1. Secure communication steps

$$|\Psi_{acb}\rangle = \frac{1}{\sqrt{2}}(|000\rangle + |111\rangle)_{acb} \rightarrow (3)$$

Alice uses three types the entangled pairs which can be regarded as three measured bases. Alice prepares N entanglement pairs with three particles for verification. Type I entanglement pairs can be written as

$$T1 = \frac{1}{\sqrt{2}}(|000\rangle + |111\rangle)_{acb} \rightarrow (4)$$

Type II entanglement pairs are to rotate qubit b for $\pi/4$ along x axis, shown in the following.

$$T2 = \frac{1}{\sqrt{2}}(|00\rangle_{ac}(|0\rangle + |1\rangle)_b + |11\rangle_{ac}(|0\rangle - |1\rangle)_b) \rightarrow (5)$$

Type III entanglement pairs are to rotate qubit b for $\pi/4$ along y axis, shown in the following.

$$T3 = \frac{1}{\sqrt{2}}(|00\rangle_{ac}(|0\rangle + i|1\rangle)_b + |11\rangle_{ac}(|0\rangle - i|1\rangle)_b) \rightarrow (6)$$

Table 1 presents the second sequence which denotes a physical measured basis. Bob receives three qubits information $|111\rangle_{456}$, where the suffix 4 represents Candy's measure basis and the suffix 6 represents Bob's measured basis. To consider the Bob's measured basis, the bases types $N_1N_2N_3$ are corresponding to the bases types $T_1T_2T_3$, wherein represents the measured basis of the qubit b which is T_i . For example, Alice transfers qubits $|111\rangle_{456}$ to Bob. then Bob checks table 1 and finds N_1 basis. Then Bob uses T_1 as his measured basis.

Table.1.Sequence of measured basis

Qbit information	Bases Types
$ 000\rangle_{456}$	$N_1N_2N_3$
$ 001\rangle_{456}$	$N_1N_2N_3$
$ 010\rangle_{456}$	$N_1N_2N_3$
$ 011\rangle_{456}$	$N_1N_3N_2$
$ 100\rangle_{456}$	$N_2N_1N_3$
$ 101\rangle_{456}$	$N_2N_3N_1$
$ 110\rangle_{456}$	$N_3N_1N_2$
$ 111\rangle_{456}$	$N_3N_2N_1$

STEP 2: Sending Entangled Quantum Qubit

When Alice sends the entangled quantum $|\Psi_{cb}\rangle$ to Candy, then Candy preserves $|\Psi_b\rangle$ to Bob.

STEP 3: Sending Acknowledge Message

When bob has received all the entangled qubits from alice, all the qubits will be checked by bob. then bob sends an acknowledge message to candy. Alice and bob have previously defined which is corrective acknowledge message. We assume that is corrective acknowledge message. If Alice receives acknowledge message is not ,then Alice judges that candy is not honest.

STEP 4: Announcing Quantum Bases

When Alice has received a acknowledge message from bob, Alice announces the type of all entangled pairs and passes all the quantum qubit information to candy. If Alice announces quantum bases in the quantum channel, bob can use this measured bases table to measure the quantum qubit correctly. Alice sends table basis set and basis element to bob. According to the agreement of measured table, bob can find the measured basis table and the measured basis element from Alice's qubit information.

STEP 5: Checking Quantum Results

Bob transfers all the measured results to Alice by using quantum qubits only. Alice and bob can check all the measured results. If all the measured results are the same, then candy is honest. Otherwise, candy is dishonest

4. Conclusion

In summary, we provide a multiparty controlled CSMA/CD scheme for quantum communication using the order rearrangement of single photon sequence and unitary transformation. It is shown that messages can be transmitted to receivers securely at one time without revealing any information to a potential eavesdropper. Compared with the previous CSMA/CD, this new scheme has many distinct advantages. In our scheme, the collision is avoided by utilizing quantum ACK and messages can only be recovered by the receivers with the permission of all controllers, which ensures the security of message transmission and realizes message sharing. For each receiver, the controllers can be different in order to enhance the applicability of the proposed quantum communication scheme. Different messages can be sent to their respective receivers simultaneously, which improves the channel utilization. So our scheme is a more efficient and feasible one with current techniques.

References

- [1] F.G.Deng and G.L.Long, "Controlled order rearrangement encryption for quantum key distribution," *phys.Rev.A*,vol.68,pp.042311-042315,October 2003.
- [2] G.P.Guo and G. C. Guo, "Quantum secret sharing without entanglement," *Phys. Lett. A*,vol.310, pp.247-251, April 2003.
- [3] Z.J.Zhang and Z. X. Man, "Multiparty quantum quantum secret sharing," *Phys.Rev.A*,vol.71,pp.04430-044304, April 2005.
- [4] P.Huang N.R. Zhou, and Y.Liu,"Secret sharing protocol based on multi-target quantum teleportation," *Journal on Communications*, vol.29, pp.114-118, March 2008.
- [5] S.J. Qin,Q.Y.Wen, and F.C.Zhu,"Cryptanalysis of multiparty quantum secret sharing of quantum state using entangled states," *chin.Phys.Lett.A*,vol.25,pp.3351-3554,October 2006.
- [6] F.G.Deng, X.H.Li, C. Y.Li, P.Zhou, and H. Y.Zhou,"Quantum secure direct communication network with Einstein-Podolsky-Rosen pairs," *Phys.Lett.A*,vol.359,pp.359-365,October 2006.
- [7] Hwayean Lee,Jongin Lim, and Hyungjin Yang,"Quantum direct Communication with authentication," *phys.Lett.A*,vol.73,pp.2301-2305, April 2006.
- [8] J.Wang,H.Q.Chen, Q. Zhang, C. J. Tang,"Multiparty controlled quantum secure direct communication protocol," *Acta Physica Sinica*,vol.56,pp.673-677,February 2007.
- [9] T.Mihara," Quantum identification schemes with entanglements," *Phys.Rev.A*,vol.65,pp.052361-052364,May 2002.
- [10] N. R.Zhou,G.H.Zeng, w. j. Zeng, and F.C.Zhu,"Cross-center quantum identification scheme based on teleportation and entanglement swapping," *Opt.Communication* vol.254,pp.380-388,October 2005.
- [11] N.R.Zhou, Y.Liu,G.H.Zeng,J.xiong, and F.C.Zhu, "Novel qubit block encryption algorithm with hybrid keys," *Physica A*, Vol.375,pp.693-698, March 2007.
- [12] c. H. Bennett, G.Brassard, C.Crepeau, R.Jozsa,A.Peres, and Wk.Wotters,"Teleporting an unknown Quantum state via dual classical and Einstein-Podolsky-Rosen channels," *Phys.Rev.Lett.*,vol.70,pp.1895-1899, March 1993.
- [13] D.Bouwmeester, J. W. Pan, K. Mattle, M.Eibl, H.Weinfurter, and A.zeilinger,"Experimental quantum teleportation," *Nature*, vol 390,pp.575-579,December 1997.
- [14] N. R. Zhou,G.H.Zeng,F.C.Zhu, and S.Q.Liu,"The Quantum Synchronous Communication Protocol for Two-army problem," *Journal of Shanghai Jiaotong University*, vol.40,pp.1885-1889,November 2006.
- [15] N. R.Zhou, G.H. Zeng,L.H.Gong,and S. Q. Liu,"Quantum Communication protocol for data link layer based on entanglement," *Acta Physica Sinica* ,vol.56,pp.5066-5070,September 2007.
- [16] G. H. Zeng, *Quantum Cryptography*. Beijing: Science Press, 2006.
- [17] K.Bostrom and T.Felbinger,"Deterministic secure direct communication using entanglement," *Phys.Rev.Lett*,vol.89,pp.187902-187904,October 2002.
- [18] Y.D. Zhang, *Principles of quantum information physics*. Beijing: Science Press, 2006.

A Location-Based User Movement Prediction Approach For Geolife Project

¹, **ZHIYUAN CHEN**, ², **BAHRAN SANJABI**, ³, **DINO ISA**

^{1,2,3}University of Nottingham, Malaysia Campus

^{1,2} School of Computer Science, ³Department of Electrical and Electronic Engineering

Abstract

Recently obtaining knowledge from raw trajectory data has been an interest of many researches. Trajectory data set consists of thousands of records. To discover valuable knowledge from these records advanced data mining techniques must be applied. Models developed from these techniques will be useful for prediction. In this paper data mining classification techniques are analyzed on trajectory dataset and Performance of these techniques is evaluated with recall, precision, kappa and accuracy.

Keywords- Classification Algorithms, WEKA, recall, precision, kappa and accuracy.

I. INTRODUCTION

We live in the era that smart phones and other GPS-enabled devices provide people the opportunity of capturing GPS trajectories everywhere at every time. Mining trajectory data leads in obtaining useful information e.g. prediction the user's behavior. Forecasting the behavior of users helps to have a better understanding of users' needs and it has many advantageous since it makes users' live simpler, more comfortable or even more secure. Considering situation that next preferred transportation mean of user is car then high quality location based services will provide to do list such as recommending car parks or gas stations on the way. Acquiring knowledge from raw trajectory data using data mining techniques has been an interest of many researches. (Zhou 2007) presented the approach that can detect important - frequent and important - non frequent locations. Using clustering algorithms and different classifiers he found the level of importance of locations in the trajectory. (Andrei Papiatseyeu, Oscar Mayora, 2008) used Naive Bayes, hidden Markov models and simple Neural Networks to analyze the performance of activity recognition from raw data collected by GPS, GSM and WIFI. The purpose of this project is applying data mining techniques (namely classification) on raw GPS records to predict the mode of transportation (such as taxi, bike, personal car and etc.) users choose once they arrive at a certain point. This paper concentrates on performance of classification algorithms. The classification algorithms considered here are Decision tree, Naive Bayes classifier, Bayesian network, Neural Network algorithm and Support Vector Machines. These classifiers are compared based on statistical parameters such as Accuracy, Recall, Precision, Confusion matrix and Kappa. It will be shown that decision tree and Bayesian network are acceptable classifiers for classifying trajectory data set. Data mining software used in this project is WEKA (Waikato Environment for Knowledge Analysis) which is a collection of data mining algorithms. The structure of this paper is as follow: next section discusses about data mining technique. Section 3 explains the data set used and the process of preprocessing data. Section 4 is allocated to the result of experiment and section 5 describes a summary of future research.

II. DATA MINING TECHNIQUE

A. classification

Data mining is extracting valuable knowledge and useful pattern from raw data. One of the well-known data mining techniques is Classification which is a supervised learning algorithm. Data classification involves two phases; training phase where the classifier algorithm builds classifier with the training set of tuples and test phase where the model is tested on testing set of tuples

B. Different classifiers

Classifiers considered in this project are Decision tree, Naive Bayes classifier, Bayesian network, Neural Network algorithm and Support Vector Machines. Decision tree: Decision tree is widely used in data mining project because it is easy to understand and gives a clear representation of how decisions are made. Decision tree consists of root node, in rnal node and leaf node. Internal nodes are between root node and leaf node. The condition is assessed at each

node if it has ositive result the data is sent to the leaf node otherwise it is sent to the non-leaf node and portioning process repeats until it reaches to leaf which assigns a class label to the data sample. Bayesian classifier: A Bayesian

classifier is based on Bayes' theorem which states: $P(Y|X) = \frac{(P(X|Y)P(Y))}{P(X)}$. In order to determine a classification using Bayes theorem, $P(Y|X)$ needs to be known for every possible value of X and Y. Two main type of Bayesian classifier are Naive Bayes Classifier and Bayesian Network. Naïve Bayes has a naïve assumption of independence between all attributes meaning that the presence or absence of one attribute has no impact on the next whereas the Bayesian Network allows conditional independence between attributes to be applied to only particular pairs of attributes. Artificial Neural Network: Artificial Neural Network is a system inspired by human neurology. The structure of ANN is like layer model. Each layer is made of numbers of interconnected nodes which connect to next layer via direct links with various weights. The first layer is called input layer that receives the input data and transmits it over next layers that are called hidden layers where the processing is applied. Hidden layers then shift the output to output layer. For a neural network to be useful, it must first be trained so that the weights of the links can be adjusted. Adjusting the weights of the links can be done in a couple of ways such as Back- propagation.

Support Vector Machine: It is based on the concept of decision planes where the training data is mapped in to a higher dimensional space and separated by a hyper plane to differentiate between two or more classes of data. The "support vectors" are those points in the input space which best define the boundary between the classes. The selected hyper plane for an SVM should be the one with the largest margin between the two classes because it creates clear boundary between them. (Bottou L., Chih-Jen Lin, n.d.)

III. DESCRIPTION OF DATA

The data set used in this project is a portion of GPS trajectory data set which was gathered for GEO life project. Recently number of researched have been done using this data set. For instance mining interesting location and travel sequence (Yu Zheng, 2009), finding similarity between users (Li, 2008) and learning automatically transportation mode (Zheng, 2008)

A. Raw data

A trajectory data set is a sequence of GPS records that are ordered by the timestamp of the records. This data set contains 17,621 trajectories that are gathered from more than 170 people and have a total distance of 1,251,654 kilometers and a total duration of 48,203 hours. Each trajectory folder is related to one particular user. These data are in PLT format and contain following fields:

Field 1: Latitude in decimal degrees.

Field 2: Longitude in decimal degrees.

Field 3: All set to 0 for this data set.

Field 4: Altitude in feet (-777 if not valid).

Field 5: Date - number of days (with fractional part) that have passed since 12/30/1899.

Field 6: Date as a string.

Field 7: Time as a string

B. Data Preprocessing

Data preparing is the vital step in data mining procedure. In this project the available data set was in PLT format. Since WEKA software accepts some distinct format the first step was converting data from PLT format to CSV format which is acceptable for WEKA. In second step impractical fields (fields 3, 4, 5) has been removed. Approximately 23% of users labeled their context by indicating the mean of transportation they used such as driving, taking a bus or taxi, using a subway, riding a bike, walking and in rare condition flying with airplane. In third step since files of trajectory and transportation label were stored separately from each other, long time has been spent to match the time and date of these files and create one complete data set. In step four, in Microsoft Excel environment the interval time user stayed in each pair of latitude and longitude point has been calculated using math function. Therefore the new data set contains latitude, longitude, date, time, transportation mode and duration. Step five was creating two tables from data set; stop table and move table. Stops can be assumed as important points of a trajectory if user stays more than a period of time. Using mathematical function in Microsoft excel the points that user stayed more than 10 minutes has been extracted and moved to stop tables. Stop tables can be used for creating location history and personal map of users. Other points have been moved to moving table. Classifying algorithms have been applied on move tables.

C. Weka

In this project WEKA "Waikato Environment for Knowledge Analysis" has been used. WEKA is an open Source Machine Learning Software that is written in Java and developed by the University of Waikato in New Zealand .It is a collection of machine learning algorithms and data preprocessing tools that helps researchers to mine different data sets. WEKA has four environments; simple CLI, explorer, experimenter and knowledge flow. In this project the explorer environment has been used. In WEKA, The results of classification is divided into several sub categories which is more

human readable and easy for evaluating. First section shows the correctly and incorrectly classified instances in numeric and percentage value. Kappa statistic, mean absolute error and root mean squared error are presented also in this category. In second part parameters for measuring accuracy of each class is shown. These parameters are FP, TP, ROC area, F-measure, Recall and precision. The third section is confusion matrix which is one of best measurement for evaluating classifiers

IV. RESULT

In GEO life project, people who collected their GPS trajectories had a different period of collaboration. Some of them have a long collaboration and carried a GPS logger for several years while some others cooperated for just a few weeks hence the size of their trajectories were different. Small size with five class of transportation, middle size with 8 class of transportation and long size with 10 class of transportation were selected for applying classification algorithms. In this paper the result of classification on small data set will be shown. This data set has 44236 instances and 5 classes. Each classifier has been tried on two test options; 10 fold cross validation and percentage split 66%.

A. Result Of Classifiers

TABLE 1-PERCENTAGE SPLIT 66%

Classifier (%)	Correctly classified instance	Incorrectly classified instance	Kappa statistic	Mean absolute error	Root mean squared error	Relative absolute error	Root relative squared error
Bayes NET	77.697	22.3023	66.79	10.96	24.51	41.5289	67.455
Naïve Bayes	58.1073	41.8927	39.14	0.19	33.45	71.9511	97.547
J48	87.296	12.7034	80.59	5.66	17.52	21.432	48.2095
Ann	66.401	33.5989	45.58	11.75	24.9	73.759	88.2569
SMO	51.491	48.5084	6.52	27.06	36.07	102.48	99.2469

TABLE 2-10 FOLD CROSS VALIDATION

Classifier (%)	Correctly classified instance	Incorrectly classified instance	Kappa statistic	Mean absolute error	Root mean squared error	Relative absolute error	Root relative squared error
Bayes Net	77.7436	22.2564	66.83	10.77	24.36	40.798	67.042
Naïve Bayes	57.468	42.532	38.18	19.13	35.69	72.474	98.250
J48	87.0617	12.9383	80.26	5.87	17.71	22.218	48.7413
Artificial Neural Network	63.7762	36.2238	43	16.58	30.72	62.814	84.559
SMO	51.5474	48.4526	6.48	27.12	36.1	102.7	99.370

B. Comparing classifiers

The performance of classifier is evaluated by parameters like accuracy, precision, recall and kappa. Correctly classified instance presents the percentage of instances which were classified correctly and this measure is often called accuracy. Precision is the fraction of instances which truly have class x among all those which were classified as class x. Recall is a fraction of instance which correctly classified as class x among all instances that belong to class x. Kappa is a measure of agreement normalized for chance agreement. $Kappa = \frac{P(A) - P(E)}{1 - P(E)}$ Where P(A) is the percentage agreement between the classifier and ground truth and P(E) is the chance agreement. A value greater than 0 shows that classifier is doing better than chance.

TABLE 3- weighted average of recall, precision and accuracy

Classifier	Weighted average of Recall	Weighted average of Precision	Number of Correctly classified instance
Decision tree(j.48)	0.871	0.871	35953
Naïve Bayesian	0.633	0.575	23733
Bayes Net	0.796	0.777	32105
Artificial Neural Network	0.637	0.638	26337
Support Vector Machine	0.323	0.515	21287

It can clearly be seen that Decision tree (j.48) has the maximum accuracy and better recall and precision. On the other hand support vector machine is the least accurate classifier. High recall demonstrates that an algorithm correctly classified most of the instance of each class. High precision means that result of an algorithm is more correct than incorrect.

TABLE 3- COMPARING KAPPA

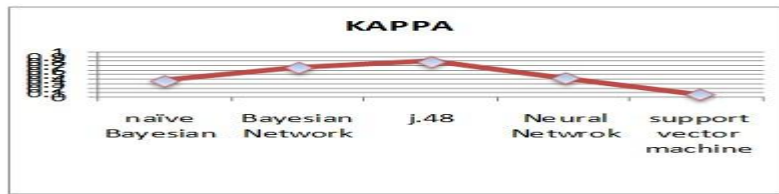


Figure 1- comparing Kappa

J.48 has the highest kappa. It means that the result is more close to truth than chance. Another important concept for evaluation the performance of classification is confusion matrix. A confusion matrix illustrates the number of correct and incorrect predictions made by the model compared with the actual classifications in the test data. The confusion matrix is an array with n size where n is the number of classes.

TABLE 4- confusion matrix obtained using decision tree classifier

a	b	c	d	e	<-- classified as
5625	6	858	1383	22	a = bike
40	2813	204	43	14	b = subway
393	17	19724	143	31	c = bus
2031	12	70	7658	1	d = walk
19	8	39	9	133	e = car

It is obvious that majority of instances are classified correctly.

V. CONCLUSION

Data mining through different technique turn raw data in to meaningful information. In this research data mining methods have been used to mine trajectory dataset which were gathered from people who have collaborated with GEO-life project. The final goal of this research is prediction the mode of transportation users use based on geographic location they are. To achieve this goal considerable effort has been put to prepare the proper data set in preprocessing level. Three sample sizes of trajectories have been selected and each of them categorized in to stop and move data set. prediction the state of transportation is achieved by applying classification algorithms on move data set .Decision tree, naïve Bayesian, Bayesian Network, Support Vector Machine and Artificial Neural Network were used as classifiers and their efficiency were evaluated by precision, Recall, Accuracy and Kappa. Decision Tree achieved the highest score and Bayesian Network was in the second place. Support vector machine illustrated weak result and it might because of the structure of data set which has lots of classes and few attributes.

VI. Futur Research

As a future extension of this study we will create models for predicting the use of public transportation or personal one in dense and popular regions. Density based clustering will be applied on trajectory data set in order to find most dense region and then by using SQL commands in data base the probability of using public transportation (bus-subway-taxi) and personal transportation (car-bike) will be calculated. Then by applying classifiers namely decision tree and Bayesian network the model for predicting the use of public or personal transportation will be build.

VII. References

- 1) Andrei Papliatseyeu, Oscar Mayora, 2008. Inferring and predicting user activities with a location aware smartphone. Advances in Soft Computing , Volume 51, pp. 343-352.
- 2) Bottou L., Chih-Jen Lin, n.d. Support Vector Machine Solvers. s.l.:s.n.
- 3) Christine Körner,Jutta Schreinemacher, 2012. Analyzing Temporal Usage Patterns of Street Segments Based on GPS. s.l., s.n.
- 4) Quannan Li1,2, Yu Zheng2, Xing Xie2,, 2008. Mining User Similarity Based on Location History. s.l., 16th ACM SIGSPATIAL international conference on Advances in geographic information systems .
- 5) Yu Zheng, 2009. Mining Interesting Locations and Travel Sequences from GPS Trajectories, s.l.: s.n.
- 6) Zheng, Y., 2008. Learning Transportation Mode from Raw GPS Data for Geographic Applications on the Web. NewYork, 17th international conference on World Wide Web .
- 7) Zhou, C., 2007. Mining Personally Important Places from GPS Tracks. Istanbul, Data Engineering Workshop, 2007 IEEE 23rd International Conference.
- 8) Remco R. Bouckaert, E. F. H., 2012. WEKA Manual for version 3.6.7. s.l.:s.n.

Hdl Implementation of Amba-Ahb Compatible Memory Controller

¹S.Ramakrishna , ²K.Venugopal, ³B.Vijay Bhasker , ⁴ R.Surya Prakash Rao
^{1,2,3,4}St Theresa college of Engineering

Abstract

Microprocessor performance has improved rapidly these years. In contrast, memory latencies and bandwidths have improved little. The result is that the memory access time has been a bottleneck which limits the system performance. Memory controller (MC) is designed and built to attacking this problem. The memory controller is the part of the system that, well, controls the memory. The memory controller is normally integrated into the system chipset. This paper shows how to build an Advanced Microcontroller Bus Architecture (AMBA) compliant MC as an Advanced High-performance Bus (AHB) slave. The MC is designed for system memory control with the main memory consisting of SRAM and ROM. Additionally, the problems met in the design process are discussed and the solutions are given in the paper.

Keywords - ARM; AMBA; Memory Controller; AHB bus

I. Introduction

With the improvement of Microprocessor these years, the memory access time has been a bottleneck which limits the system performance. Memory controller (MC) is designed and built to attacking this problem. The memory controller is the part of the system that, well, controls the memory. It generates the necessary signals to control the reading and writing of information from and to the memory, and interfaces the memory with the other major parts of the system. The memory controller is normally integrated into the system chipset. In this paper, an Advanced Microcontroller Bus Architecture (AMBA) compliant memory controller is designed for system memory control with the main memory consisting of SRAM and ROM. The memory controller is compatible with Advanced High-performance Bus (AHB) which is a new generation of AMBA bus, so we call it "AHB-MC". The AHB-MC has several

features which are shown as flows

1. Designed with synthesizable HDL for Application Specific Integrated Circuit (ASIC) synthesis
2. Supports multiple memory devices including static random access memory (SRAM), read-only memory (ROM)
3. Complies with AMBA AHB protocol
4. Supports one to four memory banks for SRAM and ROM

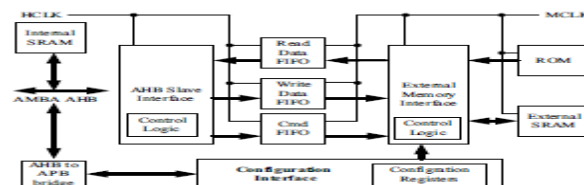
Programmable memory timing register and configuration registers

Shared data path between memory devices to reduce pin count

Asynchronous FIFO to support burst transaction up to 16-beats This paper describes how to build the AHB-MC. And combining the problem met in the process of designing, the corresponding solutions are presented. Finally, the simulation results are presented.

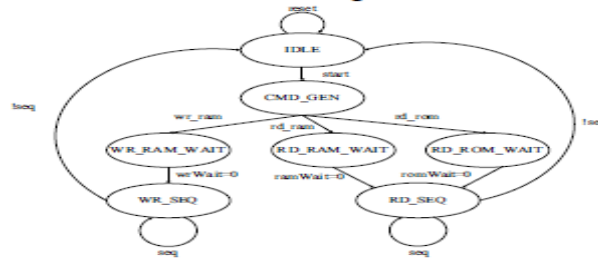
II. Architecture of Ahb-Mc

The AHB-MC mainly consists of three modules: AHB slave interface, configuration interface, and external memory interface [1]. Figure 1 shows the architecture of AHB-MC.



A. AHB slave interface

The AHB slave interface converts the incoming AHB transfers to the protocol used internally by the AHB-MC. The state



machine is shown in Figure 2.

B. External memory interface

The external memory issues commands to the memory from the command FIFO, and controls the cycle timings of these commands. The state machine is shown in Figure3.

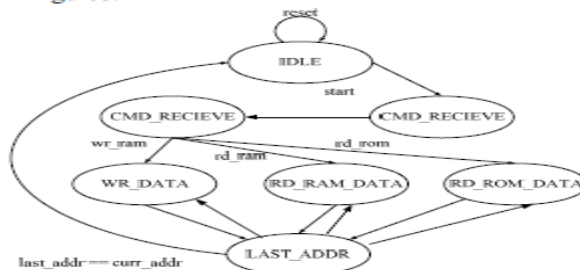


Figure 4 and Figure 5 show the timing of a read from memory and a write to memory with two wait states [2]. Figure 4. Memory read with two wait states Figure 5. Memory write with two wait states

Memory bank select

Because system will change the memory map after system boot, AHB-MC is designed to support a remap signal which is used to provide a different memory map. AHB-MC has four memory banks, which are selected by XCSN signal. The XCSN signal is controlled by the address of a valid transfer, and the system memory map mode. So before the system memory is remapped, the boot ROM at 0x3000 0000 is also mapped to the base address of 0x0000 0000 as shown in Table 1

TABLE1

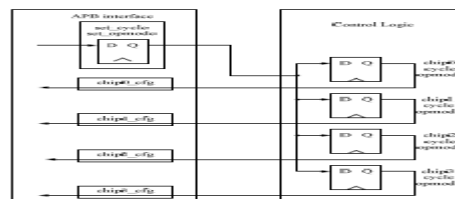
1. Memory write control

To support for writing in word (32-bits), half-word (16-bits) and byte (8-bits), the XWEN signal is used in the AHB-MC. Table 2 shows the relationship between XCSN and the inputs from AHB bus.

C. Configuration interface

The main function of the configuration interface is to change the configuration registers (SETCYCLE and SETOPMODE register) according to the commands from AHB to APB bridge which converts AHB transfers from the configuration port to the APB transfers that the configuration interface require [3]. Each memory chip supported by AHB-MC has two registers (CYCLE register and OPMODE register), which contain all the timing parameters that are required for configuration registers: SETCYCLE and SETOPMODE as shown in fig 5

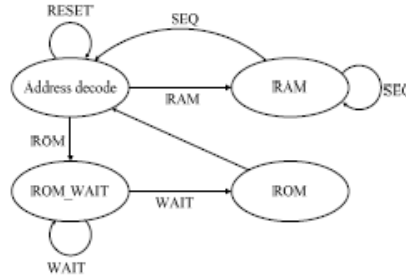
Fig 6



III. Burst Transfer Support

With the increasing system frequency, it's hard to accomplish the address decoding and memory access operations in one clock cycle. Therefore, wait states are inserted into the data cycle to ensure there is enough time for address decoding and memory accessing. But the method that inserting wait state will cause system performance drop dramatically. Therefore, a sequential-access (burst) method is presented to resolve this problem in this paper. In this method, all AHB fixed length burst types are directly translated to fixed length bursts, and all undefined length INCR bursts are converted to INCR4 bursts. Burst

operation has performance benefits because when the first beat of a burst is accepted, it contains data about the remaining beats. For example, when AHB-MC got the first beat of a read burst, all the data required to complete the transfer can be read from memory and restored in the read data FIFO. SO this first transfer has some delay before data is returned. But subsequent beats of the burst can have less delay because the data they require might have already been prepared in the FIFO. To further improve the system performance, a RETRY response is used that AHB-MC can release the bus when it is preparing the data [4]. This mechanism allows the transfer to finish on the bus and therefore allows a higher-priority master to get access to the



state machine is showed in Fig 7

IV. Memory System

In the arm architecture, instructions are all 32-bits, while instructions are 8-bits in the external ROM and SRAM. Therefore the lowest two addresses of ROM and SRAM are not connected to the external address bus. Additionally, to support byte writing, SRAM needs to be separated as four independent banks or has a byte-write enable signal. The basic memory

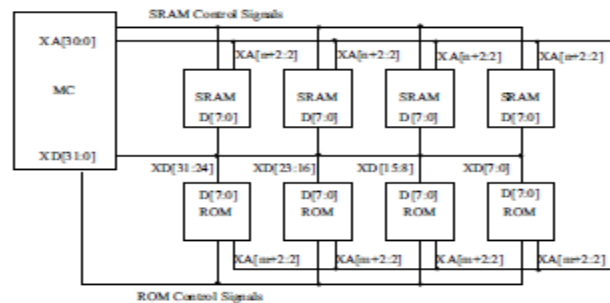


Fig 8 system architecture is shown in

V. Asynchronous Clock

The AHB-MC has two clock domains: AHB clock domain and external memory clock domain as shown in Figure 8. Asynchronous FIFO is used between two clock domains as a data buffer.

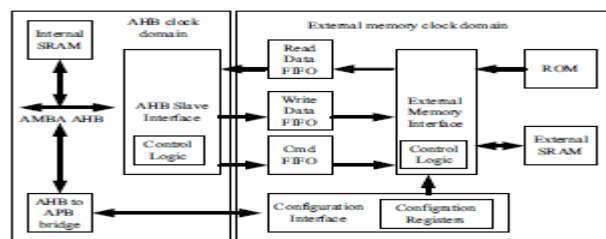


Fig 9

The main benefit of asynchronous clocking is that you can maximize the system performance, while running the memory interface at a fixed system frequency. Additionally, in sleep-mode situations when the system is not required to do much work, you can lower the frequency to reduce power consumption [5]. However, asynchronous clock will cause the flip-flop going metastable state and not converging to a legal stable state by the time the output must be sampled again as shown in Figure 10. To resolve this problem, the most common way is inserting a two-flip-flop synchronizer as shown in Figure

VI. Verification and Simulation Results

The verification method used in this paper, is to put the AHB-MC into a minimum system which consists of ARM core, AHB bus, APB bus and AHB-MC. The code used for testing is put in ROM, if the system can work correctly, then we know the test case is passed. The simulation waveforms of a simple test code are shown. Figure 13 shows read with zero wait states from the external ROM. The address is registered at rising edge of hclk (AHB bus clock), after which ex_oen (external memory read enable) signal goes high, then read data reaches hrdta (AHB read data bus) at falling edge of hclk. Figure 13 Write with zero wait states to the external RAM is shown in Figure 14. A write operation is initiated by hwrtst going high. Then the address is sent to external memory address bus and ex_wen (external memory write enable) signal goes low to enable the data from hwrtst (AHB write data bus) stored in the RAM in Figure 14.

References

- [1] "AMBA Specification (Rev2.0)", ARM Inc.
- [2] "PrimeCell AHB SRAM/NOR Memory Controller", Technical Reference Manual, ARM Inc.
- [3] "AHB Example AMBA System", Technical Reference Manual, ARM Inc.
- [4] Carter, J.; Hsieh, W., "Impulse: building a smarter memory controller", High-Performance Computer Architecture, Dept. of Comput. Sci., Utah Univ., Salt Lake City, UT.
- [5] Clifford E. Cummings, "Synthesis and scripting Techniques for Designing Multi-Asynchronous Clock Designs", Sunburst Design, Inc

IC TESTER USING 89s52 MICROCONTROLLER

¹Miss.M.A.Tarkunde, ²Prof.Mrs.A.A.Shinde

¹M.Tech.Student

^{1,2}Bharati vidyapeeth Deemed University College of Engineering
Pune,India

Abstract

An IC constitutes area of microelectronics in which many electronic components are combined in to high density modules.IC's, the main component of each and every electronic circuit can be used for wide variety of purposes and functions. IC consists of active and passive components such as resistors, capacitors, transistors on single chip which reduces size of system, power consumption and cost of overall system. But sometime due to faulty ICs the circuit doesn't work. It is lot work to debug the circuit and confirm whether the circuiting is creating problem or the IC is faulty. So the proposed project is designed to confirm whether the IC under consideration is properly working or not. The proposed project can be used to check the IC's of 74 series at gate level.

I. Introduction

The basic function of IC tester is to check digital IC for correct logical functioning as described in the truth table i.e. it used to test the variety of IC's which consists of gates,sequential circuits,combinational circuits. The input signals are applied to the input pins of the IC and output is measured at the corresponding output pin. In the various systems various IC's and components are connected to each other. During the system failure it is not possible to check the whole circuit as it requires much time ,and high cost. Therefore by checking only IC's and components on the chip the failure rate can be reduced by using the designed project. Unlike the Ic testers available in market ,this IC tester is affordable and user friendly. The 89s52 microcontroller is used in this project with keyboard and LCD display unit. It checks the gates in given IC which is placed in ZIF socket and display the result. Testing of IC is based on the inputs that provided to the gates in IC through the programming.

ii.Literature Survey

The proposed project is used to check the digital IC's. Digital IC's are consists of two types.

1.Microcontroller based

2.PC based

The proposed project checks only microcontroller based IC's. Various types of microcontrollers are available in the market to check the correct functionality of component and IC's such as

i.8051

ii.89c2051

iii.89s52

DISADVANTAGES OF 8051

1.it gulps power and so it heats up.

2.it is not CMOS compatible,only TTL compatible.

Disadvantage of 89c2051

1.it is 20 pin IC.

2.As we are testing 16/14 pin IC this IC is not sufficient.

3.it is not possible to interface keyboard and display.

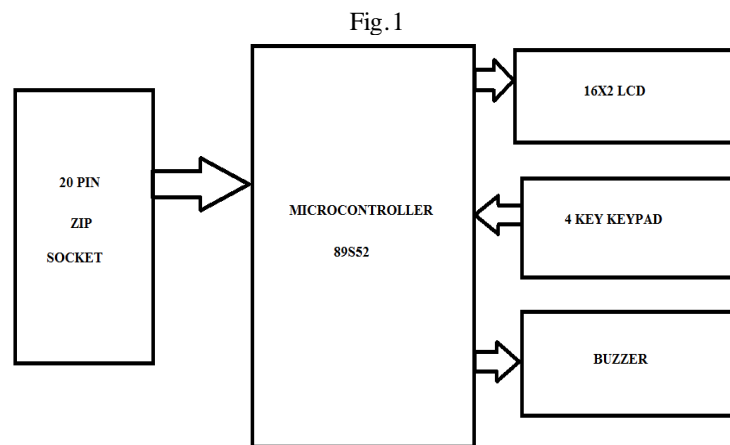
ADVANTAGES OF 89s52 MICROCONTROLLER

1.8K Bytes of In-System Programmable (ISP) Flash Memory

– Endurance: 1000 Write/Erase Cycles

- 4.0V to 5.5V Operating Range
- Fully Static Operation: 0 Hz to 33 MHz
- Three-level Program Memory Lock
- 256 x 8-bit Internal RAM
- 32 Programmable I/O Lines
- Three 16-bit Timer/ Counters
- Eight Interrupt Sources
- Full Duplex UART Serial Channel
- Low-power Idle and Power-down Modes
- Interrupt Recovery from Power-down Mode
- Watchdog Timer
- Dual Data Pointer
- Power-off Flag

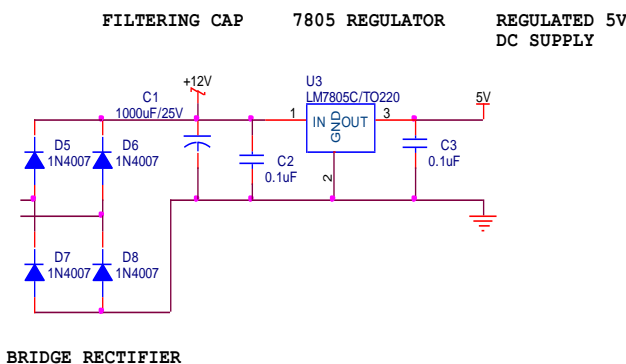
Iii.Block Diagram



Iv. Working

1.Power supply design

The basic step in the designing of any system is to design the power supply required for that system.

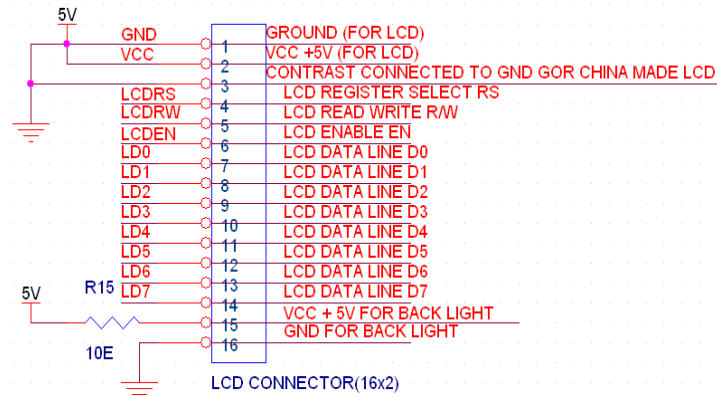


We have used Regulator

IC 7805 that gives output voltage of 5V. The minimum input voltage required for the 7805 is near about 7 v. Therefore we have used the transformer with the voltage rating 230v-10v and current rating 500 mA. The output of the transformer is 12 V AC. This Ac voltage is converted into 12 V DC by Bridge rectifier circuit.

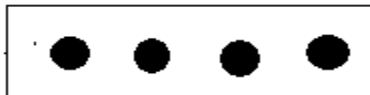
2.LCD display

We have used 16*2 LCD display which has 8 data lines and 3 control lines.
The connections of LCD are given blow



3. Keypad

It has 4 keys to select proper IC which we want to check.

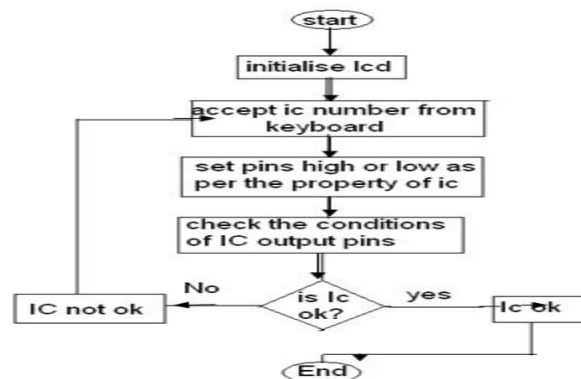


Working of gate level testing of IC

The test sequence for IC testing is as given below,

1. The ISP programmer is used to download the program in the microcontroller.
2. the project is made user friendly by interfacing keypad and LCD.
3. The IC to be tested is inserted in the ZIF socket. The user enters the IC number through keypad which is simultaneously displayed on the LCD.
4. The IC number is communicated to microcontroller which basically test the ICs for few sets of input which is given through the MCU and corresponding output. The result is again displays on the LCD.
5. If the IC tested is ok "IC TESTED OK is displayed on the LCD. Otherwise "IC TESTED FAILED" is displayed.

V. Flow Chart



Vi. Conclusion

This paper proposes an inexpensive and compact model of digital integrated circuit tester using 89s52. Different digital IC's can be tested by just writing the specific program without any change in hardware. Depending upon pre-determined data the signals from microcontroller are conditioned and corresponding output pins are checked for

correctness The system that has been implemented has shown considerable output that matched our requirement.this was achieved by small and user friendly 89s52.

Vii.References

1. Abhishek Jain, Anshul Goyal ,Siddharth Garg,"Digital IC tester"*Electronics club ,IIT Kanpur*
2. Fang pang,Canada"A reconfigurable digital IC tester implemented using ARM".
3. Ali F.Shammari"Design and implementation of digital IC interface to IBM compatible computer"Scientific journal of Kerbala,university 2010
4. www.scribd.com"digital IC Tester ieee.
5. Konemann,B Zwiehoff, G Mucha J,"Built in test for complex digital IC".solid state circuit. IEEE journal ,volume 15,issue 3
6. K.R.Botkar"Integrated circuits",Khanna publication.
7. Roshan Borkar,Ashvin Nakman,"Digital Integrated Circuit Tester",Don Bosco Institute of Technology,Mumbai.
8. Online teaching laboratory on embedded systems,"Microcontroller based diode and BJT tester".2009
9. Dhananjay v. Garde"Programming and customizing the avr microcontroller",
10. Online teaching laboratory on embedded systems,"Microcontroller based diode and BJT tester".2009
11. Dhananjay v. Garde"Programming and customizing the avr microcontroller"
12. www.scienceprog.com
13. <http://extremeelectronics.co.in/avr-tutorials>

A NOVEL APPROACH TO AUTOMATED BRAIN TUMOR CLASSIFICATION USING PROBABILISTIC NEURAL NETWORK

Varada S.Kolge¹, Prof.K.V.Kulhalli²

¹ Department of Electronics and Telecommunication, Shivaji University, DYPCET, Kolhapur, Maharashtra, India

² Department of Information Technology, Shivaji University, DYPCET, Kolhapur, Maharashtra, India

Abstract

Conventional methods of monitoring and diagnosing the diseases rely on detecting the presence of particular features by a human observer. Due to large number of patients in intensive care units and the need for continuous observation of such conditions, several techniques for automated diagnostic systems have been developed in recent years to attempt to solve this problem. Such techniques work by transforming the mostly qualitative diagnostic criteria into a more objective quantitative feature classification problem. Probabilistic Neural Network (PNN) with image and data processing techniques will be employed to implement an automated brain tumor classification. The conventional method for Medical Resonance (MR) brain images classification and tumors detection is by human inspection. Operator-assisted classification methods are impractical for large amounts of data and are also non-reproducible. Medical Resonance (MR) images contain a noise caused by operator performance which can lead to inaccuracies in classification. The use of artificial intelligent techniques like neural networks, and fuzzy logic has shown great potential in this field.

Keywords: Principal Component Analysis, Probabilistic Neural Network, Medical Resonance

1. Relevance

Brain tumor is one of the major causes in increase in mortality among children and adults. A tumor is a mass of tissue that grows out of control of the normal forces that regulates growth. The complex brain tumors can be classified into two general categories depending on the tumor origin, their growth pattern and malignancy. Primary brain tumors are tumors that arise from cells in the brain or the covering of the brain. A secondary or metastatic brain tumor occurs when cancer cells spread to the brain from a primary cancer to the other part of the body. PNN are mathematical analogous to biological neuron system. They are made up of parallel interconnected system of nodes called neurons. Combining PNN with different types of learning schemes results in a variety of PNN systems. All the PNN systems do not yield a satisfactory result in all the practical applications. Depending on the specific requirement, PNN system is to be designed. This document describes the use of PCA and PNN in automated classification of the brain tumors. PCA is a mathematical technique that is used to reduce the large dimensionality of the data and then PNN can be used for classification of the tumors.

2. Significance of PCA

PCA is a mathematical procedure that uses an orthogonal transformation to convert a set of observations of possibly correlated variables into a set of values of linearly uncorrelated variables called principal components. The number of principal components are less than or equal to the number of original variables. This transformation is defined in such a way that the first principal component has the largest possible variance (that is, accounts for as much of the variability in the data as possible), and each succeeding component in turn has the highest variance possible under the constraint that it be orthogonal to (i.e., uncorrelated with) the preceding components. Principal components are guaranteed to be independent only if the data set is jointly normally distributed. PCA is sensitive to the relative scaling of the original variables. Depending on the field of application, it is also named the discrete Karhunen–Loève transform (KLT), the Hotelling transform or proper orthogonal decomposition (POD). Technically, a principal component can be defined as a linear combination of optimally-weighted observed variables. In order to understand the meaning of this definition, it is necessary to first describe how subject scores on a principal component are computed. In the course of performing a principal component analysis, it is possible to calculate a score for each subject on a given principal component.

3. Present Theories And Practises

Artificial neural networks are finding many uses in the medical diagnosis application. According to Qeethara Kadhim Al-Shayea [1] Artificial neural networks provide a powerful tool to help doctors to analyze, model and make sense of complex clinical data across a broad range of medical applications. Most of the applications are providing solution to the classification problems. According to N. Kwak, and C. H. Choi [2] Feature selection plays an important role in

classifying systems such as neural networks (NN). In doing so higher performance with lower computational effort is expected. One of the most popular methods for dealing with this problem is the principal component analysis(PCA) method. This method transforms the existing attributes into new ones considered to be crucial. E. D. Ubeyli and I. Guler[3] used feature extraction methods in automated diagnosis of arterial diseases. Since classification is more accurate when the pattern is simplified through representation by important features, feature extraction and selection play an important role in classifying systems. T.Logeswari , and M. Karnan [5] used image segmentation based on the soft computing for improved implementation of the brain tumor detection. The MRI brain image is acquired from patients database and then Image acquisition, preprocessing, image segmentation is performed for brain tumor detection. Georgiadis. Et all [6] also did the work for improving brain tumor characterization on MRI by probabilistic neural network and non-linear transformation of textural features. According to Chettri, S. R. and Crompt, R.F., the probabilistic neural network architecture can be used for high speed classification of remotely sensed imagery. Probabilistic Neural Network can be applied to remotely sensed data.

4. Proposed Work

Here the automated classification of brain magnetic resonance images by using some prior knowledge like pixel intensity and some anatomical features are proposed[7]. Currently there are no methods widely accepted, therefore automatic and reliable methods for tumor detection are of great need and interest. The application of PNN in the classification of data for MR images problems are not fully utilized yet. These include the clustering and classification techniques especially for MR images problems with huge scale of data and consuming times and energy if done manually. Thus, fully understanding the recognition, classification or clustering techniques is essential to the developments of Neural Network systems particularly in medicine problems

Decision making will be performed in two stages:

- 1) Feature extraction using the Principal Component Analysis (PCA) and
- 2) Classification using Probabilistic Neural Network (PNN).

The performance of the PNN classifier will be evaluated in terms of training performance and classification accuracies. Probabilistic Neural Network gives fast and accurate classification and will be a promising tool for classification of the tumors.

The block diagram of the above proposed system, is as follows

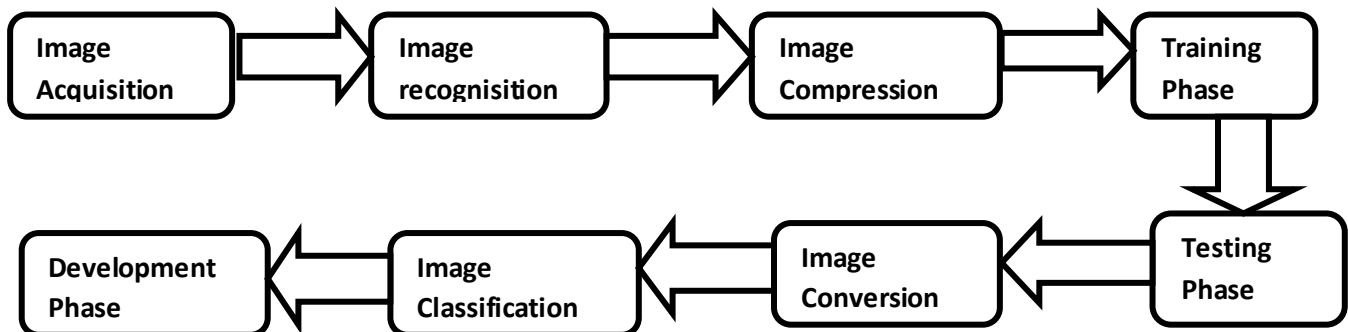


Figure 1. Block diagram of the proposed system

Image Acquisition :- Collect as many MR images of brain as possible from the Radiologists, Internet, Medical Atlases, Hospitals or other resources.

Image recognition and Image compression :- Mathematical technique of Principal Component Analysis' will be used for Image recognition and Image compression.

Training Phase :- In this phase, feature vectors for each image from the training set will be extracted.

Testing Phase :- In this phase feature vector of the test image will be computed

Image Conversion :- MR images will be converted into matrices form using MATLAB or SCILAB as a tool.

Image Classification :- Feed Forward PNN will be used to classify MR images.

Development Phase :- Performance analysis based on the result will be carried out in the development phase.

Proposed schematic diagram of MR image recognizer for automated classification of brain tumors is as shown below.

5. Proposed Schematic Diag. Of MR Image Recognizer [7]

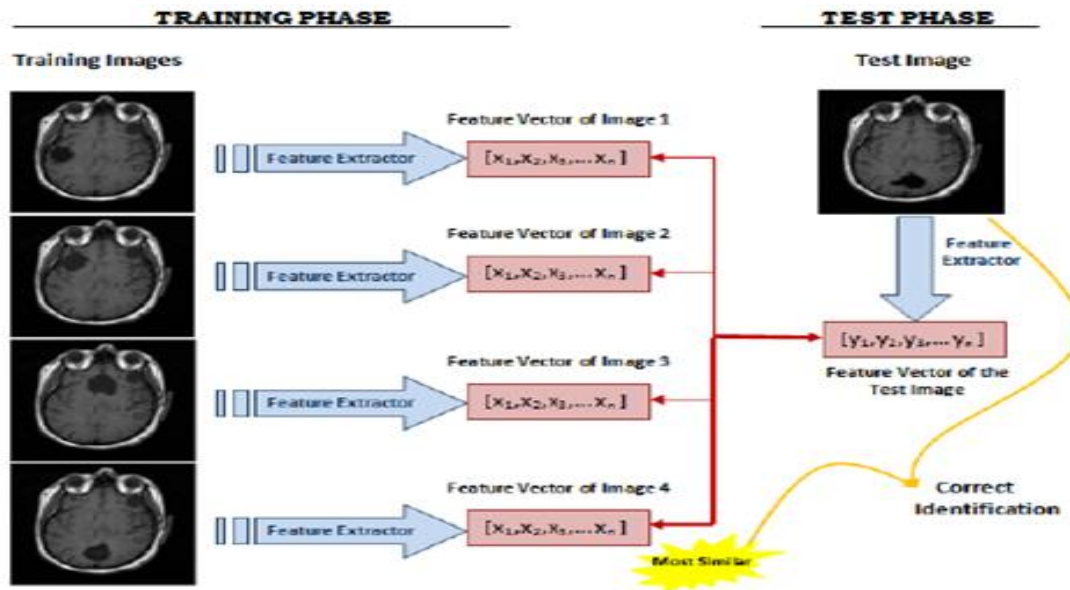


Figure 2. Proposed schematic diagram of MR image recognizer.

MR image recognition system find the identity of the given test image according to their memory[7]. The memory of a MR image recognizer is generally simulated by a training set. The training database consists of a set of MR images. The task of MR image recognizer is to find the most similar feature vector among the training set to the feature vector of a given test image. In the 'TRAINING PHASE' feature vectors are extracted for each image in the training set.

In the 'TESTING PHASE' feature vector of the test image is computed using PCA. In order to identify the test image, the similarities between the feature vectors is calculated using Euclidean distance and then output is obtained from the MR image recognizer. The MR image has been given to the input. The input image will be converted into MAT file and calculate weight also by using the Principal Component Analysis[7].

The purpose of PCA is to reduce the large dimensionality of the data. And calculate the weight also. After that create two layer network that is the PNN for classification purpose.

6. PCA Steps

- 1) Input MR Images.
- 2) Subtract the mean.
- 3) Calculate the covariance matrix.
- 4) Calculate the eigenvectors and eigen values of the covariance matrix.
- 5) Choosing components and forming a feature vector.
- 6) Deriving the new data set.

7. Conclusion

Automated classification and detection of tumors in different medical images is motivated by the necessity of high accuracy when dealing with a human life. Computer assistance is demanded in all medical applications as it will definitely improve the results of humans. The use of PCA to reduce the dimensionality of the data and the use of PNN for tumor classification will improve the speed and accuracy of the result.

8. Acknowledgment

The authors are thankful to all the staff members of Electronics and Telecommunication Dept. and Information Technology Dept, DYPCET, Shivaji University, Kolhapur, Maharashtra, India for their valuable support and continuous motivation.

9. References.

- [1] Qeethara Kadhim Al-Shayea, “Artificial Neural Networks in Medical Diagnosis” International Journal of Computer Science Issues, Vol 8, Issue 2, March 2011.
- [2] N. Kwak, and C. H. Choi, “Input Feature Selection for Classification Problems”, IEEE Transactions on Neural Networks, Vol.13, Issue 1, 143–159, 2002.
- [3] E. D. Ubeyli and I. Guler, “Feature Extraction from Doppler Ultrasound Signals for Automated Diagnostic Systems”, Computers in Biology and Medicine, Vol 35, Issue 9, 735–764, 2005.
- [4] D.F. Specht, “Probabilistic Neural Networks for Classification, mapping, or associative memory”, Proceedings of IEEE International Conference on Neural Networks, Vol.1, IEEE Press, New York, pp. 525-532, June 1988.
- [5] A. Blake and M. Isard. Active Contours. Springer, 1998.
- [6] T.Logeswari , and M. Kaman, “An improved implementation of brain tumor detection using segmentation based on soft computing”, Journal of Cancer Research and Experimental Oncology Vol 2, Issue 1.
- [7] Georgiadis. Et all , “ Improving brain tumor characterization on MRI by probabilistic neural networks and non linear transformation of textural features”, Computer Methods and program in bio medicine, vol 89, pp24-32, 2008
- [7] Mohd. Fauzi Othman and Mohd. Ariffanan Mohd. Basti, “Probabilistic Neural Network For Brain Tumor Classification”, Second International Conference on Intelligent Systems, modeling and simulation.

A New Analytical Method for the Sizing and Siting of DG in Radial System to Minimize Real Power Losses

¹Dr. A.Lakshmi Devi, ²A.Chaithanya

^{1,2}Department of EEE, S.V. University, Tirupati – 517 502

Abstract

To minimize line losses of power systems, it is crucially important to define the size and location of local generation to be placed. On account of some inherent features of distribution systems, such as radial structure, large number of nodes, a wide range of X/R ratios; the conventional techniques developed for the transmission systems generally fail on the determination of optimum size and location of distributed generations. In this study, a loss sensitivity factor, based on the equivalent current injection, is formulated for the distribution systems. The formulated sensitivity factor is employed for the determination of the optimum size and location of distributed generation so as to minimize total power losses by an analytical method without use of admittance matrix, inverse of admittance matrix or Jacobian matrix. The proposed method is in close agreement with the classical grid search algorithm based on successive load flows.

Keywords: Distributed generation, Equivalent current injection, Loss sensitivity factor, Optimum location, Optimal size, Radial system, Power losses.

1. Introduction:

One of the most important motivation for the studies on the integration of distributed resources to the grid is the exploitation of the renewable resources such as; hydro, wind, solar, geothermal, biomass and ocean energy, which are naturally scattered around the country and also are smaller in size. Accordingly, these resources can only be tapped through integration to the distribution system by means of distributed generation. Although there is no consensus on the exact definition of distributed generation (DG), there are some significant attempts, in the literature [1, 2], to define the concept. Meanwhile DG, which generally consists of various types of renewable resources, can best be defined as electric power generation within distribution networks or on the customer side of the system [1, 2], in general. This definition is preferred along this paper. DG affects the flow of power and voltage conditions on the system equipment. These impacts may manifest themselves either positively or negatively depending on the distribution system operating conditions and the DG characteristics. Positive impacts are generally called 'system support benefits', and include voltage support, loss reduction, transmission and distribution capacity release, improved utility system reliability and power quality. On account of achieving above benefits, the DG must be reliable, dispatch able, of the proper size and at the proper locations [3,4]. Energy cost of renewable-based distributed generation when compared to the conventional generating plants is generally high because the factors of social and environmental benefits could not be included in the cost account. Accordingly, most of the studies to determine the optimum location and size of DG could not consider the generation cost, directly. Although one of the most important benefits of DG is reduction on the line losses, it is crucially important to determine the size and the location of local generation to be placed. For the minimization of system losses, there have been number of studies to define the optimum location of DG. The various approaches on the optimum DG placement for minimum power losses can be listed as the classical approach: second-order algorithm method [5], the meta-heuristics approaches [6, 8] : genetic algorithm and Hereford Ranch algorithm [6], fuzzy-GA method [7], tabu search [8], and the analytical approaches [9,13]. In the analytical studies [9,11], optimal place of the DGs are determined exclusively for the various distributed load profiles such as; uniformly, increasingly, centrally in radial systems to minimize the total losses. Additionally, in [12], optimal size and place of DG is obtained and analyzed by considering the effects of static load models. These analytical studies are generally based on phasor current injection method which has unrealistic assumptions such as; uniformly, increasingly, centrally distributed load profiles. These assumptions may cause erroneous solution for the real systems. In [13] the optimal size and location of DG is calculated based on exact loss formula and compared with successive load flows and loss sensitivity methods. The method is computationally less demanding for radial and networked systems, however, it requires the calculation of the bus impedance matrix, Z_{bus} , the inverse of the bus admittance matrix, Y_{bus} . It should be noted that due to the size, complexity and specific characteristics of distribution networks, the method could not be directly applied to distribution systems. It fails to meet the requirements in robustness aspects in the distribution system environments [14]. It is already pointed out that although the heuristic methods are

intuitive, easy to understand and simple to implement as compared to analytical and numerical programming methods, the results produced by heuristic algorithms are not guaranteed to be optimal [15].

In this study, the optimum size and location of distributed generation will be defined so as to minimize total power losses by an analytical method based on the equivalent current injection technique and without the use of impedance or Jacobian matrices for radial systems. The optimum size of DG and placement for loss minimization are determined by the proposed method and validated using the 34 bus radial distribution system these results are close related to the classical grid search algorithm. The proposed method is easy to be implemented, faster and more accurate than the classical method, meta-heuristic methods and early analytical methods. It is more suitable for radial systems of considerable sizes than the analytical method proposed earlier of Nareshacharya's paper. Since the proposed method is an analytical method and exploits the topological characteristics of a distribution system, there is no need for the Jacobian matrix, the bus admittance matrix, Y_{bus} , or the bus impedance matrix, Z_{bus} . Therefore the proposed method can achieve the advantages of computation time reduction and, accuracy improvement. The derived sensitivity factor ($\partial P_{loss}/\partial P$) can be also used for various purposes such as; network planning, network reconfiguration, optimal power flow and reactive power dispatch, etc.

2. Optimum Size And Location Of DG:

The proposed method is based on the equivalent current injection that uses the bus-injection to branch-current (BIBC) and branch-current to bus-voltage (BCBV) matrices which were developed based on the topological structure of the distribution systems and is widely implemented for the load flow analysis of the distribution systems. The details of both matrices can be found in [16]. The method proposed here requires only one base case load flow to determine the optimum size and location of DG.

2.1. Theoretical analysis

In this section, the total power losses will be formulated as a function of the power injections based on the equivalent current injection. The formulation of total power losses will be used for determining the optimum size of DG and calculation of the system losses.

At each bus k , the corresponding equivalent current injection is specified by

$$I_k = \left(\frac{P_k + jQ_k}{V_k} \right)^* \quad k = 1, 2, 3, \dots, n \quad (1)$$

where V_k is the node voltage, $P_k + jQ_k$ is the complex power at each bus k , n is the total number of buses, '*' symbolizes the complex conjugate of operator

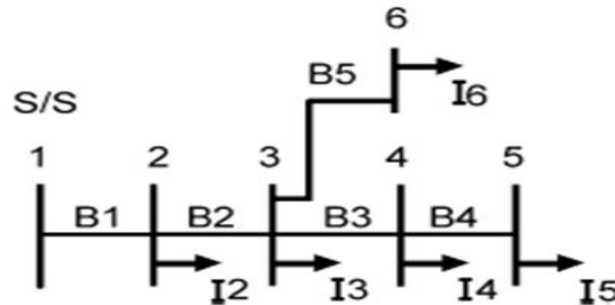


Fig.1. A Simple Distribution System

The equivalent current injection of bus k can be separated into real and imaginary parts by (2):

$$re(I_k) = \frac{P_k \cos(\theta_k) + Q_k \sin(\theta_k)}{|V_k|}, \quad im(I_k) = \frac{P_k \sin(\theta_k) - Q_k \cos(\theta_k)}{|V_k|} \quad (2)$$

where θ_k is the angle of k th node voltage. The branch current B is calculated with the help of BIBC matrix. The BIBC matrix is the result of the relationship between the bus current injections and branch currents. The elements of BIBC matrix consist of '0's or '1's:

$$[B]_{nb \times 1} = [BIBC]_{nb \times (n-1)} \cdot [I]_{(n-1) \times 1} \quad (3)$$

Where nb is the number of the branch, $[I]$ is the vector of the equivalent current injection for each bus except the reference bus. Branch currents of a simple distribution system given in Fig 1 are obtained by BIBC matrix as in (4). While the rows

of *BIBC* matrix concern with the branches of the network, on the other hand, the columns of the matrix are related with the bus current injection except the reference bus. Detailed description of *BIBC* matrix's building algorithm can be found in [16].

$$\begin{bmatrix} B_1 \\ B_2 \\ B_3 \\ B_4 \\ B_5 \end{bmatrix} = \begin{bmatrix} 1 & 1 & 1 & 1 & 1 \\ 0 & 1 & 1 & 1 & 1 \\ 0 & 0 & 1 & 1 & 0 \\ 0 & 0 & 0 & 1 & 0 \\ 0 & 0 & 0 & 0 & 1 \end{bmatrix} \begin{bmatrix} I_2 \\ I_3 \\ I_4 \\ I_5 \\ I_6 \end{bmatrix} \quad (4)$$

The total power losses can be expressed as a function of the bus current injections:

$$p_{loss} = \sum_{k=1}^{nb} |B_k|^2 \cdot R_k = [R]^T |[BIBC] \cdot [I]|^2 \quad (5)$$

where R_k is the k th branch resistance and the branch resistance vector is given in (6):

$$[R]_{nb \times 1} = [R_1 \ R_2 \ R_3 \ R_4 \ R_5 \ R_6 \ R_7 \ R_8 \ R_9 \dots \dots \dots R_{nb}]^T \quad (6)$$

The total power losses can be written as a function of the real and imaginary parts of the bus current injection:

$$P_{loss} = [R]^T |[BIBC] \cdot [I]|^2 = [R]^T |[BIBC] \cdot [re(I)] + j[BIBC] \cdot [im(I)]|^2 \quad (7)$$

where $[re(I)]$ and $[im(I)]$ are the vectors that consist of real and imaginary parts of the bus current injection:

$$p_{loss} = [R]^T (([BIBC] \cdot [re(I)])^2 + ([BIBC] \cdot [im(I)])^2) \quad (8)$$

By substituting the equivalent bus injection expression(2) into (8), the total power losses can be rewritten

$$p_{loss} = [R]^T \left([BIBC] \cdot \left[\frac{P \cos(\theta) + Q \sin(\theta)}{|V|} \right] \right)^2 + [R]^T \left([BIBC] \cdot \left[\frac{P \sin(\theta) - Q \cos(\theta)}{|V|} \right] \right)^2 \quad (9)$$

at l th branch the power loss can be obtained as

$$p_{loss_j} = R_j \cdot \left[\left(\sum_{k=2}^n BIBC(j, k-1) \frac{P_k \cos(\theta_k) + Q_k \sin(\theta_k)}{|V_k|} \right)^2 + \left(\sum_{k=2}^n BIBC(j, k-1) \frac{P_k \sin(\theta_k) - Q_k \cos(\theta_k)}{|V_k|} \right)^2 \right] \quad (10)$$

The total power losses are the sum of the each branch power losses:

$$p_{loss} = \sum_{l=1}^{nb} R_l \left[\left(\sum_{k=2}^n BIBC(j, m-1) \frac{P_m \cos(\theta_m) + Q_m \sin(\theta_m)}{|V_m|} \right)^2 + \left(\sum_{m=2}^n BIBC(j, m-1) \frac{P_m \sin(\theta_m) - Q_m \cos(\theta_m)}{|V_m|} \right)^2 \right] \quad (11)$$

The voltage drop from each bus to the reference bus is obtained with *BCBV* and *BIBC* matrices as

$$[\Delta V]_{(n-1) \times 1} = [BCBV] \cdot [BIBC] \cdot [I] \quad (12)$$

where *BCBV* matrix is responsible for the relations between branch currents and bus voltages. The elements of *BCBV* matrix consist of the branch impedances. Building algorithm of *BCBV* matrix can be found in [16]. In addition, building algorithm of *BCBV* matrix is provided as follows for convenience

- Step 1. Read *BIBC* matrix, Z_b branch impedance vector
- Step 2. Convert Z_b vector to a diagonal matrix Z by setting off diagonal elements to zero; ($Z = \text{diag}(Z_b)$).
- Step 3. Multiply transpose of *BIBC* matrix with Z matrix; ($BCBV = BIBC^T Z$).

The voltage drop of a simple distribution system given in Fig.1 is obtained as

$$[\Delta V] = [BCBV] \cdot [BIBC] \cdot [I]$$

$$\begin{bmatrix} V_1 \\ V_2 \\ V_3 \\ V_4 \\ V_5 \end{bmatrix} - \begin{bmatrix} V_2 \\ V_3 \\ V_4 \\ V_5 \\ V_{\partial 6} \end{bmatrix} = \begin{bmatrix} Z_{12} & 0 & 0 & 0 & 0 \\ Z_{12} & Z_{23} & 0 & 0 & 0 \\ Z_{12} & Z_{23} & Z_{34} & 0 & 0 \\ Z_{12} & Z_{23} & Z_{34} & Z_{45} & 0 \\ Z_{12} & Z_{23} & 0 & 0 & Z_{36} \end{bmatrix} \begin{bmatrix} 1 & 1 & 1 & 1 & 1 \\ 0 & 1 & 1 & 1 & 1 \\ 0 & 0 & 1 & 1 & 0 \\ 0 & 0 & 0 & 1 & 0 \\ 0 & 0 & 0 & 0 & 1 \end{bmatrix} \begin{bmatrix} I_2 \\ I_3 \\ I_4 \\ I_5 \\ I_6 \end{bmatrix} \quad (13)$$

2.2. The loss sensitivity factor

The derivation of the j th branch power loss per i th bus injected real power $\partial P_{loss}/\partial P_k$ can be obtained from (10) as

$$\frac{\partial p_{loss}}{\partial P_i} = 2R_l \left(\sum_{m=2}^{nb} BIBC(l, m-1) \cdot \frac{P_m \cos(\theta_m) + Q_m \sin(\theta_m)}{|V_m|} \right) \cdot XBIBC(l, k-1) \cdot \frac{\cos(\theta_k)}{|V_k|} + 2R_l \left(\sum_{m=2}^{nb} BIBC(l, m-1) \cdot \frac{P_m \sin(\theta_m) - Q_m \cos(\theta_m)}{|V_m|} \right) \cdot XBIBC(l, k-1) \cdot \frac{\sin(\theta_k)}{|V_k|} \quad (14)$$

Sum of the above expression leads to the derivation of the total power losses per k th bus injected real power, $\partial P_{loss}/\partial P_k$:

$$\frac{\partial p_{loss}}{\partial P_k} = 2 \sum_{l=1}^{nb} R_l \left(\sum_{m=2}^{nb} BIBC(l, m-1) \cdot re(I_m) \right) \cdot XBIBC(l, k-1) \cdot \frac{\cos(\theta_k)}{|V_k|} + 2 \sum_{l=1}^{nb} R_l \left(\sum_{m=2}^{nb} BIBC(l, m-1) \cdot im(I_m) \right) \cdot XBIBC(l, k-1) \cdot \frac{\sin(\theta_k)}{|V_k|} \quad (15)$$

If the i th bus is not connected the j th branch then the elements of $BIBC$ matrix is zero ($BIBC(j, i-1) = 0$) and the derivative of the corresponding element is equated to zero ($\partial P_{loss}/\partial P_i = 0$). Accordingly, the derivative of the total power losses per i th bus injected real power gives the sensitivity factor and can be expressed as

$$\frac{\partial p_{loss}}{\partial P_k} = 2 \sum_{l=1}^{nb} R_l \sum_{m=2}^n dPBIBC_k(l, m-1) \cdot \left[\frac{\cos(\theta_k)}{|V_k|} \cdot re(I_m) + \frac{\sin(\theta_k)}{|V_k|} \cdot im(I_m) \right] \quad (16)$$

The sensitivity factor with the above relation can be shown in matrix form as

$$\frac{\partial p_{loss}}{\partial P_k} = 2[R]^T \left[[dPBIBC_k] \cdot [re(I)] \cdot \frac{\cos(\theta_k)}{|V_k|} \right] + \left[[dPBIBC_k] \cdot [im(I)] \cdot \frac{\sin(\theta_k)}{|V_k|} \right] \quad (17)$$

where $[dPBIBC_i]$ matrix is constructed by a simple algorithm given step by step as follows:

- Step 1. Read BIBC matrix, i bus number for DG.
- Step 2. Set dBIBCI matrix, $dBIBCI = BIBC$.
- Step 3. Find the row with zero elements for the $(i-1)$ th column of dBIBCI matrix; ($zerorow = \text{find}(dBIBCI(:, i-1) = 0)$).
- Step 4. Convert all non zero elements of these zero; ($dBIBCI(zerorow, :) = \text{zeros}(\text{length}(zerorow), n-1)$).

To better explain $[dPBIBC_i]$ matrix building algorithm, $[dPBIBC_4]$ matrix which belongs to the sensitivity factor of the 4th bus, $\partial P_{loss}/\partial P_4$, is given in (18) for the distribution system in Fig 1.

$$dBIBC_4 = \begin{bmatrix} 1 & 1 & 1 & 1 & 1 \\ 0 & 1 & 1 & 1 & 1 \\ 0 & 0 & 1 & 1 & 0 \\ 0 & 0 & 0 & 0 & 0 \\ 0 & 0 & 0 & 0 & 0 \end{bmatrix} \quad (18)$$

2.3. Determination of optimal size:

The goal is to determine the optimum size of DG at any location so as to minimize total power losses. To determine the optimum size of DG, the derivative of the total power losses per each bus injected real powers are equated to zero as

$$\frac{\partial P_{loss}}{\partial p_k} = 0 \quad (19)$$

The expression of (16) can be shown in detail as

$$\frac{\partial P_{loss}}{\partial P_i} = 2 \sum_{j=1}^{nb} R_j \sum_{k=2}^n dPBIBC_i(j, k-1) \cdot X \left[\frac{\cos(\theta_k)}{|V_k|} \cdot re(I_k) + \frac{\sin(\theta_k)}{|V_k|} \cdot im(I_k) \right] + 2 \sum_{j=1}^{nb} R_j dPBIBC_i(j, i-1) \cdot X \left[\frac{P_i \cos^2(\theta_i) + Q_i \sin(\theta_i) \cos(\theta_i) + P_i \sin^2(\theta_i) - Q_i \cos(\theta_i) \sin(\theta_i)}{|V_i|^2} \right] \quad (20)$$

The optimal size of the added DG is extracted from (20) by equating the right hand side to zero:

$$\frac{\partial P_{loss}}{\partial P_k} = 2 \sum_{l=1}^{nb} R_l \sum_{m=2}^n dPBIBC_k(l, m-1) \cdot X \left[\frac{\cos(\theta_k)}{|V_k|} \cdot re(I_m) + \frac{\sin(\theta_k)}{|V_k|} \cdot im(I_m) \right] + 2 \sum_{l=1}^{nb} R_l dPBIBC_k(l, k-1) \cdot \frac{P_k}{|V_k|^2} = 0 \quad (21)$$

The real power injection at the bus k , P_i is extracted from as (21)

$$P_i = - \frac{|V_i| \sum_{j=1}^{nb} R_j \sum_{\substack{k=2 \\ k \neq i}}^n dPBIBC_i(j, k-1) [\cos(\theta_k) \cdot re(I_k) + \sin(\theta_k) \cdot im(I_k)]}{\sum_{j=1}^{nb} R_j dPBIBC_i(j, i-1)} \quad (22)$$

The minus sign in (22) indicates that P_k should be injected to the system. To facilitate a practical computation, can be written in matrix format by omitting the minus sign as

$$P_k = \frac{|V_k| [R]^T [dPBIBC_k] (\cos(\theta_k) [redI_k] + \sin(\theta_k) [imdI_k])}{[R]^T dPBIBC_k(:, k-1)} \quad (23)$$

where two new terms, $[redI_k]$ and $[imdI_k]$, are constructed by equating i th elements the real and imaginary part of the bus current injection vector, $[re(I)]$ and $[im(I)]$ to zero. To illustrate the concept $[redI_4]$ and $[imdI_4]$ vectors that belong to the 4th bus real power injection of the simple distribution system in Fig.1, are provided in (24):

$$[redI_4] = [re(I_2) \quad re(I_3) \quad 0 \quad re(I_5) \quad re(I_6)]^T, \quad (24)$$

$$[imdI_4] = [im(I_2) \quad im(I_3) \quad 0 \quad im(I_5) \quad im(I_6)]^T$$

The optimum size of added DG at bus i can be obtained by

$$P_{dg_k} = P_k + pload_k \quad (25)$$

2.4. Determination of optimal size and placement for DG

The objective is to minimize power losses, P_{loss} , in the system by injected power, P_{dg} . The main constraints are to restrain the [voltage along the radial system within 1 ± 0.05 pu. The proposed method to determine the optimal size and placement of DG is give step by step as follows and also as a general flowchart in Fig.2.

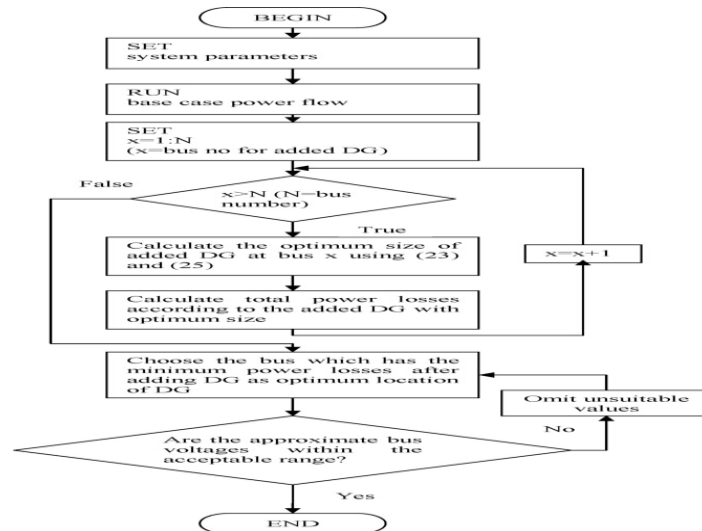


Fig. 2. General flowchart of the proposed method.

- Step 1. Run the base case power flow.
- Step 2. Find the optimum size of added DG for each bus except the reference bus using (23) and (25).
- Step 3. Calculate total power losses from(5) for each bus by placing optimum size of power to the bus.
- Step 4. Choose the bus which has the minimum power losses after adding DG as optimum location.
- Step 5. Check whether the approximate bus voltages are within the acceptable range by (12).
- Step 6. If the bus voltages are not within the acceptable range then omit DG from bus and return to Step 4.

3. The Results Of Simulations And Analysis

In order to evaluate the proposed algorithm described in Section2, 34 bus test system, taken from the literature, are used. Accordingly, optimum size and place of DG for the 34 bus distribution test system [17] are determined with the proposed method. The classical grid search algorithm is too costly because of computation time, that takes hours even days depending upon size of the system and power steps. By using variable step size, successive load flows as also known sequential load flows could be employed instead of grid search algorithm. In this case, computation time will reduce significantly.

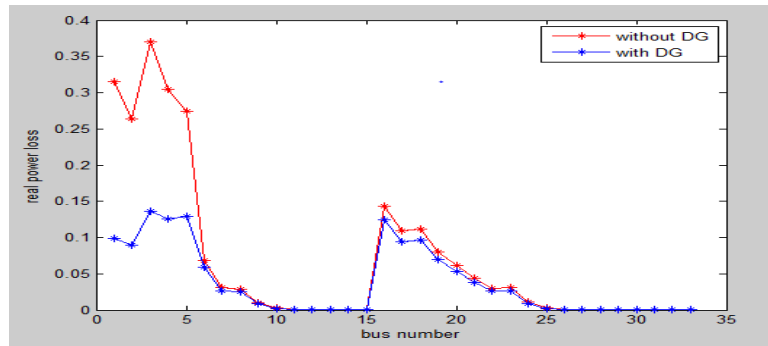


Fig 3:Variation of power loss with and without DG

The above graph in Fig 3 represents the power loss without Distribution generation(DG) & with Distributed generation(DG),In without DG the real power loss is 229.76 and after inclusion of DG real power loss is reduced to 108.6, usage of BIBC & BCBV algorithm for load flow solution and for the location of Distribution generation The loss sensitivity factor is employed & sizing is employed with the Analytical method The below graph in Fig 4 represents the Voltage variation of without Ditrubted generation & with Distributed generation. Voltage profile is improved for with installation Distributed generation.

Bus number	Reakpower (Without DG)	Realpower (With DG)	%Loss reduction
34	229.76	108.6	52.7

Table 1: Result of 34 Bus Test System

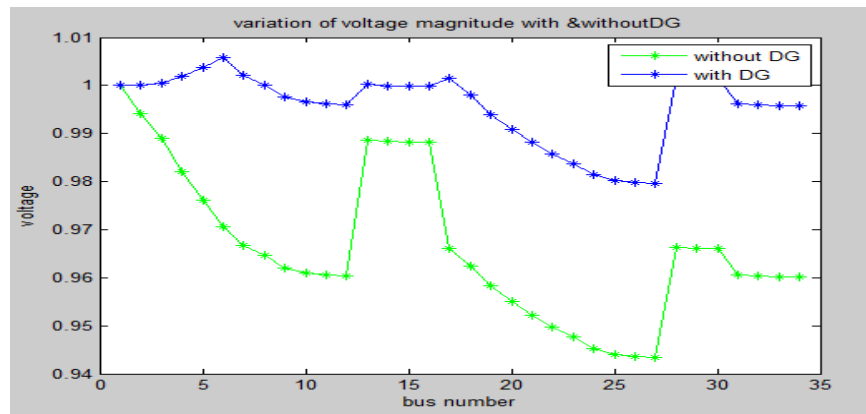


Fig 4:Variation of Voltage with and without DG

4. Conclusion

This study presents and evaluates an analytical method which can be used to determine the optimal placement and sizing of DG without use of admittance, impedance or Jacobian matrix with only one power flow for radial systems. The method is easy to be implemented and faster for given accuracy. The derived sensitivity factor is more suitable for distribution systems and could be utilized by means of simple matrix algebra. The optimal size and location of the DG, which is determined by the method, is also evaluated against Acharya's method and the classical grid search algorithm. It is found that the proposed method is in close agreement with Acharya's method and the grid search algorithm. It is appeared that the proposed method is faster than other methods in the computation time and it is appropriate for the distribution systems.

References

- [1] T. Ackermann, G. Anderson, L. Söder, Distributed generation: a definition, *Electr. Power Syst. Res.* 57 (2001) 195–204.
- [2] G. Pepermans, J. Driesen, D. Haeseldonckx, R. Belmans, W. D'haeseleer, Distributed generation: definition, benefits and issues, *Energy Policy* 33 (2005) 787–798.
- [3] P.P. Barker, R.W. de Mello, Determining the impact of distributed generation on power systems. Part 1. Radial distribution systems, in: *IEEE PES Summer Meeting*, vol. 3, 2000, pp. 1645–1656.
- [4] N. Hadjsaid, J.F. Canard, F. Dumas, Dispersed generation impact on distribution networks, *IEEE Comput. Appl. Power* 12 (April) (1999) 22–28.
- [5] S. Rau, Y.H. Wan, Optimum location of resources in distributed planning, *IEEE Trans. Power Syst.* 9 (November) (1994) 2014–2020.
- [6] K.H. Kim, Y.J. Lee, S.B. Rhee, S.K. Lee, S.-K. You, Dispersed generator placement using fuzzy-GA in distribution systems, in: *IEEE PES Summer Meeting*, vol. 3, July, 2002, pp. 1148–1153.
- [7] J.O. Kim, S.W. Nam, S.K. Park, C. Singh, Dispersed generation planning using improved Hereford Ranch algorithm, *Electr. Power Syst. Res.* 47 (October(1)) (1998) 47–55.
- [8] K. Nara, Y. Hayashi, K. Ikeda, T. Ashizawa, Application of tabu search to optimal placement of distributed generators, in: *IEEE PES Winter Meeting*, vol. 2, 2001, pp. 918–923.
- [9] H.L. Willis, Analytical methods and rules of thumb for modelling DG distribution interaction, in: *IEEE PES Summer Meeting*, vol. 3, Seattle, WA, July, 2000, pp. 1643–1644.
- [10] T. Griffin, K. Tomsovic, D. Secrest, A. Law, Placement of dispersed generation systems for reduced losses, in: *33rd Annual Hawaii International Conference on Systems Sciences*, Maui, HI, 2000, pp. 1–9.
- [11] C. Wang, M.H. Nehrir, Analytical approaches for optimal placement of DG sources in power systems, *IEEE Trans. Power Syst.* 19 (November(4)) (2004) 2068–2076.
- [12] T. Gözel, M.H. Hocaoglu, U. Eminoglu, A. Balikci, Optimal placement and sizing of distributed generation on radial feeder with different static load models, in: *Future Power Systems, 2005 International Conference*, Amsterdam, November 16–18, 2005.
- [13] N. Acharya, P. Mahat, N. Mithulananthan, An analytical approach for DG allocation in primary distribution network, *Int. J. Electr. Power Energy Syst.* 28 (December(10)) (2006) 669–678.
- [14] J.-H. Teng, C.-Y. Chang, A network-topology-based capacitor control algorithm for distribution systems, *Transm. Distrib. Conf.* 2 (2002) 1158–1163.
- [15] H.N. Ng, M.M.A. Salama, A.Y. Chikhani, Classification of capacitor allocation techniques, *IEEE Trans. Power Deliv.* 15 (January) (2000) 387–392.
- [16] J.-H. Teng, A network-topology-based three-phase load flow for distribution systems, *Proc Natl. Sci. Council. ROC(A)* 24 (4) (2000) 259–264.
- [17] D. Das, H.S. Nagi, D.P. Kothari, Novel method for solving radial distribution networks, *IEE Proc. -Gener. Transm. Dist.* 141 (July(4)) (1994) 291–298.

Route to Chaos in an Area-preserving System

Dr. Nabajyoti Das

Assistant Professor, Department of Mathematics Jawaharlal Nehru College, Boko -781123
District: Kamrup, State: Assam, Country: India

Abstract:

This paper highlights two important objectives on a two-dimensional area-preserving discrete dynamical system:

$$E(x, y) = (-y + px - (1-p)x^2, x - y + px - (1-p)x^2),$$

where p is a tunable parameter. Firstly, by adopting suitable computer programs we evaluate period-doubling:

$$\text{period } 1 \rightarrow \text{period } 2 \rightarrow \text{period } 4 \rightarrow \dots \rightarrow \text{period } 2^k \rightarrow \dots \rightarrow \text{chaos}$$

bifurcations, as a universal route to chaos, for the periodic orbits when the system parameter p varied and obtain the Feigenbaum universal constant = 8.7210972..., and the accumulation point $\alpha = 7.533284771388\dots$ beyond which chaotic region occurs.. Secondly, the periodic behaviors of the system are confirmed by plotting the time series graphs.

Key Words: Period-doubling bifurcations/ Periodic orbits / Feigenbaum universal constant / Accumulation point / Chaos / Area-preserving system

2010 AMS Classification: 37 G 15, 37 G 35, 37 C 45

1. Introduction

The initial universality discovered by Mitchell J. Feigenbaum in 1975 has successfully led to discover that large classes of nonlinear systems exhibit transitions to chaos which are universal and quantitatively measurable. If X be a suitable function space and H , the hypersurface of co-dimension 1 that consists of the maps in X having derivative -1 at the fixed point, then the **Feigenbaum universality** is closely related to the doubling operator, F acting in X defined by

$$(F\psi)(x) = -\alpha\psi(\psi(\alpha^{-1}x)) \quad \psi \in X$$

where $\alpha = 2.5029078750957\dots$, a universal scaling factor. The principal properties of F that lead to universality are

- (i) F has a fixed point x^* ;
- (ii) The linearised transformation $DF(x^*)$ has only one eigenvalue δ greater than 1 in modulus; here $\delta = 4.6692016091029\dots$
- (iii) The unstable manifold corresponding to δ intersects the surface H transversally; In one dimensional case, these properties have been proved by Lanford [2, 10].

Next, let X be the space of two parameter family of area-preserving maps defined in a domain $U \subseteq \mathbb{R}^2$, and Y , the space of two parameter family of maps defined in the same domain having not necessarily constant Jacobian. Then Y contains X . In area-preserving case, the Doubling operator F is defined by

$$F\psi = \Sigma^{-1}\psi^2\Sigma,$$

where $\Sigma: \mathbb{R}^2 \rightarrow \mathbb{R}^2, \Sigma(x, y) = (\lambda x, \mu y)$ is the scaling transformation. Here λ and μ are the scaling factors; numerically we have $\lambda = -0.248875\dots$ and $\mu = 0.061101\dots$. In the area preserving case, Feigenbaum constant, $\delta = 8.721097200\dots$. Furthermore, one of his fascinating discoveries is that if a family ψ presents period doubling

bifurcations then there is an infinite sequence $\{\mu_n\}$ of bifurcation values such that $\alpha = \lim_{n \rightarrow \infty} \frac{\mu_n - \mu_{n-1}}{\mu_{n+1} - \mu_n} = \delta$, where

δ is a universal number already mentioned above. Moreover, his observation suggests that there is a universal size-

scaling in the period doubling sequence designated as the Feigenbaum α -value, $\alpha = \lim_{n \rightarrow \infty} \frac{d_n}{d_{n+1}} = 2.5029\dots$ where d_n

is the size of the bifurcation pattern of period 2^n just before it gives birth to period 2^{n+1} [1, 6-8].

The birth and flowering of the Feigenbaum universality with numerous non-linear models has motivated me to write this paper.

2. Our Nonlinear Map and the Feigenbaum Universality:

Our concerned map:

$$E(x, y) = (-y + px - (1-p)x^2, x - y + px - (1-p)x^2) \quad (1.1)$$

where p is a tunable parameter. The Jacobian of E is the unity, so is area-preserving.

The map has one fixed point other than $(0,0)$ whose coordinates is given by

$$x = \frac{3-p}{-1+p}, y = \frac{-6+2p}{1-p}$$

From this one finds that E has no fixed point if $p = 1$. In this context, we also wish to point out that the stability theory is intimately connected with the Jacobian matrix of the map, and that the trace of the Jacobian matrix is the sum of its eigenvalues and the product of the eigenvalues equal the Jacobian determinant. For a particular value of p , the map E depends on the real parameter p , and so a fixed point \bar{x}_s of this map depends on the parameter value p , i.e. $\bar{x}_s = \bar{x}_s(p)$. Now, first consider the set, $U = (-\infty, 3) \cup (7, +\infty)$.

The fixed point \bar{x}_s remains stable for all values of p lying in U and a stable periodic trajectory of period-one appears around it. This means, the two eigenvalues

$$\lambda_1 = \frac{-5 + \sqrt{-7+p} \sqrt{-3+p} (-1+p) + 6p - p^2}{2(-1+p)},$$

$$\lambda_2 = \frac{-5 - \sqrt{-7+p} \sqrt{-3+p} (-1+p) + 6p - p^2}{2(-1+p)}$$

of the Jacobian matrix:

$$J = \begin{bmatrix} p - 2(1-p)x & -1 \\ 1 + p - 2(1-p)x & -1 \end{bmatrix}$$

at \bar{x}_s remains less than one in modulus and consequently, all the neighbouring points (that is, points in the domain of attraction) are attracted towards $\bar{x}_s(p)$, p lying in U . If we now begin to increase the value of p , then it happens that one of the eigenvalues starts decreasing through -1 and the other remains less than one in modulus. When $p = 7$, one of the eigenvalues becomes -1 and then \bar{x}_s loses its stability, i.e. $p_1 = 7$ emerging as **the first bifurcation value** of p . Again, if we keep on increasing the value of p the point $\bar{x}_s(p)$ becomes unstable and there arises around it two points, say, $\bar{x}_{21}(p)$ and $\bar{x}_{22}(p)$ forming a stable periodic trajectory of period-two. All the neighbouring points except the stable manifold of $\bar{x}_s(p)$ are attracted towards these two points. Since the period emerged becomes double, the previous eigenvalue which was -1 becomes $+1$ and as we keep increasing p , one of the eigenvalues starts decreasing from $+1$ to -1 . Since the trace is always real, when eigenvalues are complex, they are conjugate to each other moving along the circle of radius $\sqrt{p_e}$, where $p_e = p^{2^n}$ is the effective Jacobian, in the opposite directions. When we reach a certain value of p , we find that one of the eigenvalues of the Jacobian of E^2 (because of the chain rule of differentiation, it does not matter at which periodic point one evaluates the eigenvalues) becomes -1 , indicating the loss of stability of the periodic trajectory of period 2. Thus, the second bifurcation takes place at this value p_2 of p . We can then repeat the same arguments, and find that the periodic trajectory of period 2 becomes unstable and a periodic trajectory of period 4 appears in its neighbourhood. This phenomenon continues upto a particular value of p say $p_3(p)$, at which the periodic trajectory of period 4 loses its stability in such a way that one of the eigenvalues at any of its periodic points become -1 , and thus it gives the third bifurcation at $p_3(p)$. Increasing the value further and further, and repeating the same arguments we obtain a sequence $\{p_n(p)\}$ as bifurcation values for the parameter p such that at $p_n(p)$ a periodic trajectory of period 2^n arises and all periodic trajectories of period 2^m ($m < n$) remain unstable. The sequence $\{p_n(p)\}$ behaves in a universal manner such that $p_{\infty}(p) - p_n(p) \sim c(p)\delta^n$, where $c(p)$ is independent of n and δ and is the **Feigenbaum universal constant**. Since the map has constant Jacobian 1 (unity), we have the conservative case, i.e. the preservation of area and in this case δ equals 8.721097200.... Furthermore, the Feigenbaum theory says that the our map E at parameter $= p_{\infty}(p)$

has an invariant set S of Cantor type encompassed by infinitely many unstable periodic orbits of period 2^n ($n = 0, 1, 2, \dots$), and that all the neighbouring points except those belonging to these unstable orbits and their stable manifolds are attracted to S under the iterations of the map E .

3. Numerical Method For Obtaining Periodic Points [2]:

Although there are so many sophisticated numerical algorithms available, to find a periodic fixed point, we have found that the Newton Recurrence formula is one of the best numerical methods with negligible error for our purpose. Moreover, it gives fast convergence of a periodic fixed point.

The Newton Recurrence formula is

$$\bar{x}_{n+1} = \bar{x}_n - Df(\bar{x}_n)^{-1} f(\bar{x}_n),$$

where $n = 0, 1, 2, \dots$ and $Df(\bar{x})$ is the Jacobian of the map f at the vector \bar{x} . We see that this map f is equal to $E^k - I$ in our case, where k is the appropriate period. The Newton formula actually gives the zero(s) of a map, and to apply this numerical tool in our map one needs a number of recurrence formulae which are given below.

Let the initial point be (x_0, y_0) ,

Then,

$$E(x_0, y_0) = (-y_0 + px_0 - (1-p)x_0^2, x_0 - y_0 + px_0 - (1-p)x_0^2) = (x_1, y_1)$$

$$E^2(x_0, y_0) = E(x_1, y_1) = (x_2, y_2)$$

Proceeding in this manner the following recurrence formula for our map can be established.

$x_n = -y_{n-1} + px_{n-1} - (1-p)x_{n-1}^2$, and $y_n = -y_{n-1} + px_{n-1} - (1-p)x_{n-1}^2$,
where $n = 1, 2, 3, \dots$

Since the Jacobian of E^k (k times iteration of the map E) is the product of the Jacobian of each iteration of the map, we proceed as follows to describe our recurrence mechanism for the Jacobian matrix.

The Jacobian J_1 for the transformation

$E(x_0, y_0) = (-y_0 + px_0 - (1-p)x_0^2, x_0 - y_0 + px_0 - (1-p)x_0^2)$ is

$$J_1 = \begin{pmatrix} p - 2(1-p)x_0 & -1 \\ 1 + p - 2(1-p)x_0 & -1 \end{pmatrix} = \begin{pmatrix} A_1 & B_1 \\ C_1 & D_1 \end{pmatrix}$$

where $A_1 = p - 2(1-p)x_0$, $B_1 = -1$, $C_1 = 1 + p - 2(1-p)x_0$, $D_1 = -1$.

Next the Jacobian J_2 for the transformation

$E^2(x_0, y_0) = (x_2, y_2)$, is the product of the Jacobians for the transformations

$E(x_1, y_1) = (-y_1 + px_1 - (1-p)x_1^2, x_1 - y_1 + px_1 - (1-p)x_1^2)$ and

$E(x_0, y_0) = (-y_0 + px_0 - (1-p)x_0^2, x_0 - y_0 + px_0 - (1-p)x_0^2)$.

So, we obtain

$$J_2 = \begin{pmatrix} p - 2(1-p)x_1 & -1 \\ 1 + p - 2(1-p)x_1 & -1 \end{pmatrix} \begin{pmatrix} A_1 & B_1 \\ C_1 & D_1 \end{pmatrix} = \begin{pmatrix} A_2 & B_2 \\ C_2 & D_2 \end{pmatrix},$$

where $A_2 = [p - 2(1-p)x_1]A_1 - C_1$, $B_2 = [p - 2(1-p)x_1]B_1 - D_1$,

$C_2 = [1 + p - 2(1-p)x_1]A_1 - C_1$, $D_2 = [1 + p - 2(1-p)x_1]B_1 - D_1$.

Continuing this process in this way, we have the Jacobian for E^m as

$$J_m = \begin{pmatrix} A_m & B_m \\ C_m & D_m \end{pmatrix}$$

with a set of recursive formula as

$A_m = [p - 2(1-p)x_{m-1}]A_{m-1} - C_{m-1}$, $B_m = [p - 2(1-p)x_{m-1}]B_{m-1} - D_{m-1}$,

$C_m = [1 + p - 2(1-p)x_{m-1}]A_{m-1} - C_{m-1}$, $D_m = [1 + p - 2(1-p)x_{m-1}]B_{m-1} - D_{m-1}$,

($m = 2, 3, 4, 5, \dots$).

Since the fixed point of this map E is a zero of the map

$$G(x, y) = E(x, y) - (x, y),$$

the Jacobian of $G^{(k)}$ is given by

$$J_k - I = \begin{pmatrix} A_k - 1 & B_k \\ C_k & D_k - 1 \end{pmatrix}$$

$$\text{Its inverse is } (J_k - I)^{-1} = \frac{1}{\Delta} \begin{pmatrix} D_k - 1 & B_k \\ C_k & A_k - 1 \end{pmatrix},$$

where $\Delta = (A_k - 1)(D_k - 1) - B_k C_k$,

the Jacobian determinant. Therefore, Newton's method gives the following recurrence formula in order to yield a periodic point of E^k

$$x_{n+1} = x_n - \frac{(D_k - 1)(\hat{x}_n - x_n) - B_k(\hat{y}_n - y_n)}{\Delta}$$

$$y_{n+1} = y_n - \frac{(-C_k)(\hat{x}_n - x_n) + (A_k - 1)(\hat{y}_n - y_n)}{\Delta},$$

where $E^k(\bar{x}_n) = (\hat{x}_n, \hat{y}_n)$.

4. Numerical Methods For Finding Bifurcation Values [2, 4]:

First of all, we recall our recurrence relations for the Jacobian matrix of the map E^k described in the Newton's method and then the eigenvalue theory gives the relation $A_k + D_k = -1 + \text{Det}(J_k)$ at the bifurcation value. Again the Feigenbaum theory says that

$$p_{n+2} \approx p_{n+1} + \frac{p_{n-1} - p_n}{\delta} \tag{1.2}$$

where $n = 1, 2, 3, \dots$ and δ is the Feigenbaum universal constant.

In the case of our map, the first two bifurcation values p_1 and p_2 can be evaluated.

Furthermore, it is easy to find the periodic points for p_1 and p_2 . We note that if we put $I = A_k + D_k = -1 + \text{Det}(J_k)$, then I turns out to be a function of the parameter p . The bifurcation value of p of the period k occurs when $I(p)$ equals zero. This means, in order to find a bifurcation value of period k , one needs the zero of the function $I(p)$, which is given by the Secant method,

$$p_{n+1} = p_n - \frac{I(p_n)(p_n - p_{n-1})}{I(p_n) - I(p_{n-1})}.$$

Then using the relation (1.2), an approximate value p'_3 of p_3 is obtained. Since the Secant method needs two initial values, we use p'_3 and a slightly larger value, say, $p'_3 + 10^{-4}$ as the two initial values to apply this method and ultimately obtain p_3 . In like manner, the same procedure is employed to obtain the successive bifurcation values p_4, p_5, \dots etc. to our requirement.

For finding periodic points and bifurcation values for the map E , above numerical methods are used and consequently, the following **Period-Doubling Cascade**: Table 1.1, showing bifurcation points and corresponding periodic points, are obtained by using suitable computer programs:

Table 1.1

Period	One of the Periodic points	Bifurcation Pt.
1	(x=0.666666666666..., y= -1.333333333333...)	$p_1=7.0000000000$
2	(x= -0.500000000003..., y= -1.309016994376...)	$p_2=7.47213595500$
4	(x= -0.811061640408 ..., y= -1.273315586957...)	$p_3=7.525683372...$
8	(x=-0.813878975794 ..., y= -1.275108054848...)	$p_4=7.531826966...$
16	(x=-0.460474775277...,y= -1.273990103300...)	$p_5=7.532531327...$
32	(x=-0.46055735696 ..., y= -1.274198905689...)	$p_6=7.532612093...$
64	(x=-0.54742669886 ..., y= -1.356526357634...)	$p_7=7.532621354...$
128	(x=-0.547431479795 ..., y= -1.356530832564...)	$p_8=7.532636823...$
...

For the system (1.1), the values of δ are calculated as follows:

$$\delta_1 = \frac{p_2 - p_1}{p_3 - p_2} = 8.8171563807015\dots, \quad \delta_2 = \frac{p_3 - p_2}{p_4 - p_3} = 8.715976842041\dots,$$

$$\delta_3 = \frac{p_4 - p_3}{p_5 - p_4} = 8.722215813427\dots, \quad \delta_4 = \frac{p_5 - p_4}{p_6 - p_5} = 8.721026780948\dots,$$

and so on.

The ratios tend to a constant as k tends to infinity: more formally

$$\lim_{k \rightarrow \infty} \left[\frac{b_k - b_{k-1}}{b_{k+1} - b_k} \right] = \delta = 8.7210972\dots$$

And the above table confirms that the ‘universal’ Feigenbaum constant $\delta = 8.7210972\dots$

is also encountered in this area-preserving two-dimensional system.

The accumulation point p_∞ can be calculated by the formula

$$p_\infty = (p_2 - p_1) \frac{1}{\delta - 1} + p_2,$$

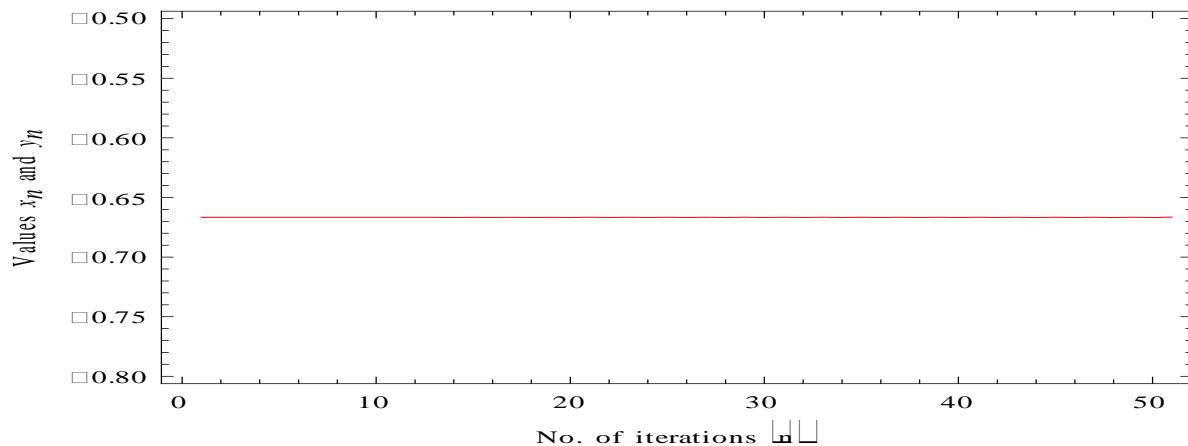
where δ is Feigenbaum constant, it is found to be **7.533284771388....** , beyond which the system (1.1) develops chaos.

5. Time Series Graphs [3]

The key theoretical tool used for quantifying chaotic behavior is the notion of a time series of data for the system [9]. A time series is a chronological sequence of observations on a particular variable. Usually the observations are taken at regular intervals. The system (1.1) giving the difference equations:

$$x_{n+1} = -y_n + px_n - (1-p)x_n^2, \quad y_{n+1} = x_n - y_n + px_n - (1-p)x_n^2, \quad n = 0,1,2,\dots \quad (1.3)$$

On the horizontal axis the number of iterations (‘time’) are marked, that on the vertical axis the amplitudes are given for each iteration. The system (1.3) exhibits the following discrete time series graphs for the values of x_n and y_n , plotted together, showing the existences of periodic orbits of periods 2^k , $k = 0, 1, 2, \dots$, at different parameter



values.

Fig. 1 Showing period-1 behavior, parameter = 1st bifurcation point

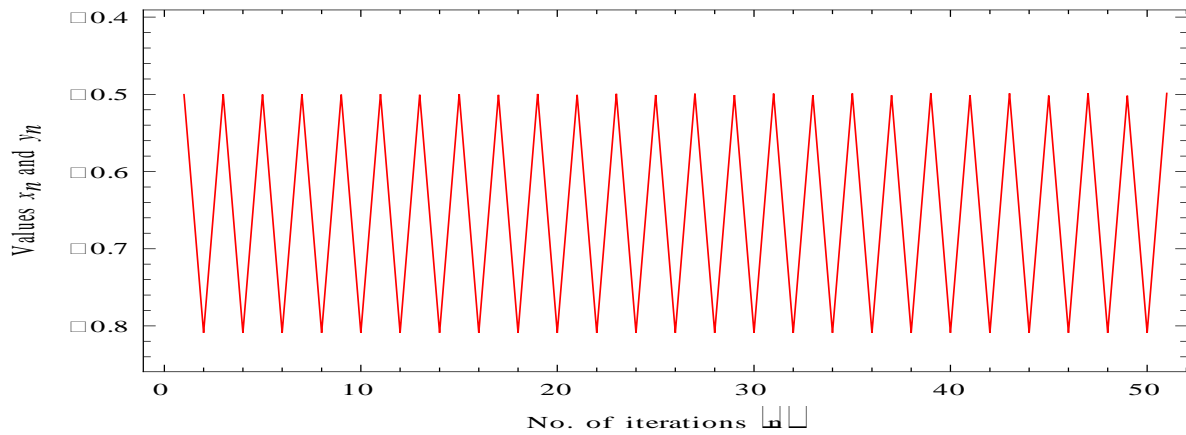


Fig. 1.2 Showing period-2 behavior, parameter = 2nd bifurcation point

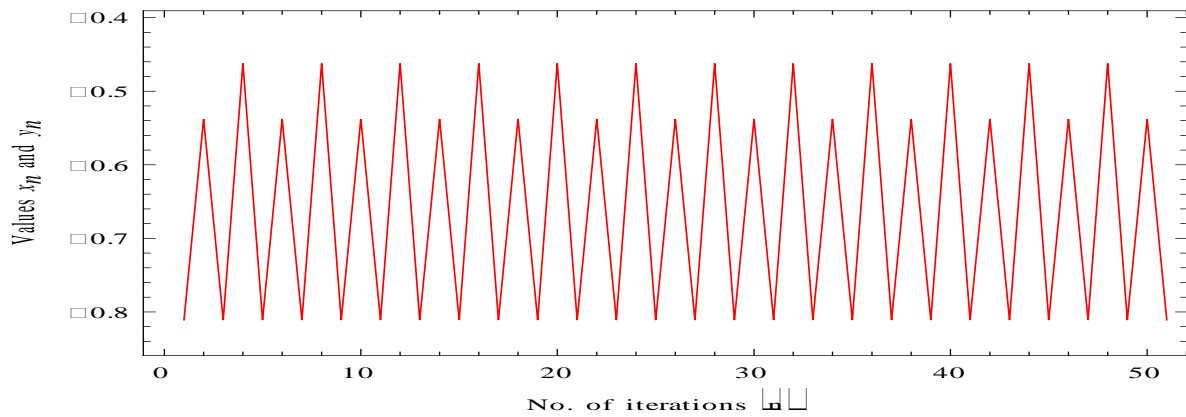


Fig. 1.3 Showing period-4 behavior, parameter = 3rd bifurcation point

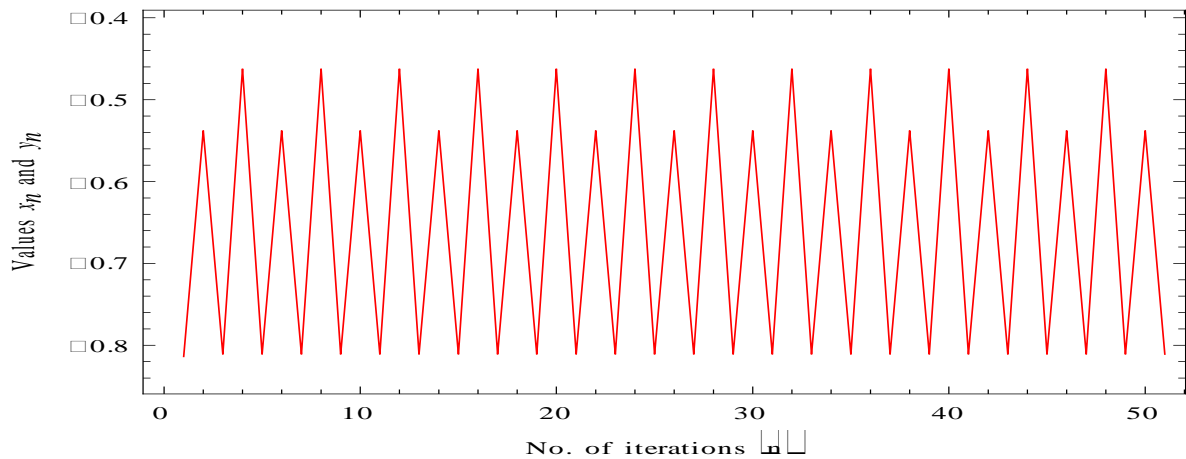


Fig. 1.4 Showing period-8 behavior, parameter = 4th bifurcation point

6. Acknowledgement:

I am grateful to **Dr. Tarini Kumar Dutta**, Senior Professor of the Department of Mathematics, Gauhati University, Assam: India, for a valuable suggestion for the improvement of this research paper.

7. References:

- [1] Deveney R.L. “ *An introduction to chaotic dynamical systems* ”, Addison-Wiseley Publishing Company,Inc
- [2] Davie A. M. and Dutta T. K., “*Period-doubling in Two-Parameter Families,*” *Physica D*, 64,345-354, (1993).
- [3] Das, N. and Dutta, N., “*Time series analysis and Lyapunov exponents for a fifth degree chaotic map*”, *Far East Journal of Dynamical Systems* Vol. 14, No. 2, pp 125- 140, 2010
- [4] Das, N., Sharmah, R. and Dutta, N., “*Period doubling bifurcation and associated universal properties in the Verhulst population model*”, *International J. of Math. Sci. & Engg. Appls.* , Vol. 4 No. I (March 2010), pp. 1 -14
- [5] Dutta T. K. and Das, N., “*Period Doubling Route to Chaos in a Two-Dimensional Discrete Map*”, *Global Journal of Dynamical Systems and Applications*, Vol.1, No. 1, pp 61 -72, 2001
- [6] Feigenbaum J M, “*Quantitative Universality For Nonlinear Transformations*” *Journal of Statistical Physics*, Vol. 19, No. 1,1978.
- [7] Chen G. and Dong X., *From Chaos to Order: Methodologies, Perspectives and Applications*, World Scientific, 1998
- [8] Peitgen H.O., Jurgens H. and Saupe D. , “ *Chaos and Fractal*”, *New Frontiers of Science*, Springer Verlag, 1992
- [9] Hilborn R. C “*Chaos and Nonlinear Dynamics*”,second edition, Oxford University Press, 1994
- [10] Lanford O.E. III, “A Computer-Assisted Proof of the Feigenbaum Conjectures,” *Bull.A m.Math.Soc.* 6, 427-34 (1982).

L^p – convergence of Rees-Stanojevic sum

Nawneet Hooda

Department of Mathematics,
DCR University of Sci& Tech, Murthal , Sonapat-131039 (INDIA)

Abstract

We study L^p -convergence ($0 < p < 1$) of Rees-Stanojevic modified cosine sum [3] and deduce the result of Ul'yanov [4] as corollary from our result.

1. Introduction

Let us consider the series

$$(1.1) \quad f(x) = \frac{a_0}{2} + \sum_{k=1}^{\infty} a_k \cos kx,$$

with coefficients $a_k \downarrow 0$ or even satisfying the conditions $a_k \rightarrow 0$ as $k \rightarrow \infty$ and $\sum_{k=1}^{\infty} |\Delta a_k| < \infty$. Riesz [Cf. 1] showed that the function $f(x)$ defined by the series (1.1) for $a_k \downarrow 0$ can be non-summable. However, they are summable to any degree p provided $0 < p < 1$.

Theorem A.[4] If the sequence $\langle a_k \rangle$ satisfies the condition $a_k \rightarrow 0$ and $\sum |\Delta a_k| < +\infty$, then for any $p, 0 < p < 1$, we have

$$\lim_{n \rightarrow \infty} \int_{-\pi}^{\pi} |f(x) - S_n(x)|^p dx = 0,$$

where $S_n(x)$ is the partial sum of the series (1.1).

Rees and Stanojevic [3] (see also Garrett and Stanojevic [2]) introduced a modified cosine sum

$$(1.2) \quad h_n(x) = \frac{1}{2} \sum_{k=0}^n \Delta a_k + \sum_{k=1}^n \sum_{j=k}^n \Delta a_j \cos kx.$$

Regarding the convergence of (1.2) in L -metric, Garrett and Stanojevic [2] proved the following result :

Theorem B. If $\{a_k\}$ is a null quasi-convex sequence . Then

$$\|h_n(x) - f(x)\| = o(1), n \rightarrow \infty,$$

where $f(x)$ is the sum of cosine series (1.1).

In this paper ,we study the L^p -convergence of this modified sum (1.2) and deduce Theorem A as corollary of our theorem.

2000 AMS Mathematics Subject Classification : 42A20, 42A32.

2. Results.

Theorem . If the sequence $\{a_k\}$ satisfies the conditions $a_k \rightarrow 0$ and $\sum |\Delta a_k| < \infty$, then for any $p, 0 < p < 1$, we have

$$\lim_{n \rightarrow \infty} \int_{-\pi}^{\pi} |f(x) - h_n(x)|^p dx = 0 .$$

Proof. We have

$$\begin{aligned} h_n(x) &= \frac{1}{2} \sum_{k=0}^n \Delta a_k + \sum_{k=1}^n \sum_{j=k}^n \Delta a_j \cos kx \\ &= \frac{a_0}{2} + \sum_{k=1}^n a_k \cos kx - a_{n+1} D_n(x) . \end{aligned}$$

Using Abel's transformation,

$$\begin{aligned} h_n(x) &= \sum_{k=0}^{n-1} \Delta a_k D_k(x) + a_n D_n(x) - a_{n+1} D_n(x) \\ &= \sum_{k=0}^n \Delta a_k D_k(x) . \end{aligned}$$

Since $D_n(x) = O(1/x^2)$ for $x \neq 0$, and $a_n \rightarrow 0$, right side tends to zero, where

$$D_n(x) = (1/2) + \cos x + \dots + \cos nx$$

represents Dirichlet's kernel.

Now,

$$f(x) - h_n(x) = \sum_{k=n+1}^{\infty} \Delta a_k D_k(x)$$

This means

$$|f(x) - h_n(x)|^p \leq \left(\frac{2}{|x|} \right)^p \left[\sum_{k=n+1}^{\infty} |\Delta a_k| \right]^p ,$$

and therefore,

$$\begin{aligned} \int_{-\pi}^{\pi} |f(x) - h_n(x)|^p dx &\leq 2^p \left[\sum_{k=n+1}^{\infty} |\Delta a_k| \right]^p \int_{-\pi}^{\pi} \frac{dx}{x^p} \\ &\rightarrow 0 \text{ as } n \rightarrow \infty . \end{aligned}$$

Corollary 1. If the sequence $\{a_k\}$ satisfies $a_k \rightarrow 0$ and $\sum |\Delta a_k| < \infty$, then for any $0 < p < 1$, we have

$$\lim_{n \rightarrow \infty} \int_{-\pi}^{\pi} |f(x) - S_n(x)|^p dx = 0 .$$

We have

$$\begin{aligned} \int_{-\pi}^{\pi} |f(x) - S_n(x)|^p dx &= \int_{-\pi}^{\pi} |f(x) - f_n(x) + f_n(x) - S_n(x)|^p dx \\ &\leq \int_{-\pi}^{\pi} |f(x) - f_n(x)|^p dx + \int_{-\pi}^{\pi} |f_n(x) - S_n(x)|^p dx \\ &= \int_{-\pi}^{\pi} |f(x) - f_n(x)|^p dx + \int_{-\pi}^{\pi} |a_{n+1} D_n(x)|^p dx \end{aligned}$$

Now,

$$\begin{aligned} \int_{-\pi}^{\pi} |a_{n+1} D_n(x)|^p dx &\leq \int_{-\pi}^{\pi} \left(\frac{2}{|x|} \right)^p |a_{n+1}|^p dx \\ &= 2^p |a_{n+1}|^p \int_{-\pi}^{\pi} (dx/x^p) \rightarrow 0 \text{ as } n \rightarrow \infty, \end{aligned}$$

also $\lim_{n \rightarrow \infty} \int_{-\pi}^{\pi} |f(x) - h_n(x)|^p dx = 0$ by our theorem. Hence the corollary follows.

References

- [1] N.K. Bari, *A Treatise on trigonometric series* (London : Pregamon Press) Vol. II (1964).
- [2] J.W. Garrett and C.V. Stanojevic, On L^1 -convergence of certain cosine sums, *Proc. Amer. Math. Soc.*, **54** (1976) 101–105.
- [3] C.S. Rees and Č.V. Stanojević, Necessary and sufficient condition for Integrability of certain cosine sums, *J. Math. Anal. Appl.* **43**(1973), 579-586.
- [4] P.L. Ul'yanov, Application of A-integration to a class of trigonometric series (in Russian) *MC* **35** (1954), 469-490.

Wireless Electricity Transmission Based On Electromagnetic and Resonance Magnetic Coupling

¹ Prof. Burali Y. N., ² Prof. Patil C.B.

¹(Head of Electrical Department, Nanasaheb Mahadik Polytechnic Institute, Peth Sangli, India)

²(Lecturer Mechanical Department, Nanasaheb Mahadik Polytechnic Institute, Peth Sangli, India)

Abstract

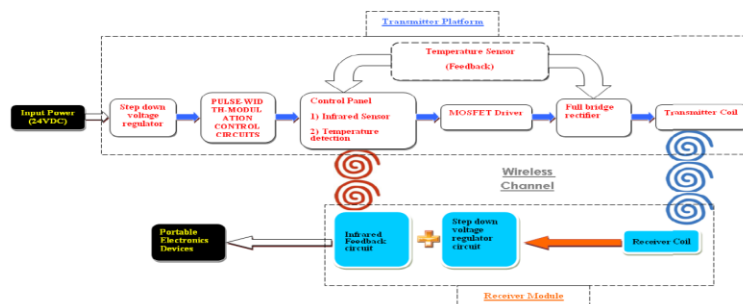
Wireless Electricity transmission is based on strong coupling between electromagnetic resonant objects to transfer energy wirelessly between them. This differs from other methods like simple induction, microwaves, or air ionization. The system consists of transmitters and receivers that contain magnetic loop antennas critically tuned to the same frequency. Due to operating in the electromagnetic near field, the receiving devices must be no more than about a quarter wavelengths from the transmitter [1]. Unlike the far field wireless power transmission systems based on traveling electro-magnetic waves, Wireless Electricity employs near field inductive coupling through magnetic fields similar to those found in transformers except that the primary coil and secondary winding are physically separated, and tuned to resonate to increase their magnetic coupling. These tuned magnetic fields generated by the primary coil can be arranged to interact vigorously with matched secondary windings in distant equipment but far more weakly with any surrounding objects or materials such as radio signals or biological tissue [4].

Keywords – AC Electricity, Wireless Electricity Device, Oscilating magnetic Field, Resonant Magnetic Coupling, Magnetic Resonance Imaging

1. INTRODUCTION

Electricity is today a necessity of modern life. It is difficult to imagine passing a day without electricity. The conventional use of electricity is made possible through the use of wires. However researchers in MIT have devised a means of providing electricity without any wires. Wireless Electricity, a portmanteau for wireless electricity, is a term coined initially and used. This principle of wireless electricity works on the principle of using coupled resonant objects for the transference of electricity. The system consists of Wireless Electricity transmitters and receivers that contain magnetic loop antennas critically Tuned to the same frequency. Wireless power transmission is not a new idea; Nikola Tesla demonstrated a "transmission of electrical energy without wires" that depends upon electrical conductivity as early as 1891. The receiver works on the same principle as radio receivers where the device has to be in the range of the transmitter. It is with the help of resonant magnetic fields that Wireless Electricity produces electricity, while reducing the wastage of power. This is unlike the principle adopted by Nikola Tesla in the later part of the 19th century; where conduction based systems were used. The present project on Wireless Electricity aims at power transmissions in the range of 100 watts. May be the products using WiTricity in future might be called Wireless Electricity So we have been able to power a 60 watt light bulb from a power source that is located about seven feet away, while providing forty percent efficiency. This was made possible using two copper coils that were twenty inches in diameter which were designed so that they resonated together in the MHz range. One of these coils were connected to a power source while the other, to a bulb. With this Wireless Electricity setup, the bulb got powered even when the coils were not in sight.

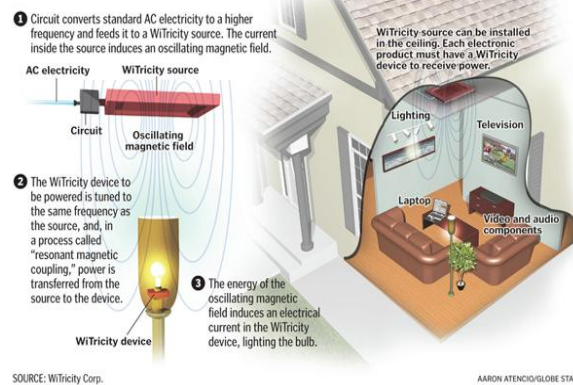
2. BLOCK DIAGRAM



I. I. WIRELESS ELECTRICITY TECHNOLOGY

Wireless electricity

WiTricity is commercializing technology developed at MIT that sends power through the air to run devices like laptops, DVD players, cellphones, and other common electronics.



Understanding what Wireless Electricity technology is transferring electric energy or power over distance without wires is quite simple. Understanding how it works is a bit more involved, but it doesn't require an engineering degree. We'll start with the basics of electricity and magnetism, and work our way up to the Wireless Electricity technology.

3. ELECTRICITY

The flow of electrons (current) through a conductor (like a wire), or charges through the atmosphere (like lightning). A convenient way for energy to get from one place to another.

4. Magnetism

A fundamental force of nature, which causes certain types of materials to attract or repel each other. Permanent magnets, like the ones on your refrigerator and the earth's magnetic field, are examples of objects having constant magnetic fields. Oscillating magnetic fields vary with time, and can be generated by alternating current (AC) flowing on a wire. The strength, direction, and extent of magnetic fields are often represented and visualized by drawings of the magnetic field lines. As electric current, I , flows in a wire, it gives rise to a magnetic field, B , which wraps around the wire. When the current reverses direction, the magnetic field also reverses its direction. The blue lines represent the magnetic field that is created when current flows through a coil. When the current reverses direction, the magnetic field also reverses its direction.

5. Electromagnetism

A term for the interdependence of time-varying electric and magnetic fields. For example, it turns out that an oscillating magnetic field produces an electric field and an oscillating electric field produces a magnetic field.

6. Magnetic Induction

A loop or coil of conductive material like copper, carrying an alternating current (AC), is a very efficient structure for generating or capturing a magnetic field. If a conductive loop is connected to an AC power source, it will generate an oscillating magnetic field in the vicinity of the loop. A second conducting loop, brought close enough to the first, may "capture" some portion of that oscillating magnetic field, which in turn, generates or induces an electric current in the second coil. The current generated in the second coil may be used to power devices. This type of electrical power transfer from one loop or coil to another is well known and referred to as magnetic induction. Some common examples of devices based on magnetic induction are electric transformers and electric generators.

7. Energy/Power Coupling

Energy coupling occurs when an energy source has a means of transferring energy to another object. One simple example is a locomotive pulling a train car the mechanical coupling between the two enables the locomotive to pull the train, and overcome the forces of friction and inertia that keep the train still and, the train moves. Magnetic coupling occurs when the magnetic fields of one object [5]. An electric transformer is a device that uses magnetic induction to transfer energy from its primary winding to its secondary winding, without the windings being connected to each other. It is used to "transform" AC current at one voltage to AC current at a different voltage. Interacts with a second object and induces an electric current in or on that object. In this way, electric energy can be transferred from a power source to a powered device. In contrast to the example of mechanical coupling given for the train, magnetic coupling does not require any physical contact between the object generating the energy and the object receiving or capturing that energy.

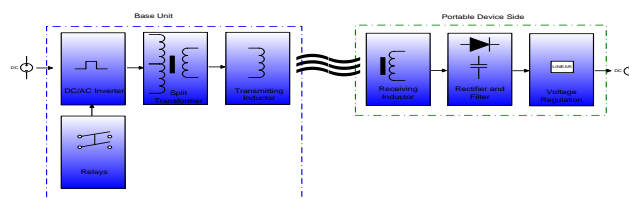
8. Resonance

Resonance is a property that exists in many different physical systems. It can be thought of as the natural frequency at which energy can most efficiently be added to an oscillating system. A playground swing is an example of an oscillating system involving potential energy and kinetic energy. The child swings back and forth at a rate that is determined by the length of the swing. The child can make the swing go higher if she properly coordinates her arm and leg action with the motion of the swing. The swing is oscillating at its resonant frequency and the simple movements of the child efficiently transfer energy to the system. The resonant frequency depends on the size, shape and thickness of the material [4].

9. Resonant Magnetic Coupling

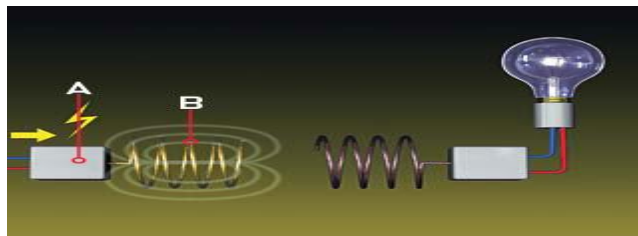
Magnetic coupling occurs when two objects exchange energy through their varying or oscillating magnetic fields. Resonant coupling occurs when the natural frequencies of the two objects are approximately the same. Two idealized resonant magnetic coils, shown in yellow. The blue and red color bands illustrate their magnetic fields. The coupling of their respective magnetic fields is indicated by the connection of the colorbands [4].

10. WORKING OF WIRELESS TECHNOLOGY



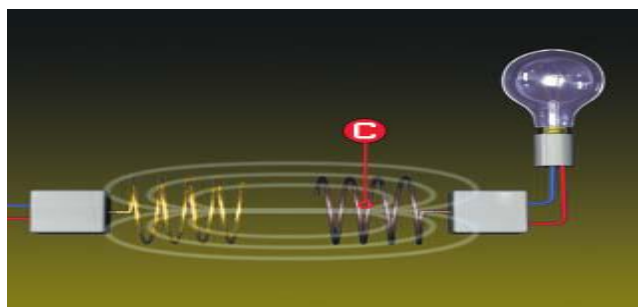
The concept of wireless electricity works on the principle of using coupled resonant objects for the transfer of electricity to objects without the use of any wires. This concept of WiTricity was made possible using resonance where an object vibrates with the application of a certain frequency of energy. So two objects having similar resonance tend to exchange energy without causing any effects on the surrounding objects.

STEP 1



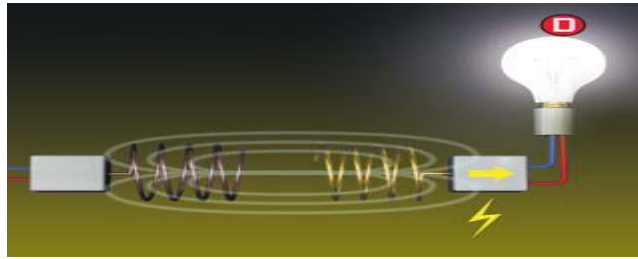
A circuit [A] attached to the wall socket converts the standard 60-hertz current to 10 megahertz and feeds it to the transmitting coil [B]. The oscillating current inside the transmitting coil causes the coil to emit a 10-megahertz magnetic field

STEP 2



The receiving coil [C] has the exact same dimensions as the sending coil and thus resonates at the same frequency and, in a process called magnetic induction, picks up the energy of the first coil's magnetic field.

STEP 3



The energy of the oscillating magnetic field induces an electrical current in the receiving coil, lighting the bulb [D].

11. MAGNETIC RESONANCE IMAGING (MRI)

MRI machines use "magnetic resonance imaging" to produce diagnostic images of soft tissue. Many people assume that WiTricity's "Resonant Magnetic Coupling" must be similar to magnetic resonance imaging (MRI) technology; however, the technologies are similar in name only. MRI is, as its name suggests, a technology for using magnetism as a basis for diagnostic imaging of soft tissue in the human body. It utilizes a strong DC magnet to orient the magnetic fields of atoms within tissues, and radio frequency fields to manipulate those atoms in a selective way, so that tissues and structures can be imaged clearly. The "resonance" referred to in "MRI" refers to the resonance of atomic structures. MRI is not considered to be a method for wireless power transfer [3].

12. ADVANTAGES OF WIRELESS ELECTRICITY

- More Convenient
- More Reliable
- More Environmentally Friendly

13. APPLICATION

- Low Power Product Category.
Example, Remote controls, game controllers, computer headsets, gaming headsets, sensors, wireless thermostats, smoke detectors.
- Full Power Product Category.
Example, iPhone/smart phones, smart phone accessories, netbooks, netbook accessories, wireless speakers.
- High Power Category
Example, Digital photo frames, laptops, laptop accessories, flat panel TV's.
- Industrial Application.
Example, Robots, packaging machinery, assembly machinery, machine tools, drilling, mining, underwater, etc.

14. CONCLUSION

Wireless Electricity technology is a non-radioactive mode of energy transfer, relying instead on the magnetic near field. Magnetic fields interact very weakly with biological organisms—people and animals—and are scientifically regarded to be safe. WiTricity products are being designed to comply with applicable safety standards and regulations. Hence witricity is technology safe.witricity can transfer power depends on the source and receivers. if it is relatively close to one another, and can exceed 95%.Efficiency is primarily determined by the distance between the power source and capture device, however, the shape may impact the efficiency. it can transfer the power through walls also. Traditional magnetic induction requires that the power source and capture device be very close to one another usually within millimeters to transfer power efficiently. Wireless Electricity technology is based on sharply resonant strong coupling, and is able to transfer power efficiently even when the distances between the power source and capture device are several times the size of the devices themselves.

15. Referances

- 1 [http://www. WiTricity-Wireless Electricity](http://www.WiTricity-Wireless Electricity).
- 2 Wireless patient monitoring system <http://www.WiTricitypower.com>
- 3 Concept Evaluation of an Inductive Charging System for Electric Vehicles. 3rd European Conference Smart Grids and E-Mobility, 17.10. - 18.10.2011, München.
- 4 "Wireless Power Transfer via Strongly Coupled Magnetic Resonances" by Andre kurs, Science 317, 83(2007); DoI:10.1126/science.1143254.
- 5 http://www.electronics-tutorials.com/filters/if_amplifier-transformers.htm IF amplifier transformers.

Design of Bovine Semen Temperature Controller Using PID

Tatag Lindu Bhakti¹, Adhi Susanto², Paulus Insap Santosa³, Diah Tri Widayati⁴

^{1,2,3}Department of Electrical Engineering and Information Technology,

Faculty of Engineering, Gadjah Mada University.

Grafika Street No. 2, Yogyakarta, 55281. INDONESIA

⁴Faculty of Animal Science, Gadjah Mada University

Fauna Street No. 3, Bulaksumur, Yogyakarta, 55281. INDONESIA

Abstract

Development of better bovine's assisted reproduction device in livestock industry requires a temperature controller to help researcher choosing best bovine's spermatozoa. This study aims to design bovine's semen temperature controller prototype which fully controlled using PID (Proportional Integral Derivative) algorithm. Temperature target is achieved using combination between peltier module's polarity switching and PWM (Pulse-Width Modulation) regulation due to its real-time error status. Testing result shows bovine's semen temperature controller prototype were able to achieve linear response ranging from -5°C to 50°C with maximum cooling rate $-0,9^{\circ}\text{C/second}$ and maximum heating rate $1,7^{\circ}\text{C/second}$.

Keywords: temperature controller, bovine's semen, assisted reproduction, PID, PWM, peltier module, temperature stage.

1. Introduction

Development of better bovine's assisted reproduction device in livestock industry requires a supporting device which can help researcher to produce high-quality bovine calf. Technical constraint due to achieve better procedure finding best spermatozoa from leading male is important issue in high-quality bovine's calf production. This study aims to find a new method to assist researcher choosing best bovine's spermatozoa through sperm motility decrement using semen cooling method. By decreasing bovine's sperm motility, we expect professional observers can get better visualization when try to recognize best bovine's spermatozoa.

2. Theoretical Basis

2.1. Peltier-Seebeck effect

Peltier effect is a phenomenon of heat exchange at thermocouple contact area in closed electricity circuit when a pair type of thermocouple is electrified in one direction. Discovery of peltier effect was published in 1834 by French physicist named J.C.A. Peltier, thirteen years after invention of thermoelectric effect by T.J. Seebeck. Both peltier and seebeck effects, they are often considered comes from an identical physical process [1].



Figure 1 Peltier module (source: www.tetech.com)

Theory about peltier and seebeck effects are based on resultant analysis of electromotive force derived from electron concentration gradient in used thermocouple materials. The theory assumes if electron concentration is associated with thermal gradient that occurs when a series of thermocouples give direct-current electricity continuously. Refer to seebeck equation in [1]; electromotive force differences (ΔU) which measured at thermocouple contact area are given by (1)

$$\Delta U = \int_{T_1}^{T_2} (S_A(T) - S_B(T)) dT \quad (1)$$

where

$$S(T) = \varepsilon_0 \frac{T}{\theta_v + T} \quad (2)$$

and

$$\varepsilon_0 = \frac{k_B}{e} = 86,17 \mu V K^{-1} \quad (3)$$

T_1 and T_2 are temperature measured at thermocouple contact area, S is seebeck coefficient which depends on type of thermocouple material used, θ_v is thermocouple characteristic temperature, k_B is Boltzmann's constant and e is elementary charge. Refer to [1]; rate of heat interchange at thermocouple contact area is proportional to amount of electrical current. This phenomena can be written as (4)

$$\frac{dQ}{dt} = \pi \frac{dq}{dt} \quad (4)$$

with

$$\pi = \frac{dQ}{dq} \quad (5)$$

where π is Peltier coefficient, Q is heat absorbed or released at thermocouple contact area and q is amount of electrical charge flowing through closed circuit. According to Thomson, Peltier coefficient is dependent to temperature and can be rewritten as (6)

$$\pi(T) = S(T) T \quad (6)$$

And if (6) is substituted with (2), it will result final Peltier's equation (7)

$$\pi(T) = \varepsilon_0 \frac{T^2}{\theta_v + T} \quad (7)$$

2.2. PID control

PID control is a control algorithm which combines proportional, integral and derivative controllers. Refer to [2][3], PID control algorithm can be shown as (8)

$$V_0 = K_p e + K_i \int_{t_0}^t e dt + K_d \frac{de}{dt} \quad (8)$$

with V_0 is controller output signal, e is input error signal, t is time, K_p is proportional constant, K_i is integral constant and K_d is derivative constant. Equation (8) represents PID control in continuous time domain. If (8) will be applied in discrete domain system then PID continuous time domain equation must be changed into PID discrete time domain. By deriving (8) we can obtain (9)

$$\frac{dV_0}{dt} = K_p \frac{de}{dt} + K_i e + K_d \frac{d}{dt} \left(\frac{de}{dt} \right) \quad (9)$$

Subsequently, if dt is substituted using short time interval (Δt) of T then (9) will change into (10)

$$\frac{\Delta V_0}{T} = K_p \frac{\Delta e}{T} + K_i e + K_d \frac{\Delta}{T} \left(\frac{\Delta e}{T} \right) \quad (10)$$

or,

$$\Delta V_0 = K_p \Delta e + K_i e T + K_d \Delta \left(\frac{\Delta e}{T} \right) \quad (11)$$

based on the definition,

$$\Delta V_o = V_{on} - V_{on-1} \quad (12)$$

$$\Delta e = e_n - e_{n-1} \quad (13)$$

so (11) can be rewritten as (14)

$$V_{on} - V_{on-1} = K_p(e_n - e_{n-1}) + K_i e_n T + \frac{K_d}{T}(\Delta e_n - \Delta e_{n-1}) \quad (14)$$

and if defined

$$\Delta e_n = e_n - e_{n-1} \quad (15)$$

$$\Delta e_{n-1} = e_{n-1} - e_{n-2} \quad (16)$$

Then by substituting (15) and (16) into (14), we can get final PID equation shown in (17)

$$V_{on} = V_{on-1} + K_p(e_n - e_{n-1}) + K_i e_n T + \frac{K_d}{T}(e_n - 2e_{n-1} + e_{n-2}) \quad (17)$$

Equation (17) represents PID control equation in discrete time domain and ready to implement into any digital controller.

2.3. Pulse-Width Modulation (PWM)

PWM is a method to control electrical power transmitted into any electrical load in an electronic system using manipulated pulse-activation period [4]. Power intensity control was performed by regulating pulse train signal to get direct-current voltage equivalencies [5] [6] and can be expressed mathematically as (18)

$$\overline{V_{DC}} = \frac{1}{T} \int_0^T V(t) dt \quad (18)$$

where $\overline{V_{DC}}$ is PWM's output direct-current voltage equivalencies, T is working period of PWM's signal activation and $V(t)$ is PWM power supply voltage function. In PWM method, transmitted power equivalency is performed through manipulated signal activation period called duty cycle (D) [4]. $V(t)$ has $V_{DC \max}$ for $0 < t < DT$ and $V_{DC \min}$ for $DT < t < T$. D ranging from 0% to 100%. Mathematically, PWM's voltage equivalencies can be declared in (19)

$$\overline{V_{DC}} = \frac{1}{T} \left(\int_0^{DT} V_{DC \max} dt + \int_{DT}^T V_{DC \min} dt \right) \quad (19)$$

because $V_{DC \max}$ and $V_{DC \min}$ are constants which independent by time, equation (19) can be changed into (20)

$$\overline{V_{DC}} = \frac{DT V_{DC \max} + (1 - D)T V_{DC \min}}{T} \quad (20)$$

and can be rewritten as (21)

$$\overline{V_{DC}} = D V_{DC \max} + (1 - D) V_{DC \min} \quad (21)$$

From (21) it can be seen if D is determining parameter which can regulate $\overline{V_{DC}}$ directly. If (21) will be applied to controlling injected power to an electronic load, it can be simply changed D -value to generate direct-current output voltage equivalencies.

2.4. ATMEGA 8 microcontroller

Microcontroller is electronic devices which can be programmed to execute specific application routine. Physically, microcontroller is an integrated circuit consists of processor, RAM (Random Access Memory), permanent memory and input/output pin which can be programmed to communicate with external electronic devices.



Figure2 ATMEGA 8microcontroller [7]

Figure2 shows physical appearance of ATMEGA 8 microcontroller. Refer to [7]; ATMEGA 8 is an 8-bit microcontroller produced by ATMEL Corp. comes with 8 Kbyte Flash PEROM (Programmable and Erasable Read Only Memory) to store main program code. ATMEGA 8 can work up to 16 MHz clock frequencies. ATMEGA 8 main processor is designed using RISC processor architecture (Reduced Instruction-Set of Computing) named ATMEL AVR®.

3. Temperature Controller Devices Construction

Bovine'ssementemperature controller device is consisted of software and hardware parts which connected each other through serialcommunication. Software construction consists of GUI (Graphical UserInterface) to handle process interaction with user and make set pointinput, moving average block is used to filtering arbitrary datum which come from temperature sensor, deferential comparatoris used to calculating errorvalue, PIDcontrolblockis used as main control and serial communication block is used to establish communication with external hardware.

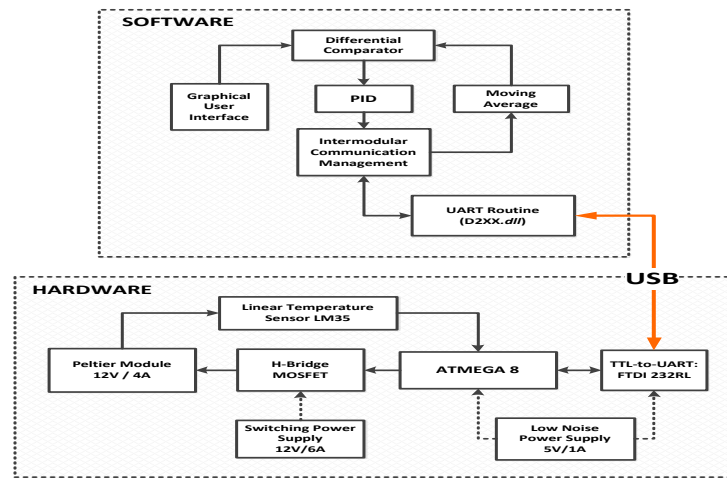


Figure 3 Block diagram of bovine'ssementemperature controller device

Hardware construction consists of serialcommunication module to make communication with main software, an AT MEGA 8 microcontrollerto generatePWM signal as ordered from software calculation, H-bridgecircuit to buffer injected current into peltier module, lineartemperaturesensorLM35 to make real time temperature measurement,switching power supplyforH-bridgeandlow noise power supply for microcontroller and signal acquisition.

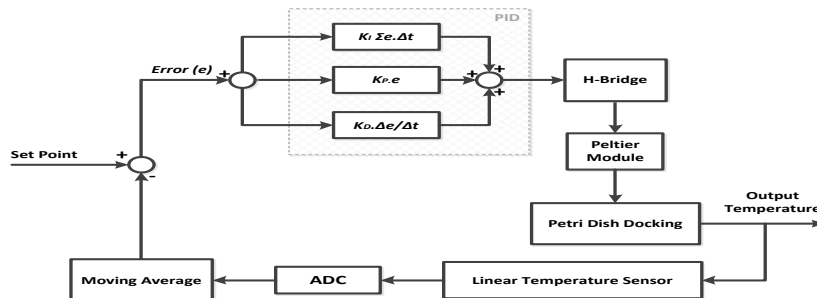


Figure4 PID control mechanism

When systemis turned on, software ordering hardware to getrealtime temperaturestatus from peltier moduleandat the same time.PIDcontrol algorithmis executed by (17)to achieve given set point as fast as possible. A duty cycle calculation result from PID issent toAT MEGA 8 through USB serialcommunication.Duty cycle order came from software then translated by

AT MEGA 8 intoreal duty cycle value. PWM output signal from AT MEGA 8 which referred (21) injected to H-bridge MOSFET circuit. At the other side, a switching power supply which connected to peltier module through H-bridge is used to supplying peltier module's power demand. Using this scheme, peltier's passed current can be fully controlled using software andat the same time, a linear temperaturesensor(LM 35) measuringpeltier module'stemperature and send it to software as feedback. PIDcalibrationis performed using reference[8].

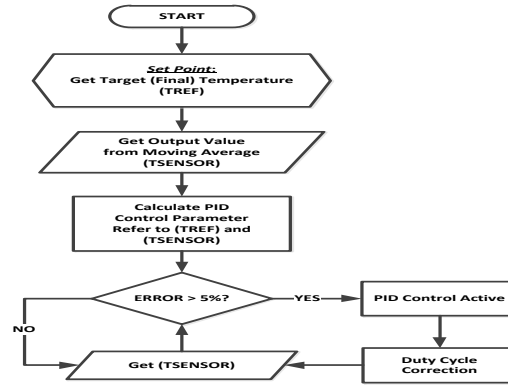


Figure5 Peltier module's temperature control method

4. Design results

Refer to diagrams in Figure3, 4 and 5; bovine's semen temperature controller consists of software and hardware which can communicate each other through serial communication lines. Figure6 shows software appearance (GUI) which has been successfully developed and Figure7 shows formed ice on preparation holder (-seered circle) when peltier module is operated at maximum cooling mode ($D = 100\%$)



Figure6 Main software appearance

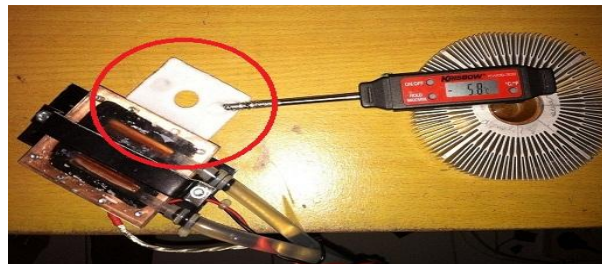


Figure7 Formed ice on bovine's semen preparation holder, see red circle
($T_{peltier} = -5,8^{\circ}C$; $D = 100\%$; $T_{ambient} = 25^{\circ}C$)

5. Testing

Overall system was tested using two methods. First testing method is using step testing signal to obtain peltier module temperature response versus input set point profile. Figure 8 shows peltier module cooling response and Figure 9 shows peltier module heating response.

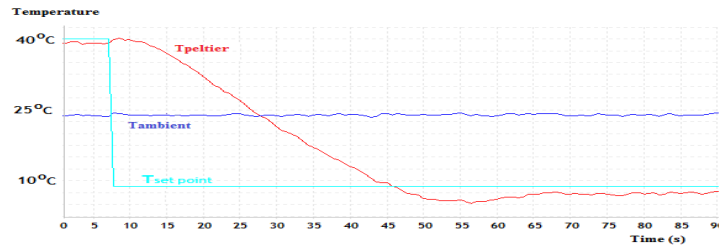


Figure 8 Peltier module's cooling response (40°C to 10°C)

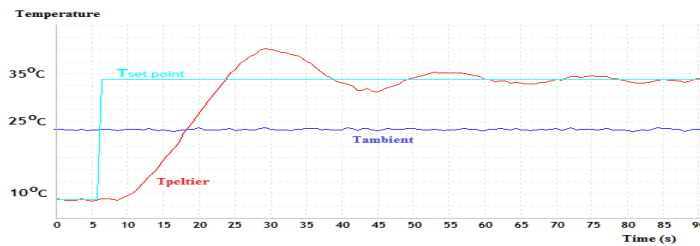


Figure 9 Peltier module's heating response (10°C to 35°C)

From Figure 8 and Figure 9, it can be known if preparation holder temperature has maximum cooling rate $-0.9^{\circ}C/second$ and maximum heating rate $1.7^{\circ}C/second$. It also seems if steady-state temperature condition is reached faster in cooling mode compared to heating mode. Overshoot is highly visible when system is operated in heating mode.

Second test method is performed by changing set point value continuously to obtain peltier module's steady-state temperature response due to any set point input. This test aims to measure hardware output temperature fidelity due to any desired input set point. Figure 10 shows peltier module's linearity response profile ranging from $-30^{\circ}C$ to $50^{\circ}C$ of set point command. Refer to Figure 10, it can be seen if hardware has linear temperature response profile ranging from $-5^{\circ}C$ to $50^{\circ}C$ in standard testing temperature pressure ($25^{\circ}C/1 atm$). Set point testing over $50^{\circ}C$ was not performed because uncontrollable overshoot potency which can damage peltier module.

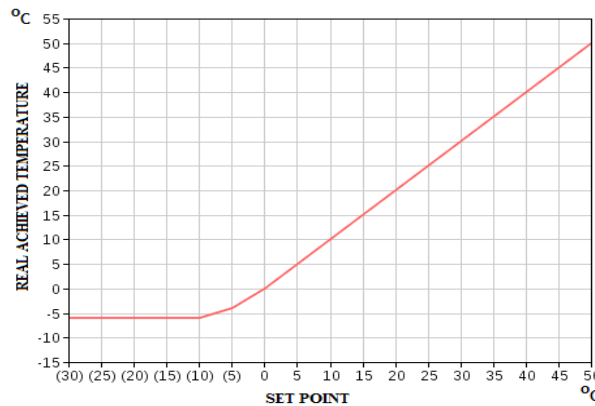


Figure 10 Setpoint temperature fidelity responses

6. Conclusion

From testing results, it can be known if bovine's semen temperature controller has linear temperature response profile ranging from -5°C to 50°C in standard testing temperature pressure ($25^{\circ}\text{C}/1\text{ atm}$). System has maximum cooling rate $-0.9^{\circ}\text{C}/\text{second}$ and maximum heating rate $1.7^{\circ}\text{C}/\text{second}$. Heating control responses above ambient (room) temperature are not symmetrical with cooling control responses below ambient temperature; therefore this control system prototype still need further research to make adaptable control system for any temperature condition given.

Acknowledgements

Authors would thank to all of Civitas Academica Electrical Engineering Department and Animal Science Department GadjahMada University and PT. Miconos Transdata Nusantara (www.miconos.co.id) which provided facility for temperature stage prototyping testing and calibration.

References

- [1] V. A. Drebuschak. The Peltier Effect. J. Thermal Anal. and Cal., Vol. 91-1, pp. 311-315, 2008.
- [2] Thiang, H. Khoswanto and E. Pangaldus. Position Control of a Manipulator Using PID Control Algorithm Based on ATmega8535 Microcontroller. Int. Conference on Instrumentation, Control & Automation (ICA) 2009, ISBN 978-979-8861-05-5, pp. 196-199, 2009.
- [3] W. Ye, J. Xu, Y. Zhu and Y. Chen. Research on Intelligent PID Control Strategy of Thermal Control Object. 3rd Int. Conference on Measuring Technology and Mechatronics Automation. 978-0-7695-4296-6/11. DOI 10.1109/ICMTMA.2011.573, IEEE pp.7-10, 2011.
- [4] S. Pongswatd, A. Chaikla, P. Ukakimapurn and K. Tirasesth. Digital Technique to Generate Variable and Multiple PWM Signals. IEEE 0-7695-2882-1/07, 2007.
- [5] X. Lu, S. Chen, C. Wu and M. Li. The Pulse Width Modulation and Its Use in Induction Motor Speed Control. 4th Int. Symposium on Computational Intelligence and Design. 978-0-7695-4500-4/11. DOI 10.1109/ISCID.2011.150. pp. 195-198, 2011.
- [6] R. Rajendran and N. Devarajan. FPGA Implementation of Space Vector PWM Technique for Voltage Source Inverter Fed Induction Motor Drive. 2nd Int. Conference on Computer and Electrical Engineering. 978-0-7695-3925-6/09 IEEE. DOI 10.1109/ICCEE. 2009.119, pp. 422-426, 2009.
- [7] Datasheet AT MEGA 8/L (Rev.2486Z-AVR-02/11). Available [Online] at <http://www.atmel.com/>
- [8] F. Haugen. Basic Dynamics and Control. ISBN 978-82-91748-13-9, 2010.

Appendix:



Figure A.1. Bovine's semen temperature control hardware

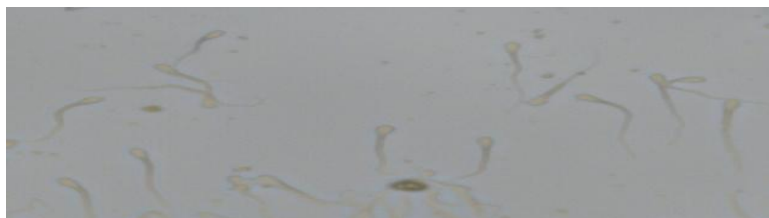


Figure A.2. Bovine's sperms at low temperature (4°C) hold for 15 minutes
(All bovine sperm's motility decreased to zero)

A Proposal for Implementation of Signature Based Intrusion Detection System Using Multithreading Technique

**Prof.D.P.Gaikwad¹, Pooja Pabshettiwar², Priyanka Musale³, Pooja Paranjape⁴,
Ashwini S. Pawar⁵**

AISSMS'S College Of Engineering,
University Of Pune

Abstract

The rapid proliferation of Internet and mobile computing applications has changed the landscape of network security. The recent denial of service attacks on major Internet sites have shown us, no open computer network is immune from intrusions. The traditional way of protecting networks with firewalls and encryption software is no longer sufficient and effective. Many intrusion detection techniques have been developed on fixed wired networks but have been turned to be inapplicable in this new environment. We need to search for new architecture and mechanisms to protect computer networks. In this paper, we are proposing signature based intrusion detection system, using multithreading technique. The multithreading approach will be used to handle network traffic. It takes the advantage of parallel processing on captured packets. We have described the proposal of our multithread based IDS system. We also suggested the algorithm which will help in updating the database which is used for IDS.

Keywords: Intrusion Detection, Multi-Threading, agent.

1. Introduction

Internet is the most important tool for carrying information in people's daily life, in recent years usage of internet has increased tremendously hence network security has become the major concern in computer network. All the computer resources in a network have become vulnerable to potential cyber threats such as network intrusion. To increase network security, use of network intrusion detection systems, firewalls, encryption and other software or hardware solution is immensely increasing.

1.1 Intrusion:

An intrusion is an act of intruding in computer network with intent of exploiting system vulnerabilities and having unauthorized access or control over the system.

1.2 Intrusion Detection:

Intrusion detection is the process of identifying and responding to malicious activities targeted at computing and networking resources. Intrusion detection systems are of two types [1].

- 1) Host-based Intrusion Detection System (HIDS)
- 2) Network-based Intrusion Detection System (NIDS)

1) Host-based Intrusion Detection System (HIDS):

A host-based intrusion detection system (HIDS) is an intrusion detection system that monitors and analyzes the internals of a computing system as well as the network packets on its network interfaces. The target of attackers is systems in corporate network having confidential information. HIDS detects which program accesses what resources and discovers that, for example, a word-processor has suddenly started modifying the system password database. HIDS also detects information present in system and check information is intact i.e. not changed by intruders.

2) Network-Based Intrusion Detection System (NIDS):

In network-based (NIDS), the packets are collected from the network. NIDS monitors network traffic on the network segment for malicious activity and unauthorized access at which it resides. In signature based IDS, signature is a formula that describes an attack. With this method, the system has some kind of knowledge about how attacks look. This means that everything in the system does not explicitly recognize as an attack is considered normal. This is usually solved by using signatures to recognize attacks. This method can be very precise and therefore should have a relatively

low false positive rate. False positive is when an alarm is generated although there is no attack. Also known as false alarm. In this paper we are proposing design of signature based intrusion detection system.

2. Literature Survey

We have reviewed various papers of researchers. The contribution of researchers has been discussed below: Ajoy Kumar and Eduardo B. Fernandez [2] have presented a paper on Security Patterns for Intrusion Detection Systems. Intrusion Detection Systems (IDS) play a very important role in the security of today's networks by detecting when an attack occurs. IDS have evolved into an integral part of network security which monitors the network traffic for attacks based , either on existing attack patterns or signatures (Signature-based IDS) or on anomalies or abnormal behavior (Behavior-Based) in the system. They have presented a pattern for abstract IDS that define their general features and patterns for Signature-Based IDS and Behavior-Based IDS. Dr. Sartid Vongpradhip and Vichet Plaimart [3] have proposed survival architecture for distributed intrusion detection system using mobile agent. In this paper they have shown the limitation of present IDS architecture and proposed new architecture that handles intrusion in network and how to survive from it. Mobile agent conceals the major resources in a network topology and network resources are divided into segments. Monitored hosts are installed on each of network segments. The architecture is designed in such a way that when a failure occurs at a single point, then we can recover the vital resources for that point from other systems in the network segments. To guarantee the correctness of message integrity, they made all of communication to pass through only secured channel by using public key cryptography and asymmetric key encryption. Even though proposed architecture can hide important resources of system but the attacker may know the location of proxy agent. So the remedy to overcome this problem is to change the location of proxy agent each time after finishing duty of region agent. Hence it is called mobile agent. Zhang Hu [4] has proposed the new feature pattern matching algorithm which first arranges letters in the pattern string form low appearance probability to high appearance probability, and then match one by one by using existing pattern matching algorithm. This algorithm first matches the rule heads, option heads and then matches the payloads of data packages to find intrusion.

The feature pattern matching reduces the comparison time. In addition to that he has given the detailed description of data acquisition module, protocol processing module, feature pattern matching module, log record module and intrusion response module. Te-Shun Chou [5] has proposed the development of an Intrusion Detection and Prevention system using technique of virtualization. In this paper instead of using real physical equipments in graduate level project of Intrusion Detection system, virtualization technology was employed to build a network with multiple machines running on the single system. In spite of running on the single system, implemented applications and services were executed by virtual machine just as a normal machine would. The advantage of this approach is, it reduces the administrative load and any error can be easily fixed and tackled, this also makes network configuration easy. Mueen Uddin, Kamran Khowaja and Azizah Abdul Rehman [6] have proposed Dynamic Multi-Layer Signature based IDS using Mobile Agents. In case of Signature based Intrusion Detection System each packet needs to be compared with every signature in database to detect an attack, this slows down the process of intrusion detection, especially when network traffic is in rush. Due to this, there is possibility of missing a potential attack. Secondly when a new service or protocol is introduced in a network, network administrator is supposed to update or add signatures into the database but this process is hectic and error prone. Degree of false positiveness is also a major concern in IDS. To overcome aforementioned drawbacks authors have proposed a new model called Dynamic Multi-Layer Signature based IDS using Mobile Agents. They have focused on detecting threats with very high success rate by dynamically and automatically creating and using small and efficient multiple databases. These databases are updated using mobile agents at particular intervals of time. Fang Yu, Zhifeng Chen, Yanlei Diao, T. V. Lakshman and Randy H. Katz [7] have proposed Fast and Memory Efficient Regular Expression Matching for Deep Packet Inspection. In IDS there is need to scan packet contents at high speed. In this paper, authors have shown that memory requirements using traditional methods are very high for many patterns used in packet scanning applications. They have developed a grouping scheme that can compile a set of regular expressions into several engines, which resulted in improvement of regular expression matching speed without much increase in memory usage. Authors have implemented a new DFA-based packet scanner using the above techniques. Their experimental results using real-world traffic and patterns have shown that their implementation achieved a factor of 12 to 42 performance improvement over a commonly used DFA based scanner. Compared to the NFA-based implementation, their DFA-based packet scanner achieved 50 to 700 times speedup. Sarang Dharmapurikar and John W. Lockwood [8] presented hardware-implementable pattern matching algorithm. This algorithm is used for content filtering applications that are scalable in terms of speed, number of patterns and pattern length. For packet content inspection and filtering multipattern matching algorithm is used which detects predefined keywords or

signatures in packets. But this algorithm requires lots of memory accesses and is poor in performance. Hence hardware implementable pattern matching algorithm is required. This algorithm is based on memory efficient multi hashing data structure called Bloom filter. They have used on cheap memory blocks in field programmable gate array to construct Bloom filters. These filters reduce a large number of memory accesses and speed up pattern matching. Based on this concept they have presented simple algorithm that scans for several thousands of short patterns i.e. up to 16 bytes with small amount of memory and few megabytes of external memory.

Zhenwei Yu, Jeffrey, J. P. Tsai and Thomas Weigert [9] have proposed An Automatically Tuning Intrusion Detection System. The proposed system will automatically tune the detection model On-the-fly according to the feedback provided by the system operator when false predictions are encountered. This system is evaluated using the KDDCup'99 intrusion detection dataset. Experimental results have shown that the system achieves up to 35% improvement in terms of misclassification cost when compared with a system lacking the tuning feature. If only 10% false predictions are used to tune the model, their system still achieves about 30% improvement. Moreover, when tuning is not delayed too long, the system can achieve about 20% improvement, with only 1.3% of the false predictions used to tune the model. The results of the experiments have shown that a practical system can be built based on ATIDS. Kapil Kumar Gupta, Baikunth Nath, and Ramamohanarao Kotagiri [10] have proposed Layered Approach Using Conditional Random Fields for Intrusion Detection. An intrusion detection system must reliably detect malicious activities in a network and must cope up with the large amount of network traffic; these issues are addressed by authors in this paper. They have demonstrated that high attack detection accuracy can be achieved by using Conditional Random Fields and high efficiency by implementing the Layered Approach. Experimental results on the benchmark KDD '99 intrusion data set shown that their proposed system based on Layered Conditional Random Fields outperforms other well-known methods such as the decision trees and the naive Bayes. The improvement in attack detection accuracy has found to be very high, especially in case of U2R attacks (34.8 percent improvement) and the R2L attacks (34.5 percent improvement). Prof. D.P.Gaikwad and Dr.R.C.Thool [1] have done survey on architecture taxonomy and product of IDS. They mention limitation of various IDS available in market that complete attack prevention is not realistically attainable due to the configuration and administration, system complexity, and abuse by user. They have discussed some aspects of IDS such as role of IDS, categories of IDS, modes of IDS. They proposed the general architecture, network parameter and architectural taxonomy. General architecture consist of three components namely Sensor (agent), Analyzer, User Interface. Sensor collects information and sends it to analyzer. Analyzer determines which intrusion occurs and user interface is used for interaction between system and users. This architecture improves performance of system. They have discussed various features of different IDS's such as Snort, MacAfee and Tripwire. As a future work author are going to develop wireless network IDS system.

3. Proposal Of Our IDS System

We propose the following system which consists of following modules:

Packet Capture Module: This module is responsible for capturing live packets from network. The captured packets are passed to packet preprocessor module. Packet preprocessor module categorizes the captured packets according to protocol like TCP, UDP, HTTP, etc. These packets are then passed to intrusion detector module. The intrusion detector checks for intrusion. If the packet is intruder then the detector creates a log of attack and generates alarm.

Intrusion Detection Module Multithreaded design:

Multi-threading is a programming feature that allows multiple threads to exist within the context of a single process. These threads share the resources, but are able to execute independently. The threaded programming model provides a useful abstraction of concurrent execution. The most interesting application of the multithreading is when it is applied to a single process to enable parallel execution. Let us consider, Detection module is a single process that decide whether the captured packet is intruder or not. A single process works well when there is normal traffic in network. However if the network is flooded or traffic is bursty, this will slow down detection process or there is possibility of missing potential attack due to dropping extra packets. To deal with this problem we are proposing the multithreaded design. The following algorithm is used to solve the problem using multithreading technique. The our algorithm will work as described below.

```

/*initially
capturedPacketCount=0
threadCount=1
Capacity=N*/
for each captured packet
{
    capturedPacketCount++;
    if (capturedPacketCount==Capacity)
    {
        capturedPacketCount=0;
        threadCount++;
        Create new thread ();
    }
}
    
```

Algorithm 1.Multithreaing

Here, capturedPacketCount keeps track of number of captured packets and threadCount will count the number of threads created by Detection process, whereas capacity (N) is a variable that holds the maximum number of packets a single thread can handle. ThreadCount is initialized to 1 as first thread will be created and it will wait for first packet. After that it will handle up to N packets. After N packets, new thread will be created to handle further packets i.e. second thread will handle N to 2N packets, third thread will handle 2N to 3N packets and so on.

Agent and DIDS-

The meaning of a word ‘agent’ is an agreement to act on one’s behalf. In software terms, agent is a program that acts for the user or some other program in a relationship of agency. Thus an agent is attributed to autonomy, authority and reactivity. The concept of an agent provides a convenient and powerful way to describe a complex software entity that is capable of acting with a certain degree of autonomy in order to accomplish tasks on behalf of its host.

Components of Agent

Figure 1 depicts the different modules of agent. Agent consists of 3 modules.

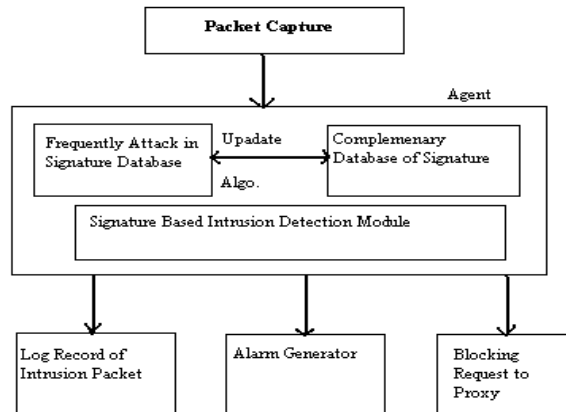


Figure 1. Modules of Agent

1] Frequent Attack Signature Database: In signature based intrusion detection method, we have a huge database of signatures. In order to check whether the incoming packet is an intruder or not, we have to match the signature of incoming packet against all the signatures in the database. However it is a time consuming process, as the database is large. To overcome this condition, we are using cache mechanism. We are going to maintain a cache of frequently occurring intruder signature database. Complementary database holds all the signatures.

2] Detection Module:

Detection Module is main component of agent. Its main task is to detect intrusion. It works as follows. The detection Module takes packet as input and extracts its signature. This extracted signature is then compared with all the signatures in cached database first, to check for intrusion. If any match occurs then packet is marked as intruder packet, resulting detection in short time. However if no match occurs then the extracted signature is then compared with all the signatures in complementary database. If match occurs then packet is intruder packet otherwise packet is considered to be a normal packet. This module incorporates multithreading logic as aforementioned.

3] Updation Module:

The updation module is responsible to keep frequent attack signature database up to date. The algorithm 2 will be used to implement the updation module. This algorithm is used to update this database from complementary database.

```

/* Let
m- max number of entries a frequent attack
database can have
n- number of entries exists in a frequently
attacking database
Initially,
    1] Frequently attacking database is empty.
    2] attackCount field of all entries in
complementary database is initialized to zero
    3] A variable maxOccurance is set to
threshold value.
*/For each record in complementary database
{
    If (count >=maxOccurance)
    {
        Move this record in frequently attacking database
        If (n<=m)
        {
            n++;
            Insert record at n location
        }
        Make its attackCount=0
    }
    Else
    {
        Search an entry in frequently attacking
database with lowest attackCount
        Swap this entry with the selected record
in complimentary database
        Make the attackCount of both records=0;
    }
}

```

Algorithm 2. For implementation of the Updation Module

We will maintain an attackCount field for each record in frequent attack database as well as complementary database. This variable attackCount will be incremented when intrusion is detected with corresponding record in database. Updation algorithm will work according to attackCount value. This algorithm will run at regular intervals. DIDS: DIDS stands for Distributed Intrusion Detection System. A distributed IDS uses multiple Intrusion Detection modules over a large network, all of which communicate with each other, or with a central server that facilitates advanced network monitoring, incident analysis, and instant attack data. By having these co-operative agents distributed across a network, network analyst and security personnel are able to know what is going on their network. It also allows to efficiently

managing its incident analysis resources by centralizing its attack records and by giving the analyst a quick and easy way to spot new threats and patterns. The figure 2 depicts the distributed IDS.

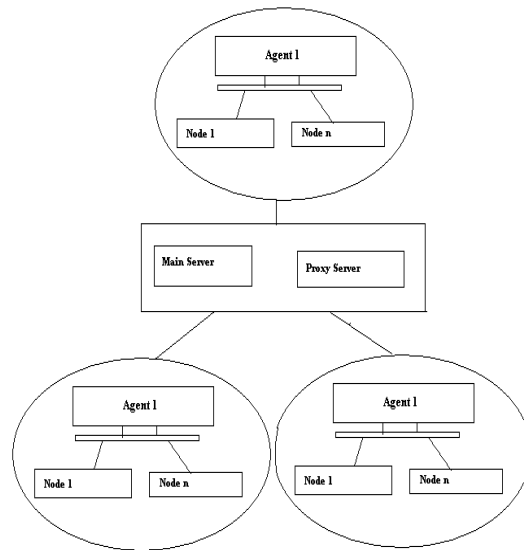


Figure 2. Distributed IDS

The Central Server

The central analysis server is the heart and soul of the operation. This server holds log of all the intrusion data. This allows the interactive querying of attack data for analysis and gives the current attack status of network. It also allows analysts to perform pre-programmed queries, such as identifies attack patterns and performs rudimentary incident analysis.

The Co-operative Agent

The co-operative agent network is one of the most important components. Every LAN in a network has Agent node. All the other nodes in LAN are connected to this agent node. And all the agent nodes are connected to central server. The agent acts in between host node and central server. Each host is having IDS program. Whenever an intrusion is detected, the host reports it to agent and agent forwards this attack information to the central server and proxy server.

The Proxy Server

The proxy server is used in DIDS system with special purpose of blocking Example- if a node has detected that packets coming from source IP address 172.34.34.3 are all intruder packets then it will give notification to agent and agent will request the proxy server to block all the packets with source IP address 172.34.34.3. This will save the time of node for intrusion detection. And deals efficiently with attacks like flooding.

4. Conclusion

The diligent management of network security is essential to the operation of networks, regardless of whether they have segments or not. It is important to note that absolute security is an abstract concept – it does not exist anywhere. All networks are vulnerable to insider or outsider attacks, and eavesdropping. No one wants to risk having the data exposed to the casual observer or open malicious mischief. Regardless of whether the network is wired or wireless, steps can and should always be taken to preserve network security and integrity. We have said that any secure network will have vulnerabilities that an adversary could exploit. This is especially true for computer networks. Intrusion Detection can compliment intrusion prevention techniques (such as encryption, authentication, secure MAC, secure routing, etc.) to improve the network security. However new techniques must be developed to make intrusion detection work better for the computer networks. We have shown that a multithreaded technique for better intrusion detection should be distributed and cooperative by applying co-operative agents to the network. Currently, the research is taking place in developing new architecture for NIDS for better security.

5. References

- [1] Prof. D.P.Gaikwad and Dr.R.C.Thool, Architecture Taxonomy and Product of IDS.
- [2] Ajoy Kumar and Eduardo B. Fernandez, Security Patterns for Intrusion Detection Systems, 1st LACCEI International Symposium on Software Architecture and Patterns (LACCEI-ISAP-MiniPLoP'2012), July 23-27, 2012, Panama City, Panama.
- [3] Dr.Sartid Vongpradhip and Vichet Plaimart, Survival Architecture for Distributed Intrusion Detection System (dIDS) using Mobile Agent, Network Computing and Applications, 2007. NCA 2007.
- [4] Zhang Hu, Design of Intrusion Detection System Based on a New Pattern Matching Algorithm, 2009 International Conference on Computer Engineering and Technology, 978-0-7695-3521-0/09 DOI 10.1109/ICCET.2009.244.
- [5] Te-Shun Chou, Development of an Intrusion Detection and Prevention Course Project Using Virtualization Technology, International Journal of Education and Development using Information and Communication Technology (IJEDICT), 2011, Vol. 7, Issue 2, pp. 46-55.
- [6] Mueen Uddin, Kamran Khowaja and Azizah Abdul Rehman, Dynamic Multi-Layer Signature Based Intrusion Detection System Using Mobile Agents, International Journal of Network Security & Its Applications (IJNSA), Vol.2, No.4, October 2010.
- [7] Fang Yu, Zhifeng Chen, Yanlei Diao, T. V. Lakshman and Randy H. Katz, Fast and Memory-Efficient Regular Expression Matching for Deep Packet Inspection.
- [8] Sarang Dharmapurikar and John W. Lockwood, Fast and Scalable Pattern Matching for Network Intrusion Detection Systems, IEEE JOURNAL ON SELECTED AREAS IN COMMUNICATIONS, VOL. 24, NO. 10, OCTOBER 2006.
- [9] Zhenwei Yu, Jeffrey, J. P. Tsai and Thomas Weigert, An Automatically Tuning Intrusion Detection System, IEEE TRANSACTIONS ON SYSTEMS, MAN, AND CYBERNETICS—PART B: CYBERNETICS, VOL. 37, NO. 2, APRIL 2007.
- [10] Kapil Kumar Gupta, Baikunth Nath, and Ramamohanarao Kotagiri, Layered Approach Using Conditional Random Fields for Intrusion Detection, IEEE TRANSACTIONS ON DEPENDABLE AND SECURE COMPUTING, VOL. 7, NO. 1, JANUARY-MARCH 2010.
- [11] M. Salour and Xiao Su, "Dynamic Two-Layer Signature-Based IDS with Unequal Databases", presented at proceeding of the International Conference on Information Technology (ITNG'07), 2007.
- [12] Hervé Debaré, An Introduction to Intrusion-Detection Systems.
- [13] P. S. Wheeler, "Techniques for Improving the Performance of Signature-Based Network Intrusion Detection Systems," in Computer Science, Davis, CA: University of California, Davis, 2006.
- [14] Karen Scarfone, Peter Mell, Guide to Intrusion Detection and Prevention Systems (IDPS), Computer Security Division Information Technology Laboratory National Institute of Standards and Technology Gaithersburg, MD 20899-8930.
- [15] Asmaa Shaker Ashoor, Prof. Sharad Gore, Importance of Intrusion Detection System (IDS), International Journal of Scientific & Engineering Research, Volume 2, Issue 1, January-2011 ISSN 2229-5518.

AN EFFICIENT VLSI IMPLEMENTATION OF IMAGE ENCRYPTION WITH MINIMAL OPERATION

¹S.Lakshmana kiran, ²P.Sunitha

¹M.Tech Student,

²Associate Professor, Dept. of ECE

^{1,2}Pragati Engineering college, Surampalem(A.P,IND)

Abstract

Traditional fast Discrete Cosine Transforms (DCT)/ Inverse DCT (mCT) algorithms have focused on reducing the arithmetic complexity. In this manuscript, we implemented a new architecture simultaneous for image compression and encryption technique suitable for real-time applications. Here, contrary to traditional compression algorithms, only special points of DCT outputs are calculated. For the encryption process, LFSR is used to generate random number and added to some DCT outputs. Both DCT algorithm and arithmetic operators used in algorithm are optimized in order to realize a compression with reduced operator requirements and to have a faster throughput. High Performance Multiplier (HPM) is being used for integer multiplications. Simulation results show that the encryption is done in the frequency domain. The throughput of this architecture is 656 M samples/s with a clock frequency of 82 MHz.

Keywords: DCT, ENCRYPTION, LFSR

I.Introduction

Security of multimedia information is used to protect the multimedia content from unauthorized access. Cryptography is the technique which is used for secure communication over the network. By using Cryptography technique readable information is converted into unreadable form. Image information is different from the text data, it has larger amount of data, higher redundancy and stronger correlation between pixels. Traditionally developed encryption algorithm such as RSA, DES is suitable for text encryption but not suitable for image encryption directly because of two reasons. One is that the image size is larger than that of text, so the traditional cryptosystems take much time to directly encrypt the image data. The other reason is that the decrypted text must be equal to the original text. However, this requirement is not necessary for image; a decrypted image containing small distortion is acceptable due to human perception [1]. Figure 1 shows how original image converted into encrypted image. At present there are many image encryption algorithms are available but these algorithms doesn't satisfy the requirement of modern cryptographic mechanism and they are prone to attacks. In the recent years, the image encryption has been developed to overcome the above disadvantages.

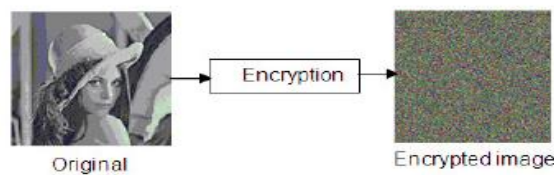


Figure1. Image Encryption System

ii.Discrete Cosine Transform

Discrete cosine transform (DCT) is one of the major compression schemes owing to its near optimal performance and has energy compaction efficiency greater than any other transform. The principle advantage of image transformation is the removal of redundancy between neighboring pixels. This leads to uncorrelated transform coefficients which can be encoded independently. DCT has that de correlation property. The transformation algorithm needs to be of low complexity. Since the DCT is separable 2-D can be obtained from two 1-D DCTs. The 2-D DCT equation is given by Equation (1)

$$C(u, v) = \alpha(u)\alpha(v) \sum_{x=0}^{N-1} \sum_{y=0}^{N-1} f(x, y) \cos \left[\frac{\pi(2x+1)u}{2N} \right] \cos \left[\frac{\pi(2y+1)v}{2N} \right],$$

For $u, v = 0, 1, 2, \dots, N-1$.

The inverse transform is defined by Equation (2)

$$f(x, y) = \sum_{u=0}^{N-1} \sum_{v=0}^{N-1} \alpha(u) \alpha(v) X(u, v) \cos \left[\frac{\pi(2x+1)u}{2N} \right] \cos \left[\frac{\pi(2y+1)v}{2N} \right],$$

For $x, y = 0, 1, 2, \dots, N-1$. The 2-D basis functions can be generated by multiplying the horizontally oriented 1-D basis functions with vertically oriented set of the same functions. In image compression, the image data is divided up into 8x8 blocks of pixels. (From this point on, each color component is processed independently, so a "pixel" means a single value, even in a color image.) A DCT is applied to each 8x8 block. DCT converts the spatial image representation into a frequency map: the low-order or "DC" term represents the average value in the block, while successive higher-order ("AC") terms represent the strength of more and more rapid changes across the width or height of the block. The highest AC term represents the strength of a cosine wave alternating from maximum to minimum at adjacent pixels.

iii. Efficient Design and Fpga Implementation of Jpeg Encoder Using Verilog Hdl

The JPEG encoder is a major component in JPEG standard which is used in image compression. It involves a complex sub-block discrete cosine transform (DCT), along with other quantization, zigzag and Entropy coding blocks. In this architecture, 2-D DCT is computed by combining two 1-D DCT that connected by a transpose buffer. For the case of 8 x 8 block region, a one-dimensional 8-point DCT followed by an internal transpose memory, followed by another one dimensional 8-point DCT provides the 2D DCT architecture. The calculation is implemented by using eight multipliers and storing the coefficients in ROMs. At the first clock, the eight inputs x_{00} to x_{07} are multiplied by the eight values in column one, resulting in eight products (P_{00} to P_{07}). At the eighth clock, the eight inputs are multiplied by the eight values in column eight resulting in eight products (P_{70} to P_{77}). From the equations for Z , the intermediate values for the first row of Z are computed. The values for Z_0 (0-7) be calculated in eight clock cycles. All 64 values of Z are calculated in 64 clock cycles and then the process is repeated. The values of Z correspond to the 1-DDCT of the input X . Once the Z values are calculated, the 2D-DCT function $Y = C * Z$.

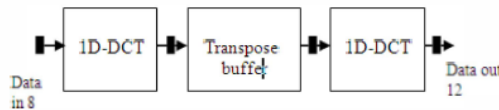


Figure 2. 2-D DCT Architecture

The maximum clock frequency is 78 MHz when implemented with a ALTERA FPGA CYCLONE-III device.

iv. Pipelined Multiplierless 2-D Dct/Idct Architecture .

The 2-D DCT architecture achieves an operating frequency of 166 MHz. This architecture is used as the core of JPEG compression hardware. The 2-D DCT calculation is made using the 2-D DCT separability property, such that the whole architecture is divided into two 1-D DCT calculations by using a transpose buffer.

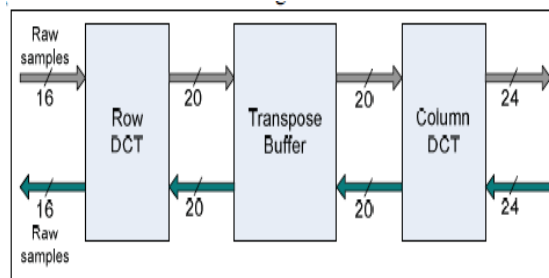


Figure .3 Architecture of 2-D DCT

Figure 3 shows the architecture of 2-D DCT. 2D-DCT/IDCT design is divided into three major blocks namely Row-DCT, Transpose Buffer, and Column-DCT. Row-DCT and Column-DCT contains both 1DDCT (Figure. 4) by Row.

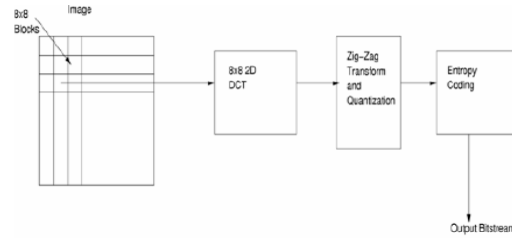


Figure. 4 Architecture of 2-D DCT

During Forward transform, 1D-DCT structure (Figure 4) is functionally active. Row-DCT block receives two 8-bit samples as an input in every cycle. Each sample is a signed 8-bit value and hence its value ranges from -128 to 127. The bit width of the transformed sample is maintained as 10-bit to accommodate 2-bit increment during

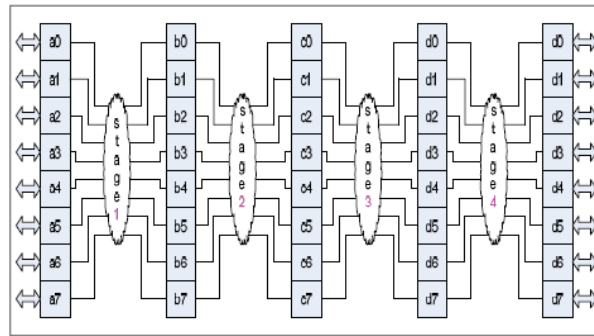


Figure .5 Four Stage Pipeline 1D-DCT.

1D-DCT computation architecture (Figure. 5) has a four stage internal pipeline shown in Figure 4. Transpose Buffer receives two 10-bit samples as an input every cycle. Each sample is a signed 10-bit value and hence its value ranges from -512 to 511. Since there is no data Manipulation in the module the output sample width remains as input sample width i.e. 10-bit. Transpose buffer has sixty-four 10-bit registers to store one 8X8 block 1D-DCT samples. Transpose operation on 8X8 block data is performed by writing the transformed samples in row-wise and reading them in column-wise and vice versa. Transpose Buffer guarantees that the nth 8X8 block data will be written into the registers after (n-1)th 8X8 block data has been completely read out for further processing. The latency of the block is 31 cycles since the data can be read only after full 8X8 block is written in the registers. Column DCT block receives two 10-bit samples as an input in every cycle. The 2D-DCT/IDCT architecture efficiently operates up to 166Mhz. Pipeline latency for the initial 8x8 block with each element of 8 bits is 45 clock cycles which is due to 7 cycles at Row-DCT, 31 cycles for Row-DCT operation to complete, 7 cycles at Column-DCT. Effectively to perform complete 2D DCT on one 8x8 will take 33 Clock cycles on availability of continuous input data to process. For operating frequency of 166 MHz, the processing time of 8x8 blocks is 0.198µs.

V. RESULT AND DISCUSSION:MODEL SIM OUTPUT:

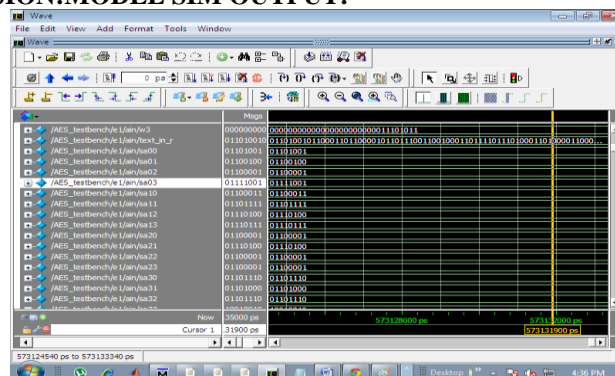


Figure 6. Simulated output.

AREA UTILIZATION REPORT:

Flow Summary	
Flow Status	Successful - Mon Nov 05 15:48:07 2012
Quartus II Version	9.0 Build 132 02/25/2009 SJ Web Edition
Revision Name	realtime
Top-level Entity Name	CODEC_MODULE
Family	Cyclone III
Device	EP3C16F484C6
Timing Models	Final
Met timing requirements	N/A
Total logic elements	3,388 / 15,408 (22 %)
Total combinational functions	3,019 / 15,408 (20 %)
Dedicated logic registers	1,747 / 15,408 (11 %)
Total registers	1747
Total pins	96 / 347 (28 %)
Total virtual pins	0
Total memory bits	0 / 516,096 (0 %)
Embedded Multiplier 9-bit elements	0 / 112 (0 %)
Total PLLs	0 / 4 (0 %)

Figure 7.Flow summary report

PERFORMANCE REPORT:

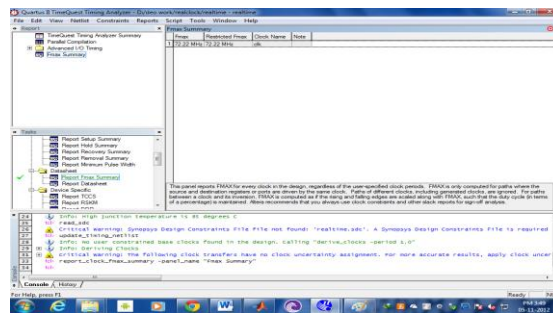


Figure 8. Fmax.Summary report of slow corner.

POWER ANALYZES:

PowerPlay Power Analyzer Summary	
PowerPlay Power Analyzer Status	Successful - Sat Jun 23 16:03:06 2012
Quartus II Version	11.0 Build 208 07/03/2011 SP 1 SJ Web Edition
Revision Name	AES_top
Top-level Entity Name	encrypt_decrypt_top
Family	Cyclone III
Device	EP3C16F484C6
Power Models	Final
Total Thermal Power Dissipation	88.58 mW
Core Dynamic Thermal Power Dissipation	0.00 mW
Core Static Thermal Power Dissipation	52.08 mW
I/O Thermal Power Dissipation	36.50 mW
Power Estimation Confidence	Low: user provided insufficient toggle rate data

Figure. 9 Power dissipation report

CONCLUSION

The proposed encryption method uses the Selective Encryption approach where the DC coefficients and some selective AC coefficients are encrypted, hence the DC coefficients carry important visual information, and it's difficult to predict the selective AC coefficients, this give a high level of security in comparison with methods mentioned above. The algorithm will not encrypt bit by bit the whole image but only selective DCT coefficients will be encrypted, and extra security has been added to the resulted encrypted blocks by using Block Shuffling method depending on two prime numbers, where these two primes will generate sequences or row and column numbers to be used in shuffling. The algorithm considered as a fast image encryption algorithm, due to the selective encryption of certain portion of the image (the DC and some AC coefficients).

References

- [1] Xiliang Liu, "Selective encryption in distribution networks: challenges and new directions", Proceedings of Communications, Internet, and Information Technology (CIIT 2003), Scottsdale, AZ, USA, Nov. 2003.
- [2] Fonteneau C., Motsch J., Babel M., and D'eforges O., "a hierarchical selective encryption technique in a scalable image codec", International Conference in Communications, Bucharest, Romania 2008.
- [3] Han Shuihua* and Yang Shuangyuan**, Non-members, "An Asymmetric Image Encryption Based on Matrix Transformation ", ecti transactions on computer and information technology vol.1, no.2 november 2005.
- [4] M. Van Droogenbroeck and R. Benedett, "Techniques for a Selective Encryption of Uncompressed and Compressed Images," in Proceedings of Advanced Concepts for Intelligent Vision Systems (ACIVS) 2002, Ghent, Belgium, Sept. 2002.

- [5] M. M. Fisch, H. Stgner, and A. Uhl, "Layered Encryption Techniques for DCT-Coded Visual Data," in European Signal Processing Conference (EUSIPCO) 2004, Vienna, Austria, Sep., 2004.
- [6] Rodrigues, J.M. Puech, W. Bors, A.G. "Selective Encryption of Human Skin in JPEG Images", IEEE International Conference on Image Processing, 2006.
- [7] L. Tang. Methods for Encrypting and Decrypting MPEG Video Data Efficiently. In Proc. ACM Multimedia, volume 3, pages 219–229, 1996.
- [8] H. Cheng and X. Li. Partial Encryption of Compressed Images and Videos. IEEE Trans. On Signal Processing, 48(8):2439–2445, Aug. 2000.
- [9] R. Lukac and K. Plataniotis. Bit-Level Based Secret Sharing for Image Encryption. Pattern Recognition, 38(5):767–772, May 2005.
- [10] C. Wu and C. Kuo. Design of Integrated Multimedia Compression and Encryption Systems. IEEE Trans. on Multimedia, 7(5):828–839, Oct. 2005.
- [11] M. V. Droogenbroeck and R. Benedett. Techniques for a Selective Encryption of Uncompressed and Compressed Images. In Proc. of Advanced Concepts for Intelligent Vision Systems (ACIVS) 2002, Ghent, Belgium, pages 90–97, Sept. 2002.

Some Dynamical Behaviors In Lorenz Model

Dr. Nabajyoti Das

Assistant Professor, Department of Mathematics, Jawaharlal Nehru College, Boko -781123
District: Kamrup, State: Assam, Country: India

Abstract

Lorenz's discovery of chaotic behaviors in nonlinear differential equations is one of the most exciting discoveries in the field of nonlinear dynamical systems. The chief aim of this paper is to develop an eigenvalue theory so that a continuous system undergoes a Hopf bifurcation, and to investigate dynamic behaviors on the **Lorenz model**:

$$\frac{dx}{dt} = -kx + ky, \quad \frac{dy}{dt} = -xz + px - y, \quad \frac{dz}{dt} = xy - qz,$$

where k, p, q are adjustable parameters.

Key Words: Nonlinear differential equation, Hopf bifurcation, Dynamic behavior, Eigenvalue theory, Chaotic behavior

2010 AMS Classification: 37 G 15, 37 G 35, 37 C 45

1. Introduction

The mathematics of differential equations is not elementary. It is one of the great achievements made possible by calculus. Lorenz's discovery of strange attractor was made in the numerical study of a set of differential equations which he had refined from mathematical models used for testing weather prediction. Although the topic of differential equations is some 300 years old, nobody would have thought it possible that differential equations could behave as chaotically as Lorenz found in his experiments [2]. In case of one-dimensional maps, the lack of hyperbolicity is usually a signal for the occurrence of bifurcations. For higher dimensional systems, these types of bifurcations also occur, but there are other possible bifurcations of periodic points as well. The most typical of these is the Hopf bifurcation. In the theory of bifurcations, a Hopf bifurcation refers to the local birth and death of a periodic solution as a pair of complex conjugate eigenvalues of the linearization around the fixed point which crosses the imaginary axis of the complex plane as the parameter varies. Under reasonably generic assumptions about the dynamical system, we can expect to see a small amplitude limit cycle branching from the fixed point [3-8]. We first highlight some related concepts for completeness of our exploration.

1.1 Limit cycles

A cyclic or periodic solution of a nonlinear dynamical system corresponds to a closed loop trajectories in the state space. A trajectory point on one of these loops continues to cycle around that loop for all time. These loops are called **cycles**, and if trajectories in the neighborhood to the cycle are attracted toward it, we call the cycle a **limit cycle** [2, 5].

1.2 The Hopf bifurcation theorem:

In this discussion we will restrict our discussion on second-order systems of nonlinear ordinary differential equations, although almost all the results and discussions given below can be extended to general n th-order systems.

We consider the system $\frac{d\bar{x}}{dt} = \xi(\bar{x}; R), \quad \bar{x} \in \mathfrak{R}^2$ (1.1)

where R denotes a real parameter on an interval I . We assume that the system is well defined, with certain smoothness on the nonlinear vector field ξ , and has a unique solution for each given initial value $\bar{x}(t_0) = \bar{x}$ for each fixed $R \in I$. We also assume that the system has an equilibrium point $\bar{x}^*(R)$ and that the associated Jacobian

$J = \frac{\partial \xi}{\partial \bar{\mathbf{x}}} \Big|_{\bar{\mathbf{x}}=\bar{\mathbf{x}}^*}$ has a single pair of complex conjugate eigenvalues $\eta(\mathbf{R}), \overline{\eta(\mathbf{R})} = \text{Re} \eta \pm i \text{Im} \eta$. Now suppose that this pair of eigenvalues has the largest real part of all the eigenvalues and is such that in a small neighborhood of a bifurcation value R_c , (i) $\text{Re} \eta < 0$ if $R < R_c$, (ii) $\text{Re} \eta = 0, \text{Im} \eta \neq 0$ if $R = R_c$ and (iii) $\text{Re} \eta > 0$ if $R > R_c$. Then, in a small neighborhood of $R_c, R > R_c$, the steady state is unstable by growing oscillations and, at least, a small amplitude limit cycle periodic solution exists about the equilibrium point. The appearance of periodic solutions (all depend on the particular nonlinear function ξ) out of an equilibrium state is called Hopf bifurcation. When the parameter R is continuously varied near the criticality R_c , periodic solutions may emerge for $R < R_c$ (this case is referred to as **supercritical bifurcation**) or for $R > R_c$ (which is referred to as **subcritical bifurcation**) [5-7]. Armed with these concepts, we now concentrate to our main study and investigation.

1.3 The principal investigation

We consider a two-dimensional system $\dot{\bar{\mathbf{x}}} = \xi(\bar{\mathbf{x}}; R), R \in \mathfrak{R}, \bar{\mathbf{x}} = (x, y) \in \mathfrak{R}^2$ where ξ depends smoothly on the real variable parameter R such that for each R near the origin $(0, 0)$ there is an equilibrium point $\bar{\mathbf{x}}^*(R)$ with the Jacobian matrix $D\xi_{\bar{\mathbf{x}}}(\bar{\mathbf{x}}^*(b), b)$ having a complex conjugate pair of eigenvalues which cross the imaginary axis as the parameter b passes through $(0, 0)$. Using complex coordinate $z = x + iy$, the system can be expressed in the variable z as $\dot{z} = \eta z + A_1 z^2 + B_1 z \bar{z} + C_1 \bar{z}^2 + M_1 z^2 \bar{z} + \dots$ (1.2) where A_1, B_1, C_1, M_1 are complex constants. By making a suitable change of variables the system can be transformed to a normal form:

$$\dot{w} = w(\eta + L|w|^2) + o(|w|^4), \quad (1.3)$$

where w, L are both complex numbers. We write $L = D + iE; D, E \in \mathfrak{R}$. The behavior of the system (1.3) is most conveniently studied using polar coordinate $w = re^{i\theta}$. From this we obtain, $\dot{w} = e^{i\theta} \dot{r} + ire^{i\theta} \dot{\theta}$. Hence $\dot{r} = r^{-1} \text{Re}(\bar{w} \dot{w})$ and $\dot{\theta} = r^{-2} \text{Im}(\bar{w} \dot{w})$ and then (1.3) implies

$$\dot{r} = Dr^3 + o(r^4), \quad \dot{\theta} = \psi + o(r^2) \quad (1.4)$$

Supercritical and subcritical Hopf bifurcation occur according as $D < 0$ and $D > 0$ respectively. If $D = 0$, considering high order terms we can draw the same conclusion. Now to determine k , we apply the transformation $w = z + \delta z^2 + \rho z \bar{z} + \theta \bar{z}^2$. We have

$$\begin{aligned} \dot{w} &= \dot{z} + 2\delta z \dot{z} + \rho \bar{z} \dot{z} + \rho z \dot{\bar{z}} + 2\theta \bar{z} \dot{\bar{z}} \\ &= \eta z + A_1 z^2 + B_1 z \bar{z} + C_1 \bar{z}^2 + M_1 z^2 \bar{z} + 2\delta z(\eta z + B_1 z \bar{z}) + \\ &\quad \rho \bar{z}(\eta z + A_1 z^2) + \rho z(\eta \bar{z} + \bar{B}_1 z \bar{z}) + 2\theta \bar{z}(\eta \bar{z} + \bar{C}_1 \bar{z}^2) \end{aligned}$$

keeping only terms upto second order, where cubic terms are neglected other than $z^2 \bar{z}$. We eliminate the quadratic terms by putting

$$\delta = -A_1 / \eta = iA_1 / \psi, \quad \rho = -iB_1 / \psi, \quad \theta = -iC_1 / 3\psi.$$

Then we obtain

$$\dot{w} = \eta w + \left(M_1 + iA_1 B_1 / \psi - i|B_1|^2 / \psi - 2i|C_1|^2 / 3\psi \right) w^2 \bar{w},$$

We conclude that $L = M_1 + iA_1 B_1 / \psi - i|B_1|^2 / \psi - 2i|C_1|^2 / 3\psi$.

and

$$D = \operatorname{Re}(M_1 + iA_1B_1 / \psi)$$

$$= \operatorname{Re}(M_1) - \psi^{-1} \operatorname{Im}(A_1B_1).$$

1.4. Extension to three order differential equations

Let us assume that we have a three-dimensional system:

$$\dot{\bar{\mathbf{x}}} = \xi(\bar{\mathbf{x}}), \quad \bar{\mathbf{x}} = (x, y, z)^T, (x, y, z) \in \mathfrak{R}^3$$

which has an equilibrium point for which there is one negative eigenvalue and an imaginary pair. The behavior of the system near the equilibrium point can be analyzed by a reduction of the system to a two-dimensional one, as follows. First we choose coordinates so that the equilibrium point is the origin and so that the linearised system is

$$\dot{v} = \rho v, \quad \dot{z} = \lambda z$$

where v is a real variable and z is complex, and $\rho < 0$, $\lambda = i\sigma$.

We can now express the system as

$$\dot{v} = \rho v + \alpha v z + \bar{\alpha} v \bar{z} + \gamma z^2 + \delta z \bar{z} + \bar{\gamma} \bar{z}^2 + \dots$$

$$\dot{z} = \lambda z + p v z + q v \bar{z} + r z^2 + s z \bar{z} + t \bar{z}^2 + d z^2 \bar{z} + \dots$$

If the equation for v were of the form $\dot{v} = \rho v + v f(v, z)$ then the plane $v = 0$ would be invariant, in the sense that solutions starting on this plane stay on it, and we could restrict attention to the behavior on this plane. What we do below is to find a change of variables which converts the system into one which is sufficiently close to this form. We try the change of variables

$$v = w + a z^2 + b z \bar{z} + \bar{a} \bar{z}^2, \text{ where } b \text{ is real.}$$

We obtain

$$\dot{w} = \rho w + \rho a z^2 + \rho b z \bar{z} + \rho \bar{a} \bar{z}^2 + \alpha w z + \bar{\alpha} w \bar{z} + \gamma z^2 + \delta z \bar{z} + \bar{\gamma} \bar{z}^2 - 2a \lambda z^2 - 2\bar{a} \bar{\lambda} \bar{z}^2,$$

neglecting terms of order 3 and higher. Then if we choose

$$a = \gamma \div (2i\sigma - \rho)$$

and

$$b = -\delta \div \rho$$

We have

$$\dot{w} = \rho w + \alpha w z + \bar{\alpha} w \bar{z} + \dots$$

which is of the desired form (as far as of second-order, which turns out to be sufficient). Putting $w = 0$, in the equation for \dot{z} , and retaining only terms of order second and those involving $z^2 \bar{z}$, we obtain

$$\dot{z} = \lambda z + r z^2 + s z \bar{z} + t \bar{z}^2 + \left(\frac{-p\delta}{\rho} + \frac{q\gamma}{2i\sigma - \rho} + d \right) z^2 \bar{z}$$

and using the two-dimensional theory we obtain

$$D = \operatorname{Real part of} \left(\frac{-p\delta}{\rho} + \frac{q\gamma}{2i\sigma - \rho} + d + \frac{irs}{\sigma} \right).$$

Supercritical and subcritical Hopf bifurcation occur according as $D < 0$ and $D > 0$ respectively. If $D = 0$, considering high order terms we can draw the same conclusions.

1.5 Our main study

For our main study we consider the **Lorenz model**:

$$\frac{dx}{dt} = -kx + ky, \quad \frac{dy}{dt} = -xz + px - y, \quad \frac{dz}{dt} = xy - qz. \quad (1.5)$$

For our purpose, the parameters are fixed as in the Lorenz model as given below [8]:

$$k = 10, \quad p = 28, \quad q = \frac{8}{3}$$

With these parameter values the equilibrium points $(x_i^*, y_i^*, z_i^*), i = 1, 2, 3$ of the system (1.5) are given by setting the left-hand sides zero and solving the resulting system of equations, to get

$$(x_1^* = 0, y_1^* = 0, z_1^* = 0),$$

$$\text{or } (x_2^* = -8.485281374238571, y_2^* = -8.485281374238571, z_2^* = 27.000000000000004),$$

$$\text{or } (x_3^* = 8.485281374238571, y_3^* = 8.485281374238571, z_3^* = 27.000000000000004).$$

Out of these equilibrium

points $(x_3^* = 8.485281374238571, y_3^* = 8.485281374238571, z_3^* = 27.000000000000004)$

is suitable for our purpose.

Let us take a linear transformation which moves the equilibrium point to the origin. We take $u = x - x_3^*, v = y - y_3^*$

and $w = z - z_3^*$. Then the system (1.5) becomes

$$\frac{du}{dt} = -k(u + x_3^*) + k(v + y_3^*) = 0u - 10v + 10w \quad (1.6)$$

$$\frac{dv}{dt} = -(u + x_3^*)(w + z_3^*) + r(u + x_3^*) - (v + y_3^*) \quad (1.7)$$

$$= -5.68434 \times 10^{-14}v + u(1 - w) - 8.48528w$$

$$\frac{dw}{dt} = (u + x_3^*)(v + y_3^*) - q(w + z_3^*) \quad (1.8)$$

$$= -5.68434 \times 10^{-14}v + u(1 - w) - 8.48528w$$

The matrix of linearized system is then of the form

$$G = \begin{bmatrix} -10 & 10 & 0 \\ 1 & -1 & -8.485281374238571 \\ 8.485281374238571 & 8.485281374238571 & -2.6666666666666665 \end{bmatrix}$$

The eigenvalues $\rho, \lambda_1, \lambda_2$ of M are

$$\rho = -13.854577914596039,$$

$$\lambda_1 = 0.09395562396468556 + 10.194505220927851i,$$

$$\lambda_2 = 0.09395562396468556 - 10.194505220927851i$$

Let us take
$$H = \begin{bmatrix} \rho & 0 & 0 \\ 0 & \lambda_1 & 0 \\ 0 & 0 & \lambda_2 \end{bmatrix}$$

as the diagonal matrix. Then we

$$\text{obtain } G^{-1}H = \begin{bmatrix} 0.718386 & -0.00173992 - 0.188787i & 0.00553639 - 0.600717i \\ -0.667072 & -0.00173992 - 0.188787i & 0.00553639 - 0.600717i \\ 0.163278 & -0.0110728 - 1.20143i & 0 + 0i \end{bmatrix}$$

In order to make the linearized system into a diagonal form, we make the coordinate change by $G^{-1}HW$, where U is the column matrix, $W = [f, g, h]^T$.

Now

$$G^{-1}HW = \begin{bmatrix} (0.718386 + 0i)f & -(0.00173992 + 0.188787i)g & (0.00553639 - 0.600717i)h \\ (-0.667072 + 0i)f & -(0.00173992 + 0.188787i)g & (0.00553639 - 0.600717i)h \\ (0.163278 + 0i)f & -(0.0110728 + 1.20143i)g & (0 + 0i)h \end{bmatrix} \text{Put in}$$

$$u = (0.718386 + 0i)f - (0.00173992 + 0.188787i)g + (0.00553639 - 0.600717i)h,$$

$$g \quad v = (-0.667072 + 0i)f - (0.00173992 + 0.188787i)g + (0.00553639 - 0.600717i)h,$$

$$w = (0.163278 + 0i)f - (0.0110728 + 1.20143i)g + (0 + 0i)h$$

in equations (1.6) and (1.7), we get

$$\frac{du}{dt} = 10((-0.667072 + 0i)f - (0.00173992 + 0.188787i)g + (0.00553639 - 0.600717i)h) \\ + 10((0.163278 + 0i)f - (0.0110728 + 1.20143i)g + (0 + 0i)h)$$

$$\frac{dv}{dt} = -5.68434 \times 10^{-14}((-0.667072 + 0i)f - (0.00173992 + 0.188787i)g + (0.00553639 - \\ 0.600717i)h) + ((0.718386 + 0i)f - (0.00173992 + 0.188787i)g + (0.00553639 - \\ 0.600717i)h)(1 - ((0.163278 + 0i)f - (0.0110728 + 1.20143i)g)) - 8.48528((0.163278 \\ + 0i)f - (0.0110728 + 1.20143i)g) \quad \text{Finally,}$$

under the stated transformation (as described in General theory) the system becomes

$$\frac{du}{dt} = -7.18386f + 0fg + 0fh + 0g^2 + 0gh + (-0.0553639 + 6.00717i)h^2 + \dots \quad (1.9)$$

$$\frac{dv}{dt} = (0.099556 + 10.1945i)g + (0.00823861 + 0.893918i)fg + (-0.000903969 - 0.0980837i)fh \\ + (0.226796 - 0.0041808i)g^2 + 0.721783gh + 0h^2 + 0g^2h + \dots \quad (1.10)$$

From above, we obtain

$$\rho = \text{Coefficient of } f \text{ in (1.9)} = -7.18386,$$

$$p = \text{Coefficient of } fg \text{ in (1.10)} = 0.00823861 + 0.893918i,$$

$$\delta = \text{Coefficient of } gh \text{ in (1.9)} = 0$$

$$q = \text{Coefficient of } fh \text{ in (1.10)} = -0.000903969 - 0.0980837i,$$

$$\gamma = \text{Coefficient of } g^2 \text{ in (1.9)} = 0$$

$$d = \text{Coefficient of } g^2h \text{ in (1.10)} = 0,$$

$$r = \text{Coefficient of } g^2 \text{ in (1.10)} = 0.226796 - 0.0041808i,$$

$$s = \text{Coefficient of } gh \text{ in (1.10)} = 0.721783,$$

$$\sigma = \text{Imaginary part of eigenvalues} = -13.854578\dots$$

Using the above values we can calculate the value of k as

$$D = \text{Real part of } \left(\frac{-p\delta}{\rho} + \frac{q\gamma}{2i\sigma - \rho} + d + \frac{irs}{\sigma} \right) \\ \approx -0.000217807$$

Hence, we have a supercritical Hopf bifurcation. Of course, this bifurcation is studied in a **rigorous manner**. Similarly, we can study the Hopf bifurcation of a given system for different values of the parameters.

[For all numerical results, used in this paper, the Computer package "MATHEMATICA" is used]

2. Conclusion:

We think, our method is quite suitable for obtaining Hopf bifurcation for any order nonlinear differential equation, if Hopf bifurcation exists.

3. Acknowledgement

I am grateful to **Dr. Tarini Kumar Dutta**, Senior Professor of the Department of Mathematics, Gauhati University, Assam: India, for a valuable suggestion for the improvement of this research paper.

4. References:

- [1] Das, N and Dutta, T. K., *Determination of supercritical and subcritical Hopf bifurcation on a two-dimensional chaotic model*, International Journal of Advance Scientific Research and Technology, Issue2, Vol. 1, February, 2012.
- [2] Hilborn, Robert C., *Chaos and Nonlinear Dynamics*, Oxford University Press, 1994
- [3] Hopf, E., *Abzweigung einer periodischen Lösung von einer stationären Lösung eines Differential systems*, Ber. Verh. Sachs. Akad. Wiss. Leipzig Math.-Nat. 94(1942), 3-22, Translation to English with commentary by L. Howard and N. Kopell, in [81; 163-205]
- [4] Marsden, J. E. and McCracken, M., *The Hopf Bifurcation and Its Applications*, Springer-Verlag, New York, 1976
- [5] Moiola, J. L. and Chen, G., *Hopf Bifurcation Analysis: a frequency domain approach*, World Scientific, 1996
- [6] Murray, J. D., *Mathematical Biology I: An Introduction*, Third Edition (2002), Springer
- [7] Roose, D. and Hlavacek, V., *A Direct Method for the computation of Hopf bifurcation points*, SIAM J. APPL. MATH., Vol. 45, No. 6, December 1985
- [8] Peitgen H.O., Jürgens H. and Saupe D., "Chaos and Fractal", New Frontiers of Science, Springer Verlag, 1992

A Novel Parallel Domain Focused Crawler for Reduction in Load on the Network

Rajender Nath¹, Naresh Kumar²

¹Professor, DCSA, Kurukshetra University, Kurukshetra, Haryana, India.

²Assistant Professor, MSIT, JanakPuri, New Delhi, India.

Abstract

World Wide Web is a collection of hyperlinked documents available in HTML format. Due to the growing and dynamic nature of the web, it has become a challenge to traverse all the URLs available in the web documents. The list of URL is very huge and so it is difficult to refresh it quickly as 40% of web pages change daily. Due to which more of the network resources specifically bandwidth are consumed by the web crawlers to keep the repository up to date. So, this paper proposes Parallel Domain Focused Crawler that searches and retrieves the Web pages from the Web, which are related to a specific domain only and skips irrelevant domains. It makes use of change in frequency of webpage change to fetch a web page from the web. It downloads only those pages that are changed and ignores those pages that are not modified since the last crawl. Experimentally, it has been found that the proposed crawler reduces the load on the network up to 40%, which is considerable.

Keywords: WWW, search engine, mobile crawler, network resources, Internet traffic, web change behavior.

1. Introduction

World Wide Web is a system of interlinked hypertext documents which is growing rapidly from few thousands of pages in 1993 to more than several billion of pages at present [1]. It is based on client server architecture that allows a user to search anything by providing the keywords to a search engine, which in turn collects and returns the required web pages from the Internet. Due to large number of pages present on the web, the search engine depends upon crawlers for collection of required pages. A crawler [15] (also called spider, walker, wanderer, worm or bot) uses the hyperlinks present in the document to download and store the web pages for the search engine. A search engine tries to cover the whole web and serve queries concerning to all possible topics. But according to [5], any search engine can cover only 16% of the entire web. And one study in [2], shows that the documents available on the web are very dynamic in nature and 40% of its contents changes daily. So, according to a study [3], to maintain the repository of search engine up to date crawler should revisit the web again and again. Due to which, the CPU utilisation, disk space, and network bandwidth etc. are consumed and overload the network. Currently web crawlers have indexed billions of web pages and 40% of Internet traffic and bandwidth utilization is due to web crawlers that download the web pages for different search engines [4]. Many suggestions [6][7][8][9] were given to maintain the web repository by using mobile crawlers. In order to filter out unwanted data locally these mobile crawlers were sent to the remote site where the data actually resides. These crawlers can reduce the network load automatically by sending the filtered data only. This paper proposes an alternate approach by using the mobile crawlers and frequency of change. These crawlers go to the remote sites, remains there and skip those pages that are not modified since the last crawl and send only the compressed modified web pages to search engine for indexing. The rest of the paper is organized as follows: The related work is discussed in section 2. Section 3 describes the problems with current crawling techniques. Section 4 describes the proposed architecture of the mobile crawler system. Sections 5 describe the URL allocation approach used by the system and section 6 describe the working of the proposed system. Section 7 shows the experimental evaluation of proposed work. Section 8 concludes the paper.

2. Related Work

In [8], last modified date, number of keywords and number of URLs were used to check the change in the page. Their purpose was to determine page change behavior, load on the network and bandwidth preservation. It was found that 63% of the total pages changed that need to be downloading and indexing, thus reducing the 37% pages on the network. It was also shown that proposed scheme reduce the load on the network to one fourth through the use of compression and preserving bandwidth of network. A fast HTML web page change detection approach based on hashing and reducing the number of similarity computations was purposed by [10]. For change detection, the web page is first converted into the XML tree structure. Two trees were compared to calculate the similarity computation. The sub trees with highest similarity were considered to be more similar. Furthermore to speed up the algorithm Hashing was used in order to provide the direct access during comparison. The experimental results have shown that web page changes were detected in seconds for small

and medium sized web pages and few seconds for large web pages. In [11], the HTML structure (tags and attributes) were taken into consideration to improve the crawling performance. Based on this structure, a robot might use the text of certain HTML elements to prioritise the documents for downloading. They also calculated the relevancy of the text to a topic by considering all the words case insensitive. They performed his experiment on *satellite navigation systems* and showed that the speed of downloading was increased. Focused Structure Parallel Crawler proposed by [12], used click stream based Link Independent web page importance metric to minimize the communication overhead. They used parallel agent's collaboration approach without using any central coordinator, the concept of crawl history, duplicate detector; distiller and classifier etc. to prove the relevancy of document with query and achieve more precision in the performance of the crawler. A distributed and parallel crawling system was proposed by [1] that shows more coverage of the web and decrease the bandwidth consumption but such type of system just distribute and localized the load but did not do anything in reducing the load. A Novel Focused Crawling Approach proposed by [13] of crawl the pages related to a specific topic based on the terms of genre and content information. To retrieve the relevant pages they applied the querying policy on the syllabi of computer science and found that the proposed architecture returns 90% relevant results and good level of precision.

The focused crawlers reported by [5][6][9][14] have the following limitations:

- [1]. The relevancy of any web page can be determined after downloading it on the search engine end only. So once a page is downloaded then what is the benefit of filtering it, because all the network resources are already used while downloading those pages.
- [2]. The another limitation related to first one is the load on the network and bandwidth is considerably large due to the downloading.
- [3]. One problem is related to the attemptation of the web space i.e. given a URL to fetch the web page require to determine quickly to which domain the URL belongs to.

3. Problem Formulation

Many mobile crawling techniques [3][7][8][12] were introduced to overcome the limitations mentioned in previous section. These techniques describe that the mobile crawlers, crawl the web pages and stay there on the remote system to monitor any change that can take place in the pages allotted to them. But these techniques also have problems given below:

- [1]. The problem of iterative computation for every web document affects the performance of the crawler.
- [2]. If the mobile web crawler stays in the memory then it consumes significant segment of memory. So what happens when more mobile crawlers from different search engines stay there? This can produce scarcity of memory on remote system site because remote system have to perform there own task also.
- [3]. Due to security reasons, remote site may not allow the mobile web crawler to stay there at the remote site.
- [4]. If a web page changes rapidly and every time a mobile crawler catches these changes and send these changed page to search engine. Then it again consumes more resources of the network including the processing of the system. To overcome these limitations, this paper proposes architecture for mobile web crawlers that use the concept of different domains and frequency change estimator for efficient URL delegation.

4. Proposed Parallel Domain Focused Crawler (PDFC)

The mobile crawlers are developed as mobile agents and sent to the web servers where they download the web documents, process them and filter out non-modified web pages. Finally, the modified web pages after compression are transmitted back to the Search Engine. The architecture of the proposed PDFC is shown in Figure 1. The major components of the PDFC are Analyzer Module (AM), Old Database File (ODF), Link Extractor (LE), Domain Name Director (DND), Crawler Hand (CH), Crawler Manager (CM), Statistics Data Base (SD), Frequency change Estimator (FCE), Remote Site/Server (RS), Comparator (CoM). Each of these modules are discussed below:

4.1 Crawler Manager (CM)

The main tasks of CM are generation of mobile crawler, delegation of URL's to the mobile crawler for crawling the web pages based on the information taken from the FCE, construction / updation of the data in ODF, updation of SD, receivable of the crawled pages from the RS, decompression and indexing them. After extracting the URL from the downloaded web pages by LE, the task of URL delegation to the mobile crawlers are also performed by the CM with the help of CoM Module.

4.2 Domain Name Director (DND)

The job of DND is to select the specific domain for the URLs that are coming from the URL queue and forward it to the particular DNS queue (such as .org, .com, .edu etc.). Given a URL to the DNS queue, the number of pages to be downloaded and time depends upon the URL itself. The distribution of the load on the CH is likely to be different depending on the frequency of demand of the domains.

4.3 Frequency Change Estimator (FCE)

This module identifies whether two versions of a web document are same or not and thus helps to decide whether the existing web page in the repository should be replaced with changed one or not. This module is the part of the client site and remains there. The FCE is used to calculate the probability of the page change means in how many days a page gets changed. This module maintains the page change frequency of every page at the SE and updates this information in SD every time a page is crawled. This information about the pages helps SE in deciding that which page is to be re-crawled and when. The CM uses this information for URL allocation to the mobile crawlers. Thus, the FCE filter out all those pages at the client site that has low probability of change and reduces the work load of the crawler on the network. The frequency change (F) is defined as follows:

$F = -1$ (for those URLs which are traversed first time).

$F = 0$ (for those pages which change at a rapid rate, so frequency parameter cannot be applied for such pages).

$F = N$ ($N > 0$; $N =$ number of days since last change of page occurred).

4.4 Statistical Database (SD)

This module is maintained at the SE and contains information about all the pages crawled by the mobile crawlers. This module has the following fields:

- a) *Name of URL*: It stores the name of the web page that is indexed by the SE in its database after downloading.

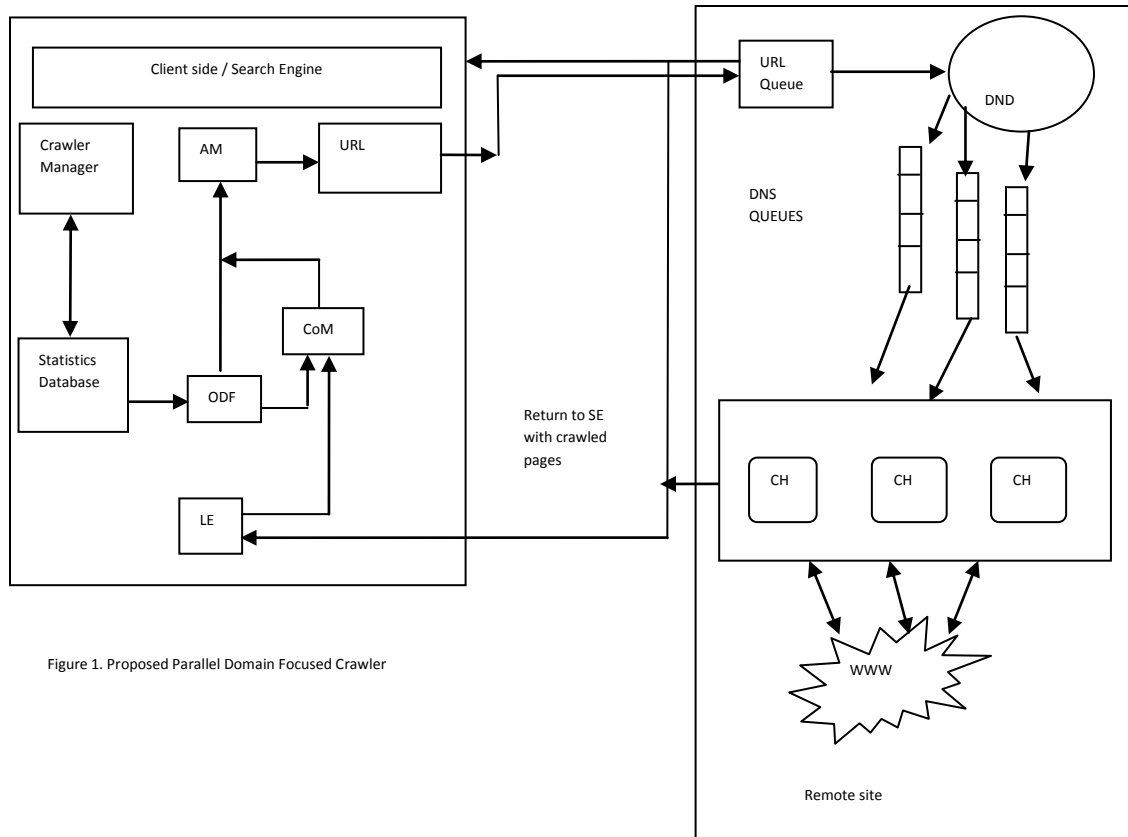


Figure 1. Proposed Parallel Domain Focused Crawler

- a) *Parent URL*: It depicts the original URL entered by the user corresponding to which the URLs in the 'Name of URL' field were fetched. For example: say the URL entered by the user is <http://xkcd.com/>. Then this URL serves as the parent URL and <http://dynamic.xkcd.com/random/comic> serves as name of URL.
- b) *ASCII count*: It shows the 'ASCII count' of a web page. It should be computed whenever the web page is downloaded.
- c) *Last Modified Date*: It refers to the date when the particular URL had been crawled the last time.
- d) *Frequency of change*: It refers to the number of days that it may take for a particular web page to change its content.
- e) *File Path*: The location of the HTML file stored in the repository of computer (at SE end) is reflected in this field.

4.5 Old Database File (ODF)

The CM constructs one ODF for each mobile crawler and contains statistics about each HTML page to be crawled. This statistics is taken from the SD. This module is sent with the corresponding mobile crawler on to the RS with two things i.e. 'Name of URL' and "ASCII count" value of web page available in the repository.

4.6 Comparator Module (CoM)

The CoM checks to see if the downloading period of a web page is reached. If yes, then send this URL of Web page to AM for further processing otherwise reject this URL. The 'Last Modified Date' and 'Frequency of Change' is taken from the ODF that were computed when the URL was previously crawled. During this comparison if the difference between the current date and the last-modified date is less than or equal to the value of "frequency of change" field, then the new URL is not processed, rather, it is ignored. On the other hand, in case the difference between these two is greater than the "frequency of change" value, then web page is processed. This module also works on both sides i.e. SE and RS. At the RS it takes the current 'ASCII count' of crawled page and compares it with the old 'ASCII count' of the same page. If both are different then it means the web page is updated and sends to SE, otherwise reject the web page.

4.7 Analyzer Module (AM)

It works on the both sites (i.e. on the SE and RS). It scans and analyzes all the pages crawled by the mobile crawlers and extract 'ASCII count' from ODF for each web page. It also calculates the 'ASCII count' of the fetched page at the RS. It is sent at the RS with the mobile crawler and a copy of it is kept in the secondary memory of RS for future use by the mobile crawler.

4.8 Link Extractor (LE)

The main aim of LE is to take the downloaded web page coming from the CH to SE. This module extracts all the links from this web page and gives them to the CoM module for further processing.

4.9 Crawler Hand (CH)

CH as shown in figure 2 retrieves the URL from the DNS queue in FCFS fashion and sends request to web server. The Crawl Worker first searches the robot.txt file maintained by the web server to verify whether the URL, it is looking for to be download, is permitted for downloading or not. If it is among the list of restricted URLs then CH stops downloading process and discards the URL, otherwise the web document for corresponding URL is fetched and send to the Manager (as shown in Figure 2). The Manager calculates the corresponding 'ASCII count' of that web page with the help of ASCII calculator. CoM Compares the new and old 'ASCII count' of the corresponding page, if they are same then reject the web page otherwise send this page to SE after compression.

4.9.1 Crawling Process

Crawling process takes URL from the crawler worker and fetch the corresponding Web page (see Figure 2). These downloaded Web pages are sent to manager for further processing. After that the new URL is taken from the Crawler Worker and fetches the next Web page. The Web Crawler can run multiple Crawling Processes at a time, so they can share the load in between different processes. Each CH is independent of other means they have no communication with each other because the crawling hand gets the seeds URL from the independent and respective DNS queue only.

5. URL Allocation Approach

Once the URLs are fetched from URL queue then they are distributed using DND to the corresponding domain queues. The CH takes the URL's from the respective domain queue. It is assumed that the pages of one domain should remain on a single server. So, the CH accepts only that page that belongs to the same server domain only. Also ODF is sent with each CH that contains information about the pages to be crawled. The CM works as given below.

- [1]. If the FCE has a value $F = 0$, then it is assumed that the information about the page change is not available because the web page is frequently changed and it is required to be processed the URL again in order to refresh the information available to SE. Furthermore, there is no need to send these pages to AM for scanning and analysis to collect the statistics about them in SD.
- [2]. If the FCE has a value $F = -1$, it shows that the URL are not previously visited. Hence the URL should be crawled in order to get updated information on the SE end. Hence forward getting the web page at the SE end, the AM scans and analyzes the web page in order to get the statistics about the web page.

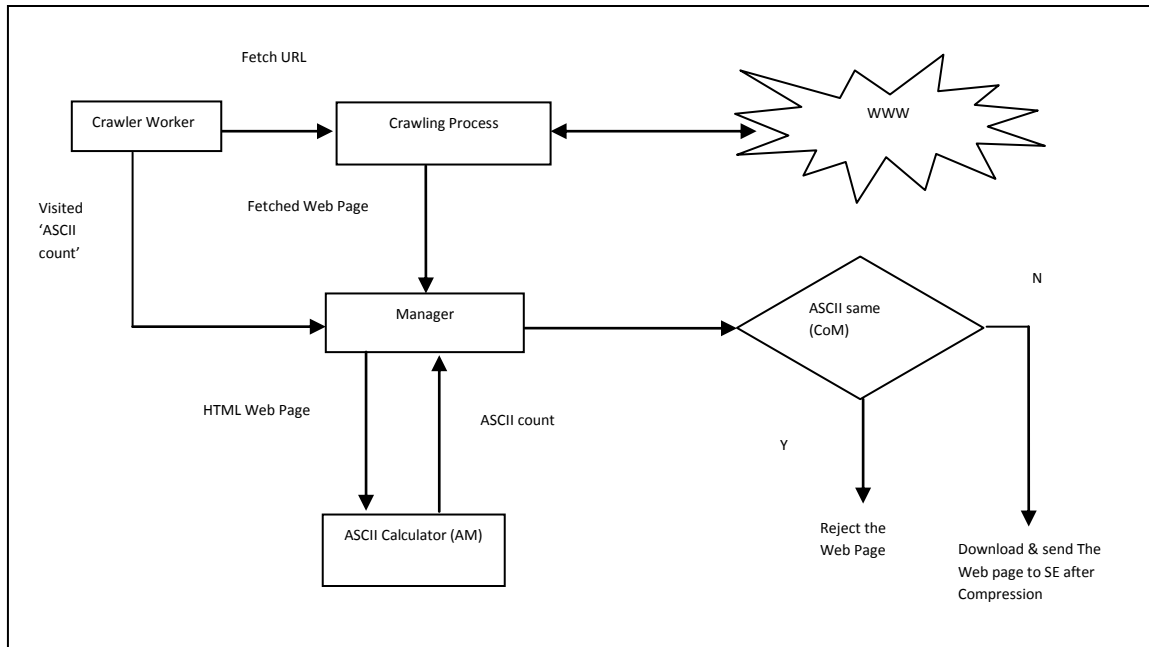


Figure 2. Crawler Hand and Web Page Change Detection

- [3]. if the FCE has a value $F = N$, it shows that in how many days the page is to be crawled. This is analyzed based on the statistics available in SD. Whenever the exact time of frequency of change occurs then the corresponding URL is assigned to the crawler for downloading and statistics of web page is not required to be sent and the value of F in FCE is not updated correspondingly. Otherwise the web page is fetched and sent to the SE in order to update the information at the client side. Also, the web page is sent to the AM that will update the Statistics of the URL accordingly. In this way, the load on the network is reduced by retrieving and indexing the web pages directly whose F value in FCE is either 0 or -1. This reduction is achieved by not storing any information in ODF or not sending any information about the web page with the crawler on the RS. It also saves the CPU time on RS used in the analysis of these web pages.

6. Working of The PDFC

The working of the PDFC is given in flow chart as shown in Figure 3. The mobile crawler used in PDFC takes the ODF, the CoM and the AM with it on the RS from where the pages are to be crawled. The mobile crawler accesses those pages one by one whose URL's are given in the ODF, calculate the 'ASCII count' of the web page and compare this new ASCII count with the previous ASCII count of the same webpage. If both are equal then this webpage is rejected. Otherwise, the web page corresponding to the URL is sent to the SE for updation of information. This is not possible all the times that last modify date is available to SE for all the web page. So, all the web page whose last modify date is not available, is directly downloaded and sent to the SE for updation without any comparison of 'ASCII count' at the RS.

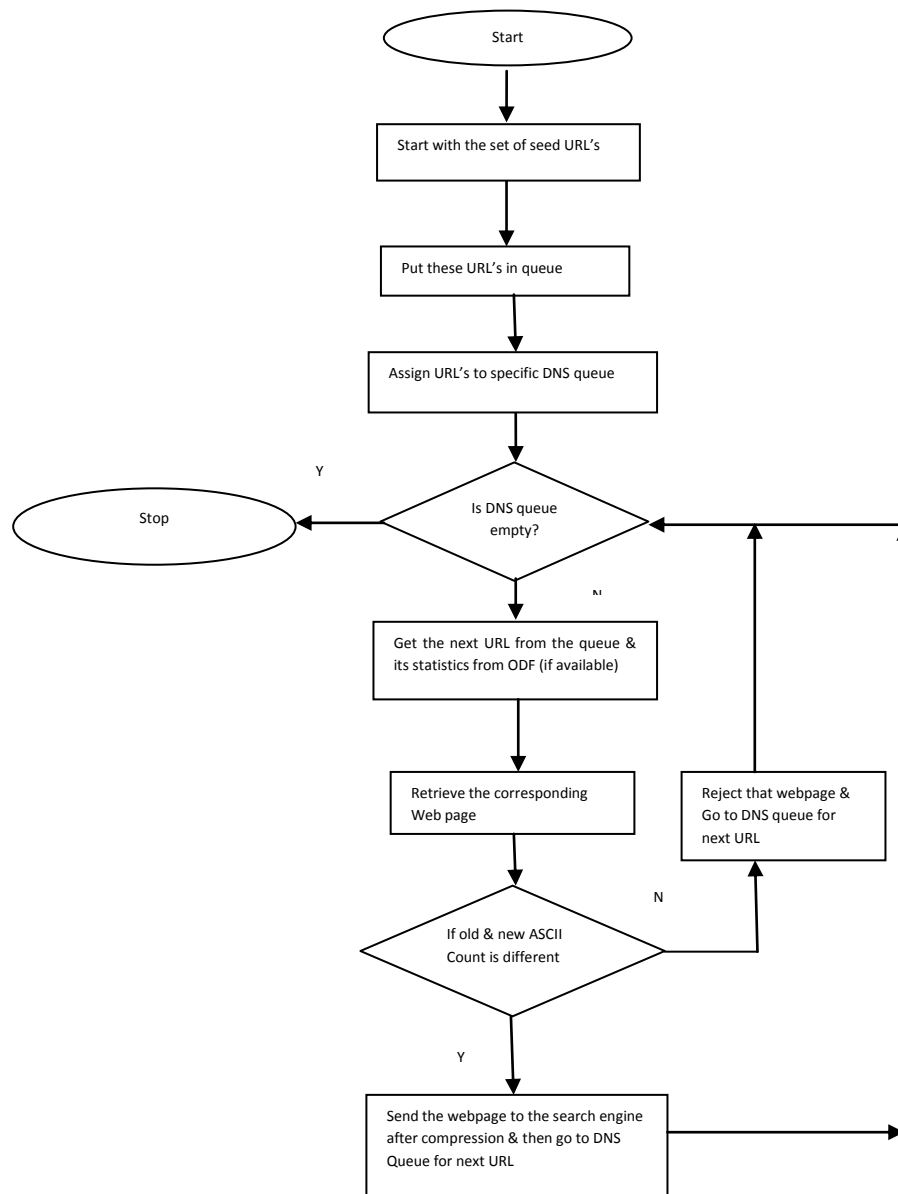


Figure 3. Flow Chart for Working of PDFC

7. Experimental Evaluation of the PDFC

PDFC is implemented in Java programming language using Netbeans IDE 7.0.1 (on Windows XP platform). The application required the JDK 1.6 version to function optimally. The database for storing information was created in MS Access. One hundred web sites were selected to perform the experiment and home pages of these web sites were downloaded. The experiment was carried over for thirty days and the data obtained from the experiment are available with the authors. On an average, each page was of 10 KB. The crawler of the PDFC visited the Remote Site (RS) and analyzed the pages for modification since the last crawl and returned only those pages that were actually modified. The crawler compares 'ASCII count' value available in ODF with 'ASCII count' value of the web page calculated at RS. The proposed PDFC is compared with the existing mobile crawlers on the following three parameters: Page change behavior, Load on the network and Bandwidth preserved are described with the help of bar charts.

[1]. **Page Change Behavior** – The page change behavior was computed based on the data collected during visiting 100 pages for 30 days. This Page change behavior was obtained by identifying the frequently changed pages and frequency of changed pages. The web pages that were found changed on every crawl are called frequently page change and the web pages that were found changed after an interval (not at a specific time) are called frequency of page change. This interval was measured in number of days. Frequency of page change is computed by summing the ASCII value of each character of a crawled HTML web page. Then compare this new computed ASCII count value with the old ASCII count value of the same webpage. If both of these values are found different then it means the newly crawled webpage is updated otherwise page is not updated. Based on above discussion and corresponding parameter representation explained in section 4.3, it was found that out of 100 web pages on an average 19 web pages were found changed due to frequency of page change and 41 pages were retrieved directly based on freshness of pages and with new URL. The bar chart given in Figure 4 shows the average number of pages retrieved due to different change criteria of PDFC. The bar chart in Figure 4 shows that out of 100 pages on the average only 60 (19+41) pages have been changed. Therefore the proposed PDFC sent 60 pages not 100 pages as in case of existing crawler. Thus saving the load of 40 pages on the network.

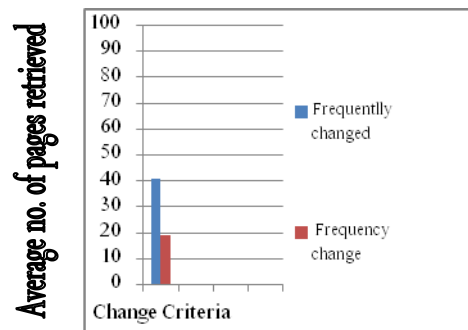


Figure 4. Average number of pages retrieved

[2]. **Load on the network.** The load on the network was measured by network graph manager and on an average it was 800Kbps when the existing mobile crawlers were used. Whereas on using PDFC without compression, the load is reduced to approximately half i.e. 480Kbps. As the PDFC retrieved on an average 60% page only, thus, the network load is approximately 60% when the crawler sends the pages to the SE without using any compression. This load is further reduced to approximately 170kbps by using standard compressing tools (e.g. WINZIP), the pages can be compressed up to 30% of the original size. The bar chart in Figure 5 shows the comparison of load on the network (in Kbps) for different types of crawlers used. Below Figure 5 shows the comparison of three mobile crawlers – existing mobile crawlers (EMC), PDFC without compression (PDFCWC) and PDFC with compression (PDFCC). It is very much clear from the Figure 5 that PDFC reduce the load up to half when the compression is not used and reduced much more when compression is applied. Thus in both cases PDFC performs better than the EMC.

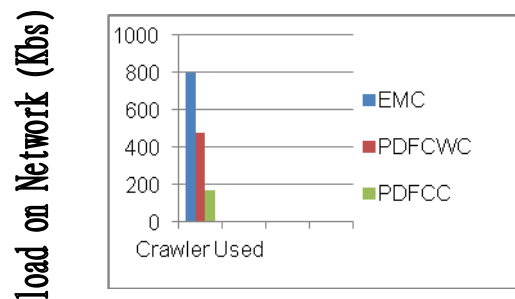


Figure 5. Load on the network.

[3]. **Bandwidth preserved** – According to Shannon- Hartley theorem, the data rate must be twice the bandwidth of the channel. So, if it is assumed that the channel is of 4 KHz without noise then the data rate of this channel would be 8 KBPS. Thus it takes 100 seconds to send the data using EMC. It takes approximately 60 seconds to send the filtered data (only those pages which are actually modified) with PDFC without compression and it takes approximately 21 seconds with PDFC with compression. The consumption of bandwidth used can be measured by software called

Bandwidth Meter Pro. The bar chart in Figure 6 had shown that EMC consumed bandwidth was 132 KHz where as in PDFC it was approximately 110 KHz. This combination of time and bandwidth has increased the data rate, which was saved by not crawling through unchanged websites. Hence, PDFC preserves bandwidth by reducing the traffic on the network by the way of filtering the unmodified pages at remote site.

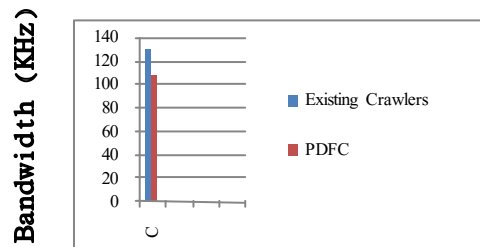


Figure 6. Comparison of Bandwidth

8. Conclusion

This paper has presented a novel Parallel Domain Focused Crawler for reduction in load on the network. The proposed crawler has made the use of the concept of ASCII count and shows experimental results in terms of reduction of load on the network, bandwidth preservation and saving memory. The proposed crawler has been intended by implementing it in Java programming language using Netbeans IDE 7.0.1. The experimental results have revealed that the proposed architecture had reduced the load on the network, has preserved bandwidth and has saved memory significantly.

References

- [1] Shkapyenyuk V. and Suel T., "Design and Implementation of A High Performance Distributed Web Crawler", in Proceedings of the 18th International Conference on Data Engineering, San Jose, California. IEEE CS Press, pp. 357-368, 2002.
- [2] Cho J. and Garcia-Molina H., "Estimating Frequency of Change", in ACM Transactions on Internet Technology (TOIT), vol. 3, no. 3, pp. 256-290, 2003.
- [3] Jan Fiedler, and Joachim Hammer, "Using the Web Efficiently: Mobile Crawlers", in Seventeenth Annual International Conference of the Association of Management (AoM/IAoM) on Computer Science, Maximilian Press Publishers, San Diego, CA, pages 324-329, August 1999.
- [4] Yuan X. and Harms J., "An Efficient Scheme to Remove Crawler Traffic from the Internet", in Proceedings of the 11th International Conferences on Computer Communications and Networks, pp. 90-95, 2002.
- [5] Lawrence S. and Giles C., "Accessibility of Information on the Web", Nature, vol. 400, no. 6740, pp. 107-109, 1999.
- [6] Nidhi Tyagi & Deepti Gupta, "A Novel Architecture for Domain Specific Parallel Crawler", in Nidhi Tyagi et. al. / Indian Journal of Computer Science and Engineering Vol 1 issue 1 .pp 44-53, 2010.
- [7] Odysseas Papapetrou and George Samaras, "Minimizing the Network Distance in Distributed Web Crawling", R. Meersman, Z. Tari (Eds.): CoopIS/DOA/ODBASE 2004, LNCS 3290, pp. 581-596, 2004.
- [8] Rajender Nath and Satinder Bal, "A Novel Mobile Crawler System Based on Filtering off Non-Modified Pages for Reducing Load on the Network", in The International Arab Journal of Information Technology, Vol. 8, No. 3, July 2011
- [9] Rajender Nath and Naresh Kumar, "A Novel Architecture for Parallel Crawler based on Focused Crawling", in International Multiconference on Intelligent Systems, Sustainable, New and Renewable Energy Technology & Nanotechnology (IISN 2012), pp.36-39, March 2012.
- [10] Hassan Artail, Kassem Fawaz, "A fast HTML web page change detection approach based on hashing and reducing the number of similarity computations", in Data & Knowledge Engineering pp. 326-337, 2008.
- [11] Ahmed Patel, Nikita Schmidt, "Application of structured document parsing to Focused web crawling", in Computer Standards & Interfaces pp. 325-331, 2011.
- [12] F. Ahmadi - Abkenari, Ali Selamat, "A Click stream-based Focused Trend Parallel Web Crawler", in International Journal of Computer Applications (0975 - 8887), Volume 9- No.5, November 2010.
- [13] Guilherme T. de Assis · Alberto H. F. Laender, Marcos André Gonçalves · Altigran S. da Silva, "A Genre-Aware Approach to Focused Crawling", in WorldWide Web (2009) 12:285-319, DOI 10.1007/s11280-009-0063-7.
- [14] Joach im Hammer, Jan Fiedler, "Using Mobile Crawlers to Search the Web Efficiently", in International Journal of Computer and Information Science, 1:1, pages 36-58, 2000.
- [15] Jungoo Cho, Hector Gracia-Molina, "Parallel Crawlers", in the proceedings of 11th international World Wide Web conference, Technical report, UCLA Computer science, 2002.

HBBABC: A Hybrid Optimization Algorithm Combining Biogeography Based Optimization (BBO) and Artificial Bee Colony (ABC) Optimization For Obtaining Global Solution Of Discrete Design Problems

Vimal Savsani

Department of Mechanical engineering, Pandit Deendayal Petroleum University, Gandhinagar 382 007, Gujarat, INDIA

Abstract

Artificial bee colony optimization (ABC) is a fast and robust algorithm for global optimization. It has been widely used in many areas including mechanical engineering. Biogeography-Based Optimization (BBO) is a new biogeography inspired algorithm. It mainly uses the biogeography-based migration operator to share the information among solutions. In this work, a hybrid algorithm with BBO and ABC is proposed, namely HBBABC (Hybrid Biogeography based Artificial Bee Colony Optimization), for the global numerical optimization problem. HBBABC combines the searching behavior of ABC with that of BBO. Both the algorithms have different solution searching tendency like ABC have good exploration searching tendency while BBO have good exploitation searching tendency. To verify the performance of proposed HBBABC, 14 benchmark functions are experimented with discrete design variables. Moreover 5 engineering optimization problems with discrete design variables from literature are also experimented. Experimental results indicate that proposed approach is effective and efficient for the considered benchmark problems and engineering optimization problems. Compared with BBO and ABC separately HBBABC performs better.

1. Introduction

Hybridization of algorithm means to combine the capabilities of different algorithm in a single algorithm. Hybridization is done to overcome the drawback in the existing algorithms and to obtain better solutions. Evolutionary Algorithms (EAs) are very popular for the hybridization due to their different capabilities in handling different types of problems. There is a continuous research to find new optimization techniques which are capable of handling variety of problems with high effectiveness, efficiency and flexibility and thus there are many such optimization algorithms like GA, SA, DE, PSO, ACO, SFLA, ABC, BBO etc. Hybridization is one of the popular methods to increase the effectiveness, efficiency and flexibility of the algorithm to produce better solution and convergence rates and thus saving computational times. Many such hybrid algorithms are available in the literature and continuous efforts are continued to develop new hybrid algorithms. Literature survey of some of the recently developed hybrid algorithm is given in Table 1. ABC is a simple and powerful population-based algorithm for finding the global optimum solutions. ABC divides the population in two main parts viz. employed bees and onlooker bees. Employed bees start the search with specific rules and onlooker bees follow the employed bees corresponding to the fitness of employed bees and it also updated the solution as employed bees. If there is no change in the fitness of employed bees for some number of generations than that bee is converted in scout bee which start for a new search and acts as a employed bees from then. Algorithm continues for predefined number of generations or until the best solution is found. So ABC finds the global solution by exploring the search space with specific rules followed by employed bees, onlooker bees and scout bees. Biogeography-Based Optimization (BBO), proposed by Simon (2008), is a new global optimization algorithm based on the biogeography theory, which is the study of distribution of species. BBO is also population-based optimization method. In the original BBO algorithm, each solution of the population is a vector of integers. BBO updates the solution following immigration and emigration phenomena of the species from one place to the other which is referred as islands by Simon. Simon compared BBO with seven other optimization methods over 14 benchmark functions and a real-world sensor selection problem. The results demonstrated the good performance of BBO. BBO has good exploitation ability as solution is updated by exchanging the existing design variables among the solution.

In order to combine the searching capabilities of ABC and BBO, in this paper, we propose a hybrid ABC with BBO, referred to as HBBABC, for the global numerical optimization problems. In HBBABC, algorithm starts by updating the solutions using immigration and emigration rates. Solution is further modified using the exploration tendency of ABC using employed, onlooker and scout bees. Experiments have been conducted on 14 benchmark functions with discrete design variables Simon (2008) and also on 5 engineering optimization problems.

2. Optimization Algorithms

2.1 Biogeography-based optimization (BBO)

BBO (Simon 2006) is a new population-based optimization algorithm inspired by the natural biogeography distribution of different species. In BBO, each individual is considered as a "habitat" with a habitat suitability index (HSI). A good solution is analogous to an island with a high HSI, and a poor solution indicates an island with a low HSI. High HSI solutions tend to share their features with low HSI solutions. Low HSI solutions accept a lot of new features from high HSI

solutions. In BBO, each individual has its own immigration rate λ and emigration rate μ . A good solution has higher μ and lower λ and vice versa. The immigration rate and the emigration rate are functions of the number of species in the habitat. They can be calculated as follows

$$\lambda_k = I \left(1 - \frac{k}{n} \right) \quad (1)$$

$$\mu_k = E \left(\frac{k}{n} \right) \quad (2)$$

where I is the maximum possible immigration rate; E is the maximum possible emigration rate; k is the number of species of the k -th individual; and n is the maximum number of species. In BBO, there are two main operators, the migration and the mutation.

2.1.1 Migration

Consider a population of candidate which is represented by design variable. Each design variable for particular population member is considered as SIV for that population member. Each population member is considered as individual habitat/Island. The objective function value indicates the HSI for the particular population member. Immigration and emigration rates are decided from the curve given in Figure 1. In Figure 1 the nature of curve is assumed to be same (linear) for immigration and emigration but with opposite slopes. S value represented by the solution depends on its HSI. S_1 and S_2 represent two solutions with different HSI. The emigration and immigration rates of each solution are used to probabilistically share information between habitats. If a given solution is selected to be modified, then its immigration rate λ is used to probabilistically modify each suitability index variable (SIV) in that solution. If a given SIV in a given solution S_i is selected to be modified, then its emigration rates μ of the other solutions is used to probabilistically decide which of the solutions should migrate its randomly selected SIV to solution S_j . The above phenomenon is known as migration in BBO. Because of this migration phenomenon BBO is well suited for the discrete optimization problems as it deals with the interchanging of design variables between the population members.

2.1.2 Mutation

In nature a habitat's HSI can change suddenly due to apparently random events (unusually large flotsam arriving from a neighbouring habitat, disease, natural catastrophes, etc.). This phenomenon is termed as SIV mutation, and probabilities of species count are used to determine mutation rates. This probability mutates low HSI as well as high HSI solutions. Mutation of high HSI solutions gives them the chance to further improve. Mutation rate is obtained using following equation.

$$m(S) = m_{\max} \left(1 - \frac{P_s}{P_{\max}} \right) \quad (3)$$

Where, m_{\max} is a user-defined parameter called mutation coefficient.

2.2 Artificial Bee Colony (ABC) technique

Artificial Bee Colony (ABC) Algorithm is an optimization algorithm based on the intelligent foraging behaviour of honey bee swarm. The colony of artificial bees consists of three groups of bees: employed bees, onlookers and scouts (Karaboga 2005, Basturk and Karaboga 2006). An employed bee searches the destination where food is available. They collect the food and returns back to its origin where they perform waggle dance depending on the amount of food available at the destination. The onlooker bee watches the dance and follows employed bee depending on the probability of the available food means more onlooker bee will follow the employed bee associated with the destination having more amount of food. The employed bee whose food source becomes abandoned convert into a scout bee and it searches for the new food source. For solving optimization problems the population is divided into two parts consisting of employed bees and onlooker bees. An employed bee searches the solution in the search space and the value of objective function associated with the solution is the amount of food associated with that solution. Employed bee updates its position using Equation (4) and it updates new position if it is better than the previous position, i.e it follows greedy selection.

$$v_{ij} = x_{ij} + R_{ij} (x_{ij} - x_{kj}) \quad (4)$$

Where v_{ij} is the new position of employes bee, x_{ij} is the current position of employed bee, k is a random number between $(1, N(\text{population size})/2) \neq i$ and $j = 1, 2, \dots, \text{Number of design variables}$. R_{ij} is a random number between $(-1, 1)$. An onlooker bees chooses a food source depending on the probability value associated with that food source, p_i , calculated using Equation (5).

$$p_i = \frac{F_i}{\sum_{n=1}^{N/2} F_n} \quad (5)$$

Where F_i is the fitness value of the solution i and $N/2$ is the number of food sources which is equal to the number of employed bees. Onlooker bees also update its position using Equation (4) and also follow greedy selection. The Employed bee whose position of the food source cannot be improved for some predetermined number of cycles than that food source is called abandoned food source. That employed bee becomes scout and searches for the new solution randomly using Equation (6).

$$x_i^j = x_{\min}^j + \text{rand}(0,1)(x_{\max}^j - x_{\min}^j) \quad (6)$$

The value of predetermined number of cycles is an important control parameter of the ABC algorithm, which is called “*limit*” for abandonment. The value of limit is generally taken as *Number of employed bees * Number of design variables* (Karaboga and Basturk 2007, Karaboga and Basturk 2008).

2.3 Hbbabc: Hybrid Biogeography Based Artificial Bee Colony Optimization

As mentioned above, ABC is good at exploring the search space and locating the region of global minimum. On the other hand, BBO has a good exploitation searching tendency for global optimization. Based on these considerations, in order to maximize the exploration and the exploitation a HBBABC approach is proposed. Step by step procedure for the implementation of HBBABC is given as follows.

Step 1: Initialize BBO and ABC parameters which are necessary for the algorithm to proceed. These parameters includes population size, number of generations necessary for the termination criteria, Maximum immigration and emigration rates, number of design variables and respective range for the design variables.

Step 2: Generate random population equal to the population size specified. Each population member contains the value of all the design variables. This value of design variable is randomly generated in between the design variable range specified. Every design variable in the population indicates SIVs for that respective population member (Habitat)

Step 3: Obtain the value of objective function for all population members. The value of objective function so obtained indicates the HSI for that Habitat (population member). If problem is constrained optimization problem than some penalty approach is used to convert constrained optimization problem to unconstrained optimization problem.

Step 4: Map the value of HSI to obtain the species count. High species count is allotted to the population member having high HSI for maximization optimization problem. If the optimization problem is of minimization type than low HSI member is given high species count.

Step 5: Modify population using the migration operator considering its immigration and emigration rates. If a given solution is selected to be modified, then its immigration rate λ is used to probabilistically modify each suitability index variable (SIV) in that solution. If a given SIV in a given solution S_i is selected to be modified, then its emigration rates μ of the other solutions is used to probabilistically decide which of the solutions should migrate its randomly selected SIV to solution S_i . Pseudo code for migration is given as follows.

For $i = 1$ to NP

Select X_i with probability proportional to λ_i

if $\text{rand}(0, 1) < \lambda_i$

For $j = 1$ to NP

Select X_j with probability proportional to μ_j

if $\text{rand}(0, 1) < \mu_j$

Randomly select a variable σ from X_j

Replace the corresponding variable in X_i with σ

Endif

Endif

End

End

Step 6: Divide the population into two equal parts to act as employed bees and onlooker bees. Obtain the value of objective function for employed bees. The value of objective function so obtained indicates the amount of nectar (food) associated with that destination (food source).

Step 7: Update the position of employed bees using Equation (4). If the value of objective function of the new solution is better than the existing solution, replace the existing solution with the new one.

Step 8: Calculate probability associated with the different solutions using Equation (5). Onlooker bee follows a solution depending on the probability of that solution. So more the probability of the solution more will be the onlooker bee following that solution.

Step 9: Update the position of onlooker bees using Equation (4). If the value of objective function of the new solution is better than the existing solution, replace the existing solution with the new one

Step 10: Identify abandon solution and replace it with the newly generated solution using Equation (6)

Step 11: Continue all the steps from step 3 until the specified number of generations are reached.

Detailed pseudo code is given below:

START

Initialize required parameters necessary for the algorithm (as mentioned above)

Generate the initial population N , Evaluate the fitness for each individual in N

For $i=1$ to number of generations

BBO loop

For each individual, map the fitness to the number of species

Calculate the immigration rate λ_i and the emigration rate μ_i for each individual X_i

For $i = 1$ to N

 Select X_i with probability proportional to λ_i

 if $\text{rand}(0, 1) < \lambda_i$

 For $j = 1$ to N

 Select X_j with probability proportional to μ_j

 if $\text{rand}(0, 1) < \mu_j$

 Randomly select a variable σ from X_j

 Replace the corresponding variable in X_i with σ

 Endif

 Endif

 End

End

ABC loop

For $i = 1$ to $N/2$

 Produce new solutions v_{ij} for the employed bees and evaluate them

 Replace new solution if it is better than the previous one

End

 Calculate the probability values p_{ij} for the solutions

 Identify onlooker bees depending on the probability p_{ij}

For $i = 1$ to $N/2$

 Produce the new solutions v_{ij} for the onlookers

 Replace new solution if it is better than the previous one

End

 Determine the abandoned solution for the scout, if exists, and replace it with a new randomly produced solution x_{ij}

End

End

STOP

It can be seen from the pseudo code that HBBABC requires small extra calculation effort than BBO but it combines the strength of both the algorithms in searching the optimum solutions. To demonstrate the effectiveness of the proposed algorithm many experiments were conducted on benchmark problems which is discussed in the next section.

3. Application On Benchmark Problems

In the field of optimization it is a common practice to compare different algorithms using different benchmark problems. In this work 14 different benchmark problems are considered having different characteristics like separability, multimodality and regularity (Simon 2008). A function is multimodal if it has two or more local optima. A function is separable if it can be written as a sum of functions of variable separately. Function is regular if it is differentiable at each point of their domain. Non separable functions are more difficult to optimize and difficulty increases if the function is multimodal. Complexity increases when the local optima are randomly distributed. Moreover complexity increases with the increase in dimensionality. Description of all the benchmark problems with respect to Multimodality, Separability and regularity are given in Table 2. All the benchmark problems are explained as follows with their optimum value and optimum design parameters.

Sphere Model $f(x) = \sum_{i=1}^{30} x_i^2$

$$-100 \leq x_i \leq 100, \quad \min(f) = f(0,0,\dots,0) = 0$$

(7)

Schwefel's Problem 2.22

$$f(x) = \sum_{i=1}^{30} |x_i| + \prod_{i=1}^{30} |x_i|$$

$-100 \leq x_i \leq 100, \quad \min(f) = f(0,0\dots0) = 0$ (8)

Schwefel's Problem 1.2

$$f(x) = \sum_{i=1}^{30} \left(\sum_{j=1}^i x_j \right)^2$$

$-100 \leq x_i \leq 100, \quad \min(f) = f(0,0\dots0) = 0$ (9)

Schwefel's Problem 2.21

$$f(x) = \max_i \{|x_i|, 1 \leq i \leq 30\}$$

$-100 \leq x_i \leq 100, \quad \min(f) = f(0,0\dots0) = 0$ (10)

Generalized Rosenbrock's Function

$$f(x) = \sum_{i=1}^{29} [100(x_{i+1} - x_i^2)^2 + (x_i - 1)^2]$$

$-30 \leq x_i \leq 30, \quad \min(f) = f(1,1\dots1) = 0$ (11)

Step Function

$$f(x) = \sum_{i=1}^{30} [x_i + 0.5]^2$$

$-100 \leq x_i \leq 100, \quad \min(f) = f(0,0\dots0) = 0$ (12)

Quartic Function

$$f(x) = \sum_{i=1}^{30} [ix_i^4]$$

$-1.28 \leq x_i \leq 1.28, \quad \min(f) = f(0,0\dots0) = 0$ (13)

Generalized Schwefel's Problem 2.26

$$f(x) = -\sum_{i=1}^{30} (x_i \sin(\sqrt{|x_i|}))$$

$-500 \leq x_i \leq 500, \quad \min(f) = f(420.9687, 420.9687\dots 420.9687) = -12569.5$ (14)

Generalized Rastrigin Function

$$f(x) = \sum_{i=1}^{30} [x_i^2 - 10 \cos(2\pi x_i) + 10]$$

$-5.12 \leq x_i \leq 5.12, \quad \min(f) = f(0,0\dots0) = 0$ (15)

Ackley's function

$$f(x) = \sum_{i=1}^{30} -20 \exp\left(-0.2 \sqrt{\frac{1}{30} \sum_{i=1}^{30} x_i^2}\right) - \exp\left(\frac{1}{30} \sum_{i=1}^{30} \cos 2\pi x_i\right)$$

$-32 \leq x_i \leq 32, \quad \min(f) = f(0,0\dots0) = 0$ (16)

Generalized Griewank function

$$f(x) = \frac{1}{4000} \sum_{i=1}^{30} x_i^2 - \prod_{i=1}^{30} \cos\left(\frac{x_i}{\sqrt{i}}\right) + 1$$

$-600 \leq x_i \leq 600, \quad \min(f) = f(0,0\dots0) = 0$ (17)

Generalized penalized function 1

$$f(x) = \frac{\pi}{30} \left[10 \sin^2(\pi y_1) + \sum_{i=1}^{29} (y_i - 1)^2 \{1 + 10 \sin^2(\pi y_{i+1})\} + (y_n - 1)^2 \right] + \sum_{i=1}^{30} u(x_i, 10, 100, 4)$$

$$-50 \leq x_i \leq 50, \quad \min(f) = f(1, 1 \dots 1) = 0 \quad (18)$$

Generalized penalized function 2

$$f(x) = 0.1 \left[\sin^2(\pi 3x_1) + \sum_{i=1}^{29} (x_i - 1)^2 \{1 + \sin^2(3\pi x_{i+1})\} + (x_n - 1)^2 (1 + \sin^2(2\pi x_{30})) \right] + \sum_{i=1}^{30} u(x_i, 5, 100, 4)$$

$$-50 \leq x_i \leq 50, \quad \min(f) = f(1, 1 \dots 1) = 0$$

$$u(x_i, a, k, m) = \begin{cases} k(x_i - a)^m & x_i > a, \\ 0, & -a \leq x_i \leq a, \\ k(-x_i - a)^m, & x_i < -a \end{cases}$$

$$y_i = 1 + 1/4(x_i + 1) \quad (19)$$

Fletcher-Powell

$$f_{14}(x) = \sum_{i=1}^{30} (A_i - B_i)^2$$

$$A_i = \sum_{j=1}^{30} (a_{ij} \sin \alpha_j + b_{ij} \cos \alpha_j), \quad B_i = \sum_{j=1}^{30} (a_{ij} \sin x_j + b_{ij} \cos x_j)$$

$$x_i, \alpha_i \in [-\pi, \pi]; a_{ij}, b_{ij} \in [-100, 100], \quad \min(f_{14}) = f_{14}(\alpha, \dots, \alpha) = 0 \quad (20)$$

3.1 Discrete optimization of benchmark problems

14 Benchmark problems were compared by implementing integer versions of all the optimization algorithms in Matlab. The granularity or precision of each benchmark function was 0.1, except for the Quartic function (Simon 2008). Since the domain of each dimension of the quartic function was only ± 1.28 , it was implemented with a granularity of 0.01. ABC was specially tuned to take integer value in each iteration modifying Equation (6) and (8) as.

$$v_{ij} = \text{round}(x_{ij} + R_{ij}(x_{ij} - x_{kj})) \quad (21)$$

And

$$x_i^j = \text{round}(x_{\min}^j + \text{rand}(0,1)(x_{\max}^j - x_{\min}^j)) \quad (22)$$

All the algorithms were run for 100 times considering different population size and number of generations depending on the complexity of problem. For BBO and HBBABC Habitat modification probability was taken as 1 and for ABC limit is set as Population size/2 * Number of design variables. Results for the discrete optimization of benchmark problems are given in Table 3 which shows the Best Value, Mean Value and T-Test Value for all the benchmark problems. Results are also shown considering different number of design variables viz. 30, 50, 100 and 200 (Dimensions). Population size is taken as 50 for all the problems and number of generation taken is equal to 50 for 30 and 50 dimensions, 100 for 100 dimensions and 200 for 200 dimensions. It is seen from the Table that out of 14 benchmark problems considering discrete design variables hybrid HBBABC has shown better result for 12 benchmark problems for the best and mean values for 100 runs. Only for Schwefel 1.2 and Schwefel 2.21 BBO has outperformed HBBABC though the best result obtained considering 200 design variables for HBBABC is better than BBO. Further statistical analysis is done to analyze the differences between different algorithms using T-test method (Hill 1970). T-test method is used to check whether the differences between the groups of data are statistically significant or not. T-test value also suggest that HBBABC is statistically significant than BBO and ABC. ABC has shown better performance than BBO for only Griewank function, but for Sphere, Schwefel 2.22, Rosenbrock, Step, and Quartic performance of ABC has increased with the number of design variables. Moreover discrete version of ABC is not so effective in comparison with HBBABC expect for some results of Schwefel 1.2 and Schwefel 2.21. Further comparison of the algorithms is done considering two more criterions like success rate and maximum number of generation required to reach the best solution. Results are shown in Table 4. Comparison is done considering the population size of 100 and number of generations as 500. If the optimum result is Not Reached than it is marked as NR. Algorithm is considered successful if the solution value is less than $1.0E-15$ and also maximum number of generation required is counted for the same value. Out of 14 benchmark problems HBBABC was able to find optimum solution for 10 benchmark problems which is quite better than BBO

(4 benchmark problems) and ABC (3 benchmark problems) also HBBABC has shown 100% success for 9 benchmark problems and about 62% for Rastrigin function which is also better than BBO and ABC. NR* indicates that though optimum solution has not reached but still the best solution achieved is better than other algorithms. It is also seen that with increase in the dimension of the problem still HBBABC is better than BBO and ABC on 12 benchmark problems. Moreover average number of generations required to reach the optimum solution (less than 1.0E-15) for 100 different runs was calculated and was rounded off in multiples of 10 (e.g. if average number of generation equals to 147 than it is rounded off to 150). These rounded values of average number of generation are shown in the Table 4. It is seen from the Table 4 that HBBABC requires less number of generations to reach the optimum solution than BBO and ABC, which indirectly indicates that HBBABC requires less computational effort than BBO and ABC. Simon (2008), founder of BBO, has compared the results of BBO with different evolutionary algorithms such as ACO, DE, ES, GA, PBIL, PSO and SGA for 14 different benchmark problems considered in this paper. The results were presented for best as well as the mean solutions. Results show that for mean solution SGA is better than BBO for Griewank, Penalty 1, Penalty 2, Quartic, Rosenbrock, Schwefel 2.26 and Step functions. For Best solution SGA is better for Fletcher, Griewank, Quartic, Schwefel 1.2, Schwefel 2.21, Sphere and Step functions while ACO is better for Penalty 1, Penalty 2 and Schwefel 2.26. To compare HBBABC with different Evolutionary algorithms results were compared with the best performing optimization algorithm in comparison with BBO considering same parameters used by Simon (2008) (i.e population size of 50, number of generations of 50, 100 number of runs, ACO parameters and SGA parameters). Results are present in Table 5 for the comparison of HBBABC with SGA and ACO. It is seen from the results that for the mean solution HBBABC has outperformed SGA for all the considered benchmark problems and for the Best solution HBBABC has also outperformed SGA and ACO except for Penalty 1, Penalty 2 and Schwefel 1.2. Here it is interesting to note that though for Penalty 1 and Penalty 2 ACO has produced better results than HBBABC but mean results for ACO is poor than HBBABC which indicates that average performance of HBBABC is better than ACO. Further investigation is done for the convergence rate which gives the value of objective function with respect to number of generations. Figure 2 shows the convergence graph for some of the benchmark problems for 100 generations. It is seen from the Figure 2 that convergence rate for HBBABC is better than BBO and ABC.

3.2 Discrete optimization of engineering problems To check the validity of the proposed hybrid algorithm 5 different real-life engineering design problems with discrete variables is considered from the literature. All the problems considered are constrained optimization problems and so it is required to convert constrained optimization problem into unconstrained optimization problem. Penalty approach is used to change the constrained optimization problem into unconstrained optimization problem. Consider an optimization problem as

$$\text{Minimize } f(X), \text{ Subjected to } g_i(X) \geq 0$$

This problem is converted in unconstrained form as

$$\text{Minimize } f(X) \text{ if } g_i(X) \geq 0, \text{ else}$$

$$\text{Minimize } f(X) + R \sum_{i=1}^n g_i(X)$$

Where R is very large number and n is number of constraints.

In this work one more term is added in the above equation to make sure that all the constraints are satisfied.

$$\text{Minimize } f(X) + R \sum_{i=1}^n g_i(X) + R_1(G)$$

Where R_1 is also a very large number and G is the number of constraints which are not satisfied.

3.2.1 Example 1: Gear Train Design

This problem was introduced by Pomrehn and Papalambros (1995) to minimize the total weight of the gear train. There are 22 discrete design variables with three different types of discreteness. The number of teeth should be integer, gear/pinion shafts must be located in discrete locations, and gears are to be manufactured from four available gear blanks. There are 86 inequality constraints considered for gear-tooth bending fatigue strength, gear-tooth contact strength, gear-tooth contact ratio, minimum pinion size, minimum gear size, gear housing constraints, gear pitch and kinematic constraints. The above problem was attempted by Khorshid and Seireg (1999) and Dolen et al. (2005). The best solution found so far is 38.13 cm³ by Khorshid and Seireg (1999).

3.2.2 Example 2: Welded Stiffened Cylindrical Shell

This problem was introduced by Jarmai et. al. (2006) to minimize the cost of welded orthogonally stiffened cylindrical shell. The problem have 5 discrete design variables with 5 inequality constraints for shell buckling, panel stiffener buckling, panel ring buckling and manufacturing limitations. The best solution given by Jarmai et. al. (2006) is $f^*(x)=55326.3$ which is the global solution for the considered problem.

3.2.3 Example 3: 10- Bar Truss Structure

This problem is taken from Rajeev and Krishnamoorthy (1992). In these problems the objective function is to minimize the weight of the structure. Constraints are based on allowable stresses and deflections with 10 discrete design variables for each bar in the structure. The above problem was also solved by many methods such as Improved Penalty

Function Method (Cai and Thiereu, 1993), Genetic Algorithms (Rajeev and Krishnamoorthy, 1992), Difference Quotient Method (Thong and Liu, 2001), Genetic Algorithms (Coello, 1994) and Simulated Annealing (Kripa 2004). The best result shown was $f^*(x)=5490.74$ which is the global optimum solution for the problem.

3.2.4 Example 4: 25- Bar Truss Structure

This problem is also taken from Rajeev and Krishnamoorthy (1992). In these problems the objective function is to minimize the weight of the structure. Constraints are based on allowable stresses and deflections with 8 discrete design variables for different sets of bar in the structure. The above problem is also solve by many methods such as Improved Penalty Function Method (Cai and Thiereu, 1993) , Genetic Algorithms (Rajeev and Krishnamoorthy, 1992), Brach and Bound (Zhu, 1986), Difference Quotient Method (Thong and Liu, 2001), Genetic Algorithms (Coello, 1994), Simulated Annealing (Kripa 2004). The best result is equal to $f^*(x)=484.85$

3.2.5 Example 5: Multispeed Planetary Transmission

This problem is taken from Simionescu et. al. (2006) for the teeth number synthesis of Multispeed Planetary Transmission. The objective function is to minimize the error between imposed and actual transmission ratios. There are 12 kinematic constraints with 10 discrete design variables. The best global solution for the problem is $f^*(x)=0.526$. The result for the above considered problems are shown in Table 6. It can be seen that for all the considered problems HBBABC has given global solutions. The results given by HBBABC are better than BBO and ABC in terms of mean solutions and success rate. Algorithm is considered to be successful if the solution has reached 99% of the global solution. Only for Example 1 algorithm is considered successful if it gives feasible solution. For Example 1 HBBABC has given better results than reported in the literature.

4. Conclusions

A hybrid HBBABC algorithm using two well known algorithms viz. Biogeography Based Optimization and Artificial Bee colony Optimization is proposed in this work. It combined the exploitation capacity of BBO and exploration capacity of ABC. To verify the performance of the proposed method it was experimented on 14 benchmark problems considering discrete design variables and 5 engineering design optimization problems. Comparison of different algorithm is done considering different criteria such as Best solution, Mean Solution, T-test, Success rate, Average number of generations required to reach the optimum solution and Convergence rate. Experimental results show that the overall performance of HBBABC is better than BBO and ABC considering above criteria.

References

- [1]. Ali HK, Huseyin C, Tamer A, Gurhan G (2010) PSOLVER: A new hybrid particle swarm optimization algorithm for solving continuous optimization problems. *Expert Systems with Applications* 37: 6798–6808
- [2]. Ali RY (2009) A novel hybrid immune algorithm for global optimization in design and manufacturing. *Robotics and Computer-Integrated Manufacturing* 25: 261-270
- [3]. Basturk B, Karaboga D (2006) An Artificial Bee Colony (ABC) Algorithm for Numeric function Optimization. *IEEE Swarm Intelligence Symposium*, Indianapolis, Indiana, USA
- [4]. Behnamian J, Zandieh M, Fatemi Ghomi SMT (2009) Parallel-machine scheduling problems with sequence-dependent setup times using an ACO, SA and VNS hybrid algorithm. *Expert Systems with Applications* 36: 9637-9644
- [5]. Behnamian J, Fatemi Ghomi SMT (2010) Development of a PSO–SA hybrid metaheuristic for a new comprehensive regression model to time-series forecasting. *Expert Systems with applications* 37: 974–984
- [6]. Berna D, Fulya A, Onder B (2010) Design of reliable communication networks: A hybrid ant colony optimization algorithm. *IIE Transactions*. 42: 273 - 287
- [7]. Cai JB, Thiereut G (1993) Discrete optimization of structures using an improved penalty function method. *Engineering Optimization* 21: 293-306
- [8]. Changsheng Z, Jiaxu N, Shuai L, Dantong O, Tienan D (2009) A novel hybrid differential evolution and particle swarm optimization algorithm for unconstrained optimization. *Operations Research Letters* 37: 117-122
- [9]. Chin KH, Hong TE (2009) GACO - a hybrid ant colony optimization metaheuristic for the dynamic load-balanced clustering problem in ad hoc networks. *Applied Artificial Intelligence* 23: 570 - 598
- [10]. Coello CA (1994) Discrete Optimization of Trusses using Genetic Algorithms. *Expert Systems Applications and Artificial Intelligence*, J.G. Cheng, F.G. Attia and D.L. Crabtree (Editors), (I.I.T.T. International, Technology Transfer Series): 331-336
- [11]. Cuneyt O, Zafer B (2009) Application of heuristic and hybrid-GASA algorithms to tool-path optimization problem for minimizing airtime during machining. *Engineering Applications of Artificial Intelligence*. 22: 389-396
- [12]. Dolen M, Kaplan H, Seireg A (2005) Discrete parameter-nonlinear constrained optimisation of a gear train using genetic algorithms. *International Journal of Computer Applications in Technology*. 24(2): 110 - 121
- [13]. Dong HK, Ajith A, Jae HC (2007) A hybrid genetic algorithm and bacterial foraging approach for global optimization. *Information Sciences* 177: 3918-3937
- [14]. Fan SKS, Zahara E (2007) A hybrid simplex search and particle swarm optimization for unconstrained optimization. *European Journal of Operational Research* 181: 527–548
- [15]. Guohui Z, Xinyu S, Peigen L, Liang G (2009) An effective hybrid particle swarm optimization algorithm for multi-objective flexible job-shop scheduling problem. *Computers & Industrial Engineering* 56: 1309-1318

- [16]. Hill G (1970) Algorithm 395: Students t-distribution'. *Communication of ACM* 13: 617-619
- [17]. Hui L, Zixing C, Yong W (2010) Hybridizing particle swarm optimization with differential evolution for constrained numerical and engineering optimization. *Applied Soft Computing* 10: 629-640
- [18]. Jarmai K, Snyman JA, Farkas J (2006) Minimum cost design of a welded orthogonally stiffened cylindrical shell. *Computers and Structures* 84: 787-797
- [19]. Jerome HK, Darren R (2009) A hybrid CMA-ES and HDE optimisation algorithm with application to solar energy potential. *Applied Soft Computing* 9: 738-745
- [20]. Jing-Ru Z, Jun Z, Tat-Ming L, Michael RL (2007) A hybrid particle swarm optimization-back-propagation algorithm for feedforward neural network training. *Applied Mathematics and Computation* 185: 1026-1037
- [21]. Karaboga D (2005) An Idea Based On Honey Bee Swarm For Numerical Optimization. *Technical Report-TR06, Erciyes University, Engineering Faculty, Computer Engineering Department*
- [22]. Karaboga D, Basturk B (2007) Artificial Bee Colony (ABC) Optimization Algorithm for Solving Constrained Optimization Problems. *P. Melin et al. (Eds.): IFSA 2007, LNAI 4529, Springer-Verlag Berlin Heidelberg*, pp. 789-798.
- [23]. Karaboga D, Basturk B (2008) On the performance of artificial bee colony (ABC) algorithm. *Applied Soft Computing* 8: 687-697
- [24]. Karen I, Yildiz AR, Kaya N, Ozturk N, Ozturk F (2006) Hybrid approach for genetic algorithm and Taguchi's method based design optimization in the automotive industry. *International Journal of Production Research* 44: 4897 - 4914
- [25]. Khorshid E, Seireg A (1999) Discrete nonlinear optimisation by constraint decomposition and designer interaction. *International Journal of Computer Applications in Technology* 12: 76-82
- [26]. Kripa M (2004) Discrete Optimization of Trusses by Simulated Annealing. *Journal of the Brazilian Society of Mechanical Science & Engineering* 26: 170-173
- [27]. Liao TW (2010) Two hybrid differential evolution algorithms for engineering design optimization. *Applied Soft Computing*: doi:10.1016/j.asoc.2010.05.007
- [28]. Ling W (2005) A hybrid genetic algorithm-neural network strategy for simulation optimization. *Applied Mathematics and Computation* 170: 1329-1343
- [29]. Nenzi W, Yau-Zen C (2002) A Hybrid Search Algorithm for Porous Air Bearings Optimization. *Tribology Transactions* 45: 471 - 477
- [30]. Nourelfath M, Nahas N, Montreuil B (2007) Coupling ant colony optimization and the extended great deluge algorithm for the discrete facility layout problem. *Engineering Optimization* 39: 953 - 968
- [31]. Pomrehn LP, Papalambros PY (1995) Discrete optimal design formulations with application to gear train design. *ASME Journal of Mechanical Design* 117: 419-424
- [32]. Pradeep KG, Ranjan G (2005) An automated hybrid genetic-conjugate gradient algorithm for multimodal optimization problems. *Applied Mathematics and Computation* 167: 1457-1474
- [33]. Qian-jin G, Hai-bin Y, Ai-dong X (2006) A hybrid PSO-GD based intelligent method for machine diagnosis. *Digital Signal Processing* 16: 402-418
- [34]. Rajeev S, Krishnamoorthy CS (1992) Discrete Optimization of Structures Using Genetic Algorithms. *Journal of Structural Engineering* 118: 1233-1250
- [35]. Shahla N, Mohammad EB, Nasser G, Mehdi HA (2009) A novel ACO-GA hybrid algorithm for feature selection in protein function prediction. *Expert Systems with Applications* 36: 12086-12094
- [36]. Shu-kai SF, Yun-chia L, Erwie Z (2004) Hybrid simplex search and particle swarm optimization for the global optimization of multimodal functions. *Engineering Optimization* 36: 401 - 418
- [37]. Shun-Fa H, Rong-Song H (2006) A hybrid real-parameter genetic algorithm for function optimization. *Advanced Engineering Informatics* 20: 7-21
- [38]. Simionescu PA, Beale D, Dozier GV (2006) Teeth Number Synthesis of Multispeed Planetary Transmission Using An Estimation of Distribution Algorithm. *Journal of mechanical design* 128: 108-115
- [39]. Simon D (2008) Biogeography based optimization. *IEEE transactions on Evolutionary Computations* 99(1): 1-13
- [40]. Taher N (2010) A new fuzzy adaptive hybrid particle swarm optimization algorithm for non-linear, non-smooth and non-convex economic dispatch problem. *Applied Energy* 87: 327-339
- [41]. Taher N, Babak A (2010) An efficient hybrid approach based on PSO, ACO and k-means for cluster analysis. *Applied Soft Computing* 10: 183-197
- [42]. Tamer A, Ali HK, Huseyin C, Gurhan G (2009) Hybridizing the harmony search algorithm with a spreadsheet 'Solver' for solving continuous engineering optimization problems. *Engineering Optimization* 41(12): 1119 - 1144
- [43]. Thong WHT, Liu GR (2001) An optimization procedure for truss structures with discrete design variables and dynamic constraints. *Computers and Structures* 79: 155-162
- [44]. Victoire TAA, Jeyakumar AE (2004) Hybrid PSO-SQP for economic dispatch with valve-point effect *Electric Power Systems Research* 71: 51-59
- [45]. Vincent K, Florin C, Olivier L, Louis W (2008) A hybrid optimization technique coupling an evolutionary and a local search algorithm. *Journal of Computational and Applied Mathematics* 215: 448-456
- [46]. Wen-Yi L (2010) A GA-DE hybrid evolutionary algorithm for path synthesis of four-bar linkage. *Mechanism and Machine Theory* 45: 1096-1107
- [47]. Xiaoxia Z, Lixin T (2009) A new hybrid ant colony optimization algorithm for the vehicle routing problem. *Pattern Recognition Letters* 30: 848-855
- [48]. Yannis M, Magdalene M (2010) A hybrid genetic - Particle Swarm Optimization Algorithm for the vehicle routing problem. *Expert Systems with Applications* 37: 1446-1455
- [49]. Ying-Pin C (2010) An ant direction hybrid differential evolution algorithm in determining the tilt angle for photovoltaic modules. *Expert Systems with Applications* 37: 5415-5422

[50]. Yi-Tung K, Erwie Z (2008) A hybrid genetic algorithm and particle swarm optimization for multimodal functions. Applied Soft Computing 8: 849-857

Table 1 Details of different hybrid algorithms

Hui et. al. (2010)	PSO + DE
Behnamian and Ghomi (2010)	PSO + SA
Ali et. al. (2010)	PSO + Spread Sheet ‘Solver’
Wen (2010)	GA + DE
Ying (2010)	ACO + DE
Liao (2010)	DE + Random walk
	DE + Harmony Search
Berna et. al. (2010)	ACO + SA
Taher and Babak (2010)	ACO + Fuzzy adaptive PSO + k-means Algorithm
Taher (2010)	Fuzzy Adaptive PSO + Nelder–Mead simplex Search
Yannis and Magdalene (2010)	GA + PSO
Chin and Hong (2009)	GA + ACO
Tamer et. al. (2009)	Harmony Search + Spread Sheet ‘Solver’
Changsheng et. al. (2009)	DE + PSO
Guohui etl al. (2009)	PSO + Tabu Search Algorithm
Shahla et. al. (2009)	GA + ACO
Ali (2009)	Immune + Hill climbing algorithm
Cuneyt and Zafer (2009)	GA + SA
Jerome and Darren (2009)	Covariance Matrix Adaptation Evolution Strategy + DE + Backwards Ray Tracing Technique
Xiao xia and Lixin (2009)	ACO + Scatter Search
Behnamian et. al. (2009)	ACO + SA + Vaialbe Neighborhood Search (VNS)
Vincent et. al. (2008)	GA + Local Search Interior Point Method
Yi and Erwir (2008)	GA + PSO
Fan and Zahara (2007)	PSO + Simplex search
Nourelfath et. al. (2007)	ACO + Extended Great Deluge (EGD) Local Search Technique
Jing et. al. (2007)	PSO + Back Propogation Algorithm
Dong et. al. (2007)	Genetic Algorithm (GA) + Bacterial Foraging (BF)
Karen et. al. (2006)	Taguchi's method + GA
Qian et. al. (2006)	PSO + Gradient Descent (GD) Methods
Shun and Rong (2006)	GA + SA
Pradeep and Ranjan (2005)	GA + Local Optimizing Gradient Based Algorithm
Ling (2005) [34]	GA + Neural Network Strategy
Shu et. al. (2004)	Nelder-Mead (NM) + PSO
Victoire and Jeyakumar (2004)	PSO + SQP
Nenzi and Yan (2002)	GA + Simplex Method (SM)

Table 2

Characteristics of benchmark problems

Name	Multimodal?	Separable?	Regular?
Sphere	no	yes	yes
Schwefel 2.22	no	no	no
Schwefel 1.2	no	no	yes
Schwefel 2.21	no	no	no
Rosenbrock	no	no	yes
Step	no	yes	no
Quartic	no	yes	yes
Schwefel 2.26	yes	yes	no
Rastrigin	yes	yes	yes
Ackley	yes	no	yes
Griewank	yes	no	yes
Penalty #1	yes	no	yes
Penalty #2	yes	no	yes

Fletcher-Powell yes no no

Table 3

Best results and Mean results for the benchmark problems considering discrete design variables for different dimensions. **'Bold value'** indicates better solution found. T-Test value is significant with 49 degree of freedom at $\alpha=0.05$ by two tailed test

		BBO		ABC		HBBABC		TTEST	
		Best	Mean	Best	Mean	Best	Mean	BBO	ABC- -HBBABC
Sphere	30	1.078	2.504	3.215	7.815	0.050	0.143	23.430	29.171
	50	15.692	20.509	18.615	22.885	3.296	4.460	13.085	16.615
	100	45.958	61.804	27.373	40.423	7.781	9.968	17.866	13.356
	200	117.133	149.820	59.827	80.398	19.351	22.552	16.962	15.481
Schwefel 2.22	30	3.600	7.128	4.000	6.720	0.000	0.066	38.917	40.539
	50	32.300	41.890	30.800	37.780	8.100	11.160	17.982	15.549
	100	82.000	97.790	58.600	72.260	19.500	25.220	21.983	18.078
	200	194.700	214.280	123.800	138.030	49.300	60.100	33.147	18.453
Schwefel 1.2	30	1687	4971	5926	13556	7369	12276	-23.507	2.671
	50	21581	30233	38196	55858	51359	75257	-7.424	-2.901
	100	92822	113219	156135	226183	178278	228703	-7.208	-0.113
	200	303333	355509	571897	728556	64230	440653	-0.991	2.924
Schwefel 2.21	30	25.500	47.082	37.900	60.934	36.900	58.062	-8.525	2.559
	50	63.900	66.868	78.800	79.914	81.500	79.874	-1.306	0.004
	100	69.400	82.640	86.500	92.610	85.800	91.070	-3.862	1.053
	200	88.300	92.390	94.500	96.150	94.300	96.380	-4.888	-0.423
Rosenbrock	30	48.997	117.287	107.642	205.920	19.963	28.034	25.096	28.686
	50	517.953	698.683	406.147	582.530	94.113	148.841	13.327	9.478
	100	1572.754	1915.736	796.838	1001.431	237.627	311.123	16.249	11.844
	200	3617.898	4706.759	1534.069	1857.636	559.278	668.473	17.562	20.332
Step	30	302	912	742	2828	16.000	75.080	21.255	27.929
	50	7304	11185	5636	7105	1460.000	2083.600	12.164	15.180
	100	15464	22224	10566	14859	3826.000	5361.400	11.514	7.596
	200	38448	52700	24749	29931	11132.000	13777.100	17.361	11.279
Quartic	30	0.019	0.094	0.037	0.195	0.000	0.000	15.777	18.343
	50	3.695	9.161	0.850	1.351	0.062	0.140	6.199	9.436
	100	19.336	40.968	2.877	4.984	0.331	0.870	8.778	8.410
	200	169.447	239.505	18.221	24.612	2.674	5.074	17.581	12.171
Schwefel 2.26	30	-11138	-10749	-8907	-8258	-11963.61	-11410.21	17.710	65.308
	50	-16262	-15778	-12171	-11514	-18411	-18016	11.659	22.303
	100	-32854	-30841	-24535	-22835	-35535	-34632	8.903	34.811
	200	-59440	-58118	-47483	-44980	-65880	-64368	10.302	22.015
Rastrigin	30	18.769	35.180	90.180	129.927	16.141	30.555	4.725	56.078
	50	144.350	159.983	467.228	536.967	96.676	147.285	1.290	26.909
	100	355.272	398.947	1020.308	1115.391	234.206	280.601	7.932	36.907
	200	838.478	907.235	2162.628	2353.384	458.595	541.145	20.615	61.021
Ackley	30	6.037	8.169	7.691	16.911	0.231	1.772	58.213	36.810
	50	10.609	12.483	19.923	19.930	5.335	6.822	14.892	50.080
	100	12.825	13.621	19.923	19.930	6.736	8.197	18.019	46.156
	200	13.927	14.501	19.925	19.931	7.605	8.441	27.032	70.353
Griewank	30	3.642	9.014	2.064	5.826	1.101	1.434	25.258	19.911
	50	53.643	72.828	25.408	39.197	8.034	13.328	11.365	6.976
	100	155.753	211.611	67.133	80.182	29.081	35.830	18.913	12.919
	200	385.648	484.405	127.770	161.764	86.818	113.142	19.470	4.391
Penalty 1	30	6.024	125269	15722	1422426	0.336	1.983	1.900	5.799
	50	767251	5781793	1342867	4503053	12.175	101.366	5.194	5.923
	100	4319626	16831372	5053622	11357689	50.224	556.008	5.718	5.933
	200	29233477	57270741	3980933	10125942	238.834	9106.955	6.687	6.496
Penalty 2	30	248	362503	172745	5265971	3.573	31.627	5.919	12.768
	50	6234168	18773181	6881823	16165647	296.413	45020.198	6.299	6.449
	100	54117223	97087010	15026298	34967350	45358	123262	7.160	6.761
	200	114373923	194879393	17566913	35550460	236611	727595	9.840	8.964
Fletcher	30	24917	68364	40390	105468	4829	28120	14.217	18.507

50	789748	1154052	1844496	2626204	499324	646130	6.500	9.428
100	3500122	4555957	10863455	12910759	2164663	2974089	5.744	20.746
200	16068045	20570768	45431035	53360024	9868405	14269770	5.199	16.630

Table 4

Success rate and Average minimum number of generation required for benchmark problems considering discrete design variables. '**Bold value**' indicates better value found.

Benchmark Functions	BBO		ABC		HBABC	
	SR*	AMG* SR	AMG	SR	AMG	SR
Sphere	0.550	400	NR	NR	1	110
Schwefel 2.22	0.360	300	0.920	45	1	40
Schwefel 1.2	NR*	NR*	NR	NR	NR	NR
Schwefel 2.21	NR*	NR*	NR	NR	NR	NR
Rosenbrock	NR	NR	NR	NR	NR*	NR*
Step	NR	NR	NR	NR	1	160
Quartic	1	180	NR	NR	1	150
Schwefel 2.26	NR	NR	NR	NR	NR*	NR*
Rastrigin	0.520	210	NR	NR	0.620	350
Ackley	NR	NR	0.900	350	1	50
Griewank	NR	NR	1	310	1	90
Penalty 1	NR	NR	NR	NR	1	210
Penalty 2	NR	NR	NR	NR	1	220
Fletcher	NR	NR	NR	NR	NR*	NR*

SR* Success Rate

AMG* Average number of Maximum Generations Required

Table 5

Comparison of HBABC with other optimization techniques. '**Bold value**' indicates better value found.

	Mean			Best		
	ACO	SGA	HBABC	ACO	SGA	HBABC
Griewank	-	7.63059	1.434	-	2.4531	1.1006
Penalty 1	67850279.99	7.98258	1.982893	0.23161	-	0.33582
Penalty 2	159465175.9	17083.97	31.62655	0.24281	-	3.5728
Quartic	-	0.023493	0.000479	-	0.001395	0.00005127
Rosenbrock	-	107.2454	28.03401	-	-	-
Schwefel 2.26	-	-8410.10	-11410.2	-3953.9	-	-11963.61
Step	-	618.6	75.08	-	222	16
Schwefel 1.2	-	-	-	-	3484.908	7369
Fletcher	-	-	-	-	20876.64	4829
Sphere	-	-	-	-	0.9543	0.050393

Table 6

Best results, Mean results and Success rate for the engineering optimization problems considering discrete design variables. '**Bold value**' indicates better solution found

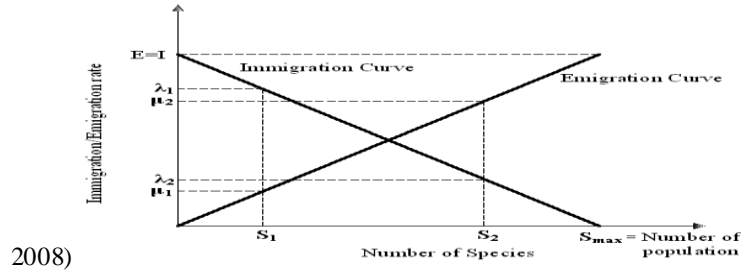
	BBO			ABC			HBABC			
	Best	Mean	SR*	Best	Mean	SR	Best	Mean	SR	
Gear Train	N50G100*	6.7E+05	1.6E+08	0.00	2.0E+06	1.9E+08	0.00	46.20	1.3E+07	0.08
	N100G100	43.64	4.6E+06	0.24	40.41	2.2E+07	0.36	35.36	52.49	1.00
Welded Structure	N50G100	55698.95	57160.11	0.04	55326.29	55980.17	0.60	55326.29	55729.30	0.72
	N100G100	55326.29	56877.94	0.12	55326.29	55769.47	0.72	55326.29	55381.83	0.96
10- Truss	N50G100	5556.28	5776.11	0.00	5498.37	5797.23	0.16	5490.74	5594.76	0.68
	N100G100	5559.91	5695.93	0.04	5491.72	5646.59	0.36	5490.74	5513.63	0.92
25- Truss	N50G100	494.83	510.92	0.00	484.85	489.20	0.80	484.85	484.95	1.00
	N100G100	485.77	501.17	0.12	484.85	487.16	0.88	484.85	484.85	1.00

Planetary Transmission	N50G100	0.527	0.629	0.04	0.536	0.556	0.00	0.526	0.536	0.48
	N100G100	0.533	0.607	0.04	0.530	0.538	0.12	0.526	0.529	0.84

SR* Success Rate

N50G100* Population size = 50, Number of Generation = 100

Figure 1 Species model for single habitat showing two candidate solutions (Simon ,



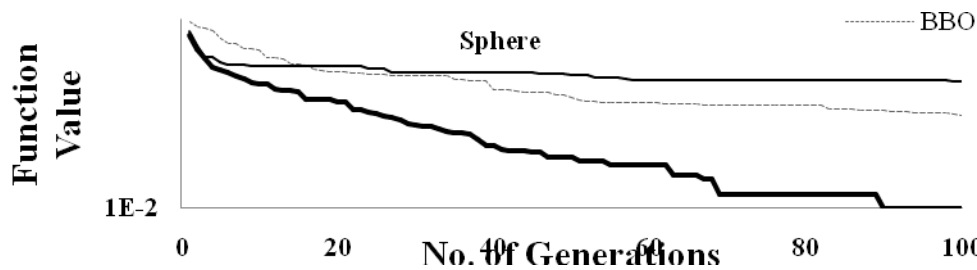
2008)

Figure 2

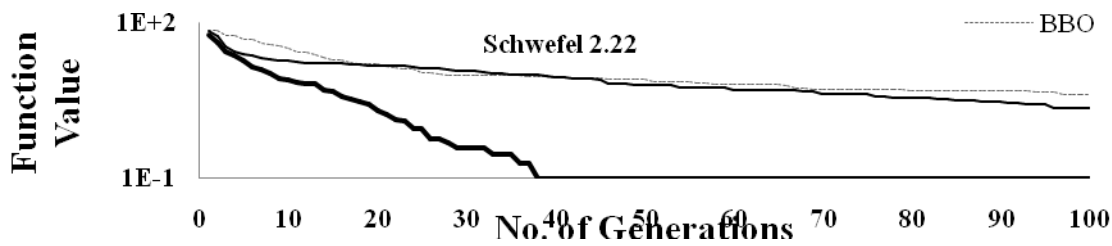
Convergence curve for different benchmark problems considering discrete design variables

(a) Sphere, (b) Schwefel 2.22, (c) Rastrigin (d) Fletcher

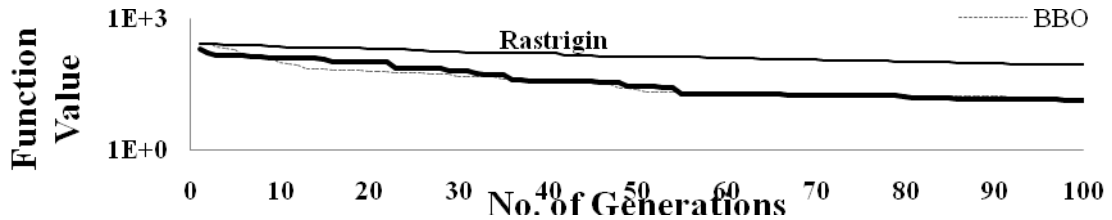
(a)



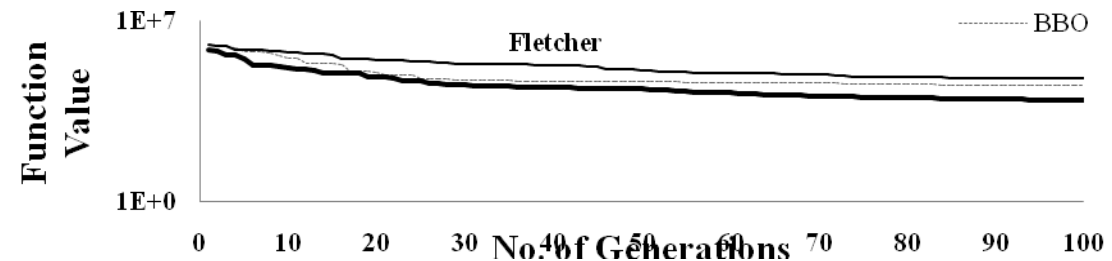
(b)



(c)



(d)



Video Compression Using Spiht and Neural Network

¹Sangeeta Mishra, ²Sudhir Sawarkar

Abstract

Apart from the existing technology on image compression represented by series of JPEG, MPEG and H.26x standards, new technology such as neural networks and genetic algorithms are being developed to explore the future of image coding. Successful applications of neural networks to basic propagation algorithm have now become well established and other aspects of neural network involvement in this technology. In this paper different algorithms were implemented like gradient descent back propagation, gradient descent with momentum back propagation, gradient descent with adaptive learning back propagation, gradient descent with momentum and adaptive learning back propagation and Levenberg-Marquardt algorithm. The compression ratio obtained is 1.1737089:1. It was observed that the size remains same after compression but the difference is in the clarity.

Keyword: Macroblock, Neural Network, SPIHT

1. Introduction

Reducing the transmission bit-rate while concomitantly retaining image quality is the most daunting challenge to overcome in the area of very low bit-rate video coding, e.g., H.26X standards [3].[6]. The MPEG-4 [2] video standard introduced the concept of content-based coding, by dividing video frames into separate segments comprising a background and one or more moving objects. This idea has been exploited in several low bit-rate macroblock-based video coding algorithms [1][8] using a simplified segmentation process which avoids handling arbitrary shaped objects, and therefore can employ popular macroblock-based motion estimation techniques. Such algorithms focus on moving regions through the use of regular pattern templates, from a pattern codebook (Figure 1), of non-overlapping rectangular blocks of 16×16 pixels, called macroblocks (MB).

2. SPIHT

When the decomposition image is obtained, we try to find a way how to code the wavelet coefficients into an efficient result, taking redundancy and storage space into consideration. SPIHT [2] is one of the most advanced schemes available, even outperforming the state-of-the-art JPEG 2000 in some situations. The basic principle is the same; a progressive coding is applied, processing the image respectively to a lowering threshold. The difference is in the concept of zerotrees (spatial orientation trees in SPIHT). This is an idea that takes bounds between coefficients across subbands in different levels into consideration. The first idea is always the same: if there is an coefficient in the highest level of transform in a particular subband considered insignificant against a particular threshold, it is very probable that its descendants in lower levels will be insignificant too, so we can code quite a large group of coefficients with one symbol. SPIHT makes use of three lists – the List of Significant Pixels (LSP), List of Insignificant Pixels (LIP) and List of Insignificant Sets (LIS). These are coefficient location lists that contain their coordinates. After the initialization, the algorithm takes two stages for each level of threshold – the sorting pass (in which lists are organized) and the refinement pass (which does the actual progressive coding transmission). The result is in the form of a bitstream. Detailed scheme of the algorithm is presented in Fig. 3. The algorithm has several advantages. The first one is an intensive progressive capability – we can interrupt the decoding (or coding) at any time and a result of maximum possible detail can be reconstructed with one-bit precision. This is very desirable when transmitting files over the internet, since users with slower connection speeds can download only a small part of the file, obtaining much more usable result when compared to other codec such as progressive JPEG. Second advantage is a very compact output bitstream with large bit variability – no additional entropy coding or scrambling has to be applied. It is also possible to insert a watermarking scheme into the SPIHT coding domain [3] and this watermarking technique is considered to be very strong regarding to watermark invisibility and attack resiliency. But we also have to consider disadvantages. SPIHT is very vulnerable to bit corruption, as a single bit error can introduce significant image distortion depending of its location. Much worse property is the need of precise bit synchronization, because a leak in bit transmission can lead to complete misinterpretation from the side of the decoder. For SPIHT to be employed in real-time applications, error handling and synchronization methods must be introduced in order to make the codec more resilient.

3. Principle Of SPIHT Coder:

SPIHT is based on three principles: i) Exploitation of the hierarchical structure of the wavelet transform, by using a tree-based organization of the coefficients;

- ii) Partial ordering of the transformed coefficients by magnitude, with the ordering data not explicitly transmitted but recalculated by the decoder; and
- iii) Ordered bit plane transmission of refinement bits for the coefficient values.

This leads to a compressed bitstream in which the most important coefficients are transmitted first, the values of all coefficients are progressively refined, and the relationship between coefficients representing the same location at different scales is fully exploited for compression efficiency. SPIHT is a very effective, popular and computationally simple technique for image compression, it belongs to the next generation of wavelet encoders. SPIHT exploits the properties of the wavelet-transformed images to increase its efficiency. It offers better performance than previously reported image compression techniques. In this technique the pixels are divided into sets and subsets. Under the same assumption of zerotrees used in EZW, SPIHT coder scans wavelet coefficients along quad tree instead of subband and SPIHT identifies significance of wavelet coefficients only by the magnitude of coefficients and encodes the sign separately into a new bit stream. Initial threshold is calculated using the equation. The significance test is applied to these pixels. If these pixels are found to be significant with respect to threshold, they are taken into consideration for transmission otherwise ignored.

The Coding / decoding algorithm has following steps:

1) **Initialization:** Set $n = \lfloor \log_2 (\max_{(i,j)} \{ |c(i,j)| \}) \rfloor$ & transmit n .

Set the LSP as an empty set list, and add the coordinates

$(i, j) \in \square H$ to the LIP and only those with descendants also to the LIS, as the type A entries.

2) **Sorting pass:**

2.1 for each entry (i, j) in the LIP do:

2.1.1 output $S_n(i, j)$;

2.1.2 if $S_n(i,j)=1$, move (i,j) to the LSP and output the sign of $c_{i,j}$;

2.2 for each entry (i, j) in the LIS do:

2.2.1 if the entry is of type A then

2.2.1.1 output $S_n(D(i, j))$;

2.2.1.2 if $S_n(D(i, j)) = 1$ then

2.2.1.2.1 for each $(k, l) \in \square O(i, j)$ do:

2.2.1.2.1.1 output $S_n(k, l)$;

2.2.1.2.1.2 if $S_n(k, l) = 1$, add (k, l) to the LSP and output the sign of $c_{k,l}$;

2.2.1.2.1.3 if $S_n(k, l) = 0$, add (k, l) to the LIP;

2.2.1.2.2 if $\xi(i, j) \neq 0$, move (i, j) to the end of the LIS as an entry of type B and go to Step 2.2.2 ;

otherwise, remove entry (i, j) from the LIS;

2.2.2 if the entry is of type B then

2.2.2.1 output $S_n(\xi(i, j))$;

2.2.2.2 if $S_n(\xi(i, j)) = 1$ then

2.2.2.2.1 add each $(k, l) \in \square O(i, j)$ to the end of the LIS as entry of type A;

2.2.2.3 remove (i, j) from the LIS;

3) **Refinement pass:** for each entry (i, j) in the LSP, except those included in the last sorting pass (i.e. with same n), output the n th most significant bit of $|c_{i,j}|$;

4) **Quantization step update:** decrement n by 1 and go to Step 2 if needed.

4. Neural network

1. Neural network outline

Neural network (NN) is a nonlinearity complex network system which consists of large quantities of processing unit analogizing neural cells, has the capability of approaching the nonlinear function, very strong fault-tolerant ability and the quick study speed of local network. Among them, feed forward network consists of three layers: the input layer, the hidden layer and the output layer. The hidden layer may have many layers, each layer neurons only accepts the previous layer neurons' output. And then, this realizes the input and output nonlinear mapping relationship by adjusting the connected weighted value and the network structure[1]. At present the neural network research method has formed many schools, the most wealthiest research work includes: the multi-layer network BP algorithm, Hopfield neural network model, adaptive resonance theory, self-organizing feature map theory and so on. This paper is based on researching BP neural network training

quantification parameter [2], presents a network that is better than BP (Back Propagation) network in its property of optimal approximation.

2. Feed Forward Network

A single-layer network of neurons having R inputs is shown below in fig. 1, full detail on the left and with a layer diagram on the right.

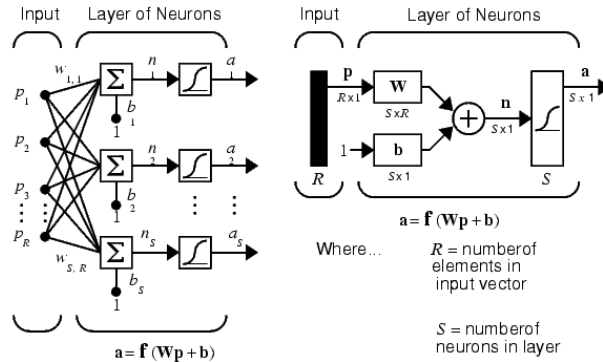


Fig.1. Feed Forward Network

Feed forward networks often have one or more hidden layers of sigmoid neurons followed by an output layer of linear neurons. Multiple layers of neurons with nonlinear transfer functions allow the network to learn nonlinear and linear relationships between input and output vectors. The linear output layer lets the network produce values outside the range -1 to +1. For multiple-layer networks we use the number of the layers to determine the superscript on the weight matrices. The appropriate notation is used in the two-layer tansig/purelin network shown in fig 2.

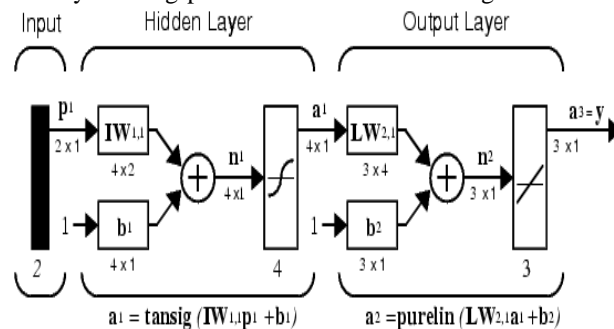


Fig.2 Multiple Layer Input

This network can be used as a general function approximation. It can approximate any function with a finite number of discontinuities, arbitrarily well, given sufficient neurons in the hidden layer.

3. Back propagation algorithm:

Back propagation was created by generalizing the Widrow-Hoff learning rule to multiple-layer networks and nonlinear differentiable transfer functions. Input vectors and the corresponding target vectors are used to train a network until it can approximate a function, associate input vectors with specific output vectors, or classify input vectors in an appropriate way as defined by you. Networks with biases, a sigmoid layer, and a linear output layer are capable of approximating any function with a finite number of discontinuities. Standard back propagation is a gradient descent algorithm, as is the Widrow-Hoff learning rule, in which the network weights are moved along the negative of the gradient of the performance function. The term *back propagation* refers to the manner in which the gradient is computed for nonlinear multilayer networks. There are a number of variations on the basic algorithm that are based on other standard optimization techniques, such as conjugate gradient and Newton methods. There are generally four steps in the training process:

1. Assemble the training data
2. Create the network object
3. Train the network
4. Simulate the network response to new inputs

The generalized delta rule, also known as back propagation algorithm is explained here briefly for feed forward Neural Network (NN). The NN explained here contains three layers. These are input, hidden, and output Layers. During the training phase, the training data is fed into to the input layer. The data is propagated to the hidden layer and then to the output layer. This is called the forward pass of the back propagation algorithm. In forward pass, each node in hidden layer gets input from all the nodes from input layer, which are multiplied with appropriate weights and then summed. The output of the hidden node is the non- linear transformation of this resulting sum. Similarly each node in output layer gets input from all the nodes from hidden layer, which are multiplied with appropriate weights and then summed. The output of this node is the non-linear transformation of the resulting sum. The output values of the output layer are compared with the target output values. The target output values are those that we attempt to teach our network. The error between actual output values and target output values is calculated and propagated back towards hidden layer. This is called the backward pass of the back propagation algorithm. The error is used to update the connection strengths between nodes, i.e. weight matrices between input-hidden layers and hidden-output layers are updated.

4. Results And Discussions

During the testing phase no learning takes place i.e., weight matrices are not changed. Each test vector is fed into the input layer. The feed forward of the testing data is similar to the feed forward of the training data. Various algorithms were tried and tested.



Fig. 3 Original Residue Frame



Fig.4 Frame after SPIHT with gradient descent with momentum and adaptive learning back propagation



Fig.5 Frame after SPIHT with gradient descent with adaptive learning back propagation



Fig.6 Frame after SPIHT with gradient descent with momentum back propagation

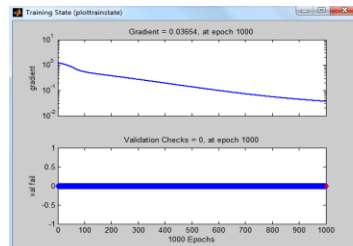


Fig.7 Training Achieved

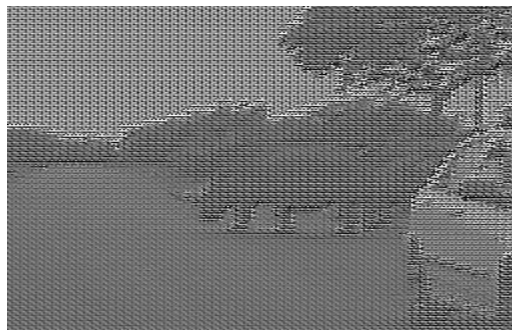


Fig.8 Frame after SPIHT with gradient descent back propagation



Fig.9 Frame after SPIHT with Levenberg-Marquardt algorithm

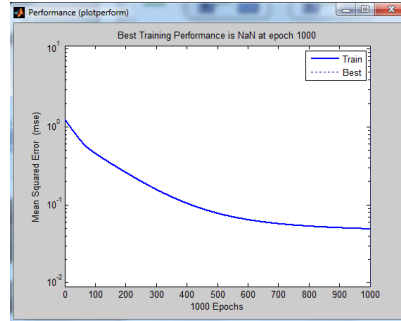


Fig.10 Performance Achieved

5. References

1. M.Vetterli and J Kovacevic, Wavelets & Subband Coding, Prentice Hall PTR, Englewood cliffs, NJ, 1995.
2. C. Sidney Burrus, Ramesh A Gopinath, and Haitao Guo, Introduction to Wavelets & Wavelets Transforms, Prentice Hall Inc, Upper Saddle River, NJ,1998.
3. O Rioul and M Vetterli,“Wavelets and signal processing,” IEEE Signal Processing Magazine, vol. 8, no. 4, pp. 14–38, 1991.
4. A. Said, W. A. Pearlman, “SPIHT Image Compression: Properties of the Method”, Html
5. A. Said, W.A. Pearlman: “A New Fast and Efficient Image Codec Based on Set Partitioning in Hierarchical Trees”, IEEE Transactions on Circuits and Systems for Video Technology, vol. 6,1996.
6. J.A.Freeman and D.M.Skapura, Neural Networks: algorithms, Applications and Programming Techniques Addition-Wesley), 1991.
7. H.Demuth and M. Beale. Neural Network TOOLBOX User’s Guide. For use with MATLAB. The Math Works Inc.. (1998)
8. Kiamal Z. Pekmestzi. Multiplexer-Based Array Multipliers. IEEE Transcation on computers, vol, 48 , JAN (1998)
9. Hennessy. J.L and Patterson. D.A. Computer Architecture: A quantitative Approach. Morgan Kaufmanns, (1990)
10. J. Jiang. Image compression with neural networks. Signal Processing: Image Communication 14 (1999) 737-760

Matching Dominating Sets of Euler Totient Cayley Graphs

^{1,2}**M.Manjuri, ²B.Maheswari**

^{1,2}Department of Applied Mathematics, Sri Padmavati Women's University,
Tirupati - 517502, Andhra Pradesh, India.

Abstract

Graph Theory has been realized as one of the most useful branches of Mathematics of recent origin, finding widest applications in all most all branches of sciences, social sciences, computer science and engineering. Nathanson[3] paved the way for the emergence of a new class of graphs, namely, Arithmetic Graphs by introducing the concepts of Number Theory, particularly, the Theory of congruences in Graph Theory. Cayley graphs are another class of graphs associated with the elements of a group. If this group is associated with some arithmetic function then the Cayley graph becomes an arithmetic graph. The Cayley graph associated with Euler Totient function is called an Euler Totient Cayley graph and in this paper we study the matching domination parameters of Euler Totient Cayley graphs.

Keywords: Euler Totient Cayley Graph, Matching Dominating sets.

1. Introduction

Cayley graph

Let (X, \cdot) be a group and S , a symmetric subset of X not containing the identity element e of X . The graph G whose vertex set $V = X$ and edge set $E = \{(g, gs) / s \in S\}$ is called the Cayley graph of X corresponding to the set S and it is denoted by $G(X, S)$. Madhavi [2] introduced the concept of Euler totient Cayley graphs and studied some of its properties.

Euler Totient Cayley Graph

For each positive integer n , let Z_n be the additive group of integers modulo n and S be the set of all numbers less than n and relatively prime to n . The Euler totient Cayley graph $G(Z_n, \varphi)$ is defined as the graph whose vertex set V is given by $Z_n = \{0, 1, 2, \dots, n-1\}$ and the edge set is given by $E = \{(x, y) / x - y \in S \text{ or } y - x \in S\}$. Clearly as proved by Madhavi [2], the Euler totient Cayley graph $G(Z_n, \varphi)$ is

1. a connected, simple and undirected graph,
2. $\varphi(n)$ - regular and has $\frac{n \cdot \varphi(n)}{2}$ edges,
3. Hamiltonian,
4. Eulerian for $n \geq 3$,
5. bipartite if n is even and
6. complete graph if n is a prime.

2. Matching Dominating Sets of Euler Totient Cayley Graphs

The theory of domination in Graphs introduced by Ore [4] and Berge [1] is an emerging area of research today. The domination parameters of Euler Totient Cayley graphs are studied by Uma Maheswari [6] and we present some of the results without proofs and can be found in [5].

Theorem 2.1: If n is a prime, then the domination number of $G(Z_n, \varphi)$ is 1.

Theorem 2.2: If n is power of a prime, then the domination number of $G(Z_n, \varphi)$ is 2.

Theorem 2.3: The domination number of $G(Z_n, \varphi)$ is 2, if $n = 2p$ where p is an odd prime.

Theorem 2.4: Suppose n is neither a prime nor $2p$. Let $n = p_1^{\alpha_1} p_2^{\alpha_2} \dots p_k^{\alpha_k}$, where p_1, p_2, \dots, p_k are primes and $\alpha_1, \alpha_2, \dots, \alpha_k$ are integers ≥ 1 . Then the domination number of $G(Z_n, \varphi)$ is given by $\gamma(G(Z_n, \varphi)) = \lambda + 1$, where λ is the length of the longest stretch of consecutive integers in V , each of which shares a prime factor with n . A matching in a graph $G(V, E)$ is a subset M of edges of E such that no two edges in M are adjacent. A matching M in G is called a

perfect matching if every vertex of G is incident with some edge in M . Let $G(V, E)$ be a graph. A subset D of V is said to be a dominating set of G if every vertex in $V - D$ is adjacent to a vertex in D . The minimum cardinality of a dominating set is called the domination number of G and is denoted by $\gamma(G)$. A dominating set D of G is said to be a matching dominating set if the induced subgraph $\langle D \rangle$ admits a perfect matching. The cardinality of the smallest matching dominating set is called the matching domination number and is denoted by γ_m .

Theorem 1: The matching domination number of $G(Z_n, \varphi)$ is 2, if n is a prime.

Proof: Let n be a prime. Then $G(Z_n, \varphi)$ is a complete graph. It is clear that $\{0\}$ is a minimal dominating set as it dominates all other vertices of $\{1, 2, \dots, n-1\}$. Therefore $\gamma(G(Z_n, \varphi)) = 1$. For any $t \in \{1, 2, \dots, n-1\}$, vertex 0 is adjacent to vertex t . So if $D_m = \{0, t\}$, then the induced subgraph $\langle D_m \rangle$ admits a perfect matching with minimum cardinality. Hence D_m is a minimal matching dominating set of $G(Z_n, \varphi)$. Therefore $\gamma_m(G(Z_n, \varphi)) = 2$. ■

Theorem 2: If n is power of a prime, then the matching domination number of $G(Z_n, \varphi)$ is 2.

Proof: Consider $G(Z_n, \varphi)$ for $n = p^\alpha$ where p is a prime. Then the vertex set V of $G(Z_n, \varphi)$ is given by $V = \{0, 1, 2, \dots, p^\alpha - 1\}$. This set V falls into disjoint subsets as below.

1. The set S of integers relatively prime to n ,
2. The set M of multiples of p ,
3. Singleton set $\{0\}$. Let $D_m = \{0, t / \text{GCD}(t, n) = 1\}$ where $t \in \{0, 1, 2, \dots, p^\alpha - 1\}$. Then D_m becomes a minimum dominating set of $G(Z_n, \varphi)$ as in Theorem 2.2. Since $\text{GCD}(t, n) = 1$, $t \in S$, the vertices 0 and t are adjacent. This gives that $\langle D_m \rangle$ admits a perfect matching. So D_m is a matching dominating set of $G(Z_n, \varphi)$ of minimum cardinality. Hence it follows that $\gamma_m(G(Z_n, \varphi)) = 2$. ■

Theorem 3: The matching domination number of $G(Z_n, \varphi)$ is 4 if $n = 2p$, where p is an odd prime.

Proof: Let us consider the Euler totient Cayley graph $G(Z_n, \varphi)$ for $n = 2p$, p is an odd prime. Then the vertex set $V = \{0, 1, 2, \dots, 2p - 1\}$ falls into the following disjoint subsets.

1. The set S of odd numbers which are less than n and relatively prime to n ,
2. The set M of non-zero even numbers,
3. The set D_m of numbers 0 and p .

Then $D_m = \{0, p\}$ becomes a minimum dominating set of $G(Z_n, \varphi)$ as in Theorem 2.3. Further the vertices in D_m are non-adjacent because $\text{GCD}(p, n) \neq 1$. This gives that $\langle D_m \rangle$ does not admit a perfect matching. So D_m is not a matching dominating set of $G(Z_n, \varphi)$. In order that D_m admits a perfect matching, we need to add at least two vertices adjacent to each of the vertex in D_m so that $\gamma_m(G(Z_n, \varphi)) \geq 4$. Let $D'_m = \{0, p, r, p+r / \text{GCD}(r, n) = 1\}$. Then $D_m \subset D'_m$. This implies that D'_m is a dominating set of $G(Z_n, \varphi)$. Moreover, since $\text{GCD}(r, n) = 1$, vertex 0 is adjacent to vertex r and vertex p is adjacent to vertex $p+r$. Further we have $\text{GCD}(p, n) \neq 1$. Hence 0 and p are non-adjacent and similarly r and $p+r$ are non-adjacent. So $\langle D'_m \rangle$ admits a perfect matching. Hence D'_m is a matching dominating set of minimum cardinality. Thus $\gamma_m(G(Z_n, \varphi)) = 4$. ■

Theorem 4: Let n be neither a prime nor $2p$ and $n = p_1^{\alpha_1} p_2^{\alpha_2} \dots p_k^{\alpha_k}$, where p_1, p_2, \dots, p_k are primes and $\alpha_1, \alpha_2, \dots, \alpha_k$ are integers ≥ 1 . Then the matching domination number of $G(Z_n, \varphi)$ is given by

$$\gamma_m(G(Z_n, \varphi)) = \begin{cases} \lambda + 1 & \text{if } \lambda \text{ is odd} \\ \lambda + 2 & \text{if } \lambda \text{ is even} \end{cases}$$

Where λ is the length of the longest stretch of consecutive integers in V each of which shares a prime factor with n .

Proof: Let us consider $G(Z_n, \varphi)$ for $n = p_1^{\alpha_1} p_2^{\alpha_2} \dots p_k^{\alpha_k}$ where n is neither a prime nor $2p$. The vertex set V of $G(Z_n, \varphi)$ is given by $V = \{0, 1, 2, \dots, n-1\}$. Then the set V falls into disjoint subsets as follows.

1. The set S of integers relatively prime to n ,
2. The set $X = \{S_i\}$, where S_i is a collection of consecutive positive integers such that for every x in S_i , $\text{GCD}(x, n) > 1$,
3. The singleton set $\{0\}$.

Let S_λ be the largest set in X with maximum cardinality λ . Suppose

$S_\lambda = \{x_1, x_2, \dots, x_\lambda\}$, where $\text{GCD}(x_i, n) > 1$ for $i = 1, 2, 3, \dots, \lambda$. Then $D_m = \{0, 1, 2, \dots, \lambda\}$ is a dominating set of minimum cardinality, as in Theorem 2.4. Now two cases arise.

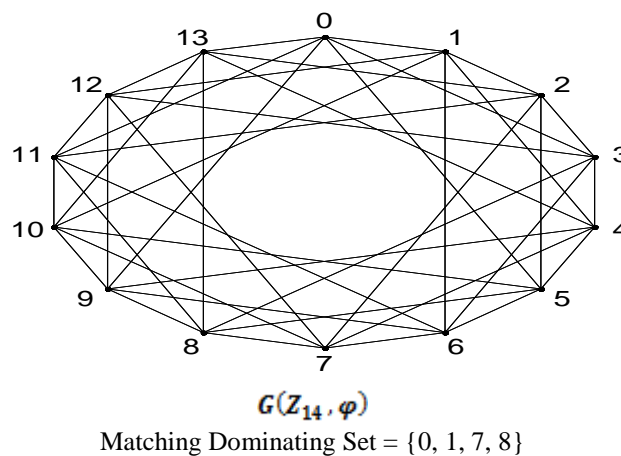
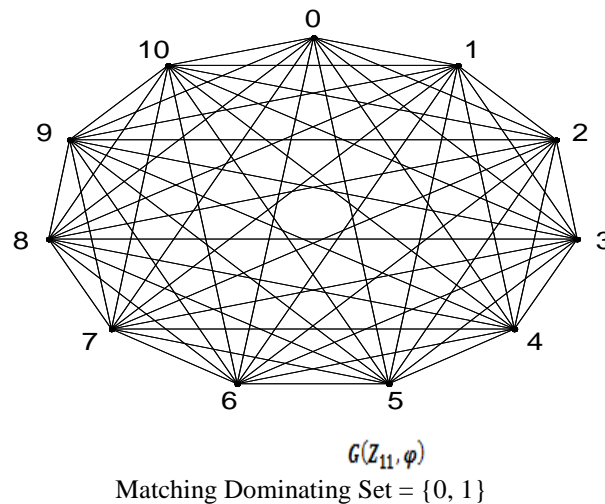
Case 1: Suppose λ is an odd number.

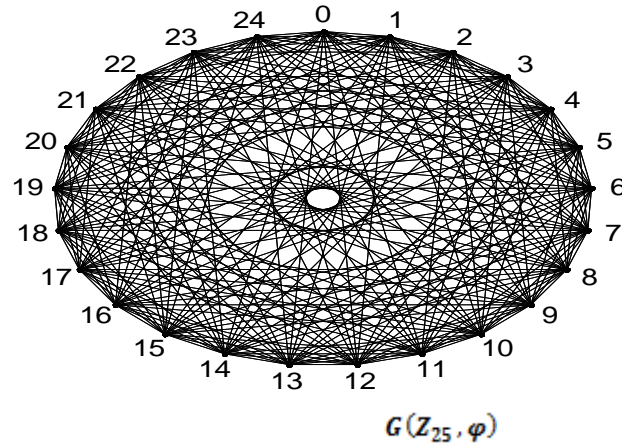
Consider the set $E_1 = \{(0,1), (2,3), \dots, (\lambda-1, \lambda)\}$. Each pair $(2i, 2i+1)$, $0 \leq i \leq \frac{\lambda-1}{2}$ is an edge of $G(Z_n, \varphi)$ as $(2i+1) - 2i = 1 \in S$. So E_1 is a set of edges in $G(Z_n, \varphi)$. Obviously, no two edges in E_1 are adjacent. So $\langle E_1 \rangle$ admits a perfect matching. Hence D_m becomes a matching dominating set of $G(Z_n, \varphi)$. Since $\gamma(G(Z_n, \varphi)) = \lambda + 1$, we have $\gamma_m(G(Z_n, \varphi)) \geq \lambda + 1$. As $|D_m| = \lambda + 1$, it follows that D_m is a minimum matching dominating set of $G(Z_n, \varphi)$. Therefore $\gamma_m(G(Z_n, \varphi)) = \lambda + 1$, if λ is an odd number.

Case 2: Suppose λ is an even number.

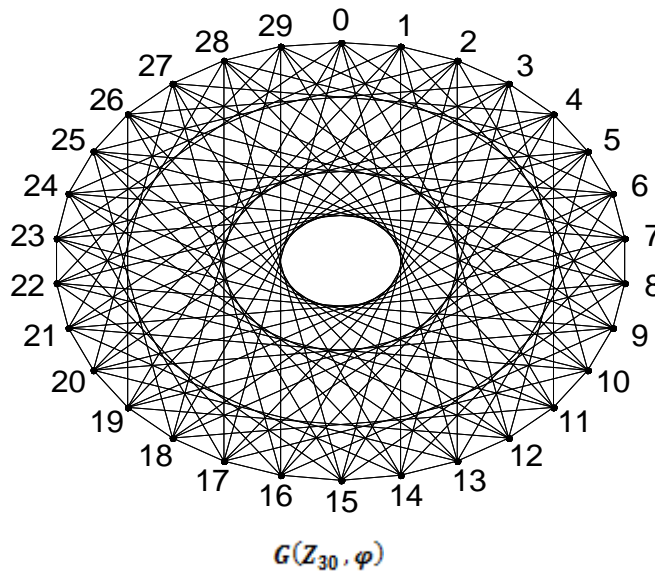
Let $D'_m = \{0, 1, 2, \dots, \lambda, \lambda + 1\}$. Since $D_m \subset D'_m$ it follows that D'_m is a dominating set of $G(Z_n, \varphi)$. Consider the set $E_2 = \{(0,1), (2,3), \dots, (\lambda, \lambda + 1)\}$. As $(2i + 1) - 2i = 1 \in S$, each pair $(2i, 2i + 1)$, $0 \leq i \leq \frac{\lambda}{2}$ is an edge of $G(Z_n, \varphi)$. So E_2 is a set of edges in $G(Z_n, \varphi)$. Again it can be seen that no two edges in E_2 are adjacent. So $\langle E_2 \rangle$ admits a perfect matching. Hence D'_m is a matching dominating set of $G(Z_n, \varphi)$. Now λ is an even number implies that $\lambda + 1$ is an odd number. Since the matching domination number is always even it follows that $\gamma_m(G(Z_n, \varphi)) \geq \lambda + 2$. Therefore D'_m is a minimal matching dominating set of $G(Z_n, \varphi)$. Hence $\gamma_m(G(Z_n, \varphi)) = \lambda + 2$, if λ is an even number. ■

3. Illustrations





Matching Dominating Set = {0, 1}



Matching Dominating Set = {0, 1, 2, 3, 4, 5}

References

1. Berge, C. - The Theory of Graphs and its Applications, Methuen, London (1962).
2. Madhavi, L. - Studies on domination parameters and enumeration of cycles in some Arithmetic Graphs, Ph. D. Thesis submitted to S.V.University, Tirupati, India, (2002).
3. Nathanson and Melvyn B. - Connected components of arithmetic graphs, Monat.fur.Math, 29,219 – 220 (1980).
4. Ore, O. - Theory of Graphs, Amer. Math. Soc. Colloq. Publ., 38, Providence, (1962).
5. Uma Maheswari, S and Maheswari, B. – Domination parameters of Euler Totient Cayley Graphs, Rev.Bull.Cal.Math.Soc. 19, (2), 207-214(2011).
6. Uma Maheswari, S. - Some Studies on the Product Graphs of Euler Totient Cayley Graphs and Arithmetic V_n Graphs, Ph. D. Thesis submitted to S.P.Women's University, Tirupati, India, (2012).

Preparation and Characterization of Natural Degradable Microcapsules

M. Geetha Devi¹, Susmita Dutta², Ashraf Talib Al- Hinai³ and S.Feroz⁴

^{1, 2} Department of Chemical Engineering, National Institute of Technology Durgapur, India

³ Department of Chemistry, Sultan Qaboos University, Sultanate of Oman

⁴ Caledonian College of Engineering, Sultanate of Oman

Abstract

In this work, multilayer microcapsules of size 350 nm were prepared by layer-by-layer (L-b-L) assembly of oppositely charged chitosan and dextran sulphate on silica template, followed by removal of silica using Hydrofluoric acid. Particular emphasis is given on synthesis of monodisperse silica particles (310nm) with fine spherical shape. The hollow microcapsules obtained by the removal of the colloidal template with hydrofluoric acid solution were characterized by Scanning Electron Microscopy (SEM) and Energy Dispersive X-ray Analysis (EDX). The size distribution of silica particle was analyzed by Dynamic Light Scattering (DLS) method. Scanning electron microscopy (SEM) and Energy dispersive X-ray spectroscopy (EDX) measurements proved the purity of the hollow capsules. These microcapsules can be used for drug encapsulation and release in pharmaceutical applications.

Keywords: Biodegradable polymers, Chitosan, Dextran sulphate, L-b-L technique, Polyelectrolytes.

1. Introduction

Drug delivery is becoming a whole interdisciplinary field of research gaining much attention in pharmaceutical industry. Controlled release technologies are more popular in modern medicine and pharmaceuticals. Various drug delivery systems have been formulated using different types of materials such as micelles [1], lipid vesicles [2], micro particles [3, 4] and hydrogels [5]. Capsules were fabricated using wide variety of polymers such as synthetic polyelectrolytes, polysaccharides, polynucleotides etc. The layer-by-layer (L-b-L) self-assembly technique is a useful technology to fabricate multilayer thin films of nanometer precision [6]. L-b-L technology takes advantage of the charge-charge interaction between substrate and polyelectrolytes to create multilayers by electrostatic interactions. The main attractions of L-b-L method include the process is simple, inexpensive, fine tuning of layer thickness and independent of shape and geometry of template. Capsules in the nanometer to micrometer range are important for a range of different applications, including the encapsulation and controlled release of substances. The permeability of capsule wall and release of encapsulated drug depend on the thickness and composition of the shell.

During last few years much attention have been given to polysaccharides such as carboxy methyl cellulose [7], chitosan sulphate [8], chitosan [9] and dextran sulphate [10] for capsule preparation due to their excellent properties like biodegradation, biocompatibility, non-toxicity, and adsorption. The applications of Chitosan in pharmaceutical industry showed a great potential as a drug carrier system [11-21]. Chitosan is a non-toxic, biocompatible polymer that has found a number of applications in controlled drug delivery. Predominantly, polystyrene (PS), melamine Formaldehyde (MF), CaCO₃, MnCO₃ etc. has been employed as templates for the L-b-L preparation of capsules. Each of these sacrificial cores has certain limitations associated with their application. The main attraction of silica particles is it can be used in the presence of biological materials without significantly affecting bioactivity. The biodegradable and biocompatible nature of dextran sulphate has been used for the controlled release of basic drugs. The negatively charged sulphate groups of dextran sulphate binds with positively charged amino groups of chitosan to form polyelectrolyte complexes [22]. Biodegradability is one of the most important requirements in biomedical applications. In this paper, fabrication of microcapsules by layer-by-layer technique using chitosan and dextran sulphate was presented. These microcapsules can be used for drug encapsulation and release in pharmaceutical applications.

2. Materials and Methods

2.1 Materials

Chitosan (Mw 650000Da, degree of deacetylation >75%) and Dextran sulphate (Mw 500000Da), were obtained from Sigma Aldrich, Bangalore, India. Monodisperse colloidal silica particles of size 310 nm was synthesised in our laboratory. TEOS (tetra ethyl ortho silicate), NH₄OH, C₂H₅OH, NaCl, HCl and HF were obtained from Merck, India. Millipore water (18.2MΩ resistivity) was used in all experiments.

2.2 Methods

2.2.1 Silica template preparation

The synthesis of monodisperse silica particles were carried out based on Stober's protocol [23]. The mean diameter and particle size distribution of silica particles were measured by Dynamic Light Scattering (DLS) method using a Brookhaven B1 9000AT analyzer (Brookhaven Instruments Corporation, USA).

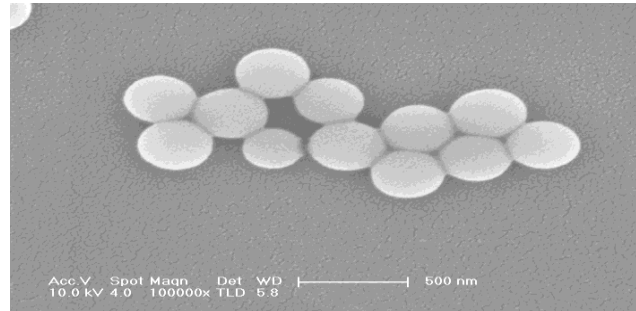


Figure 1. Scanning Electron Micrograph of Silica Particles

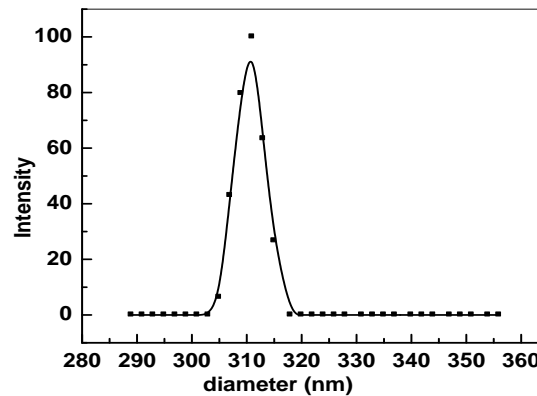


Fig. 2. Size distribution of Silica Particles

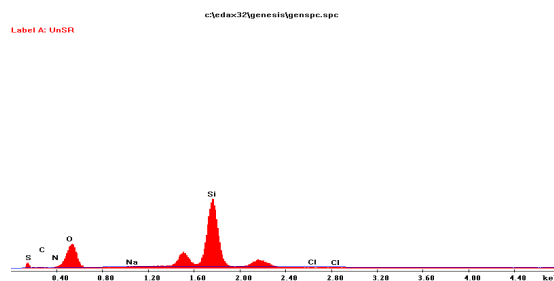


Fig.3. EDX Spectra of Silica Particles

2.2.2. Preparation of capsules

Capsules were prepared by the L-b-L technique [24, 25] with chitosan as the first layer. The adsorption of polyelectrolytes (1mg/ml) was conducted in 1M NaCl solution for 15 minutes followed by three washings in water. Then the respective oppositely charged polyelectrolytes were adsorbed. After the desired number of layers was deposited, the coated particles were treated with 1M HF to remove silica core. The resulting hollow capsules were washed with pure water and centrifuged 5 times to remove traces of HF. The capsules were characterised by SEM (FEI- Sirion, Eindhoven, The

Netherlands) at an operating voltage of 3kV. Samples were prepared by placing a drop of capsule suspension on a pre-cleaned silicon wafer, dried under a nitrogen stream followed by gold sputtering.

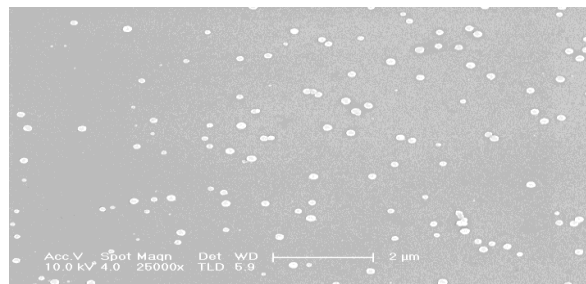


Fig.4. Chitosan - Dextran sulphate hollow capsules

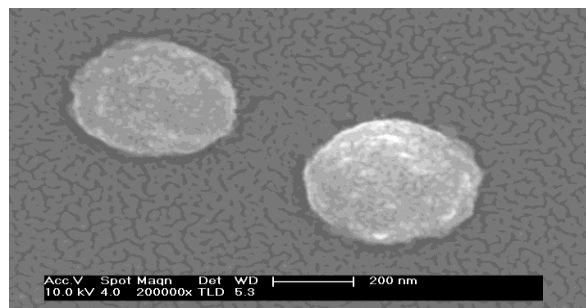


Fig.5. Chitosan - Dextran sulphate hollow capsules at high magnification

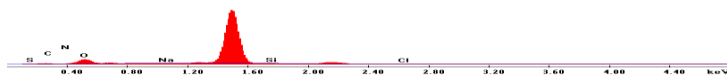


Fig.6. EDX Spectra of Chitosan - Dextran sulphate hollow capsules

3. Results and Discussion

Silica particles were synthesized by the Stober's protocol. The Scanning Electron Micrograph as shown in Fig.1 illustrates that the particles are spherical, well dispersed and of uniform size. Particle size analysis in Fig.2 showed a narrow size distribution with an average size of 310nm. Figure 3 shows the EDX spectra of silica particles. All analyses were repeated six times and the results were averaged. DLS measurements were done with a laser wavelength of 658.0 nm and at 27°C. Eight layers of polyelectrolytes were deposited followed by core dissolution. The capsules were rinsed 3 times with water before use. Fig.4 and Fig.5 shows the micrograph of hollow capsules. The capsules showed good integrity and high yield with diameter around 350 nm. The capsule wall appears thick due to the high molecular weight of the polyelectrolytes used. EDX spectra in Fig.6 reveal that the silica cores have been completely removed from the capsules. No aggregation of the capsules was observed which is critical from application point of view. L-b-L self-assembly has the advantages of accurate control over size, composition, and the thickness of the multilayer shell make these capsules very promising for a number of applications in materials and biomedical science.

4. Conclusion

In this study, chitosan- dextran sulphate hollow capsules of about 350 nm were prepared by the layer-by-layer technique using silica as template. The employability of silica particles as template proves the successful fabrication of capsules. The surface texture of the particle surface determines the morphology of the derived capsules as well as the capsule wall thickness. The obtained capsules are of special interest in pharmaceutical applications due to their desirable wall thickness ,

surface texture and high surface area. The layer-by-layer (L-b-L) templating technique has attracted significant interest as a simple, highly versatile approach that has been widely used to prepare nanostructured materials with tailored properties.

5. Acknowledgements

The authors express their sincere thanks to Dr. David K Daniel, VIT University, for providing laboratory facilities. We also thank Dr. Ashok and Dr. Sankar for the fruitful discussions and technical support.

References

- [1]. A.V. Ambade, E.N. Savariar, and S. Thayumanavan. Dendrimeric micelles for controlled drug release and targeted delivery. *Mol. Pharm*, 2: 264–272, 2005.
- [2]. X. Guo and F. Szoka. Chemical approaches to triggerable lipid vesicles for drug and gene delivery. *Acc. Chem. Res*, 36: 335–341, 2003.
- [3]. Q.H. Zhao, B.S. Han, C.Y. Gao, C.H. Peng, and J.C. Shen. Hollow chitosan–alginate multilayer microcapsules as drug delivery vehicle: doxorubicin loading and in vitro and in vivo studies, *Nanomed. NBM*, 3 : 63–74, 2007.
- [4]. Q.H. Zhao, Z.W. Mao, C.Y. Gao, and J.C. Shen, Assembly of multilayer microcapsules on CaCO₃ particles from biocompatible polysaccharides. *J. Biomater. Sci. Polym. Ed*, 17: 997–1014, 2006.
- [5]. Y.L. Luo, K.P. Zhang, Q.B. Wei, Z.Q. Liu, and Y.S. Chen, Poly(MAA-co-AN) hydrogels with improved mechanical properties for theophylline controlled delivery. *Acta Biomater*, 5: 316–327, 2009.
- [6]. G. Decher. Fuzzy Nano assemblies: toward layered polymeric multicomposites. *Science*, 277: 1232 -1237, 1997.
- [7]. P. Caiyu, Z. Qinghe, and G.Changyou. Sustained delivery of doxorubicin by porous CaCO₃ and chitosan/alginate multilayers-coated CaCO₃ microparticles. *Colloids and Surfaces A: Physicochemical. Eng. Aspects*, 353: 132-139, 2010.
- [8]. B. Gisela, C. Helmut, D. Herbert. Physicochemical and chemical characterization of chitosan in dilute aqueous solution. *Progress in Colloid and Polymer Science*, 119: 50-57, 2002.
- [9]. Y. Shiqu, W. Chaoyang, L. Xinxing, T. Zhen, R. Beye, and Z. Fang. New loading process and release properties of insulin from polysaccharide microcapsules fabricated through layer-by-layer assembly. *J. Control. Release*, 112: 79, 2006.
- [10]. Y. Itoh, M. Matsusaki, T. Kida, and M. Akashi, Enzyme-Responsive Release of Encapsulated Proteins from Biodegradable Hollow Capsules. *Biomacromolecules*, 7: 2715-2718, 2006.
- [11]. Y. Hu, Y. Ding, D. Ding, M. Suun, L. Zhang, X. Jiang, and C. Yang. Hollow chitosan/poly (acrylic acid) Nano spheres as drug carriers. *Biomacromolecules*, 8: 1069-1076, 2007.
- [12]. X. Z. Shu and K. J. Zhu. Controlled drug release properties of ionically cross-linked chitosan beads: the influence of anion structure. *International Journal of Pharmaceutics*, 223: 217-225, 2002.
- [13]. N.V.R. Majeti. A review of chitin and chitosan applications. *Reactive & Functional Polymers*, 46: 1-27, 2000.
- [14]. T. Chandy and C. P. Sharma. Chitosan beads and granules for oral sustained delivery of nifedipine. *Biomaterials*, 12: 949-955, 1992.
- [15]. T. Chandy and C. P. Sharma. Chitosan matrix for oral sustained delivery of ampicillin. *Biomaterials*, 14: 939-944, 1993.
- [16]. X. Qiu, S. Leporatti, E. Donath, and H. Mohwald. Studies on the Drug Release Properties of Polysaccharide Multilayers Encapsulated Ibuprofen Microparticles. *Langmuir*, 17: 5375-5380, 2001.
- [17]. V. R. Patel and M. M. Amiji. Preparation and characterization of freeze-dried chitosan poly (ethylene oxide) hydrogels for site-specific antibiotic delivery in the stomach, *Pharm. Res*, 13: 588-593, 1996.
- [18]. O. Felt, P. Buri, R. Gurny. Chitosan: a unique polysaccharide for drug delivery, *Drug Dev. Ind. Pharm*, 24 : 979-993, 1998.
- [19]. L. Illum. Chitosan and its use as a pharmaceutical excipient. *Pharm. Res*, 15: 1326 -1331, 1998.
- [20]. K.C. Gupta and M.N.V.R. Kumar. Drug release behaviour of beads and micro granules of Chitosan. *Biomaterials*, 21: 1115-1119, 2000.
- [21]. G. I. Kinci, S.S. Enel, H. Akincibay, S. Kas, S. Ercis, C. G. Wilson, and A. A. Hincal. Effect of chitosan on a periodontal pathogen *Porphyromonas gingivalis*. *International Journal of Pharmaceutics*, 235: 121-127, 2002.
- [22]. S.C. chatz, A. Domard, and C. Viton. Versatile and efficient formation of colloids of biopolymer-based polyelectrolyte complexes. *Bio macromolecules*, 5: 1882-1892, 2004.
- [23]. W. Stober, A. Fink, and E. Boahn. Controlled Growth of Monodisperse Silica Spheres in the Micron Size Range. *J. Colloid Interface Science*, 26: 62-69, 1968.
- [24]. F. Caruso and H. Mohwald. Protein multilayer formation on colloids through a stepwise Self-assembly technique. *Am. Chem. Soc*, 121: 6039-6046, 1999.
- [25]. Z. P. Liang, C. Y. Wang, Q. L. Sun, and Z. Tong. Novel microcapsule fabricated by L-b-L nano self- assembly. *Prog. Chem*, 16: 485- 491, 2004.

WATER MARKING SCHEME WITH HIGH CAPACITY CDMA

Dr K RameshBabu¹, Vani.kasireddy²

¹ Professor, ECE Dept, hitam, jntuh, Hyderabad, AP, India

² vani.kasireddy ,PG student,ECE dept,hitam,jntuh,Hyderabad,AP,India

Abstract:

In this paper, we propose a high capacity CDMA based watermarking scheme based on orthogonal pseudorandom sequence subspace projection. We introduced a novel idea to eliminate the interference due to the correlation between the host image and the code sequences in the watermark extraction phase, and therefore, it improve the robustness and message capacity of the watermarking scheme. We give the implementation steps of the proposed scheme and test its performance under different attack conditions by a series of experiments. Experimental results show higher robustness than the canonical scheme under different attack conditions.

Keywords: CDMA, watermarking, high capacity, oval approach sub space projection, and wavelet transform.

1. Introduction

A. Digital watermarking life-cycle phases

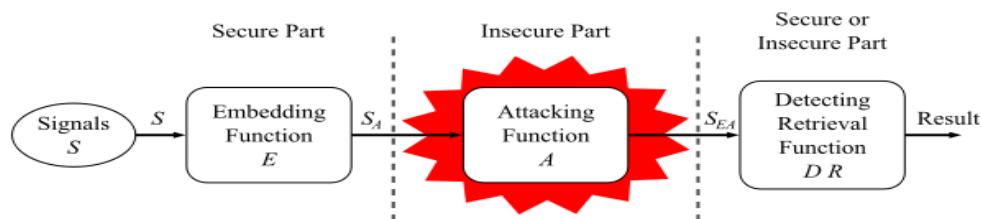


Fig 1.1 Digital watermarking life-cycle phases

Then the watermarked digital signal is transmitted or stored, usually transmitted to another person. If this person makes a modification, this is called an attack. While the modification may not be malicious, the term attack arises from copyright protection application, where pirates attempt to remove the digital watermark through modification. There are many possible modifications, for example, lossy compression of the data (in which resolution is diminished), cropping an image or video or intentionally adding noise. Detection (often called extraction) is an algorithm which is applied to the attacked signal to attempt to extract the watermark from it. If the signal was unmodified during transmission, then the watermark still is present and it may be extracted. In robust digital watermarking applications, the extraction algorithm should be able to produce the watermark correctly, even if the modifications were strong. In fragile digital watermarking, the extraction algorithm should fail if any change is made to the signal.

B Digital Watermark: Also referred to as simply watermark, a pattern of bits inserted into a digital image, audio, video or text file that identifies the file's copyright information (author, rights, etc.). The name comes from the faintly visible watermarks imprinted on stationary that identify the manufacturer of the stationery. The purpose of digital watermarks is to provide copyright protection for intellectual property that's in digital format.

C. General Framework for Digital Watermarking: Digital watermarking is similar to watermarking physical objects except that the watermarking technique is used for digital content instead of physical objects. In digital watermarking a low-energy signal is imperceptibly embedded in another signal. The low energy signal is called watermark and it depicts some metadata, like security or rights information about the main signal. The main signal in which the watermark is embedded is referred to as cover signal since it covers the watermark. The cover signal is generally a still image, audio clip, video sequence or a text document in digital format.

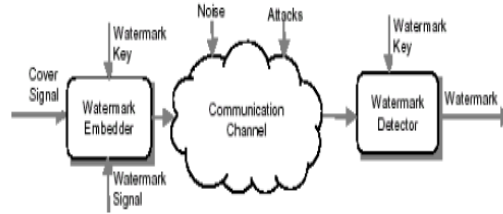


Fig 1.3: watermark embedded and a watermark detector

D. Digital Watermarking System: The digital watermarking system essentially consists of a watermark embedded and a watermark detector (see Figure). The watermark embedded inserts a watermark onto the cover signal and the watermark detector detects the presence of watermark signal. Note that an entity called watermark key is used during the process of embedding and detecting watermarks. The watermark key has a one-to-one correspondence with Watermark signal (i.e., a unique watermark key exists for every watermark signal). The watermark key is private and known to only authorized parties and it ensures that only authorized parties can detect the watermark. Further, note that the communication channel can be noisy and hostile (i.e., prone to security attacks) and hence the digital watermarking techniques should be resilient to both noise and security attacks. A watermark is an identifying feature, like a company logo, which can be used to provide protection of some “cover” data. A watermark may be either visible i.e. perceptible or invisible i.e. Imperceptible both of which offer specific advantages when it comes to protecting data. Watermarks may be used to prove ownership of data, and also as an attempt to enforce copyright restrictions.

Types of watermarking:

- i) Visible watermarking.
- ii) Invisible watermarking
- iii) Watermarking applications:

2. Cdma Watermarking:

2.1. Development of CDMA water marking model

There are several prior references to CDMA watermarking of digital video. Hartung and Girod’s work is notable in recognizing CDMA as a viable choice for video watermarking. Their approach parses the video into a linear stream of individual pixel elements. A watermark represented by a binary pattern is then expanded by an *m*-sequence and added pixel-by-pixel to the uncompressed video. Watermark recovery is done by matched filtering. In this paper we build upon the work reported in by developing a more complete model for CDMA-based video watermarking in a multi-user/multiple media environment. In particular, instead of linearizing the video as a 1-D pixel stream, we model the video as a *bit plane* stream; the 2D counterpart of bit stream used in (1). By closely following the conventional CDMA model, it is possible to address a variety of watermark removal/destruction attempts that go beyond random noise attacks. For example, any spread spectrum watermarking that relies on *m*-sequences is extremely sensitive to timing errors. Frame drops, intentional or otherwise, destroy the delicate pattern of an *m*-sequence and can seriously challenge watermark identification. We model digital video as a function in time and space represented by $I(x, y, t)$. $I(x, y, t)$ can then be sequenced along the time axis as bit planes: Where $i(.)$ is the *n*th bit plane of the *j*th frame positioned at $t = jT_f + nT_b$. T_f and T_b are frame length and bit plane spacing respectively and are related by $T_f = bT_b$ where *b* is the number of bit planes per frame.

$$I(x, y, t) = \sum_j \sum_{n=0}^b i(x, y, t - (jT_f + nT_b)) \quad \text{Eq.3}$$

Two questions arise at this point, 1): how is a watermark defined? and 2): where in the bit plane stream is it inserted. We define the watermark by a bit plane, $w(x, y)$, spatial dimensions of which match that of the video frames. The content of the watermark plane can be selected to suite varied requirements. It can contain a graphical seal, textual information about the source or any other data deemed appropriate for watermarking. In the context of CDMA, $w(x, y)$ can be thought of as the message. This message is then spread using a 2D *m*-sequence or *m*-frames $f(x, y, t)$. To generate *m*-frames, a one dimensional *m* sequence is rearranged in a 2D pattern. Depending on the period of the *m*-sequence and the size of each video frame, the 1D to 2D conversion may span up to *k* frames and will repeat afterwards. Spreading of the “message”, i.e. the watermark $w(x, y)$ is now defined by a periodic frame sequence given

by $w_{ss} = w(x, y) \sum_{j=0}^{k-1} \phi_j(x, y, t_j) \dots\dots \text{Eq. 4}$

Where $f_j(x, y, t_j)$ is f_j positioned at yet to be determined locations $t = t_j$. wss must now be aligned with and inserted into video bit plane stream in (3). The embedding algorithm works as follows. In every frame the bit plane at $t = t_j$ is tagged then removed and replaced by $f_j(x, y, t_j)$. The question now is which bit planes are tagged and in what order? It is safe to assume that in most cases the LSB plane bit distribution is random and can be safely replaced by the watermark. However, LSB plane is vulnerable to noise and other disturbances but bit planes can be used to embed a watermark with small to negligible effect on quality. In one example, watermark placement in one of 4 lower bit planes did not significantly impact video quality. In order to embed wss in the video, we define a separate multilevel sequence v and use $v(j)$ as pointer to the j th bit plane position. There are many ways to create v . One simple method is to start with a binary m -sequence u and add 3 cyclically shifted versions. Let $u = (u_0, u_1, \dots, u_{p-1})$ be an m -sequence of period p . Define D as an operator that cyclically shifts the elements of u to the left $D(u) = (u_1, u_2, \dots, u_{p-1}, u_0)$. We define v by $v = u + D(u) + D^2(u)$ where D^k is the k th cyclic shift of u . The new sequence now has two key properties, 1): it is still periodic with period p and 2): it is a 4 valued sequence taking on amplitudes in the range $\{0, 1, \dots, 3\}$. The significance of 4 values is that the watermark will be limited to 4 lower bit plane positions. This number can clearly change. We can now align wss in (4) with the timeline

$$\text{defined in (3)} \quad w_{ss} = w(x, y) \sum_{j=0}^{k-1} \phi(x, y, v(j)T_b) \quad \dots \quad \text{Eq. 5}$$

wss is now a spread spectrum version of the watermark at pseudorandom locations determined by $v(j)$. The second task is accomplished by using $v(j)T_b$ as pointers to the candidate bit planes where the watermark must be inserted. In order to take the last step, the designated bit planes must be removed and replaced by the corresponding elements of wss. The formalism to achieve this goal is through the use of a gate function defined by

$$\text{gate}(t - v(j)T_b) = \begin{cases} 0 & \text{for } t \neq v(j)T_b \\ 1 & \text{for } t = v(j)T_b \end{cases} \quad 0 \leq t \leq T_c \quad \dots \quad \text{Eq. 6}$$

Multiplying video bit plane stream in (3) by the gate function above removes the bit plane at $v(j)$. The spread watermark bit plane stream in (5) is positioned such that the individual planes correspond exactly to the planes just nulled by the gate function. Putting it all together, CDMA watermarked video can be written as

$$I_{wm}(x, y, t) = \sum_j \left\{ \sum_{n=0}^{b-1} i(x, y, jT_f + nT_b) \text{gate}(t - jT_f - v(n)T_b) + w(x, y) \phi(x, y, jT_f + v(n)T_b) \right\}$$

$$\Phi_j + \kappa = \Phi_j \quad \text{Eq. 7}$$

3. Wavelet Transforms:

It provides the time-frequency representation. often times a particular spectral component occurring at any instant can be of particular interest. In these cases it may be very beneficial to know the time intervals these particular spectral components occur. For example, in EEGs, the latency of an event-related potential is of particular interest. Wavelet transform is capable of providing the time and frequency information simultaneously, hence giving a time-frequency representation of the signal.

3.1. The Continuous Wavelet Transform: The continuous wavelet transform was developed as alternative approaches to the short time Fourier transform to overcome the resolution problem. The wavelet analysis is done in a similar way to the STFT analysis, in the sense that the signal is multiplied with a function, [it the wavelet], similar to the window function in the STFT, and the transform is computed separately for different segments of the time-domain signal. However, there are two main differences between the STFT and the CWT: 1. The Fourier transforms of the windowed signals are not taken, and therefore single peak will be seen corresponding to a sinusoid, i.e., negative frequencies are not computed. 2. The width of the window is changed as the transform is computed for every single spectral component, which is probably the most significant characteristic of the wavelet transform. The continuous wavelet transform is defined as follows

$$CWT_x^\psi(\tau, s) = \Psi_x^\psi(\tau, s) = \frac{1}{\sqrt{|s|}} \int x(t) \psi^* \left(\frac{t - \tau}{s} \right) dt \quad \dots \quad \text{Eq 3.1}$$

As seen above variables, **tau** and **s**, the **translation** and **scale** parameters, respectively. **psi(t)** is the transforming function, and it is called **the mother wavelet**.

The scale

The parameter **scale** in the wavelet analysis is similar to the scale used in maps. As in the case of maps, high scales correspond to a non-detailed global view (of the signal), and low scales correspond to a detailed view. Similarly, in terms of frequency, low frequencies (high scales) correspond to a global information of a signal (that usually spans the entire signal), whereas high frequencies (low scales) correspond to a detailed information of a hidden pattern in the signal (that usually lasts a relatively short time). Cosine signals corresponding to various scales are given as examples in the following figure.

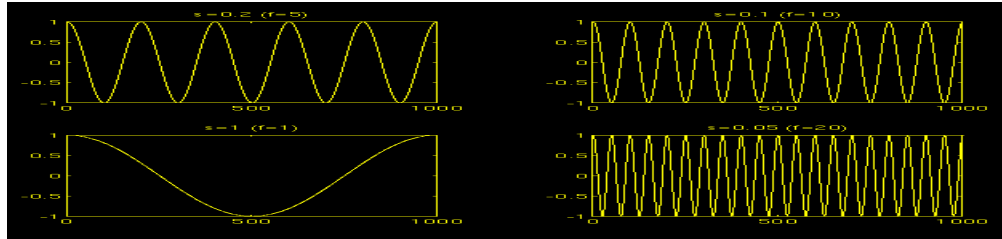


Fig 3.1: Cosine signals corresponding to various scales

Fortunately in practical applications, low scales (high frequencies) do not last for the entire duration of the signal, unlike those shown in the figure, but they usually appear from time to time as short bursts, or spikes. High scales (low frequencies) usually last for the entire duration of the signal. Scaling, as a mathematical operation, either dilates or compresses a signal. Larger scales correspond to dilated (or stretched out) signals and small scales correspond to compressed signals. All of the signals given in the figure are derived from the same cosine signal, i.e., they are dilated or compressed versions of the same function. In the above figure, $s=0.05$ is the smallest scale, and $s=1$ is the largest scale. In terms of mathematical functions, if $f(t)$ is a given function $f(st)$ corresponds to a contracted (compressed) version of $f(t)$ if $s > 1$ and to an expanded (dilated) version of $f(t)$ if $s < 1$. However, in the definition of the wavelet transform, the scaling term is used in the denominator, and therefore, the opposite of the above statements holds, i.e., scales $s > 1$ dilates the signals whereas scales $s < 1$, compresses the signal. This interpretation of scale will be used throughout this text.

3.2 Computations of Cwt

Interpretation of the above equation will be explained in this section. Let $x(t)$ is the signal to be analyzed. The mother wavelet is chosen to serve as a prototype for all windows in the process. All the windows that are used are the dilated (or compressed) and shifted versions of the mother wavelet. There are a number of functions that are used for this purpose. The Morlet wavelet and the Mexican hat function are two candidates, and they are used for the wavelet analysis.

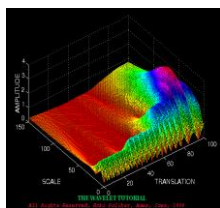


Fig 3.2: (CWT) of this signal

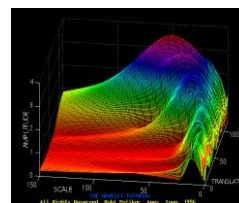


Fig 3.3 CWT signal with high frequencies

Note that in Figure 3.2 that smaller scales correspond to higher frequencies, i.e., frequency decreases as scale increases, therefore, that portion of the graph with scales around zero, actually correspond to highest frequencies in the analysis, and that with high scales correspond to lowest frequencies. Remember that the signal had 30 Hz (highest frequency) components first, and this appears at the lowest scale at translations of 0 to 30. Then comes the 20 Hz component, second highest frequency, and so on. The 5 Hz component appears at the end of the translation axis (as expected), and at higher scales (lower frequencies) again as expected. Now, recall these resolution properties: Unlike the STFT which has a constant resolution at all times and frequencies, the WT has a good time and poor frequency resolution at high frequencies, and good frequency and poor time resolution at low frequencies. Figure 3.3 shows the same WT in Figure 3.2 from another angle to better illustrate the resolution properties: In Figure 3.3, lower scales (higher frequencies) have better scale resolution (narrower in scale, which means that it is less ambiguous what the exact value of the scale) which correspond to poorer

frequency resolution :Similarly, higher scales have scale frequency resolution (wider support in scale, which means it is more ambitious what the exact value of the scale is) , which correspond to better frequency resolution of lower frequencies. The axes in Figure 3.2 and 3.3 are normalized and should be evaluated accordingly. Roughly speaking the 100 points in the translation axis correspond to 1000 ms, and the 150 points on the scale axis correspond to a frequency band of 40 Hz (the numbers on the translation and scale axis **do not correspond to seconds and Hz, respectively** , they are just the number of samples in the computation).

4. Discrete Wavelet Transforms

4.1. Need of Discrete Wavelet Transform

Although the DWT enables the computation of the continuous wavelet transform by computers, it is not a true discrete transform. As a matter of fact, the wavelet series is simply a sampled version of the CWT, and the information it provides is highly redundant as far as the reconstruction of the signal is concerned. This redundancy, on the other hand, requires a significant amount of computation time and resources. The discrete wavelet transform (DWT), on the other hand, provides sufficient information both for analysis and synthesis of the original signal, with a significant reduction in the computation time. The DWT is considerably easier to implement when compared to the CWT.

4.2. Discrete wavelet transforms (DWT): The foundations of the DWT go back to 1976 when Croiser, Esteban, and Galand devised a technique to decompose discrete time signals. Crochiere, Weber, and Flanagan did a similar work on coding of speech signals in the same year. They named their analysis scheme as **sub band coding**. In 1983, Burt defined a technique very similar to sub band coding and named it **pyramidal coding** which is also known as multi resolution analysis. Later in 1989, Vetterli and Le Gall made some improvements to the sub band coding scheme, removing the existing redundancy in the pyramidal coding scheme. Sub band coding is explained below. A detailed coverage of the discrete wavelet transform and theory of multi resolution analysis can be found in a number of articles and books that are available on this topic, and it is beyond the scope of this tutorial.

4.2.1 The Sub band Coding and the Multi resolution Analysis: The frequencies that are most prominent in the original signal will appear as high amplitudes in that region of the DWT signal that includes those particular frequencies. The difference of this transform from the Fourier transform is that the time localization of these frequencies will not be lost

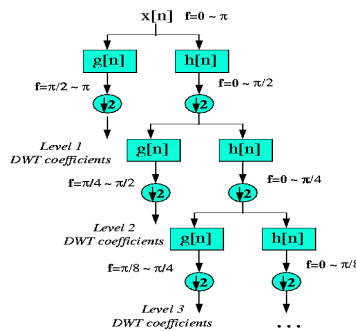


Fig 4.1. Bandwidth of the signal at every level

However, the time localization will have a resolution that depends on which level they appear. If the main information of the signal lies in the high frequencies, as happens most often, the time localization of these frequencies will be more precise, since they are characterized by more number of samples. If the main information lies only at very low frequencies, the time localization will not be very precise, since few samples are used to express signal at these frequencies. This procedure in effect offers a good time resolution at high frequencies, and good frequency resolution at low frequencies. Most practical signals encountered are of this type. The frequency bands that are not very prominent in the original signal will have very low amplitudes, and that part of the DWT signal can be discarded without any major loss of information, allowing data reduction. Figure 4.2 illustrates an example of how DWT signals look like and how data reduction is provided. Figure 4.2a shows a typical 512-sample signal that is normalized to unit amplitude. The horizontal axis is the number of samples, whereas the vertical axis is the normalized amplitude. Figure 4.2b shows the 8 level DWT of the signal in Figure 4.2a. The last 256 samples in this signal correspond to the highest frequency band in the signal, the previous 128

samples correspond to the second highest frequency band and so on. It should be noted that only the first 64 samples, which correspond to lower frequencies of the analysis, carry relevant information and the rest of this signal has virtually no information. Therefore, all but the first 64 samples can be discarded without any loss of information. This is how DWT provides a very effective data reduction scheme.

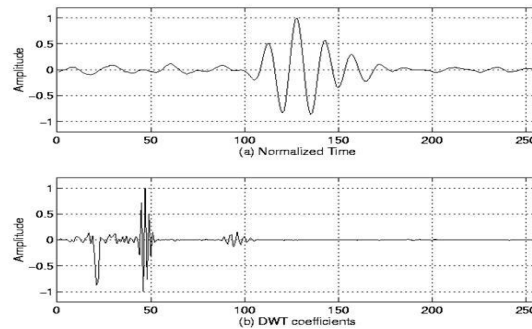


Fig 4.2 a,b Example of a DWT

One important property of the discrete wavelet transform is the relationship between the impulse responses of the high pass and low pass filters. The high pass and low pass filters are not independent of each other, and they are related by

$$g[L-1-n] = (-1)^n h[n]$$

Where $g[n]$ is the high pass, $h[n]$ is the low pass filter, and L is the filter length (in number of points). Note that the two filters are odd index alternated reversed versions of each other. Low pass to high pass conversion is provided by the $(-1)^n$ term. Filters satisfying this condition are commonly used in signal processing, and they are known as the Quadrature Mirror Filters (QMF). The two filtering and sub sampling operations can be expressed by

$$y_{high}[k] = \sum_n x[n].g[-n+2k]$$

$$y_{low}[k] = \sum_n x[n].h[-n+2k]$$

The reconstruction in this case is very easy since half band filters form orthonormal bases. The above procedure is followed in reverse order for the reconstruction. The signals at every level are up sampled by two, passed through the synthesis filters $g'[n]$, and $h'[n]$ (high pass and low pass, respectively), and then added. The interesting point here is that the analysis and synthesis filters are identical to each other, except for a time reversal. Therefore, the reconstruction formula becomes (for

each layer)

$$x[n] = \sum_{k=-\infty}^{\infty} (y_{high}[k].g[-n+2k]) + (y_{low}[k].h[-n+2k])$$

However, if the filters are not ideal half band, then perfect reconstruction cannot be achieved. Although it is not possible to realize ideal filters, under certain conditions it is possible to find filters that provide perfect reconstruction. The most famous ones are the ones developed by Ingrid Daubechies, and they are known as Daubechies' wavelets. Note that due to successive sub sampling by 2, the signal length must be a power of 2, or at least a multiple of power of 2, in order this scheme to be efficient. The length of the signal determines the number of levels that the signal can be decomposed to. For example, if the signal length is 1024, ten levels of decomposition are possible. Interpreting the DWT coefficients can sometimes be rather difficult because the way DWT coefficients are presented is rather peculiar. To make a real long story real short, DWT coefficients of each level are concatenated, starting with the last level. An example is in order to make this concept clear: Suppose we have a 256-sample long signal sampled at 10 MHz and we wish to obtain its DWT coefficients. Since the signal is sampled at 10 MHz, the highest frequency component that exists in the signal is 5 MHz. At the first level, the signal is passed through the low pass filter $h[n]$, and the high pass filter $g[n]$, the outputs of which are sub sampled by two. The high pass filter output is the first level DWT coefficients. There are 128 of them, and they represent the signal in the [2.5 5] MHz range. These 128 samples are the last 128 samples plotted. The low pass filter output, which also has 128 samples, but spanning the frequency band of [0 2.5] MHz, are further decomposed by passing them through the same $h[n]$

And $g[n]$. The output of the second high pass filter is the level 2 DWT coefficients and these 64 samples precede the 128 level 1 coefficients in the plot. The output of the second low pass filter is further decomposed, once again by passing it through the filters $h[n]$ and $g[n]$. The output of the third high pass filter is the level 3 DWT coefficients. These 32 samples precede the level 2 DWT coefficients in the plot. The procedure continues until only 1 DWT coefficient can be computed at level 9. This one coefficient is the first to be plotted in the DWT plot. This is followed by 2 level 8 coefficients, 4 level 7 coefficients, 8 level 6 coefficients, 16 level 5 coefficients, 32 level 4 coefficients, 64 level 3 coefficients, 128 level 2 coefficients and finally 256 level 1 coefficients. Note that less and less number of samples is used at lower frequencies, therefore, the time resolution decreases as frequency decreases, but since the frequency interval also decreases at low frequencies, the frequency resolution increases. Obviously, the first few coefficients would not carry a whole lot of information, simply due to greatly reduced time resolution. To illustrate this richly bizarre DWT representation let us take a look at a real world signal. Our original signal is a 256-sample long ultrasonic signal, which was sampled at 25 MHz. This signal was originally generated by using a 2.25 MHz transducer; therefore the main spectral component of the signal is at 2.25 MHz. The last 128 samples correspond to [6.25 12.5] MHz range. As seen from the plot, no information is available here; hence these samples can be discarded without any loss of information. The preceding 64 samples represent the signal in the [3.12 6.25] MHz range, which also does not carry any significant information. The little glitches probably correspond to the high frequency noise in the signal. The preceding 32 samples represent the signal in the [1.5 3.1] MHz range. As you can see, the majority of the signal's energy is focused in these 32 samples, as we expected to see. The previous 16 samples correspond to [0.75 1.5] MHz and the peaks that are seen at this level probably represent the lower frequency envelope of the signal. The previous samples probably do not carry any other significant information. It is safe to say that we can get by with the 3rd and 4th level coefficients, that are we can represent this 256 sample long signal with $16+32=48$ samples, a significant data reduction which would make your computer quite happy.

One area that has benefited the most from this particular property of the wavelet transforms is image processing. As you may well know, images, particularly high-resolution images, claim a lot of disk space. As a matter of fact, if this tutorial is taking a long time to download, that is mostly because of the images. DWT can be used to reduce the image size without losing much of the resolution. Here is how: For a given image, you can compute the DWT of, say each row, and discard all values in the DWT that are less than a certain threshold. We then save only those DWT coefficients that are above the threshold for each row, and when we need to reconstruct the original image, we simply pad each row with as many zeros as the number of discarded coefficients, and use the inverse DWT to reconstruct each row of the original image. We can also analyze the image at different frequency bands, and reconstruct the original image by using only the coefficients that are of a particular band. I will try to put sample images hopefully soon, to illustrate this point. Another issue that is receiving more and more attention is carrying out the decomposition (sub band coding) not only on the low pass side but on both sides. In other words, zooming into both low and high frequency bands of the signal separately. This can be visualized as having both sides of the tree structure of Figure 4.1. What result is what is known as the wavelet packages we will not discuss wavelet packages in this here, since it is beyond the scope of this tutorial. Anyone who is interested in wavelet packages or more information on DWT can find this information in any of the numerous texts available in the market. And this concludes our mini series of wavelet tutorial. If I could be of any assistance to anyone struggling to understand the wavelets, I would consider the time and the effort that went into this tutorial well spent. I would like to remind that this tutorial is neither a complete nor a through coverage of the wavelet transforms. It is merely an overview of the concept of wavelets and it was intended to serve as a first reference for those who find the available texts on wavelets rather complicated. There might be many structural and/or technical mistakes, and I would appreciate if you could point those out to me. Your feedback is of utmost importance for the success of this tutorial.

5 Water Marking Schemes

5.1. the Channel Model of Canonical CDMA based Watermarking Schemes

Since discrete wavelet transform (DWT) is believed to more accurately models aspects of the Human Visual System (HVS) as compared to the FFT or DCT, watermark information are embedded in the wavelet domain for many CDMA based watermarking schemes. The host image is first transformed by orthogonal or bi orthogonal wavelets to obtain several sub band images (each sub band image consists of wavelet coefficients). Then some of them are selected for watermark embedding. Suppose sub band image I is chosen for watermark embedding and the message is represented in binary form $b = (b_1, b_2, \dots, b_L)$ where $b_i \in \{0,1\}$ we first transform b into a binary polar sequence m of $\{-1,1\}$ by the following formula

$$m_i = 1 - 2b_i, \quad i=1, 2, \dots, L. \quad (1)$$

According to the CDMA principles, the message m is encoded by L uncorrelated pseudo sequences $\{s_1, s_2, \dots, s_L\}$ generated by a secret key, such as m sequences, gold sequences, etc.. Since it is possible to make them orthogonal with each other, we simply assume that they are orthogonal unit vectors, i.e.,

$$\langle s_i, s_j \rangle = \delta = \begin{cases} 0, & i \neq j, \\ 1, & i = j. \end{cases} \quad i, j = 1, 2, \dots, L. \quad (2)$$

Where, $\langle \bullet, \bullet \rangle$ denotes inner product operation. The pseudorandom noise pattern W is obtained as follows

$$W = \sum_{i=1}^L m_i s_i, \quad (3)$$

This submerges the watermark message. Then the pseudorandom noise pattern W is embedded into the sub band image I as follows

$$I_w = I + \lambda W, \quad (4)$$

Where λ is a positive number, called the water mark strength parameter. Then an inverse wavelet transform is performed to obtain the water marked image.

In the water marked extracting phase, the water marked image is transformed by the same wavelet transform that is used in the watermark embedding phase to obtain the sub band image \hat{I}_w that contains the watermark message, i.e.,

$$\hat{I}_w = I + \lambda W + n, \quad (5)$$

Where n is the distortion due to attacks or simply quantization errors if no other attack is performed. Then the orthogonal pseudo sequences $\{s_1, s_2, \dots, s_L\}$ are generated using the key, and the inner product between each s_i and \hat{I}_w is computed:

$$\langle s_i, \hat{I}_w \rangle = \langle s_i, I \rangle + \lambda m_i + \langle s_i, n \rangle \quad (6)$$

The canonical CDMA based methods decide the sign of m_i by computing the inner product on the left most of (6), i.e.,

$$\hat{m}_i = \begin{cases} 1, & \text{if } \langle s_i, \hat{I}_w \rangle > 0, \\ -1, & \text{otherwise.} \end{cases} \quad (7)$$

Where \hat{m}_i denotes the estimated value of m_i . This equivalent to neglecting of correlation between s_i and the host image I , and the host image I , and the correlation between s_i and the attack distortion n . When the message size is small, we can take a large watermark strength parameter λ , so we have no problem to neglect those small values. But when the message size is large, problem occurs. For the convenience of analysis, we ignore the third term in (6) at present. Then we have

$$\langle s_i, \hat{I}_w \rangle \approx \langle s_i, I \rangle + \lambda m_i. \quad (8)$$

As the message size increases, the watermark strength parameter λ becomes smaller and smaller in order to keep the imperceptibility. So the influence of the host image's contents becomes more and more prominent as the message size increases. Experimental results also confirm this fact. So we must find a way to eliminate or reduce the interference of the host image so that we can improve the robustness of the CDMA watermarking scheme considerably.

5.2. High Capacity CDMA Watermarking Scheme: In the previous subsection we have analyzed, the influence of the host image's content to the robustness of the canonical CDMA watermarking schemes. In order to eliminate this influence, we project the host image onto the linear subspace S generated by the orthogonal pseudorandom sequences, i.e.

$$P_s(I) = \sum_{i=1}^L \langle s_i, I \rangle s_i. \quad (9)$$

If we keep the projection coefficients $\{c_i = \langle s_i, I \rangle : i = 1, 2, \dots, L\}$ as a secret key, then we can subtract $P_s(I)$ from the watermarked sub band image I , Before watermark extraction, therefore, we can decide the sign of \hat{m}_i by computing

$$\langle s_i, \hat{I}_w - P_s(I) \rangle \approx \langle s_i, I + \lambda W - P_s(I) \rangle = \lambda \langle s_i, W \rangle = \lambda m_i, \quad (10)$$

Which is not affected by the host image's contents, and therefore, provides a more robust way for CDMA based watermarking.

5.2.1. Watermark Embedding Process: The watermark embedding process of the proposed high capacity CDMA scheme is the same as the canonical one except for a preprocessing step of calculating the projection coefficients $\{c_i = \langle s_i, I \rangle : i = 1, 2, \dots, L\}$, which should be kept as a key for watermark extraction. Fig. 1 gives the flow chart of the watermark embedding process.

Here we give the watermark embedding steps:

Step 1: decompose the host image into sub band images using orthogonal or bi orthogonal discrete wavelet transform (DWT), and chose one or several sub band images I for watermark embedding;

Step2: generate the orthogonal pseudorandom sequences $\{s_1, s_2, \dots, s_L\}$ using the secret key (key1);

Step3: project the sub band images I onto the linear subspace S generated by the orthogonal pseudo sequences, and keep the projection coefficients $\{c_i = \langle s_i, I \rangle : i = 1, 2, \dots, L\}$ as the second secret key (key2) which will be used in the watermark extraction phase;

Step4: encode the watermark information using formula (1) and (3) to get the pseudorandom noise pattern W;

Step5: embed the pseudorandom noise pattern W into the sub band image I using formula (4);

Step6: perform inverse discrete wavelet transform (IDWT) to obtain the watermarked image.

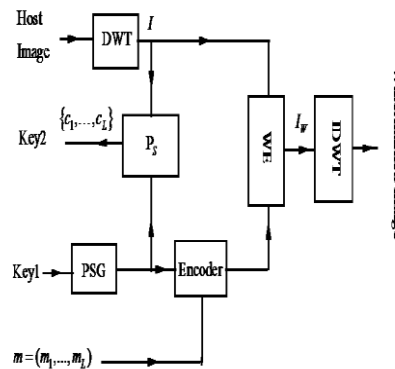


Fig 5.1 the watermark embedding process of the proposed scheme.

Key1 is the key used to generate the orthogonal pseudo sequences; PSG is the pseudo sequence generator; P_s is the orthogonal projection operator; Key2 is generated by the projection operator, which consists of the projection coefficients, will be used in the watermark extraction phase; DWT denotes the discrete wavelet transform; WE denotes watermark embedding; IDWT denotes inverse wavelet transform.

Watermark Extraction Process: Now we give the watermark extraction steps:

Step1: decompose the received image into sub band images using the same wavelet transform as the one used in the watermark embedding phase, and choose the corresponding sub band images \hat{I}_w for watermark extraction;

Step2: generate the orthogonal pseudorandom sequences $\{s_1, s_2, \dots, s_L\}$ using the secret key (key1);

Step3: eliminate the projection component from \hat{I}_w by

$$\tilde{I}_w = \hat{I}_w - P_s(I) = \hat{I}_w - \sum_{j=1}^L c_j s_j \quad (11)$$

Where C_i are the projection coefficients kept in the second secret key (key2);

Step4: extract the embedded message $m = (m_1, m_2, \dots, m_L)$ by correlation detection

$$\hat{m}_i = \begin{cases} 1, & \text{if } \langle s_i, \tilde{I}_w \rangle > 0, \\ -1, & \text{otherwise} \end{cases} \quad (12)$$

Step5: transform the extracted message $m = (m_1, m_2, \dots, m_L)$ into the original watermark $b = (b_1, b_2, \dots, b_L)$ by

$$b_i = (1 - m_i) \div 2, i = 1, 2, \dots, L \quad (13)$$

6. Performance Test

We have performed a series of experiments to test the robustness of the proposed scheme. Seven 512x512 grayscale images (a. airplane, b. baboon, c. Barbara, d. boats, e. gold hill, f. Lena, g. pepper.) are chosen as test images. The watermarks are binary sequences of different size. The pseudorandom sequences we used are generated by pseudorandom number generators and we orthogonalize them by Cholesky decomposition method. Of course other choices of pseudo sequences such as m sequences, gold sequences may be more suitable for watermarking; we will test them in the future.

A. Capacity VS Bit Error Rate (BER)

The first test we have performed is to test the relationship between message capacity and the bit error rate of the extracted watermark for both the canonical and newly proposed schemes. The bit error rate (BER) is calculated by the following formula:

$$BER = \frac{1}{mn} \sum_{i=1}^m \sum_{j=1}^n |W(i, j) - EXW(i, j)| \quad (14)$$

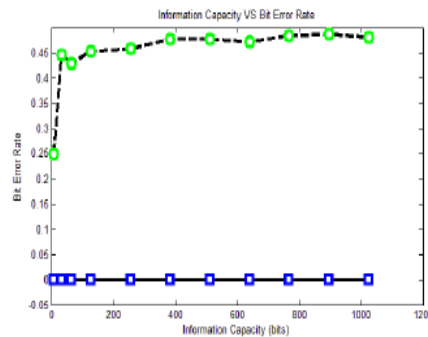


Fig 5.2 the relationship between message capacity and the bit error rate

Where W denotes the original watermark, ExW denotes the extracted watermark. In this test, we embed the watermarks into the lower resolution approximation image (LL) of the 2-level biorthogonal discrete wavelet decomposition of the test image using both canonical and the newly proposed CDMA based schemes, no attack is performed on the watermarked image except for quantization errors. Then extract watermarks from the watermarked image using corresponding watermark extraction schemes and compare the extracted watermark with the original one. The watermark size (number of information bits) vary from 16 to 1015, we have chosen 11 discrete values for our test. For each watermark size value, we perform the watermark embedding and extracting process on all 7 test images, and calculate the average BER. In the whole test we carefully adjust the watermark strength parameter λ so that the peak signal to noise ratio (PSNR) of the watermarked image take approximately the same value for different watermark sizes and different test images. Fig. 2 gives the experimental results. The horizontal axis indicates the information capacity, i.e., the number of bits embedded in the test image. The vertical axis indicates the average BER. From fig. 2 we see that as the information capacity increases the BER of the canonical CDMA based scheme increases and approaches to 0.5. But for the proposed scheme, the bit error rate keeps to be zero until the message capacity takes the value of 1024 bits. Of course, if the message capacity keeps on increasing, the bit error rate cannot always be zero, it will increase and approach to 0.5 in the long run. On the hand, for the canonical scheme, if the message size is large, the bit error rate is high even no attack is performed on the watermarked image. This phenomenon has not taken place in the tests for the proposed scheme yet. The reason is that the interference of the correlations between the test image and the pseudorandom sequences used for encoding the watermark message is cancelled in the proposed scheme. Fig. 2 also shows that the proposed scheme has higher information capacity than the canonical CDMA based watermarking scheme when no attack other than quantization errors is performed.

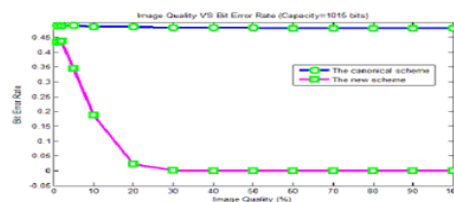


Fig 5.3 Image quality VS BER for JPEG attacks of different attack intensity

B. Robustness to Noising Attacks: The second test is to test the robustness to noising attacks of both schemes. In this test, we first generate binary watermarks of capacity 128, 256, 512 and 1015 bits, then embed them into the 7 test images using both watermark embedding schemes to generate 14 watermarked images, and then add Gaussian noise of different intensity to the watermarked images to generate the noising attacked images, then extract watermarks from those attacked images using corresponding watermark extraction scheme. The intensity of noising attack is measured by noise Rate RI , i.e.,

$$RI = \frac{\sigma}{R}, \quad (15)$$

Where σ is the standard deviation of the noise, R is the range the pixel values of the image I , i.e., $R = \max_{x,y} I(x, y) - \min_{x,y} I(x, y)$. (16)

We have added Gaussian noise with RI vary from 0.05 to 0.5 and calculated the average BER of the extracted watermark for each RI value and each value of watermark capacity. Fig. 3 gives the BER-RI plot with watermark capacity=1015, 512, 256,128. We see that BER of the new scheme is much smaller than the one of the canonical scheme.

C. Robustness to JPEG Attacks :The third test is to test the robustness to JPEG attacks of both schemes. In this test, we compress the watermarked images using JPEG compressor (JPEG imager v2.1) with quality factors vary from 100% to 1% before watermark extraction. Fig. 4 shows the BER of both schemes under JPEG compression attacks with different quality factors. The horizontal axis indicates the quality factor that measures the extent of lossy JPEG compression, the smaller the quality factor, the higher the compression extent. From fig. 4 we see that the proposed scheme is highly robust to JPEG compression.

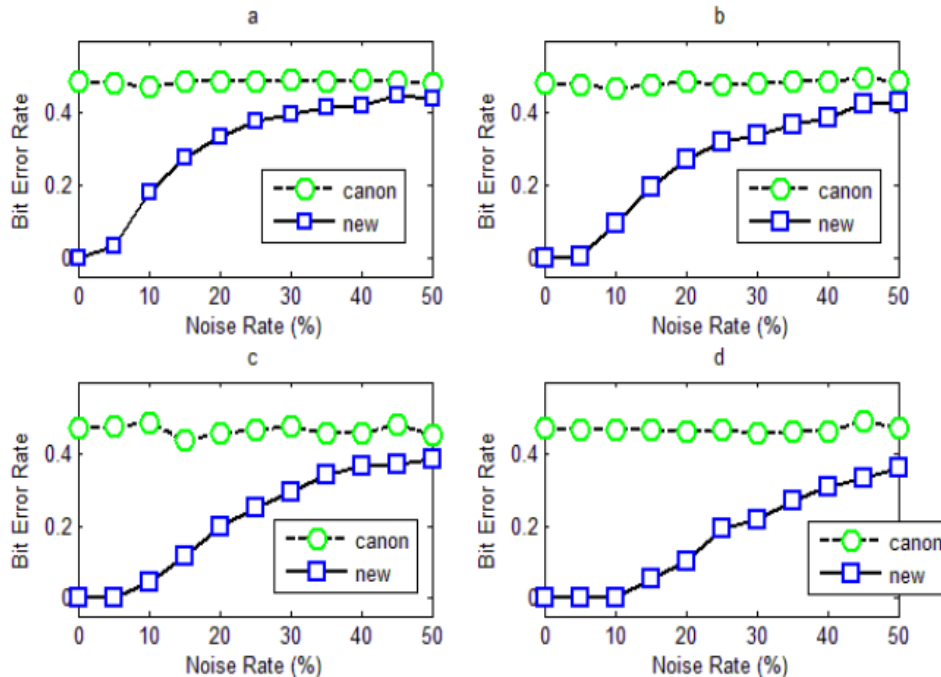


Fig 5.4 BER-RI plot with different values of watermark capacity.

a. watermark capacity=1015; b. watermark capacity=512; c. watermark capacity=256; d. watermark capacity=128. ‘canon’ in the legend indicates the canonical scheme; ‘new’ indicates the new scheme.

D. Robustness to other Attacks

We test the robustness to median filtering and jitter attacks of both schemes. In the median filtering test, we filter the watermarked image using a 5x5 median filtering template before watermark extraction. In the jitter attack test, before watermark extraction, we first randomly drop a row and a column of the watermarked image, then randomly duplicate a row and a column to keep the image size unchanged. This attack can destroy the synchronization of the watermark, which often leads to the failure of watermark extraction for many existing watermarking schemes. The experimental data are list in table I. We see that the proposed scheme is robust to both attacks but the canonical scheme is not.

7. Code:

```

Clc;Clear all; Close all;
start_time=cputime;
i=uigetfile('.jpg','select the host image');
s0=imfinfo(i);
i=imread(i);
i=imresize(i,[256 256]);
imbytes=size(i,1)*size(i,2)*s0.BitDepth;
imshow(i),title('original image');
bpp=numel(i)/imbytes
if size(i,3)>1
i=rgb2gray(i);
end
g=im2double(i);
% canonical CDMA based watermarking% % % % %
[LL LH HL HH]=dwt2(g,'haar',1);
I=LL;
lambda=0.1; % set the gain factor for embedding
disp('Embedded Bits')
b=[1 1 1 1 1]
% b=randint(1,128);
L=length(b);
for i0=1:L
m(i0)=1-2.*b(i0); % % eq-1
end
for i1=1:L
for j1=1:L
if i1==j1
s(i1,j1)=1;
else % % eq-2(key-1)
s(i1,j1)=0;
end end end
for i2=1:L
W(i2)=sum(m(i2).*s(i2)); % % eq-3
end
W=imresize(W,size(I));
% W=round(2*(rand(128,128)-0.5));
iw=I+lambda.*W; % % eq-4
IW=idwt2(iw,LH,HL,HH,'haar');
imwrite(IW,'watermarked.jpg')
figure,imshow(IW,[]);title('watermarked image')
n=randn(size(I));
IW1=I+lambda.*W+n; % % eq-5
iss=s(1:L).*I(1:L)+lambda.*m+s(1:L).*n(1:L); % % eq-6
%iss=ceil(iss);
for i3=1:length(iss)
if iss(i3) > 0
m1(i3)=1; % % eq-7
else
m1(i3)=-1;
end
end
%-----Proposed methodology-----% % %
for i4=1:L
P(i4)=sum((s(i4).*I(i4)).*s(i4)); % % eq-9
end

```

```

for i5=1:L
    c(i5)=s(i5).*I(i5); %%-----key-2-----
end
I1=imread('watermarked.jpg');
I1=im2double(I1);
A=input('Select Attack \n (1) Gussian Noise \n (2) Salt & Pepper Nose \n (3) JPEG Compression      ');
switch (A)
    Case 1
        WI=imnoise (I1,'gaussian', 0.01);
        PSNR_Attack=psnr (I1, WI)
        BER=biter (I1, WI)
    Case 2
        WI=imnoise (I1,'salt & pepper', 0.02);
        PSNR_Attack=psnr (I1, WI)
        BER=biter (I1, WI)
    Case 3
        T = dctmtx (8);
        B = blkproc (I1,[8 8],'P1*x*P2',T,T);
        Mask= [1 1 1 1 0 0 0 0
              1 1 1 0 0 0 0 0
              1 1 0 0 0 0 0 0
              1 0 0 0 0 0 0 0
              0 0 0 0 0 0 0 0
              0 0 0 0 0 0 0 0
              0 0 0 0 0 0 0 0
              0 0 0 0 0 0 0 0];
        B2 = blkproc (B, [8 8],'P1.*x', mask);
        WI = blkproc (B2, [8 8],'P1*x*P2', T', T);
        PSNR_Attack=psnr (I1, WI)
        BER=biter (I1, WI)
end
figure, imshow(WI); title('Attacked Watermarked Image');
L1=medfilt2 (WI, [3 3]);
figure, imshow(L1); title('De-noised Image');
Dim=imsubtract (WI, L1);
figure, imshow(Dim); title('Difference Image');
[LL1 LH1 HL1 HH1]=dwt2 (WI,'haar', 1);
IW2=LL1;
IW2=IW2 (1: L)-P;      %% eq-11
for i6=1:L
    iss (i6)=s(i6).*IW2(i6);
end
for i7=1:length(iss)
    if iss(i7) > 0
        m2 (i7) =1;      %%eq-7
    else
        m2(i7)=-1;
    end ;end
disp('Received Bits')
b1=(1-m2)./2  %% received bits
% display processing time
elapsed_time=cputime-start_time
sigma=0.05;
R=max(max(I))-min(min(I));
RI=sigma/R;
Q=[0:10:100];

```

```

for jj=1:length(Q)
    mnn=jpogcomp(i,Q(jj));
    brr(jj)=biter( double(i),mnn);
end
br=[1:4;          br1=[5:11];      brr=[br/0.45 br1/0.45];
figure,plot(Q,1./(brr),'k*-' )
xlabel('image quality');
ylabel('--->BER');title('image quality Vs BER ');
cap=[0 10 20 30 40 50 100 150 200 250 300 350 400 450 500 550 600];
ber1= [0.066 0.066 0.066 0.066 0.066 0.066 0.066 0.066 0.066 0.066 0.066 0.066 0.066 0.066 0.066 0.066 0.066];
figure, plot(cap,ber1,'-rs');
title ('Information capacity VS Bit Error Rate');
xlabel ('Information capacity (no.of.bits)');
ylabel ('Bit Error Rate');

```

8.Comparisons:

Watermarking scheme	Median Filtering		Jitter Attack	
	PSNR(db)	BER	PSNR(db)	BER
The canonical Scheme	43.9731	0.4732	44.0650	0.4836
The Proposed Scheme	44.0235	0.0856	44.0167	0.0664

9. Conclusions

In this paper, we propose a high-capacity CDMA based watermarking scheme based on orthogonal pseudorandom sequence subspace projection. The proposed scheme eliminates the interference of the host image in the watermark extraction phase by subtracting the projection components (on the linear subspace generated by the pseudorandom sequences) from the host image. So it is more robust than the canonical CDMA based scheme. We analyzed and test the performance of the proposed scheme under different attack conditions and compared with the canonical CDMA based scheme. We find that the proposed scheme shoes higher robustness than the canonical scheme under different attack conditions. The expense of high robustness is that an additional key that consists of projection coefficients is needed for the water mark extraction. But this additional memory cost is worthwhile in many situations since it improves both robustness and security of the watermarking system. In the near future we will analyze and test the proposed scheme intensively and use it to design watermarking systems resistant to geometrical attacks and print-and-scan attacks.

References

- [1] Santi P. Maity, Malay K. Kundu, "A Blind CDMA Image Watermarking Scheme In Wavelet Domain," International Conference on Image Processing, vol. 4, Oct. 2004, pp. 2633-2636.
- [2] J. K. Joseph, Ó. Ruanaidh, P. Thierry, "Rotation, Scale and Translation Invariant Spread Spectrum Digital Image Watermarking", Signal Processing. Vol. 66(3), 1998, pp. 303-317
- [3] C. G. M. Silvestre, W. J. Dowling, "Embedding Data in Digital Images Using CDMA Techniques". In: Proc. of IEEE Int. Conf. on Image Processing, Vancouver, Canada 1(2000)589-592
- [4] T. Kohda, Y. Ookubo, K. Shinokura, "Digital Watermarking Through CDMA Channels Using Spread Spectrum Techniques". In: IEEE 6th Int. Sym. on Spread Spectrum Techniques and Applications, Parsippany, NJ, USA, Vol. 2, 2000, pp. 671 –674
- [5] B. Vassaux , P. Bas, J. M. Chassery, "A New CDMA Technique for Digital Image Watermarking Enhancing Capacity of Insertion and Robustness". In: Proc. of IEEE Int. Conf. on Image Processing, Thessalonica, Greece, Vol. 3, 2001, pp. 983 -986
- [6] G. M. Bijan, "Exploring CDMA for Watermarking of Digital Video". Villanova University, Villanova, PA, USA, 1985, <http://www.ece.villanova.edu/~mobasser/mypage/3657-10.pdf>.
- [7] G. M. Bijan, "Direct Sequence Watermarking of Digital Video Using m- frames". In: Proc. Of IEEE Int. Conf. on Image Processing, Chicago, Illinois, USA, Vol. 2(1998) 399 -403.
- [8] L. Xie and G. R. Arce, "Joint wavelet compression and authentication watermarking," in Proc. IEEE ICIP, Chicago, USA, vol. 2, pp. 427–431, Oct., 1998.

- [9] H. Inoue, A. Miyazaki, A. Yamamoto, and T. Katsura, "A digital watermark based on the wavelet transform and its robustness on image compression," in Proc. IEEE ICIP, Chicago, USA, vol. 2, pp. 391–395, Oct., 1998.
- [10] Jong Ryul Kim and Young Shik Moon, "A robust wavelet-based digital watermark using level-adaptive thresholding," in: Proc. ICIP, Kobe, Japan, pp.202-212, Oct. 1999.
- [11] G. Langelaar, I. Setyawan, R.L. Lagendijk, "Watermarking Digital Image and Video Data", in IEEE Signal Processing Magazine, Vol 17, pp. 20-43, September 2000.
- [12] M. Hsieh, D. Tseng, and Y. Huang, "Hiding digital watermarks using multiresolution wavelet transform," IEEE Trans. on Indust. Elect. vol. 48, pp. 875–882, Oct. 2001.
- [13] Y. Seo, M. Kim, H. Park, H. Jung, H. Chung, Y. Huh, and J. Lee, "A secure watermarking for jpeg-2000," in Proc. IEEE ICIP, 2001, Thessaloniki, Greece, vol. 2, pp. 530-533, Oct. 2001.
- [14] P. Su, H. M. Wang, and C. J. Kuo, "An integrated approach to image watermarking and jpeg-2000 compression," J. VLSI Signal Processing, vol. 27, pp. 35–53, Jan. 2001.
- [15] P. Meerwald, A.Uhl, "A Survey of Wavelet-Domain Watermarking Algorithms", in: Proc. of SPIE, Security and Watermarking of Multimedia Contents III, San Jose, USA, Jose, CA, USA, vol.4314, pp. 505-516, Jan. 2001.
- [16] Santi P. Maity, Malay K. Kundu, "A Blind CDMA Image Watermarking Scheme In Wavelet Domain," in: International Conference on Image processing, vol. 4, Oct. 2004, pp. 2633-2636.
- [17] O. Alkin and H. Caglar, "Design of efficient m-band coders with linear phase and perfect reconstruction properties," IEEE Trans. Signal Processing, vol. 43, pp. 1579-1590, 1995.
- [18] P. Steffen, P. N. Heller, R. A. Gopinath, and C. S. Burrus, "Theory of regular M-band wavelet bases," IEEE Trans. Signal Process., vol. 41, no. 12, pp. 3497–3510, Dec. 1993.
- [19] Y. Fang, N. Bi, D. Huang, and J. Huang, "The m-band wavelets in image watermarking," in Proc. IEEE ICIP, 2005, vol. 1, pp. 245–248.

Authors Brief Profile:



Dr K Rameshbabu¹

Dr K.RameshBabu professor, ECE Hyderabad Institute of Technology And Management, Hyderabad, holding B.E (ece),M.E, PhD having 16+years of experience in electronics and communication Engineering area .he is member in ISTE,IEEE & Java Certified Programmer(2,0)PGDST holder. he has lot of experience in academics and industrial related real time projects. He is paper setter for many autonomous universities and visiting professor for many areas like image processing, electron devices etc. he can be reached at: dr.kprb.ece@gmail.com



vani.kasireddy²

Vani.kasireddy is Good student, pursuing M.Tech vlsid from ECE dept, Hitam.she is active member, in technical education along the student related motivation activities.lot of interest in research areas related to, image processing digital Electronics, trouble shooting hardware kits etc. she can reach at: vanisri234@gmail.com

FPGA implementation of wavelet-based denoising technique to analysis of EEG signal

¹T.Chaitanya, ²G.S.Siva kumar

¹M.Tech student,

Pragati Engineering College, Surampalem (A.P, IND).

²Assistant Professor, Dept.Of ECE

Abstract

The electroencephalogram (EEG) is widely used clinically to investigate brain disorders. However, abnormalities in the EEG in serious psychiatric disorders are at times too subtle to be detected using conventional techniques. This paper describes the application of the wavelet transform, for the classification of EEG signals. The data reduction and preprocessing operations of signals are performed using the wavelet transform. Five classes of EEG signals were used: Alpha, beta, Gamma, Delta, Theta. The EEG signal is generated with the help of MATLAB. After several iteration we found the suitable wavelet coefficients which will able to correctly classify all five class of EEGs, respectively. The wavelet transform thus provides a potentially powerful technique for classification of EEG signals. Finally we carried out FPGA implementation of these resulting parameters.

Keywords: FPGA, Wavlet, MATLAB, etc.

1. Introduction

The purpose of this paper is to illustrate the potential of the High Resolution EEG techniques when applied to the analysis of brain activity related to the observation of TV commercials, political advertising, and PSAs to localize cerebral areas mostly emotionally involved. In particular, we would like to describe how, by using appropriate statistical analysis, it is possible to recover significant information about cortical areas engaged by particular scenes inserted within the video clip analyzed. The brain activity was evaluated in both time and frequency domains by solving the associate inverse problem of EEG with the use of realistic head models.

Successively, the data analyzed were statistically treated by comparing their actual values to the average values estimated during the observation of the documentary. Statistical estimators were then evaluated and employed in order to generate representations of the cortical areas elicited by the particular video considered. Electroencephalography (EEG) is the recording of electrical activity along the scalp produced by the firing of neurons within the brain.^[2] In clinical contexts, EEG refers to the recording of the brain's spontaneous electrical activity over a short period of time, usually 20–40 minutes, as recorded from multiple electrodes placed on the scalp. In neurology, the main diagnostic application of EEG is in the case of epilepsy, as epileptic activity can create clear abnormalities on a standard EEG study.^[3] A secondary clinical use of EEG is in the diagnosis of coma, encephalopathies, and brain death. EEG used to be a first-line method for the diagnosis of tumors, stroke and other focal brain disorders, but this use has decreased with the advent of anatomical imaging techniques such as MRI and CT. Derivatives of the EEG technique include evoked potentials (EP), which involves averaging the EEG activity time-locked to the presentation of a stimulus of some sort (visual, somatosensory, or auditory). Event-related potentials (ERPs) refer to averaged EEG responses that are time-locked to more complex processing of stimuli; this technique is used in cognitive science, cognitive psychology, and psychophysiological research.

The processing of information takes place by the “firing” or pulsing of many individual neurons. The pulse is in the form of membrane depolarization travelling along the axons of neurons. A series of pulses in the neurons, also known as a spike train, can be considered the coded information processes of the neural network. The EEG is the electrical field potential that results from the spike train of many neurons. Thus, there is a relationship between the spike train and the EEG and the latter also encodes information processes of the neural-network. Measurement and analysis of the EEG can be traced back to Berger's experiments in 1929. Since then it has had wide medical applications, from studying sleep stages to diagnosing neurological irregularities and disorders. It was not until the 1970's that researchers considered using the EEG for communication.

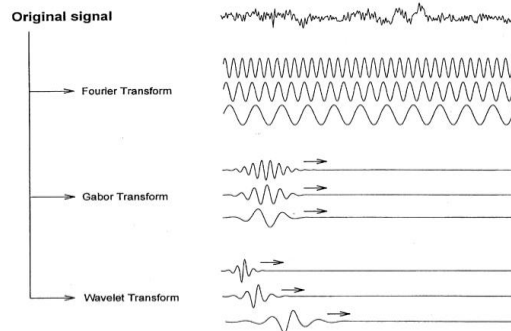


Fig. 1.1 various methods of EEG signal Analysis

2. 2. Analysis Methods

2.1 QUANTITATIVE EEG ANALYSIS

In quantitative EEG analysis the spectral contents of measured EEG can be quantified by various parameters obtained from the power spectral density (PSD) estimate. Typically several representative samples of EEG are selected and an average spectrum is calculated for these samples. Traditionally EEG is divided into four bands: δ (0 - 3.5 Hz), θ (3.5 - 7 Hz), α (7 - 13 Hz) and β (13 - 30 Hz). PSD estimates can be calculated by either nonparametric (e.g. methods based on FFT) or parametric (methods based on autoregressive time series modeling) methods.

EEG signal generation using MATLAB

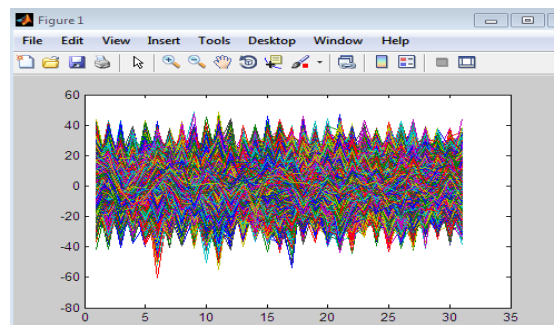


Fig 1.2 EEG signal.

2.2 TIME-VARYING EEG ANALYSIS

In the analysis of non-stationary EEG the interest is often to estimate the time-varying spectral properties of the signal. A traditional approach for this is the spectrogram method, which is based on Fourier transformation. Disadvantages of this method are the implicit assumption of stationarity within each segment and rather poor time/frequency resolution. A better approach is to use parametric spectral analysis methods based on e.g. time-varying autoregressive moving average (ARMA) modeling. The time-varying parameter estimation problem can be solved with adaptive algorithms such as least mean square (LMS) or recursive least squares (RLS). These algorithms can be derived from the Kalman filter equations. Kalman filter equations can be written in the form

$$\begin{aligned}
 \hat{\theta}_{t|t-1} &= \hat{\theta}_{t-1} \\
 C_{\hat{\theta}_{t|t-1}} &= C_{\hat{\theta}_{t-1}} + C_{w_{t-1}} \\
 K_t &= C_{\hat{\theta}_{t|t-1}} \varphi_t^T \left(\varphi_t^T C_{\hat{\theta}_{t|t-1}} \varphi_t + C_{e_t} \right)^{-1} \\
 C_{\hat{\theta}_t} &= \left(I - K_t \varphi_t^T \right) C_{\hat{\theta}_{t|t-1}} \\
 \epsilon_t &= z_t - \varphi_t^T \hat{\theta}_{t|t-1} \\
 \hat{\theta}_t &= \hat{\theta}_{t|t-1} + K_t \epsilon_t
 \end{aligned}$$

Where θ is the state vector of ARMA parameters, ϕ includes the past measurements, C denotes for covariance matrices and K is the Kalman gain matrix. All these adaptive algorithms suffer slightly from tracking lag. This can however be avoided by using Kalman smoother approach. Here we demonstrate the ability of several time-varying spectral estimation methods, with an EEG sample recorded during a eyes open/closed test. This test is a typical application of testing the desynchronization /synchronization (ERD/ERS) of alpha waves of EEG. The occipital EEG recorded while subject having eyes closed shows high intensity in the alpha band (7-13 Hz). With opening of the eyes this intensity decreases or even vanishes. It can be assumed that EEG exhibits a transition from a stationary state to another. One such transition from desynchronized state to synchronized state is presented below.

Analysis Based On Modes

The EEG signal is closely related to the level of consciousness of the person. As the activity increases, the EEG shifts to higher dominating frequency and lower amplitude. When the eyes are closed, the alpha waves begin to dominate the EEG. When the person falls asleep, the dominant EEG frequency decreases. In a certain phase of sleep, rapid eye movement called (REM) sleep, the person dreams and has active movements of the eyes, which can be seen as a characteristic EEG signal. In deep sleep, the EEG has large and slow deflections called delta waves. No cerebral activity can be detected from a patient with complete cerebral death.

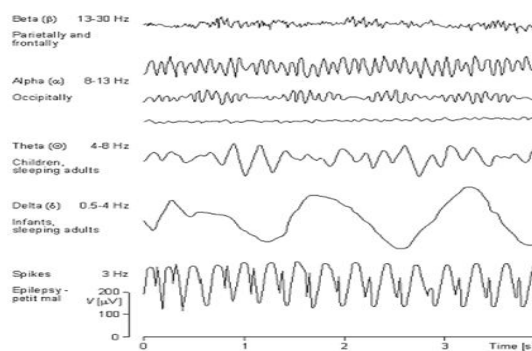


Fig. 1.3 various stages of EEG signal's

Power Spectra Calculation

Using Auto-Regressive (AR) parameter model method to compute the self-power spectra estimated value of the EEG signal [23]: The AR model of the EEG time series x_n is provided by the following formula

$$x_n = -\sum_{k=1}^p a_k x_{n-k} + w_n \quad (2)$$

Here p is the order of the AR model; $a_k (k = 1, 2, \dots, p)$ is AR model parameter; w_n is the unpredictable part of x_n , namely residual error. If the model can well match the EEG time series, w_n should be white noise process. According to the AR model

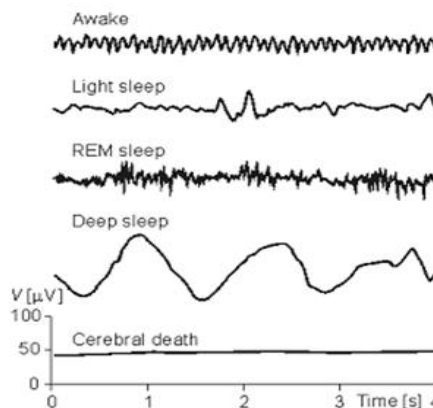


Figure 1.4 EEG activity depends on level of consciousness

given by formula (2), we can get the estimated value of the AR spectra

$$P_x(\omega) = \frac{\sigma_{\omega}^2}{|A(e^{j\omega})|^2} = \frac{\sigma_{\omega}^2}{\left|1 + \sum_{k=1}^p a_k e^{-j\omega k}\right|^2} \quad (3)$$

Here σ_{ω}^2 is the variance of AR model residual error. From the formulas (2) and (3), we know the key to get the AR spectra estimation is to estimate the AR parameters $a_k(k = 1, 2, \dots, p)$ through the EEG time series. Usually, Yule-Walker equation and Levinson-Durbin algorithm are used to estimate AR parameters. In this paper, we use Burg algorithm. Burg algorithm is an auto regression power spectra estimated method, on the premise of Levinson-Durbin recursion restraint, making the sum of the front and back forecast error energy smallest. Burg algorithm avoids the computation of self-correlation function. It can distinguish the extremely close sine signal in low noise signals, and may use less data record to estimate, and the result is extremely close to real values. Moreover, the forecasting error filter obtaining from Burg algorithm is minimum phase. The choice of the model order p is a critical problem in the AR model spectra estimate. If p is too low, it will cause smooth spectra estimate; while if p is too high, it will cause spectral line excursion and spectral line abrupt and generate general statistic instability. In this paper, we adopt Akaike information criterion(AIC) to estimate the value of the order

$$AIC(p) = N \ln \tilde{\rho}_p + 2p,$$

Here N is the number of the data points, $\tilde{\rho}_p$ is the estimated value of the white noise variance (forecasting error power) of p order AR model.

The Determinism Computation of EEG Signals

Whether the brain is a deterministic system, determines the applicability of the nonlinear dynamic method of studying EEG signal [16]. Generally, the deterministic computation of the EEG signal requires much data; and supposes the spread of adjacent lines of EEG series in the phase space are similar. However, unstable data often generates false results. CTM algorithm is a method to express the second-order difference plot (SODP) characteristic of trajectory tangent vector quantificationally. It can be used in the deterministic computation of nonlinear time series effectively. This algorithm is real-time, stable and anti-noisy [17]. The tangent vector of trajectory in the reconstructing phase space is

$$F(t) = x(t+1) - x(t).$$

The angle between the tangent vectors can be expressed by its cosine value

$$A(t) = \frac{Y(t+1) \cdot Y(t)}{\|Y(t+1)\| \|Y(t)\|}.$$

Compared with the angle itself, the cosine value can resist noises better. The SODP of signal expresses the change rate of the tangent vectors angle $A(n+2) - A(n+1)$ to $A(n+1) - A(n)$, its CTM value is The value of CTM reflects the smooth degree of the attractors' trajectory: the smaller the CTM value is, the less the changes of tangent vector angle, the smoother the trajectory is; and vice versa. The determinacy of the signal S can be measured by the ratio of the CTM value of the EEG series data and the surrogate data. The bigger S is, the stronger the randomness of EEG signal is. The researches show: the deterministic signal $S < 0.3$; the random signal $S > 0.7$; as to part deterministic signal $0.3 < S < 0.7$.

2.3 Phase Graph Analysis

Using the phase space reconstruct technique from one-dimensional time series to determine the time delay τ : In the experimental system, it should be through repeated trial method to confirm choice of τ . If τ is undersize, the track of the phase space will approach to a straight line; per contra τ is oversize, the data point will centralize in a small range of the phase space, and we can't get the attractors' local structures from the reconstructed phase graph [13]. Testing repeatedly, we find that selecting $\tau = 3$, data point $N = 2000$, it can well reconstruct the EEG attractors. We construct the EEG attractors of all five kinds of consciousness activities of 7 subjects and find that EEG attractors of various patterns have similar characteristics. Fig.2 is a representative one. As can be seen from Fig. 2, the attractors' track often rotate in an extremely complex way, even smear a group black in the plane, but there is still internal structure when the attractors is magnified. The attractors of relaxation, mental composition of a letter and visualizing a 3-dimensional object being revolved about an axis often distribute in a small ellipse region, while the point in the attractors of mental arithmetic of multiplication and visualizing numbers being written or erased on a blackboard centralize nearby the 45 degree line and there is a large distributing range along the 45 degree line. This is because while proceeding rational computation such

as mathematics or imagination, the value of the adjacent sampling points of EEG signals are close, and the amplitude values of the whole EEG signals are great.

FPGA

A field-programmable gate array (FPGA) is an integrated circuit designed to be configured by the customer or designer after manufacturing—hence "field-programmable".

3. Result and Discussion: Model Sim Output:

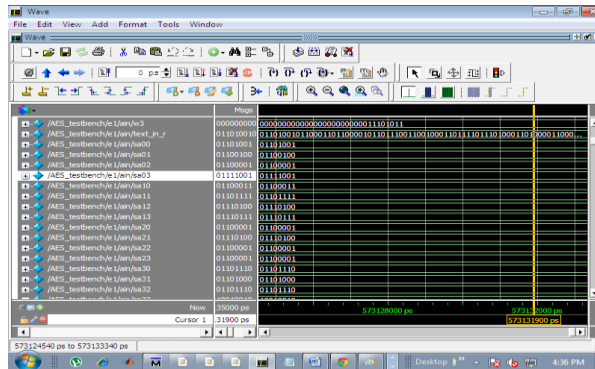


Figure 1.5.Simulated output.

CLASSIFIED EEG SIGNALS.

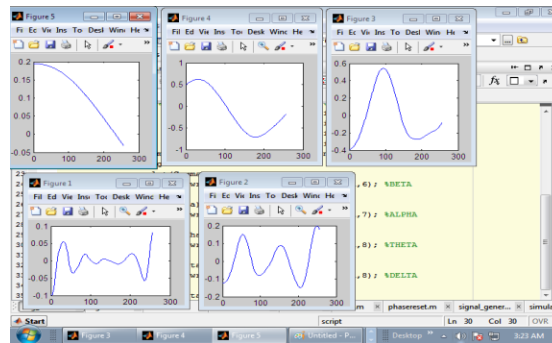


Fig 1.6 classified EEG signals

4. Synthesis Report:

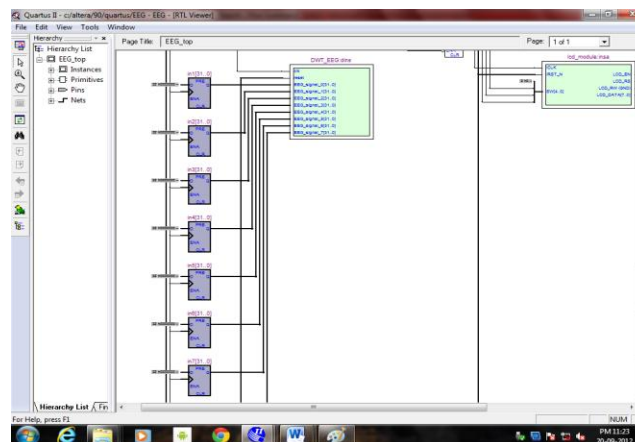


Fig1.7 RTL Schematic report

Area Utilization Report: Figure

Flow Summary	
Flow Status	Successful - Thu Sep 20 23:17:24 2012
Quartus II Version	9.0 Build 132 02/25/2009 SJ Web Edition
Revision Name	EEG
Top-level Entity Name	EEG_top
Family	Cyclone III
Device	EP3C16F484C6
Timing Models	Final
Met timing requirements	N/A
Total logic elements	174 / 15,408 (1 %)
Total combinational functions	169 / 15,408 (1 %)
Dedicated logic registers	61 / 15,408 (< 1 %)
Total registers	61
Total pins	57 / 347 (16 %)
Total virtual pins	0
Total memory bits	0 / 516,096 (0 %)
Embedded Multiplier 9-bit elements	0 / 112 (0 %)
Total PLLs	0 / 4 (0 %)

Fig 1.8.Flow summary report

MAP VIEWER:

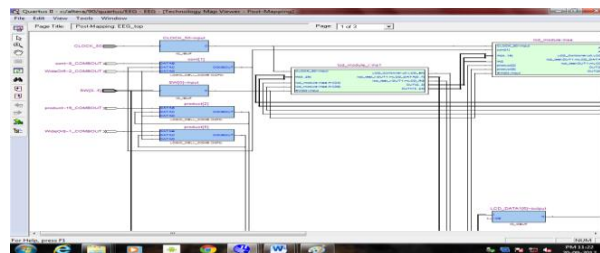


Fig 1.9.Technology map viewer

POWER ANALYZES

PowerPlay Power Analyzer Summary	
PowerPlay Power Analyzer Status	Successful - Thu Sep 20 23:21:22 2012
Quartus II Version	9.0 Build 132 02/25/2009 SJ Web Edition
Revision Name	EEG
Top-level Entity Name	EEG_top
Family	Cyclone III
Device	EP3C16F484C6
Power Models	Final
Total Thermal Power Dissipation	69.32 mW
Core Dynamic Thermal Power Dissipation	0.00 mW
Core Static Thermal Power Dissipation	51.74 mW
I/O Thermal Power Dissipation	17.57 mW
Power Estimation Confidence	Low: user provided insufficient toggle rate data

Fig. 1.10 Power dissipation report

Conclusion

A wavelet-chaos methodology was presented for analysis of EEGs and delta, theta, alpha, beta, and gamma sub bands of EEGs for detection of seizure and epilepsy. Although it is observed that the filters are used for EEG signal denosing classification is not possible with the help of filters. The accuracy of wavlet based EEG classification is for better than any other methods.

References

- [1] Seizures and Epilepsy: Hope through Research National Institute of Neurological Disorders and Stroke (NINDS), Bethesda, MD, 2004 .
- [2] H. Adeli, Z. Zhou, and N. Dadmehr, "Analysis of EEG records in an epileptic patient using wavelet transform," *J. Neurosci. Meth.*, vol. 123,no. 1, pp. 69–87, 2003.
- [3] P. J. Durka, "From wavelets to adaptive approximations: Time-frequency parameterization of EEG," *BioMedical Engineering OnLine*,vol. 2, no. 1, pp. 1(1)–1(30), 2003 [Online]. Available: <http://www.biomedical-engineering-online.com/>
- [4] L. D. Iasemidis, L. D. Olson, J. C. Sackellares, and R. S. Savit, "Timedependencies in the occurrences of epileptic seizures: A nonlinear approach,"*Epilepsy Res.*, vol. 17, pp. 81–94, 1994.
- [5] H. Adeli and S. L. Hung *Machine Learning – Neural Networks, Genetic Algorithms, and Fuzzy Sets*. New York: Wiley, 1995.

Area Optimized and Pipelined FPGA Implementation of AES Encryption and Decryption

¹Mg Suresh, ²Dr.Nataraj.K.R

¹Asst Professor Rgit, Bangalore, ²Professor

^{1,2}Department Of Electronics And Communication Sjb Institute Of Technology, Bangalore

Abstract

Advanced Encryption Standard (AES), a Federal Information Processing Standard (FIPS), and categorized as Computer Security Standard. The AES algorithm is a block cipher that can encrypt and decrypt digital information. The AES algorithm is capable of using cryptographic keys of 128, 192, and 256 bits. The Rijndael cipher has been selected as the official Advanced Encryption Standard (AES) and it is well suited for hardware. This paper talks of AES 128 bit block and 128 bit cipher key and is implemented on Spartan 3 FPGA using VHDL as the programming language. Here A new FPGA-based implementation scheme of the AES-128 (Advanced Encryption Standard, with 128-bit key) encryption and decryption algorithm is proposed in this paper. The mode of data transmission is modified in this design so that the chip size can be reduced. The 128-bit plaintext and the 128-bit initial key, as well as the 128-bit output of cipher text, are all divided into four 32-bit consecutive units respectively controlled by the clock. This system aims at reduced hardware structure and high throughput. ModelSim SE PLUS 6.3 g software is used for simulation and optimization of the synthesizable VHDL code. Synthesizing and implementation (i.e. Translate, Map and Place and Route) of the code is carried out on Xilinx - Project Navigator, ISE 12.1i suite.

Keywords : AES, FPGA, FIPS, VHDL, Plaintext, Ciphertext

1. Introduction

With the rapid development and wide application of computer and communication networks, the information security has aroused high attention. Information security is not only applied to the political, military and diplomatic fields, but also applied to the common fields of people's daily lives. With the continuous development of cryptographic techniques, the long-serving DES algorithm with 56-bit key length has been broken because of the defect of short keys. So AES (Advanced Encryption Standard) substitutes DES and has already become the new standard. AES algorithm is already supported by a few international standards at present, and AES algorithm is widely applied in the financial field in domestic, such as realizing authenticated encryption in ATM, magnetism card and intelligence card. In 1997, an effort was initiated to develop a new American encryption standard to be commonly used well into the next century. This new standard was given a name AES, Advanced Encryption Standard. A new algorithm was selected through a contest organized by the National Institute of Standards and Technology (NIST). By June 1998, fifteen candidate algorithms have been submitted to NIST by research groups from all over the world. After the first round of analysis was concluded in August 1999, the number of candidates was reduced to final five. The five algorithms selected were MARS, RC6, RIJNDAEL, SERPENT and TWOFISH. The conclusion was that the five Competitors showed similar characteristics. On October 2nd 2000, NIST announced that the Rijndael Algorithm as the winner of the contest. The primary criteria used by NIST to evaluate AES candidates included security, efficiency in software and hardware, and flexibility. Rijndael Algorithm developed by Joan Daemen and Vincent Rijmen. Was chosen since it had the best overall scores in security, performance, efficiency, implementation ability and flexibility. Hence chosen as the standard AES (Advanced Encryption Standard) algorithm's a symmetric block cipher that can process data blocks of 128 bits through the use of cipher keys with lengths of 128, 192, and 256 bits. The hardware implementation of the Rijndael algorithm can provide either high performance or low cost for specific applications.

AES algorithm is widely applied in the financial field in domestic, such as realizing authenticated encryption in ATM, magnetism card and intelligence card. On the current situation of researching at home and abroad, AES algorithm emphasizes its throughput using pipeline pattern. Its biggest advantage is to improve the system throughput, but there is a clear disadvantage that is at the cost of on-chip resources. And in accordance to that AES algorithm is used in the low requirements of the terminal throughput at present, the high safety and cost-effective reduced AES system is designed and validated on the xilinx spartan 3 chip aiming at reduced hardware structure. The advantages in this system are high speed, high reliability, a smaller chip area, and high cost-effective. These will effectively promote the AES algorithm to be used in the terminal equipments. Hardware security solution based on highly optimized programmable FPGA provides the parallel processing Capabilities and can achieve the required encryption performance benchmarks. The current area-optimized algorithms of AES are mainly based on the realization of S-box mode and the minimizing of the internal registers which could save the area of IP core significantly.

Cryptographic algorithms are most efficiently implemented in custom hardware than in software running on general purpose processors. Hardware implementations are of extreme importance in case of high performance, security against system intruders and busy systems, where a cryptographic task consumes too much time. Traditional ASIC solutions have the well-known drawback of reduced flexibility compared to software solutions. Hence the implementation of the AES algorithm based on FPGA devices has certain advantages over the implementation based on ASICs. One new AES algorithm with 128-bit keys (AES-128) was described in this paper, which was realized in VHDL. The 128-bit plaintext and 128-bit key, as well as the 128-bit output data were all divided into four 32-bit consecutive units respectively. The pipelining technology was utilized in the intermediate nine round transformations so that the new algorithm achieved a balance between encryption speed and chip area, which met the requirements of practical application. The data of each column (32 bits) in the state matrix was used to be an operand of encryption, when the operation of ShiftRows and SubBytes were incorporated. And each round of the intermediate nine Round Transformations of encryption was processed by pipelining technology. The main problem in older algorithms is area utilization on chip is more. These are of low performance and low throughput architectures. Further, many of the architectures are not area efficient and can result in higher cost when implemented in silicon. In this proposed method, for maintaining the speed of encryption, the pipelining technology is applied and the mode of data transmission is modified in this design so that the chip size can be reduced. The 128-bit plaintext and the 128-bit initial key, as well as the 128-bit output of ciphertext, which are all divided into four 32-bit consecutive units respectively controlled by the clock. Hence we overcome the area utilization problem. Here area and throughput are carefully trading off to make it suitable for wireless military communication and mobile telephony where emphasis is on the speed as well as on area of implementation.

A. Objective

The main objective of the paper is to design and development of AES system using FPGA in computer communication networks such as internet and to perform the verification and validation of the developed system.

- First design the AES encryption algorithm using VHDL Language in Xilinx 12.2 and simulation is done by Modelsim 6.3f.
- Second design the AES decryption algorithm using VHDL Language in Xilinx 12.2 and simulation is done by Modelsim 6.3f. In the standard AES algorithm, there are four steps like SubByte, ShiftRow, MixColumn and Add Round Key in normal rounds. In Our design we highlight some following modifications:
 - 1) Exclusion of Shift Row OR Merging of Sub Byte and Shift Row
 - 2) Pipelining for high Throughput
 - 3) Optimizing the design to keep handy balance between Throughput and Silicon Area .

B. Existing System:

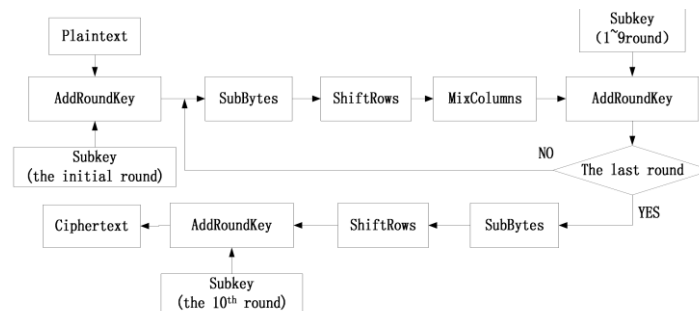


Figure1. The Structure of Rijndael Encryption Algorithm

Rijndael algorithm consists of encryption, decryption and key schedule algorithm. The main operations of the encryption algorithm among the three parts of Rijndael algorithm include: bytes substitution (SubBytes), the row shift (ShiftRows), column mixing (MixColumns), and the round key adding (AddRoundKey). Similarly Decryption includes: Inverse bytes substitution (InvSubBytes), the Inverse row shift (InvShiftRows), Inverse column mixing (InvMixColumns), and the round key adding (AddRoundKey). Exclusive-OR operation is an inverse of itself, so there is no need for specific InvAddRoundKey transformation the same AddRoundKey operation is used during both encryption and decryption rounds. Encryption algorithm processes Nr+1 rounds of AddRoundKey transformation of the plaintext for the ciphertext. Decryption algorithm processes Nr+1 rounds of InvAddRoundKey transformation of the ciphertext for the plaintext. The value of Nr in AES algorithm whose packet length is 128 bits should be 10 for the key length of 128.

2. Implementation Of Area Optimized And Pipelined AES Encryption And Decryption

A.The Design of Improved AES Algorithm

2. Two main processes of improved AES Encryption and Decryption algorithm:

The AES Encryption algorithm can be divided into two parts, the key schedule and round transformation. similarly in decryption also. Key schedule consists of two modules: key expansion and round key selection. Key expansion means mapping N_k bits initial key to the so-called expanded key, while the round key selection selects N_b bits of round key from the expanded key module. Round Transformation involves four modules by ByteSubstitution, ByteRotation, MixColumn and AddRoundKey in the Encryption .where as in Decryption the Round Transformation involves four modules Inv ByteSubstitution, InvByteRotation,InvMixColumn and AddRoundKey

2) Key points for the design:

In the AES-128, the data in the main process mentioned above is mapped to a 4x4 two-dimensional matrix. The matrix is also called state matrix, state matrix in at the begin of Encryption process will have the plain text. Where as at the start of Decryption process will contain cipher text which is shown as Figure.2.

a_{00}	a_{01}	a_{02}	a_{03}
a_{10}	a_{11}	a_{12}	a_{13}
a_{20}	a_{21}	a_{22}	a_{23}
a_{30}	a_{31}	a_{32}	a_{33}

Figure 2: The state matrix

In the four transformation modules of round transformation of the Encryption process, the Byte Rotation, Mix Column and Add Round Key are all linear transformations except the Byte Sub. Similar in Decryption process the modules of round transformation the Inv Byte Rotation, Inv Mix Column and AddRoundKey are all linear transformations except the Inv Byte Sub.

Take analysis of the AES Encryption and Decryption algorithm principle and we can find:

- Byte Substitution(Sub Bytes) operation simply replaces the element of 128-bit input plaintext with the element corresponding to the Galois field $GF(2^8)$, whose smallest unit of operation is 8 bits/ group. Inv Byte Substitution Transformation in the Decryption(inverse cipher) is the inverse of Byte Substitution (Sub Bytes).
- Byte Rotation(Shift Rows) operation takes cyclic shift of the 128-bit state matrix, in which one row (32 bits) is taken as the smallest operand. . Inv Byte Rotation Transformation in the Decryption(inverse cipher) is the inverse of Byte Rotation (Shift Rows).
- Mix Column operation takes multiplication and addition operations of the results of Byte Rotation with the corresponding irreducible polynomial $x^8 + x^4 + x^3 + x + 1$ in $GF(2^8)$, whose minimum operating unit is 32 bits. . Inv Mix Column Transformation in the Decryption(inverse cipher) is the inverse of Mix Column.
- Add round key operation takes a simple XOR operation with 8-bit units. Since Exclusive-OR operation is an inverse of itself, so there is no need for specific Inv Add Round Key transformation the same Add Round Key operation is used during both Encryption and Decryption rounds.

The inputs of plaintext and initial key, intermediate inputs and outputs of round transformation, as well as the output of cipher text in the AES Encryption algorithm are all stored in the state matrixes. Similarly the inputs of ciphertext and initial key, intermediate inputs and outputs of round transformation, as well as the output of plaintext in the AES Decryption algorithm are all stored in the state matrixes which are processed in one byte or one word. Thus, in order to take operations at least bits, the original 128-bit data should be segmented. We design some external controllers in the new algorithm, so that the data transmission and processing can be implemented on each column of the state matrix (32bit). That means the data should be packed and put into further operations. Take the independent and reversible bytes substitution operation of S-box as example. Firstly, the state matrix is divided into four columns. And then byte replacement is achieved by the operation of look-up table shown as Figure 3.

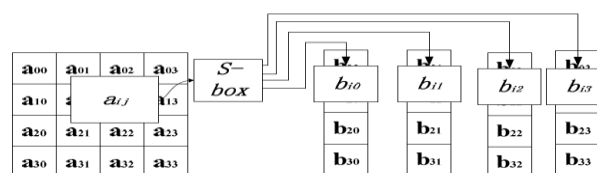


Figure 3: Bytes Segmentation and replacement processing

Therefore, the original 128-bit inputs and key will be replaced with four consecutive 32-bit input sequences respectively. In order to decrease the output ports, four continuous 32-bit output sequences have taken place of the original 128-bit output by adding a clock controller. The 128-bit data in the round transformation is also split into four groups of 32-bit data before the operation of pipelining.

B.PROPOSED MODEL :

In the proposed method architectural optimization has been incorporated which includes pipelining techniques. Speed is increased by processing multiple rounds simultaneously but at the cost of increased area. The corresponding hardware realization is optimal in terms of area and offers high data throughput. An optimized code for the implementation of this algorithm for 128 bits has been developed and experimentally tested using Xilinx device. So the focal approach of our design on hardware platform is to attain speed up (i.e. high throughput No. of block processed per second) at the same time, silicon area optimization. From the above analysis, we can find that the process of AES encryption and Decryption can be mainly divided into two parts: key schedule and round transformation. The improved structure is also divided into these two major processes. The initial key will be sent to the two modules: Key expansion and Key selection, While the plaintext is to be sent to the round transformation during Encryption and cipher text is sent to round transformation after the round key is selected. But the operand of data transmission is turned into a 32-bit unit.

The process of new algorithm is shown as Figure 4(a) & (b).

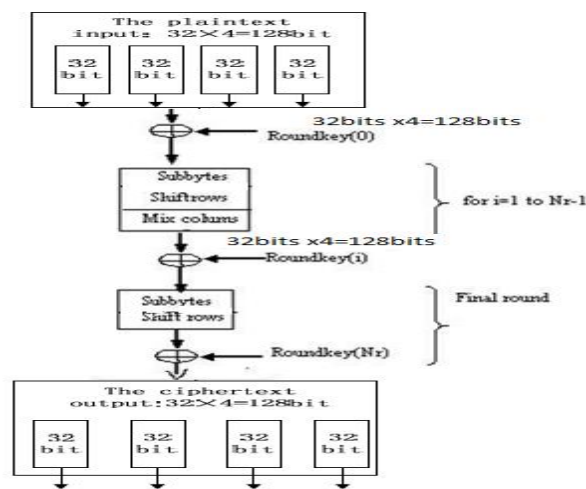


Figure 4(a): Proposed AES algorithm for Encryption

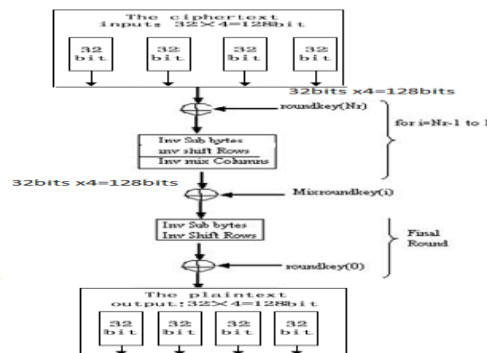


Figure 4(b) Proposed AES algorithm for Decryption Flow

In AES Encryption and Decryption process, first of all, a initial round of transformation has to be performed

3. The initial round of encryption

Which XORs the original 128 bits of input data with the original 128 bits of key i.e. four packets of consecutive 32-bit plaintext (Encryption) or four packets of consecutive 32-bit Ciphertext (Decryption) have been put into the corresponding registers. Meanwhile, another four packets of consecutive 32-bit initial key (128 bits) have been put into other registers by the control of the enable clock signal. Furthermore, this module should combine the plaintext and initial key by using the XOR operator during Encryption where as in the Decryption this module should combine the ciphertext and initial key by using the XOR operator.

4. Round Transformation in the intermediate steps:

A round transformation mainly realizes the function of SubBytes and MixColumns with 32-bit columns during Encryption and InvSubBytes and InvMixColumns with 32-bit columns during Decryption. Here **Exclusion of Shift Row** is performed by calling required shifted element from the data matrix, instead of calling element one by one sequentially from the data matrix. Thereby SUB-BYTE and SHIFT ROW for encryption (which is known as BYTE ROTATE when the shift is done on register or 32 bit word) operations are carried out in one-step instead of two similarly for Decryption. Four packets of round transformation are processed independently. Then the results of MixColumns and InvMix Column and the 32-bit keys sourced from Key expansion are combined by using XOR operators respectively. Here, the round transformation is a module with 64 input ports (32-bit plaintext+32-bit key) and 32 output ports. The function of SubByte and Inv SubByte is realized by Look-Up Table (LUT). It means that the operation is completed by the Find and Replace after all replacement units are stored in a memory ($256 \times 8 \text{bit} = 1024 \text{ bit}$). The implementation of MixColumn and InvMixColumn is mainly based on the mathematical analysis in the Galois field $GF(2^8)$ and Inv Galois field $GF(2^{-8})$. Only the multiplication module and the 32-bit XOR module of each processing unit(one column) are needed to design, because the elements of the multiplication and addition in Galois field are commutative and associative. Then the function of MixColumn and InvMixColumn can be achieved.

Figure.5 is a block diagram for the introduction of pipelining technology used in the round transformation.

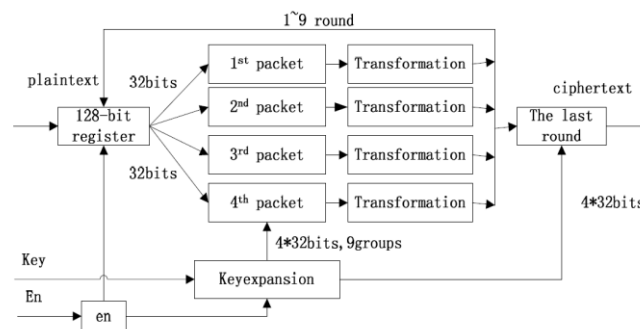


Figure5: The Process of Pipelining

In the process of pipelining, the 128-bit data is divided into four consecutive 32-bit packets that take round transformation independently. The operation of the above four groups of data can be realized in pipelining technology. In brief, it can be described as follows: store the unprocessed data in the 128-bit register, and control the clock for restarting the 128-bit register to read the new data when the four groups' operations have been overcome. Thus the 128-bit round-operating unit has been transformed into four 32-bit round-operating elements. The internal pipelining processing should be implemented during the whole nine intermediate Round Transformations of the four packets before achieving the 128-bit ciphertext for Encryption and 128-bit plaintext for Decryption.

5. The process of the last round:

The final round is a 128-bit processor. After nine rounds of operations included Shiftrows, SubByte and Mixclumns during Encryption and After nine rounds of operations included InvShiftrows, InvSubByte and InvMixclumns during Decryption. The 128-bit intermediate resultant data will be used in XOR operation with the final expanded key ($4 * 32 \text{bit}$), which is provided by the key expansion module. The output of final round of Encryption in the processor is the desired 128-bit ciphertext. Similarly, the ciphertext is divided into four packets of 32-bit data by an external enable signal. The output of final round of Decryption in the processor is the desired 128-bit plaintext. Similarly, the plaintext is divided into four packets of 32-bit data by an external enable signal. The proper selection of the module and data path for a particular round is done by the control signals. These signals also control the Key Scheduling module so that valid keys are called for the particular round.

6. Key expansion and Key extraction

This module is implemented basically the same with the traditional way as another part of the AES encryption algorithm.

The only difference lies on the mode of data transmission. The initial key and expanded keys are divided into four 32-bit data before being extracted.

All of the above modules can be decomposed into basic operations of seeking and XOR if the AES algorithm is Implemented on FPGA. So the basic processing unit (look-uptable) of FPGA can be used. The operation of AddRoundKey is taken first in each round. When the plaintext and initial key are input, the encryption module starts running, and the expanded keys are stored into the registers at the same time. This implementation method is independent on a specific FPGA.

7. SIMULATION RESULTS

ModelSim SE PLUS 6.3 g software is used for simulation and optimization of the synthesizable VHDL code. Synthesizing and implementation (i.e. Translate, Map and Place and Route) of the code is carried out on Xilinx - Project Navigator, ISE 12.1i suite. Initially we designed AES module in such a way that it should be implemented on a single chip, but when we implemented on FPGA kit (SPARTAN-III), our design exceeded more than 4 lakhs gates. This made impossible to implement the AES design module to dump on a single chip. As a result we implemented the AES Encryption module on a FPGA for the verification of the hardware implementation of the design. When we feed 16 bytes (128 bit four 32 bits packets) of data in case of AES encryption into Modelsim simulator, In Figure6 we can observe that all the 16 bytes of encrypted data for AES, can be observed on the output of FPGA also In terms of 8 bits of chunk. For verification of the working of Decryption we have feed the output of encryption to the decryption module and observed that the output has regenerated the original text at the output in Figure7. We have forced HELLO WORLD as an input to the design and obtained the original data back after the decryption of the encrypted message with the use of same key as seen in Figure8. We have also monitored that if the single bit of the decryption key is change we are not in a position to retrieve the original data back.



Figure6: Simulation of 128-bit AES Encryption

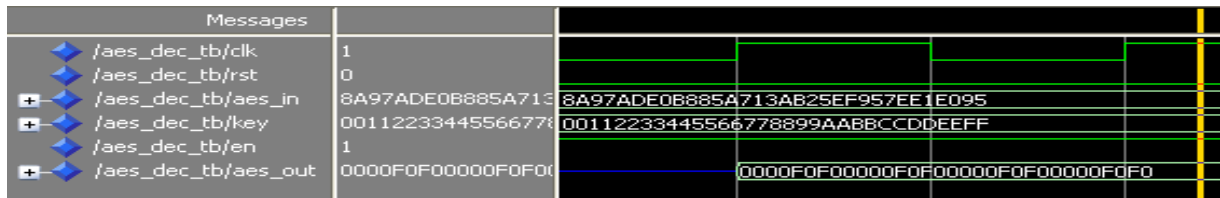


Figure7: Simulation of 128-bit AES decryption

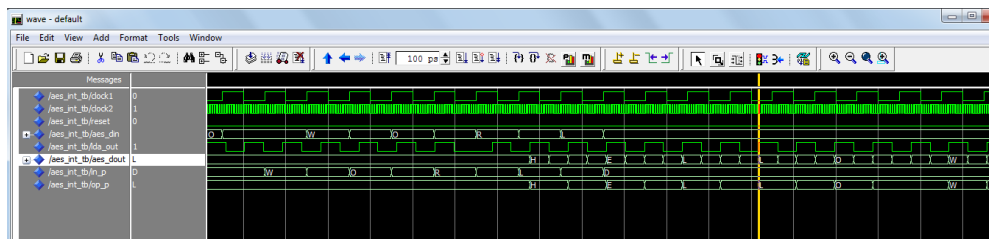


Figure8: HELLO WORLD is forced as input to the design and obtained the original data back

8. Conclusion And Future Work

From our work we have concluded that the concept of Pipelined AES architecture can be practically implemented . It has been observed that the implementation of AES Encryption on the FPGA is successful and several data input. The cipher key can be changed with respect to the user requirements. The result shows that the design with the pipelining technology and special data transmission mode can optimize the chip area effectively. Meanwhile, this design reduces power consumption to some extent, for the power consumption is directly related to the chip area. Therefore the encryption device implemented in this method can meet some practical applications. As the S-box is implemented by look-up-table in this design, the chip area and power can still be optimized. So the future work should focus on the implementation mode of S-box. Mathematics in Galois field (2^8) can accomplish the bytes substitution of the AES algorithm, which could be another idea of further research. While implementing the AES Algorithm, the critical aspect was the area utilization. Which was done using implementation of functions for different sub modules in the algorithm the work has approximately reduced around 10% utilization on chip as compared to basic available modules .

We have successfully implemented AES encryption on FPGA. We have achieved the data encryption as per 100% accuracy as compared to data encryption module available online. The next step is to study the behavior of the AES Model in extreme conditions and to implement as an ASIC. There is a provision and flexibility to remove or add any other cryptographic standards.

References

1. [Oded Goodrich](#), *Foundations of Cryptography, Volume 1: Basic Tools*, Cambridge University Press, 2001.
2. "[Cryptology \(definition\)](#)". *Merriam-Webster's Collegiate Dictionary* (11th edition.). Merriam-Webster. <http://www.merriam-webster.com/dictionary/cryptology/>. Retrieved on 2008-02-01.
3. <http://Advanced Encryption Standard - Wikipedia, the free encyclopedia.html>
4. J.Yang, J.Ding, N.Li and Y.X.Guo, "FPGA -based design and implementation of reduced AES algorithm" IEEE Inter.Conf. Chal Envir Sci Com Engin(CESCE), Vol.02, Issue.5-6, pp.67-70, Jun 2010.
5. A.M.Deshpande, M.S.Deshpande and D.N.Kayatanavar, "FPGA Implementation of AES Encryption and Decryption" IEEE Inter.Conf. Cont, Auto, Com, and Ener., vol.01, issue04, pp.1-6, Jun.2009.
6. Hiremath.S. and Suma.M.S., "Advanced Encryption Standard Implemented on FPGA" IEEE Inter. Conf. Comp Elec Engin. (IECEE), vol.02, issue.28, pp.656-660, Dec. 2009.
7. Abdel-hafeez.S., Sawalmeh.A. and Bataineh.S., "High Performance AES Design using Pipelining Structure over GF(28)" IEEE Inter Conf. Signal Proc and Com, vol.24-27, pp.716-719, Nov. 2007.
8. Rizk.M.R.M. and Morsy, M., "Optimized Area and Optimized Speed Hardware Implementations of AES on FPGA", IEEE Inter Conf. Desig Tes Wor., vol.1, issue.16, pp.207-217, Dec. 2007.
9. Liberatori.M., Otero.F., Bonadero.J.C. and Castineira.J. "AES-128 Cipher. High Speed, Low Cost FPGA Implementation", IEEE Conf. Southern Programmable Logic (SPL), vol.04, issue.07, pp.195-198, Jun. 2007.
10. Abdelhalim.M.B., Aslan.H.K. and Farouk.H. "A design for an FPGA based implementation of Rijndael cipher", ITICT. Ena Techn N Kn Soc.(ETNKS), vol.5, issue.6, pp.897-912, Dec.2005.
11. Pong P. Chu, *RTL Hardware Design Using VHDL*, John Wiley & Sons, Inc., Hoboken, New Jersey, 2006.
12. National Institute of Standards and Technology, "Specification for the ADVANCED ENCRYPTION STANDARD (AES)", Federal Information Processing Standards Publication 197, November 26, 2001 (<http://www.csrc.nist.gov>).
13. Łukasz Krukowski, "Realizacja algorytmów szyfrowania w układach FPGA", dissertation for M.Sc. degree, Wrocław University of Technology, Faculty of Electronics, 2007 (in Polish).
14. A. Menezes, P. van Oorschot, and S. Vanstone, *Handbook of Applied Cryptography*, CRC Press, New York, 1997, p. 81-83.
15. Joseph Zambreno, Student member, IEEE, Dan Honbo, student Member, IEEE, Alok Choudhary, Fellow, IEEE, Rahul Simha, Member, IEEE, and Bhagirath Narahari, "High performance Software Protection Using Reconfigurable Architectures", Proceedings of the IEEE, volume 94, No. 2, February 2006.
16. Thomas Wollinger, Jorge Guajardo and Christ of Paar, "Cryptography on FPGAs: State of the Art Implementations and Attacks", Special Issue on Embedded Systems and Security of the ACM Transactions in Embedded Computing Systems (TECS).

NUMERICAL INVESTIGATION FOR EXHAUST GAS EMISSIONS FOR A DUAL FUEL ENGINE CONFIGURATION USING HYDROGEN AND COMPRESSED NATURAL GAS (CNG)

PREMAKUMARA. G¹, AKHIL THOMAS², JAYAKRISHNAN .K³, ANIRUDH VUYVALA⁴, L.M. DAS⁵

¹(CENTRE FOR ENERGY STUDIES, INDIAN INSTITUTE OF TECHNOLOGY, DELHI, INDIA)

²(DEPARTMENT OF MECHANICAL ENGINEERING, INDIAN INSTITUTE OF TECHNOLOGY, BHUBANESWAR, INDIA)

ABSTRACT

A simulation for numerical analysis of internal combustion engines, both spark-ignited and compression-ignited systems, running on dual fuel of Hydrogen and any hydrocarbon developed is presented in this report. The program coded using Matlab is used to simulate various engine conditions and discern its effect on the emissions. The engine emissions, including species like NO_x, CO, and CO₂, in accordance with the extent of hydrogen fraction, the equivalence fuel-air ratio, combustion equilibrium temperature and pressure are simulated. The paper focuses on simulation of exhaust emissions while using H-CNG blend. Simulation attempts to find an optimum extent of dual-fuelling, equivalence ratio, combustion temperature with regard to quality of emissions.

Key words:Hydrogen,Matlab,CNG,emissions etc

1. Introduction

Our history tells us one thing that all along the past men was consistently tending to go wrong, as if he always beholds to the Murphy's Law which says, 'if anything can go wrong, then it will'. Such an error made by man was his incorrect assessment on availability of petroleum fuels. Till the early 1970s, petroleum was considered as the eternal fuel source when it was realized that the petroleum-based fuels were dwindling fast and at the same time, the rate of consumption of these fuels was increasing at a much faster rate and this presents the trillion dollar quest today, for the best alternative fuel [1]. Looking at this problem, we have a broader aim than just an alternative to the present fuels, but a better one in terms of its emissions. Considering the effect of global warming which has already made big impact giving us serious warning of its effects has led to the need for an alternative fuels which produce minimum emissions. But there also lies another big problem in terms of economic viability. So, taking all these factors, we look for an environment friendly, economically viable alternative fuel for the existing internal combustion engines. Over the years, liquefied petroleum gas (LPG), alcohols (both ethanol and methanol), compressed natural gas (CNG), Bio-fuels (including biodiesel), hydrogen and so many other fuels has been investigated as alternative fuels for both the spark ignition (SI) and compression ignition (CI) engines [1]. Performance studies were done in engines running on these fuels and many methods have been implemented to improve the emissions as well as engine performance. CNG is one fuel which had been able to replace gasoline in spark ignited engines. In order to reduce the emissions from these engines, lean burn strategy is being implemented. But this has a setback on the engine power output. It is clear that the lower flame speed of CNG significantly reduce the power output available. It has additional drawbacks as they are difficult to ignite, which results in misfire and increases un-burned hydrocarbon emissions, and wastes fuel. Adding hydrogen as a blend with CNG helps in reducing these defects. Hydrogen's high flame speed (high burning speed), low ignition energy makes the hydrogen-CNG mixture easier to ignite, thus avoiding misfire and improving the emissions [7]. It also improves the mixture's energy density at lean zone which improves the power output.

Far sighting the potential of H-CNG dual fuelling, studies have been done on various fields in view of developing this concept. It is, however a necessity that we have to optimize all the factors that affects the performance of the engine. Conducting experiments is the obvious way of doing this, but it always has its own limitations as many of the possible combination of factors may not be brought up practically. So, an intelligent way of doing this is by theoretical analysis. There was a time when analytical methods were time consuming and extremely challenging. But today, the scenario is different. With the development of technology, there are enormous and effective ways of theoretically analyzing situations. This paper attempt to numerically analyze the exhaust gas emissions from an engine run on dual fuel involving Hydrogen-CNG blends. The paper involves an indigenously developed simulation program with graphical user interface which is capable of calculating the mole fraction of different components in exhaust emission.

2. THE PROGRAM

The developed program is capable of simulating the effects of various factors, such as extent of dual-fuelling, the equivalence fuel-air ratio, combustion equilibrium temperature and pressure, on the emission properties as well as calculating the emission properties for a specific set of input values. The species which could be analyzed in the exhaust are CO, NO, CO₂, H₂O, O₂, H₂, O, H, OH and N₂.

For simulating the effects of input parameters on exhaust emissions, we considered three main input parameters, Temperature, equivalence ratio, and extent of dual fuelling, on the exhaust species CO, NO, and CO₂. Out of the different methods possible of simulating the effect, we found three-dimensional surface plots as the apt one in our analysis. In two-dimensional plots, when simulating the effect of two factors on output, there is a limitation that there can be only one variable factor and the effect of other has to be analyzed for various constant values. Surface plots give a wider scope of simulation, since in addition to what is possible in two-dimensional plots, we can simulate the effect of two factors, both being variables at a time on the exhaust properties. And this approach makes it more comparable with real engine simulations.

Table 1. Notations used

p	Number of carbon atoms in primary fuel
q	Number of hydrogen atoms in primary fuel
r	Number of oxygen atoms in primary fuel
s	Number of nitrogen atoms in primary fuel
t	Temperature (K)
x	Fraction of Hydrogen in blend
Pres	Pressure (atm)
equ	Equivalence ratio
sto	Stoichiometric fuel-air ratio
K	Equilibrium constant
ni	Concentration of 'i'th product

2.1 PROGRAM INTERFACE

A user friendly interface is given to the program as seen in **Fig.1** that enables the user to control the hydrocarbon fuel data (the number of Carbon, Hydrogen, Nitrogen, and Oxygen atoms), fraction of Hydrogen in the fuel blend, combustion conditions including equilibrium combustion temperature and pressure, and the equivalence fuel-air ratio. According to the user's choice, the output will be the mole fractions of the compounds CO₂, H₂O, N₂, O₂, CO, H₂, H, O, OH, and NO corresponding to the input set of values or the simulated change in mole fraction of the species with the change in input parameters.

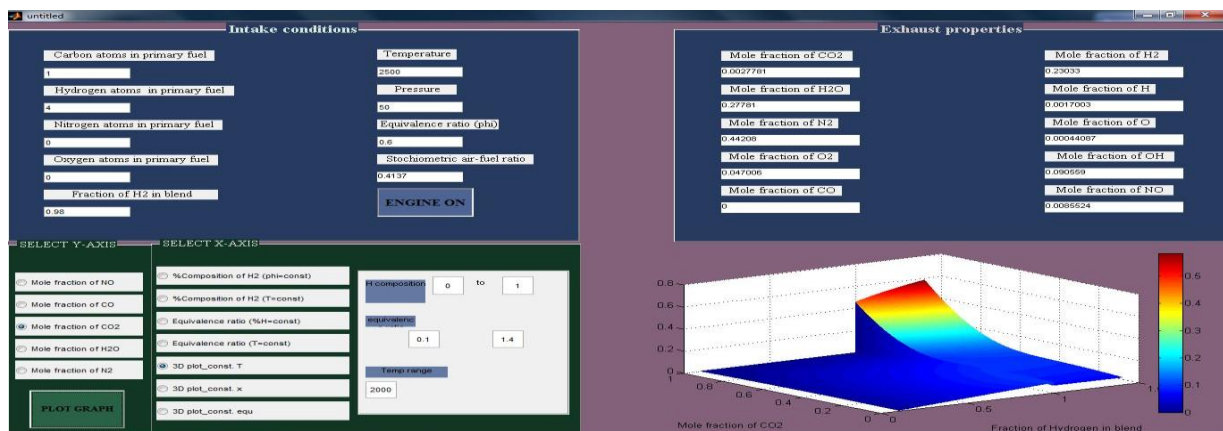


Fig.1: Interface of the program

3. SIMULATIONS

Mole fractions of NO, CO, H₂O, N₂ and CO₂ can be simulated against varying

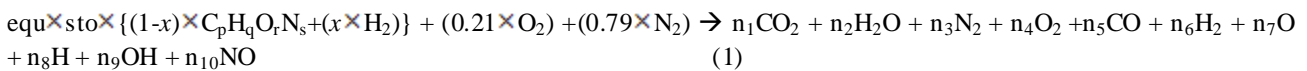
- Extent of blending (fraction of hydrogen in blend) for five different values of combustion temperature with equivalence fuel-air ratio kept as a constant in a 2- dimensional plot.
- Extent of blending for five different values of equivalence fuel-air ratio with combustion temperature kept as a constant.
- Equivalence fuel-air ratio for five different values of combustion temperature with extent of blending kept as a constant.
- Equivalence fuel-air ratio for five different values of extent of blending with combustion temperature kept as a constant.

- Equivalence fuel-air ratio and extent of blending for a constant value of temperature in a three dimensional surface plot.
- Equivalence fuel-air ratio and Temperature for a constant value of composition of hydrogen in a three dimensional surface plot.
- Temperature and composition of hydrogen for a constant value of equivalence fuel-air ratio in a three dimensional surface plot.

4. Formation Of Equations

The program uses a modified version of equilibrium constant method applied by Olikara and Borman to find the solution for the properties of equilibrium gas phase products of combustion of Hydrocarbon fuels. [3] The coding is done for any general dual fuel blend involving hydrogen. The reactant mixture is a blend of a primary fuel of formula $C_pH_qO_rN_s$ and H_2 and air. Lagrange multiplier approach [3] is done with the help of NASA simulation program [5] to restrict the number of species to be considered in the equilibrium constant method. The data showed that if fuel-air ratio is less than 3, the only species of importance because of dissociation are O, H, OH, and NO. In accordance with the results, we considered only 10 products of combustion.

The combustion reaction is hence written as:



Here, stoichiometric fuel-air ratio:

$$\text{sto} = 0.21 \times \left(\frac{1-x}{p+0.25q-0.5r} + 2x \right) \quad (2)$$

Balancing of atoms leads to:

$$C: \text{equ} \times \text{sto} \times (1-x) \times p = n_1 + n_5 \quad (3)$$

$$H: \text{equ} \times \text{sto} \times (1-x) \times q + 2x = 2n_2 + 2n_6 + n_8 + n_9 \quad (4)$$

$$O: \text{equ} \times \text{sto} \times (1-x) \times r + 0.42 = 2n_1 + n_2 + 2n_4 + n_5 + n_7 + n_9 + n_{10} \quad (5)$$

$$N: \text{equ} \times \text{sto} \times (1-x) \times s + 1.58 = 2n_3 + n_{10} \quad (6)$$

Applying the following approximations, we developed the equations:

$$\text{For } \text{equ} < 1: n_5 = 0 \quad (7)$$

$$\text{For } \text{equ} > 1: n_4 = 0 \quad (8)$$

The equations of products for equivalence fuel-air ratio < 1 are:

$$n_1 = (1-x) \times p \times \text{equ} \times \text{sto} \quad (9)$$

$$n_2 = 1 \times q \times \text{equ} \times \text{sto} / 2 \quad (10)$$

$$n_3 = 1 \times 0.79 + (1-x) \times s \times \text{equ} \times \text{sto} / 2 \quad (11)$$

$$n_4 = (1) \times 0.21 \times (1-\text{equ}) \quad (12)$$

$$n_5 = 0 \quad (13)$$

$$n_6 = 0.42x \quad (14)$$

And for equivalence fuel-air ratio > 1 ;

In this case, considering the equilibrium constant for the water gas reaction [3] and taking values from JANAF tables [7] we get the following equations:

$$K = e^{0.273 - (1.761 \div \frac{t}{1000}) - (1.611 \div (\frac{t}{1000})^2) + (0.283 \div (\frac{t}{1000})^3)} \quad (15)$$

$$a = 1 \times (1-K) \quad (16)$$

$$b = (1-x) \times (0.42 - \text{equ} \times \text{sto} \times (2-r) + k \times (0.42 \times (\text{equ}-1)) + p \times \text{equ} \times \text{sto}) + x \times (0.42 - 2 \times \text{equ} \times \text{sto} + K \times 0.42 \times (\text{equ}-1)) \quad (17)$$

$$c = -(1-x) \times (0.42 \times \text{equ} \times \text{sto} \times p \times (\text{equ}-1) \times k) \quad (18)$$

$$n_5 = \frac{-b \pm \sqrt{b^2 - 4ac}}{2a} \quad (19)$$

$$n_1 = (1-x) \times (p \times \text{equ} \times \text{sto} - n_5) + x \times n_5 \quad (20)$$

$$n_2 = (1-x) \times (0.42 + \text{equ} \times \text{sto} \times (2p-r) + n_5) - x \times (0.42 + n_5) \quad (21)$$

$$n_3 = (1-x) \times (0.79 + s \times \text{equ} \times \text{sto} / 2) + 0.79x \quad (22)$$

$$n_4 = 0 \quad (23)$$

$$n_6 = (1-x) \times (0.42 \times (\text{equ}-1) - n_5) + 0.42x \quad (24)$$

Mole fractions of these products are found out using the equation:

$$y_i = n_i / \sum n_i \quad (25)$$

The six gas-phase reactions are introduced which include the dissociation of hydrogen, oxygen, water, carbon dioxide, and equilibrium OH and NO formation [3]. The equilibrium constants of these reactions [3] had been curve fitted to JANAF table by Olikara and Borman for $600 < t < 4000$ K. Their expressions are of the form:

$$\log_{10} K_i = A_i \times \ln \frac{t}{1000} + \frac{B_i}{t} + C_i + D_i \times t + E_i \times t^2 \quad (26)$$

The values of A, B, C, D, E are obtained from JANAF table [7].

The mole fraction of rest species are found out using these equilibrium constant values in accordance with the following equations:

$$y_7 = \frac{K_1}{p_{res}^{0.5}} \times y_6^{0.5} \quad (27)$$

$$y_8 = \frac{K_2}{p_{res}^{0.5}} \times y_4^{0.5} \quad (28)$$

$$y_9 = K_3 \times y_6^{0.5} \times y_4^{0.5} \quad (29)$$

$$y_{10} = K_4 \times y_4^{0.5} \times y_3^{0.5} \quad (30)$$

5. RESULTS

Simulations are done for CNG – H₂ fuel blend emissions under various conditions as discussed before. The results are presented below:

5.1 CO EMISSIONS

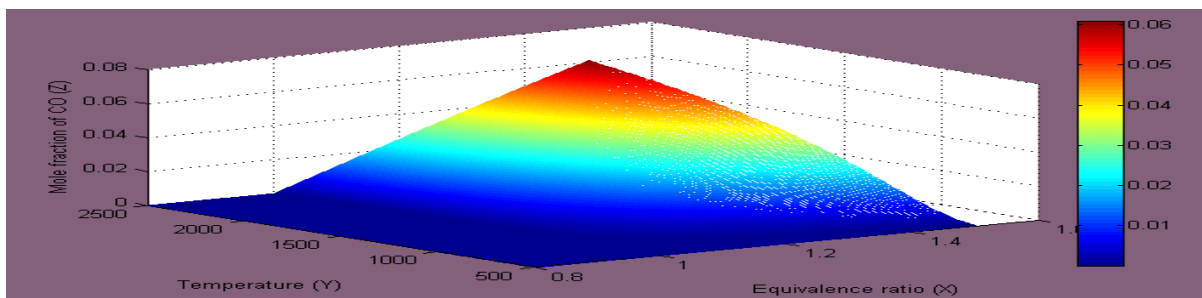


Fig.2: Effect of Temperature and equivalence ratio on mole fraction of CO for $\phi=0.3$

Fig.2 shows that for lean mixtures ($\phi < 1$), the CO emissions are negligible which is due to complete combustion of fuel. On the other hand for rich mixtures ($\phi > 1$), it can be observed that mole fraction of CO increases with increasing equivalence ratio. This can be attributed to the occurrence of incomplete combustion.

It can also be observed that CO emissions increase with increase in temperature. This result is due to the increase in dissociation of CO₂ at higher temperatures which boosts the formation of CO. It can be noted that the emissions of CO are more prevalent for $T=2500K$ and $\phi=1.4$ in the plot.

5.2 CO₂ EMISSIONS

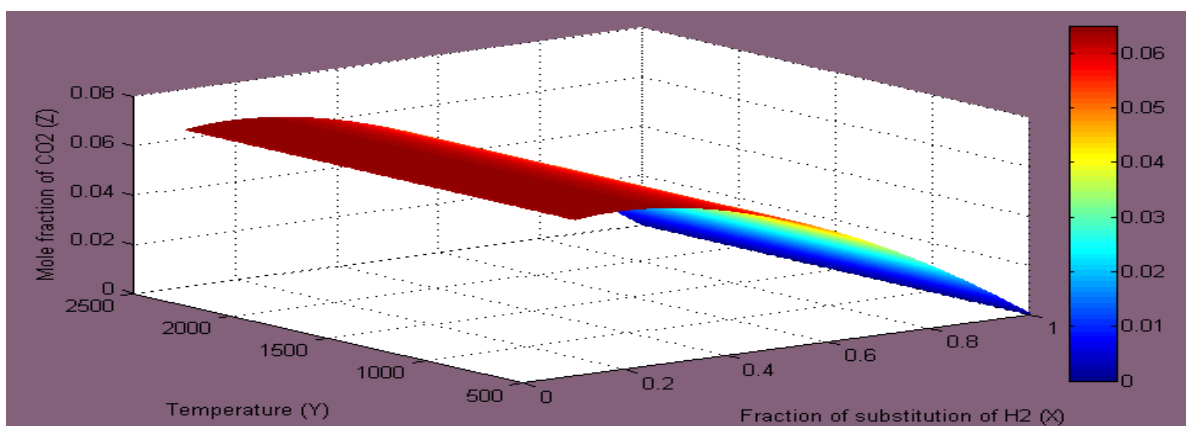


Fig.3: Variation of Mole fraction of CO₂ with change in Temperature and Hydrogen fraction at $\phi=0.3$

In Fig.3, with increase in hydrogen fraction, CO₂ emissions decrease as the carbon content in the fuel (CNG fraction) is decreasing, for a lean mixture ($\phi=0.3$). This trend was found to be the same for all other values of ϕ less than one. For the hydrogen fraction of 0.2, the value of CO₂ mole fraction is 0.06, and for 0.9 the value of mole fraction is 0.01, which gives an average decrease of 83%.

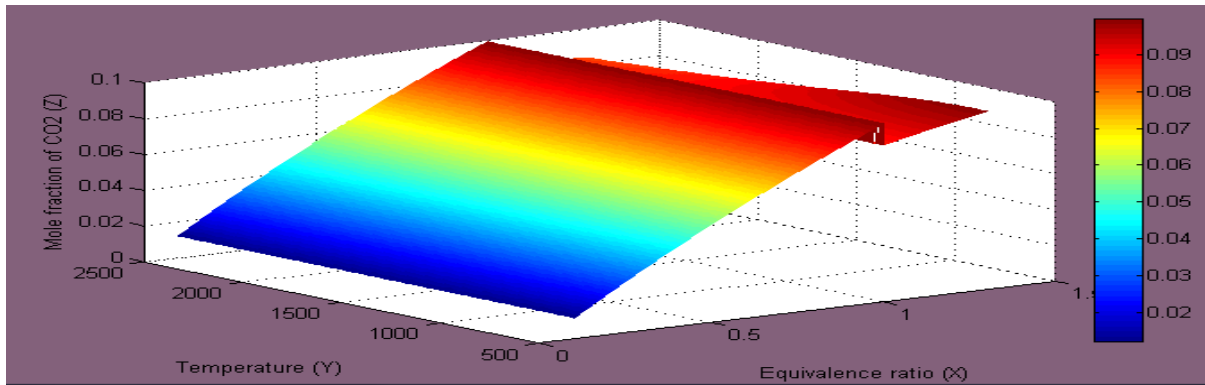


Fig.4: Effect of equivalence ratio and temperature on the mole fraction of CO_2 at $x=0.3$

In Fig.4, it can be observed that for lean mixtures, the mole fraction of CO_2 is almost independent on temperature. However, for rich mixtures it is seen that the mole fraction decreases with increase in temperature. From the plot, the mole fraction for $T=2500\text{K}$ is much less than $T=500\text{K}$. This can be explained as temperature increases, dissociation of CO_2 increases which, on the other hand leads to the increase in mole fraction of CO , a product due to incomplete combustion of rich mixtures. It is also noticeable that mole fraction of CO_2 shows an increasing trend with increase in equivalence ratio, which can be accredited to the increase in carbon content (due to increased fuel content).

NO_x EMISSIONS

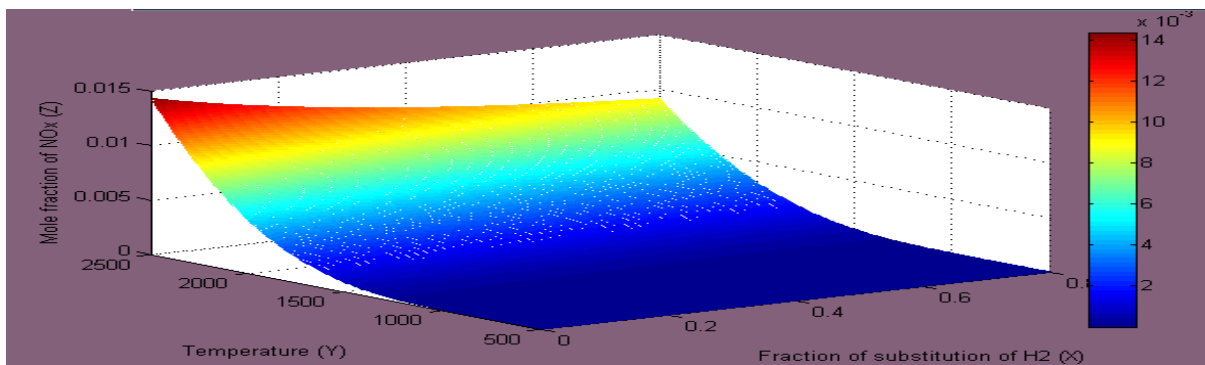


Fig.5: Effect of Temperature and Hydrogen fraction on mole fraction of NO_x at $\text{equ}=0.6$

The Fig.7 shows that for all hydrogen fractions, mole fraction of NO increases with increase in temperature. This is due to the very high dissociation energy of N_2 atoms which demands higher temperatures for its dissociation, which is in turn essential for NO formation. It can also be observed that for a fixed temperature, NO emissions show a slightly decreasing trend with increase in hydrogen fraction.

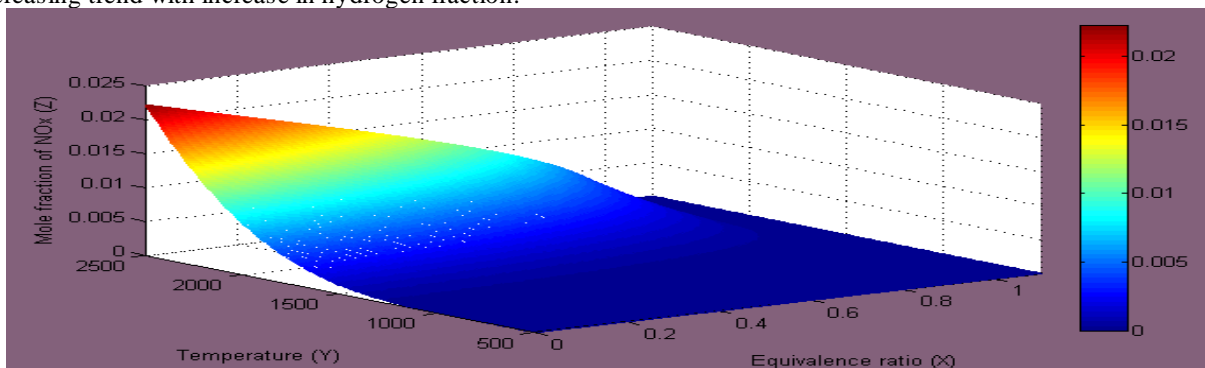


Fig.6: Effect of Temperature and equivalence ratio on mole fraction of NO_x

From the Fig.8, it is clear that effect of temperature on NO emission is consistent with the earlier result. It can also be observed that as equivalence ratio increases for a given temperature, NO_x emissions decrease. This can be explained by the decrease in availability of Oxygen with increase in equivalence ratio.

6. CONCLUSIONS

The results from the simulation were successfully verified with experimental values, which give credibility to the algorithm used. But there are many limitations to the program as it cannot be used for simulating very high temperatures ($T > 3000\text{K}$) due to the assumptions involved in derivation of the formula.

The effects of equivalence ratio, Temperature and Hydrogen fraction on emission of different species in an H-CNG blend can be concluded as follows:

- The emission of CO is negligible for lean mixtures and increases with equivalence ratio for rich mixtures. Also for rich mixtures, the CO emissions increase with increase in combustion equilibrium temperature.
- For lean mixtures, CO₂ emissions decrease with increase in hydrogen fraction and increase with increase in equivalence ratio. It is also independent on temperature for lean mixtures, but decrease with increase in temperature for rich mixtures.
- The emission of NO is negligible for rich mixtures and decreases with equivalence ratio for lean mixtures. NO emissions also decrease slightly with increase in hydrogen fraction. Also, the emissions increase with increase in temperature.

REFERENCES

- [1] L.M.Das. 'Hydrogen engine: research and development (R&D) programmes in Indian Institute of Technology (IIT), Delhi'. International Journal of Hydrogen Energy 27 (2002) 953 – 965
- [2] Ferguson CR. Internal combustion engines – applied thermo sciences. John Wiley and Sons; 1986.
- [3] Mathur HB, Khajuria PR. 'Performance and emission Characteristics of a hydrogen-fuelled spark ignition engine.' Int J Hydrogen Energy, 1984:729–36.
- [4] Svehla, R.A and Mcbridge, B.J. "Fortran IV computer program for calculation of thermodynamic and transport properties of complex chemical system", NASA technical notes TND-7056, 1973
- [5] Deshpande NV et.al, Exhaust gas simulation. IE (I) Journal–MC; 2004.
- [6] Yun Xiao. 'Thermodynamic simulation for Engine combustion simulations' UM-MEAM-90-07
- [7] S.O Bade Shrestha, G.A.Karim, Hydrogen as an additive to methane for spark ignition engine applications, International Journal of Hydrogen Energy 24(1999)577-586

An Affine Combination of TVLMS Adaptive Filters for Echo Cancellation

¹B. Srinivas, M.Tech, ²Dr. K. Manjunathachari,

¹Miste (Life Member)

²M.Tech, Ph.D

¹Assistant Professor, ECE Department, Sagar Institute of Technology

² Professor & HOD, ECE Department, GITAM University, Hyderabad

Abstract

This paper deals with the statistical behaviour of an affine combination of the outputs of two TVLMS adaptive filters that simultaneously adapting the same white Gaussian inputs and it's cancelling the echoes by system identification. The purpose of the combination is to obtain TVLMS adaptive filters with faster convergence and small steady-state mean-square deviation (MSD). The linear combination is used in this paper, is a generalization of the convex combination, in which the combination factor $\lambda(n)$ is restricted to interval (0, 1). The viewpoint is taken that each of the two Filters produces dependent estimates of the unknown channel. Thus, there exists a sequence of optimal affine combining coefficients which minimizes the MSE and it find's the unknown system response. These results will be verified on the MAT LAB 7.8.0 version software by using signal processing tool box. The applications of this paper are System Identification with low MSE and Echo Cancellation. Now a day in real time applications can be implemented using an affine combination of TVLMS adaptive filters because, it is easy way to design, implementation, robustness, with low MSE, and high level noise cancellation and it requires less number of computational operations.

Keywords—Adaptive filters, affine combination, analysis, time varying least mean square (TVLMS), stochastic algorithms.

1.INTRODUCTION

The design of many adaptive filters requires a trade-off between convergence speed and steady-state mean-square error (MSE). A faster (slower) convergence speed yields a larger (smaller) steady-state mean-square deviation (MSD) and MSE. This property is usually independent of the type of adaptive algorithm, i.e., least mean-square (LMS), normalized least mean-square (NLMS), recursive least squares (RLS), or affine projection (AP). This design trade-off is usually controlled by some design parameter of the weight update, such as the step size in LMS or AP, the step size or the regularization parameter in NLMS or the forgetting factor in RLS. Variable step-size modifications of the basic adaptive algorithms offer a possible solution to this design problem. Fig. 1 shows where $W_1(n)$ adaptive filter uses a larger step size than adaptive filter $W_2(n)$.

The key to this scheme is the selection of the scalar mixing parameter $\lambda(n)$ combining the two filter outputs. The mixing parameters adaptively optimized using a stochastic

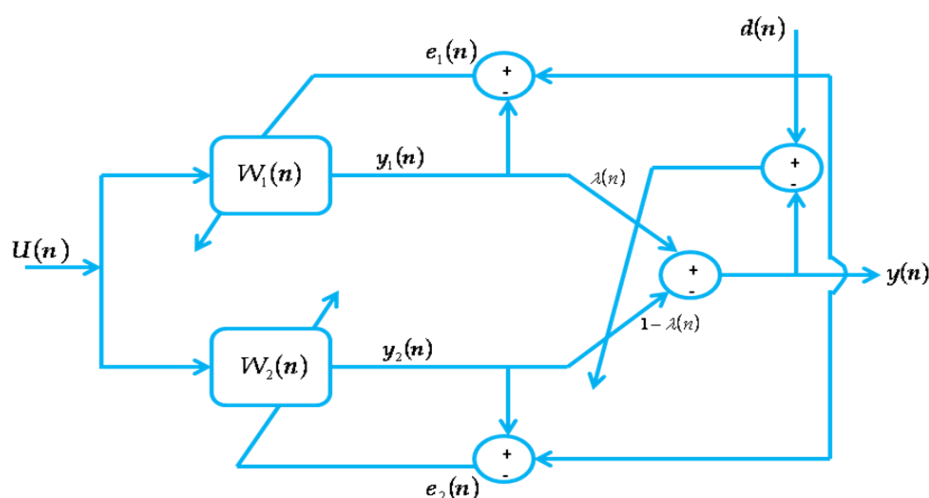


Fig.1 Adaptive combining of two transversal adaptive fitters

gradient search which minimizes the quadratic error of the overall filter. The convex combination performed as well as the best of its components in the MSE sense. These results indicate that a combination of adaptive filters can lead to fast convergence rates and good steady-state performance, an attribute that is usually obtained only in variable step-size algorithms. Thus, there is great interest in learning more about the properties of such adaptive structures. This paper provides new results for the performance of the combined structure. The achievable performance is studied for an affine combination of two TVLMS adaptive filters using the structure shown in Fig. 1 with stationary signals. Here, the combination parameter $\lambda(n)$ is not restricted to the range (0, 1). Thus, Fig. 1 is interpreted from the viewpoint of a linear combiner. Each adaptive filter is estimating the unknown channel impulse response using the same input data. Thus, $W_1(n)$ and $W_2(n)$ are statistically dependent estimates of the unknown channel. There exists a single combining parameter sequence $\lambda(n)$ which minimizes the MSD. The parameter $\lambda(n)$ does not necessarily lie within (0, 1) for all. Thus, the output in Fig. 1 is an affine combination of the individual outputs $y_1(n)$ and $y_2(n)$ the convex combination is a particular case [1] - [2].

2. THE OPTIMAL AFFINE COMBINER

A. THE AFFINE COMBINER

The system under investigation is show in Fig. 1. Each filter uses the LMS adaption rule but with different step size $\mu_i, i = 1,2$;

$$W_i(n+1) = W_i(n) + \mu_i e_i(n) U_i(n), i = 1,2 \quad (2.1)$$

$$\text{Where } e_i(n) = d(n) - W_i^T(n)U(n), i = 1,2 \quad (2.2)$$

$$d(n) = e_o(n) + W_o^T(n)U(n), i = 1,2 \quad (2.3)$$

Where $W_i(n), i = 1,2$ are the N-dimensional adaptive coefficient vectors, $e_o(n)$ is assumed zero-mean, and statistically independent of any other signal in the system, and the input process $u(n)$ is assumed wide-sense stationary, $U(n) = [u(n), \dots, u(n-N+1)]^T$ is the input vector. It will be assumed, without loss, that $\mu_1 \geq \mu_2$, so that $W_1(n)$ will, in general, converge faster than $W_2(n)$. Also $W_2(n)$ will converge to the lowest individual steady-state weight maladjustments. The weight vectors $W_1(n)$ and $W_2(n)$ are coupled both deterministically and statistically through $U(n)$ and $e_o(n)$ [2] - [4].

The outputs of the two filters are combined as in Fig. 1:

$$y(n) = \lambda(n)y_1(n) + [1 - \lambda(n)]y_2(n) \quad (2.4)$$

Where $y_i(n) = W_i^T(n)U(n), i = 1,2$ can be any real number and the overall system error is given by

$$e(n) = d(n) - y(n) \quad (2.5)$$

The adaptive filter output combination is an affine combination, as $y(n)$ can assume any value on the real line. This setup generalizes the combination of adaptive filter outputs, and can be used to study the properties of the optimal combination.

B. The Optimal mixing parameter

Equation (2.4) can be written as

$$\begin{aligned} y(n) &= \lambda(n)W_1^T(n)U(n) + [1 - \lambda(n)]W_2^T(n)U(n) = \{\lambda(n)[W_1(n) - W_2(n)] + W_2(n)\}^T U(n) \\ &= \{\lambda(n)W_{12}(n) + W_2(n)\}^T U(n) \end{aligned} \quad (2.6)$$

$$\text{Where } W_{12}(n) = W_1(n) - W_2(n)$$

Equation (2.6) shows that $y(n)$ can be interpreted as a combination of $W_2(n)$ and weighted version of the difference filter $W_{12}(n)$. It also shows that the combined adaptive filter has an equivalent weight vector given by

$$W_{eq}(n) = \lambda(n)W_{12}(n) + W_2(n) \quad (2.7)$$

Subtracting Equation (2.1) for $i=2$ from Equation (2.1) for $i=1$ yields a recursion for $W_{12}(n)$:

$$W_{12}(n+1) = [I - \mu_1 U(n)U^T(n)]W_{12}(n) + (\mu_1 - \mu_2)e_2(n)U(n) \quad (2.8)$$

Next, let us consider a rule for choosing $\lambda(n)$ that minimizes the conditional MSE at time n $E[e^2(n) | W_1(n), W_{12}(n)]$.

Writing $e(n)$ in equation (2.5) as

$$e(n) = e_o(n) + [W_{o2}(n) - \lambda(n)W_{12}(n)]^T U(n) \quad (2.9)$$

Where $W_{o2}(n) = W_o(n) - W_2(n)$ yields

$$\frac{\partial E[e^2(n) | W_1(n), W_{12}(n)]}{\partial \lambda(n)} = -2E[e(n)W_{12}^T(n)U(n) | W_2(n), W_{12}(n)] = 0 \tag{2.10}$$

Using equation (2.9), taking the expectation over $U(n)$ and defining the input conditional autocorrelation matrix

$$R_u = E[U(n)U^T(n) | W_{12}(n), W_{12}(n)] \tag{2.11}$$

Solving Equation (2.11) for $\lambda(n) = \lambda_o(n)$

$$\lambda_o(n) = \frac{W_{o2}^T(n)R_u W_{12}(n)}{W_{12}^T(n)R_u W_{12}(n)} \tag{2.12}$$

3.SYSTEM IDENTIFICATION

In the class of applications dealing with identification, an adaptive filter is used to provide a linear model that represents the best fit to an unknown plant. Here, same input is given to both the adaptive filter and the plant. The output of the plant will serve as the desired signal for the adaptation process. In this application the unknown system is modelled by an FIR filter with adjustable coefficients. Both the unknown time –variant system and FIR filter model are excited by an input sequence $u(n)$. The adaptive FIR filter output $y(n)$ is Compared with the unknown system output $d(n)$ to produce an estimation error $e(n)$. The estimation error represents the difference between the unknown system output and the model (estimated) output. The estimation error $e(n)$ is then used as the input to an adaptive control algorithm which corrects the individual tap weights of the filter. This process is repeated through several iterations until the estimation error $e(n)$ becomes sufficiently small in some statistical sense. The resultant FIR filter response now represents that of the previously unknown system. It can show in Fig. 2 and Fig 3.

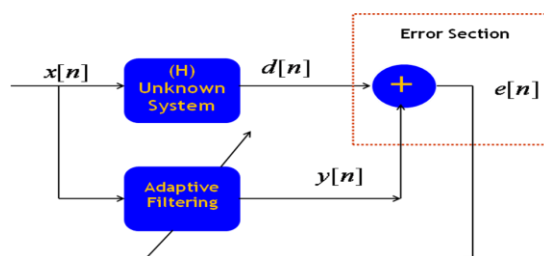


Fig.2 Block diagram of the System Identification

In Fig 3, instead of Adaptive algorithm, we can take the affine combination of two TVLMS algorithm, because it provides new better results for the performance of the combined structure for system identification [5].

The following toolboxes are used during programming of above algorithms

1. Signal processing Toolbox.
2. Filter design toolbox.
3. General purpose commands.

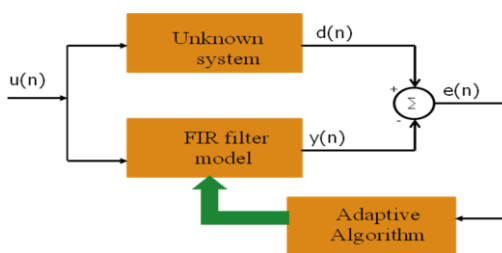


Fig.3 Block diagram of the System Identification model

4. Applications

A. Advantages and Disadvantages of TVLMS algorithm

- (i). The TVLMS algorithm changes (adapts) the filter tap weights so that $e(n)$ is minimized in the mean-square sense. When the processes are $x(n)$ and $d(n)$ are jointly stationary or Non-stationary, this algorithm converges to a set of tap-weights which, on average, are equal to the wiener-Hopf solution [3] – [4].
- (ii). Simplicity in implementation,
- (iii). inherently stable and robustness performance against different signal conditions, and
- (iv). slow convergence (due to eigenvalue spread).

B. Applications

Because of their ability to perform well in unknown environments and track statistical time-variations, adaptive filters have been employed in a wide range of fields. However, there are essentially four basic classes of applications for adaptive filters. These are: Identification, inverse modeling, prediction, and interference cancellation, with the main difference between them being the manner in which the desired response is extracted. The adjustable parameters that are dependent upon the applications at hand are the number of filter taps, choice of FIR or IIR, choice of training algorithm, and the learning rate. Beyond these, the underlying architecture required for realization is independent of the application. Therefore, this thesis will focus on one particular application, namely noise cancellation, as it is the most likely to require an embedded VLSI implementation. This is because it is sometimes necessary to use adaptive noise cancellation in communication systems such as handheld radios and satellite systems that are contained on a 16 single silicon chip, where real-time processing is required. Doing this efficiently is important, because adaptive equalizers are a major component of receivers in modern communications systems and can account for up to 90% of the total gate count [2].

1. System Identification
2. Inverse modelling
3. Prediction
4. Interference Cancellation: Adaptive Noise cancellation, Echo cancellation

5. RESULT ANALYSIS

Fig.4.shows the adaptive noise cancellation by using affine combination of TVLMS adaptive filters.

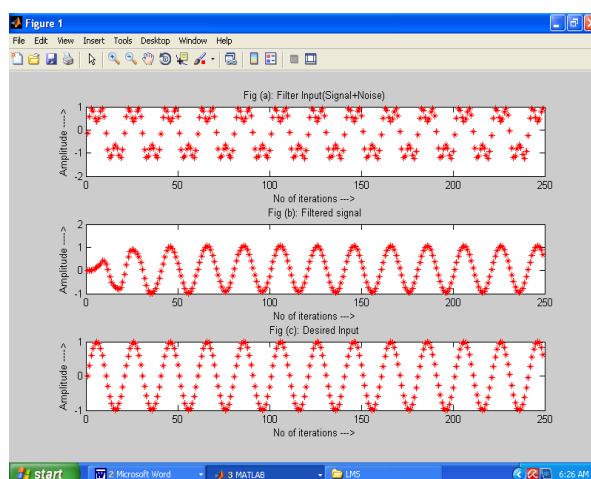


Fig.4: The adaptive noise cancellation

For simulations a sinusoidal signal of frequency 1500HZ is used as desired input. The input to the filter is a noisy signal consisting of multiple sine frequencies and Gaussian random noise. The simulation results are also obtained for the adaptive filter with standard LMS, TV-LMS, RLS, Affine combination of LMS and TVLMS algorithms using the same configuration. The results are generated for different number of iterations ranging from 50 to 1000. Finally, the performance of the TV LMS algorithms is compared with standard LMS, Affine LMS and RLS algorithms are good and easiest one in the implementation part.

No. of iterations	Affine combination of two TVLMS Adaptive filters MSE
50	0.0262
100	0.0147
500	0.0066
850	0.0057
900	0.0057
950	0.0056
1000	0.0055

Table 5.1: Iterations Vs MSE of TVLMS algorithm for de-noising noisy-sine wave

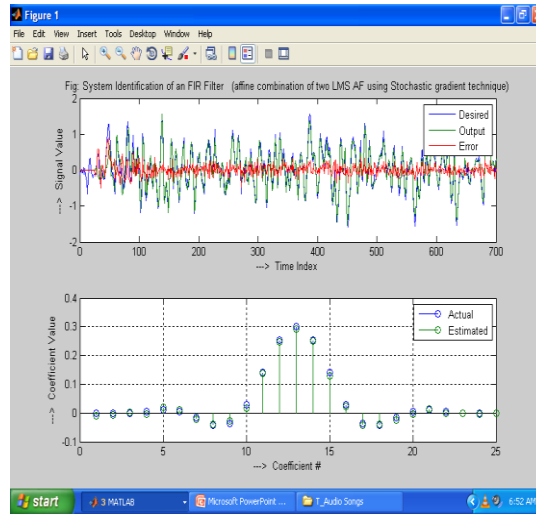


Fig.5: System identification of an FIR filter with 700 iterations (An affine combination of LMS adaptive filters using stochastic gradient technique)

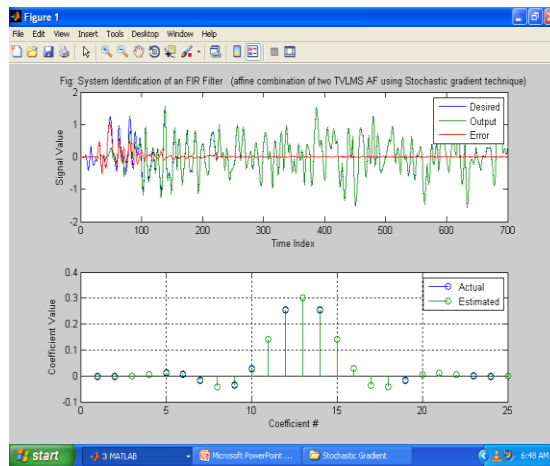


Fig.6: System identification of an FIR filter with 700 iterations (An affine combination of TVLMS adaptive filters using stochastic gradient technique)

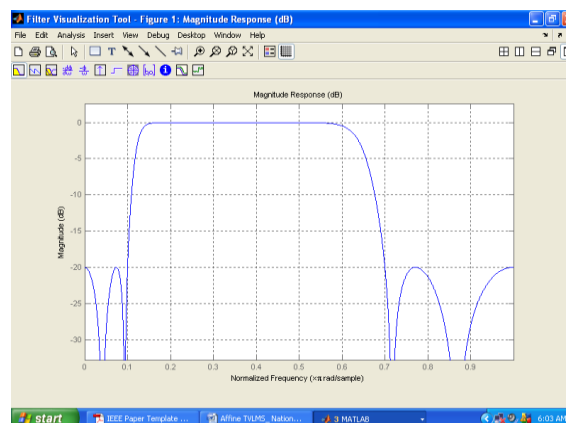


Fig.7: The magnitude response of FIR model

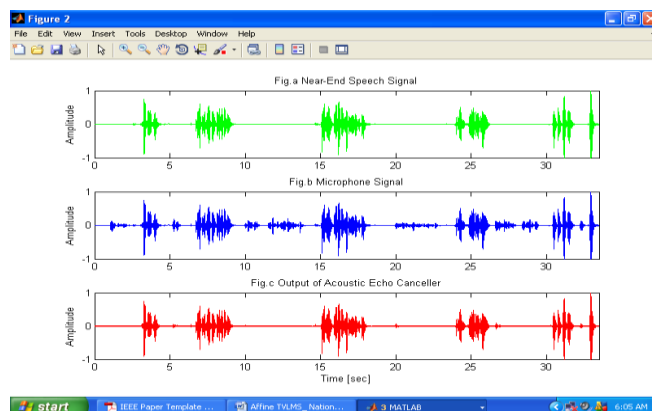


Fig.7: The adaptive Echoes cancellation

6. Conclusions

This paper has studied the statistical behaviour of an affine combination of the outputs of two time varying LMS adaptive filters that simultaneously adapt using the same Gaussian inputs. The purpose of the affine combination is to obtain a TVLMS adaptive filter with faster convergence and small steady state Mean Square Deviation. First, the optimal unrealizable affine combiner was studied and provided the best possible performance. Then, two new schemes were proposed for practical applications. The first scheme performed nearly as well as the optimal unrealizable combiner, providing the same convergence time and steady-state behaviour. A second new scheme was investigated that depended upon the time-averaged instantaneous squared error of each adaptive filter. The viewpoint is taken that each of the two Filters produces dependent estimates of the unknown channel. Thus, there exists a sequence of optimal affine combining coefficients which minimizes the mean-square error (MSE) and it find's the unknown system response. Now a day in real time applications, video conferences can be implemented using an affine combination of LMS adaptive filters because, it is easy way to design, implementation, robustness, with low MSE, and high level noise cancellation and it requires less number of computational operations.

References

- [1] LJUNG,L, and S.GUNNARSSON (1990). "Adaption and Tracking in system identification-A survey." Automatic am, vol. 26. pp. 7-21.
- [2] "Adaptive Filter Theory" – SIMON HAYKIN, Prentice Hall, Third Edition.
- [3] Digital Signal Processing Primer – C.BITTON and RORABAUGH, TMH.
- [4] "Adaptive Noise Cancelling: principles and applications," Proc, IEEE vol. 63, pp. 1692-1716.
- [5] Neil J.Bershad and JC M. Bermudez, "IEEE Trans.. On Signal Processing", vol

AUTHORS



Mr. B.Srinivas, an M.Tech from JNT University, Hyderabad, has an experience of more than 6.5 years of Teaching. At present Mr. B. Srinivas serving the Sagar Institute of Technology (Sagar Group of Institutions), Chevella, Ranga Reddy, and A.P, as an Assistant Professor of the department of Electronics and Communication Engineering. He is the Life member of ISTE.



Dr. K. Manjunathachari, an M.Tech from JNT University, Hyderabad, and Ph.D from JNT University, Hyderabad, A.P, has an experience of more than 16 years of Teaching and 3 years of Industry. At present Dr. K. Manjunathachari serving the GITAM University, Hyderabad and A.P, as a Professor and Head of the department of Electronics and Communication Engineering.

Facts Placement for Maximum Power Transfer Capability And Stability in a Transmission Line

C.Vasavi¹, Dr. T.Gowri Manohar²

¹ Department of EEE, SVU College of Engineering, Tirupati, Andhra Pradesh, India.

² Associate Professor, Department of EEE, SVU College of Engineering, Tirupati, Andhra Pradesh, India

Abstract:

Maximum power transfer capability in the transmission line is the utmost important consideration in power systems. Facts devices are very effective and capable of increasing power transfer capability of a line, as thermal limit permits, while maintaining the same degree of stability. So, as to transfer maximum power to the consumer through a transmission line. Shunt FACTS devices are placed at the midpoint of the transmission line and degree of series compensation is provided to get the maximum possible benefit. It is observed that the optimal location of facts devices deviates from the centre of the line towards the generator side with the increase in the degree of series compensation. This paper presents a two stage approach a conventional method is used to determine the optimal location of shunt facts device in a series compensated line and then Fuzzy logic is used to determine the optimal placement. The proposed method is considered for 13.8KV Base, 6*350 MVA, 360 km long transmission line.

Keywords: Fuzzy logic, Maximum power transfer, optimal placement, shunt FACTS devices, series compensation, stability.

1. Introduction

During the past two decades, the increase in electrical energy demand has presented higher requirements from the power industry, including deregulation in many countries; numerous changes are continuously being introduced to a once predictable business. Although electricity is a highly engineered product, it is necessarily being considered and handles as a commodity, is necessary to study the stability and security of the transmission system. Thus transmission systems are being pushed closer to their stability and thermal limits while the focus on the quality of power delivered is greater than ever.

In the modern days, the financial and market forces are, and will continue to demand a more optimal and profitable operation of a power system with respect to generation, transmission and distribution. Now, more than ever the demands of the power system are lower power losses, faster response to parameter change, higher stability and reliability .to achieve both operational and financial profitability Flexible AC Transmission systems(FACTS)[1]based on the success of research in power electronics switching devices and advanced control technology of choice in voltage control, reactive/active power flow control, transient and steady state stabilization and improves the functionality of existing transmission system[2]

FACTS technologies is allowed for improved transmission system operation with minimum infrastructure investment. Environmental constraints and economical impact are the two important constraints forced the power utilities to meet the future demand by utilizing the existing transmission system without building the new lines. FACTS are effective and capable of increasing power transfer capability of line, as thermal limits permits, while maintaining the same degree of stability.

Benefits of utilizing FACTS devices in electrical transmission systems can be summarized as follows.

1. Better utilization of existing transmission system assets.
2. Increases transmission system reliability and availability.
3. Increases dynamic and transient grid stability.
4. Increases quality of supply for sensitive industries.
5. Environmental Benefits.

FACTS devices can be connected to a transmission line in various ways .the series FACTS devices (SSSC, TCSC) which are connected in series with transmission line is known as series compensation. The shunt FACTS devices such as (SVC, STATCOM)connected in shunt with the transmission line is known as shunt compensation.

Series compensation aims to directly control the overall series line impedance of the transmission line. The AC power transmission is primarily limited by the series reactive impedance of the transmission line. A series connected can add a voltage in opposition to the transmission line voltage drop, therefore reducing the series line impedance. The voltage magnitudes of sending end and receiving end are assumed are equal $V_S=V_R=V$. And the phase angle between them is δ the transmission line model is assumed lossless and represented by the reactance X_L .

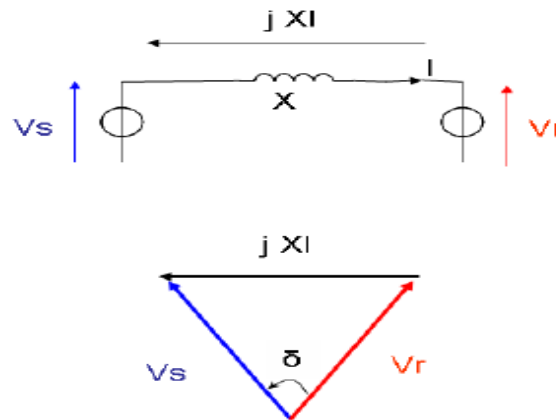


Figure .1 series compensation

shunt compensation ,especially shunt reactive compensation is used in transmission system to improve voltage quality and to enhance the system stability[4]shunt reactors used to reduce the over-all voltages while shunt capacitors are used to maintain voltage levels of the transmission line.

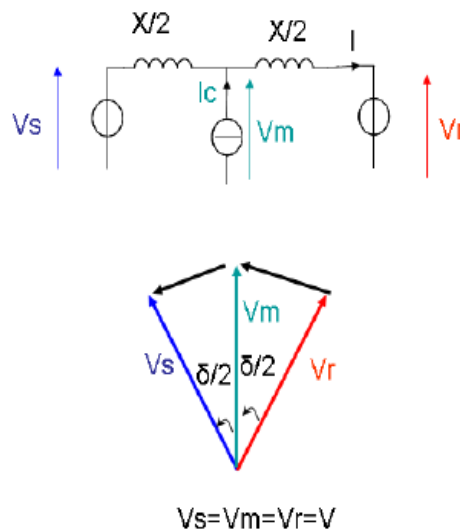


Figure.2 shunt compensation

Optimal location of facts Devices

In power systems, optimal location[5] of these devices is important, properly placed FACTS devices enhances the stability of the system ,where as improperly placed FACTS may become counterproductive. Many researchers found that the optimal location is at $K=0.5$ at the midpoint of the transmission line .in this paper a series compensation is provided to a transmission line. One of the objectives of this paper is to find the maximum power flow corresponding optimal location of shunt FACTS device, when a series compensation level changes (%C). The rating of shunt FACTS device is selected in such a way so as to control the voltage equal to sending end voltage at the bus of shunt FACTS device. It is observed that

the optimal location of shunt FACTS device deviates from the centre of the line towards the generator side with the change in degree of series compensation (%C)

Transmission line model

In this study, it is considered that the transmission line parameters are uniformly distributed and the line can be modeled by 2 port-4 terminal network.

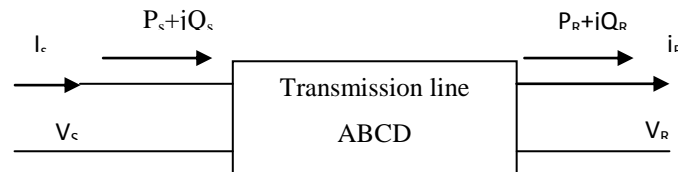


Figure 3: Two – port four terminal model of a transmission line

The relationship between the sending end(SE)and receiving end(RE)quantities of the line can be written as

$$V_S = AV_R + BI_R \quad (1)$$

$$I_S = CV_R + DI_R \quad (2)$$

The ABCD constants of a line length l , having a series impedance of $Z \Omega/\text{km}$ and shunt admittance of $Y \text{ S}/\text{km}$ are given by

$$A = D = \cosh(\gamma l) \quad B = Z_c \sinh(\gamma l) \quad C = \sinh(\gamma l) / Z_c \quad (3)$$

Where $y = \sqrt{Z_c Y}$ and $Z_c = \sqrt{Z / Y}$

The active and reactive power flows at the SE and RE of the line cab be written as [11]

$$P_S = C_1 \cos(\beta - \alpha) - C_2 \cos(\beta + \delta) \quad (4)$$

$$Q_S = C_1 \sin(\beta - \alpha) - C_2 \sin(\beta + \delta) \quad (5)$$

$$P_R = C_2 \cos(\beta - \delta) - C_3 \cos(\beta - \alpha) \quad (6)$$

$$Q_R = C_2 \sin(\beta - \delta) - C_3 \sin(\beta - \alpha) \quad (7)$$

Where

$$C_1 = AV_S^2 / B, C_2 = V_S V_R / B, C_3 = AV_R^2 / B$$

$$A = A \angle \alpha, B = B \angle \beta, V_R \angle \theta = V_S \angle \delta$$

It is clear from eqn 6 that the RE power P_R reaches the maximum value when the angle δ becomes β . However the SE power P_S of eqn 4 becomes maximum at $\delta = (\pi - \beta)$. for the simplified model of the line, the resistance and capacitance are neglected. For such model, the ABCD constants of the line become

$$A = D = 1 \angle 0^\circ \quad B = X \angle 90^\circ \quad C = 0 \quad (8)$$

Here X is the series reactance of the line in Ω/km . In this case, the line is represented by only a lumped series reactance $X = X_L$ and both P_R and P_S become maximum at $\delta = 90^\circ$. such model may provide reasonably a good results for short transmission line .when a shunt fact device is connected in a long transmission line to increase the power transfer capability the following model is designed.

In this paper, it is considered that the line is transferring power from a generation station to a load and is equipped with a series capacitor 'C' at the centre and shunt FACTS device at a point 'm' as shown in figure 4 .parameter 'K' is used to show the fraction of line length. In this study we considered 13.8 KV Base, 6*350 MVA and it is supplying a load of 30,000MVA ,735 KV is considered , the series impedance of the line is found to be $Z = (0.01273 + j0.9337) \Omega/\text{Km}$ at 60 Hz

respectively. Here the transmission line is divided in to two sections (section1 and 2) and section 2 is further divided in to two sections. Each section is represented by a separate 2 port, 4-terminal network.

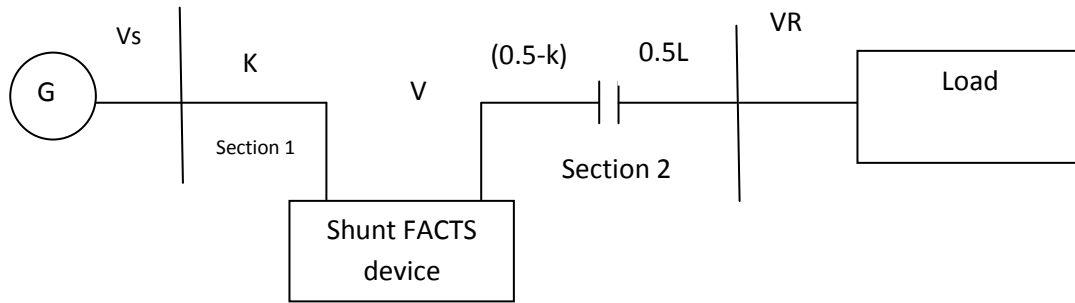


Figure .4: Series compensated transmission line with a shunt FACT device

Maximum power transfer capability

First consider that the line is represented by its simplified model and there is no facts device connected to the line, for such case, the maximum power transfer through the line for given values of SE and RE voltage magnitudes, cab be written as

$$P = P_m \sin \delta \quad (9)$$

Here the maximum power pm is $V_s V_R / x$ and it occurs at an angle $\delta^m = 90^\circ$. when a shunt facts device is connected to the line , both P_m and δ^m are increased and their values depends upon the k factor. For $k=0.5$ and $V_s = V_R = V_M$ both P_M and δ^m become double or increases to $2 V_s V_R / x$ and 180° , respectively [8]. when k exceeds 0.5 both P^M and δ^m decreases after reaching the maximum value. In this paper (%c) degree of series compensation is provided for a long transmission line. As the (%c) increases, the value of k changes the maximum power and corresponding angle are first determined for various values of k.

A sophisticated computer program has been carried out to determine the various characteristics of the system of fig.3 using the simplified and actual models of the line sections. The constraints of the same RE power of section1 and SE power section2 ($P_{R1} = P_{S2}$) is incorporated in to the problem, in all cases , $V_s = V_R = V_M = 1.0$ p. Unless specified the maximum power P^m and corresponding angle δ^M are determined for various values of location K.

The figure (5) to (9) shows the variation in maximum RE power (P_R^m), maximum SE power (P_S^m) and transmission angle (δ^m) with respect to degree of series compensation (%c).

From fig (5) it can be noted that when %C = 0, the value of (P_S^m) increases as the value of k is increased from zero and reaches maximum value at 13.5 p.u. when % C = 15, the value of P_S^m increases, and reaches to 19.5 p.u. when %C=45 the value P_S^m increases and reaches maximum value 35 p.u. at k = 0.3.

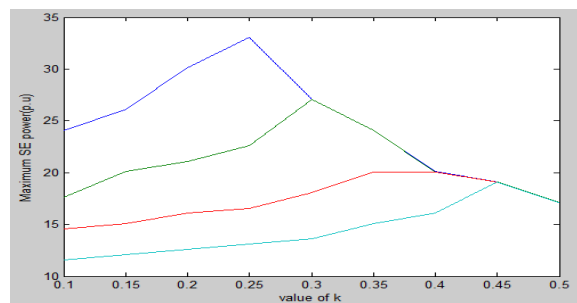


Figure 5: Variation in maximum sending end power for the different values of %c

Similarly for RE power (P_R^m) can be observed in fig (6) when the series compensation in the line is taken into account. We observe that the optimal location of the shunt facts device will change and shift towards the generator side. It can be observed that when %C = 45 we obtain the optimal location of shunt fact device at $k = 0.225$ and P_R^m increases to value of 22.5 pu

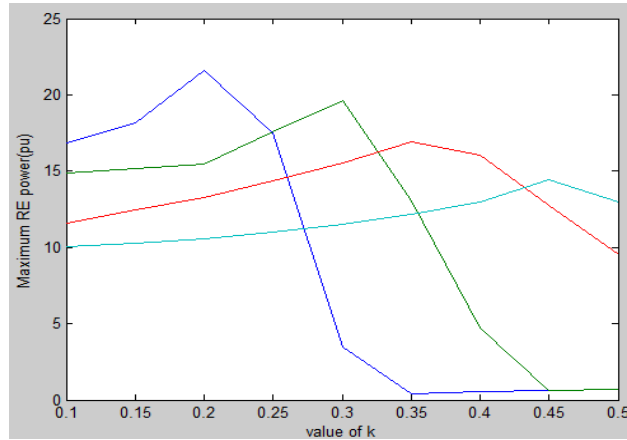


Figure 6: Variation in maximum receiving end power for the different values of %C

In figure (7), It can be observed by using both SVC and STATCOM, the angle at SE power increases when % C = 0 at $k = 0$ the value of δ^m increases from 96.7° to its maximum value 169° when % C=45 the value of δ^m increases 189.5° at $k = 0.225$. As the degree of series compensation increases, the stability, of the system increases and the optimal location of the shunt fact device changes.

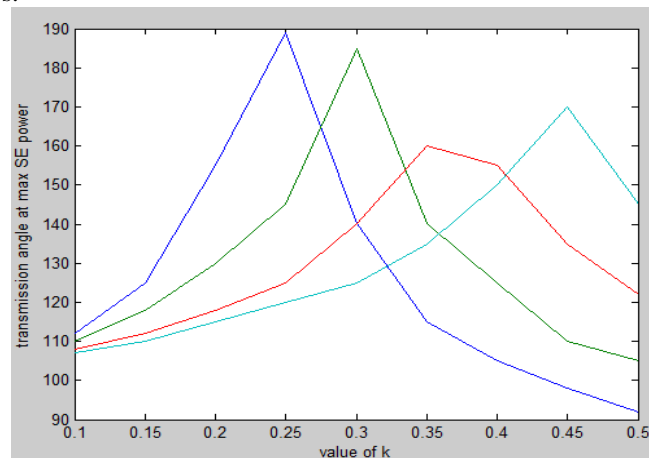


Figure 7: Variation in transmission angle at the maximum SE power for the different values of %c

Optimal location of shunt facts device

Fig (8) shows the variation of maximum RE power of section (1) (P_{R1}^m) and maximum SE power of section (2) (P_{S2}^m) against the value of K for different series compensation levels (%c). When %C =0 the value of $k = 0.45$ for uncompensated line similarly when %C = 45 the value of $k = 0.25$

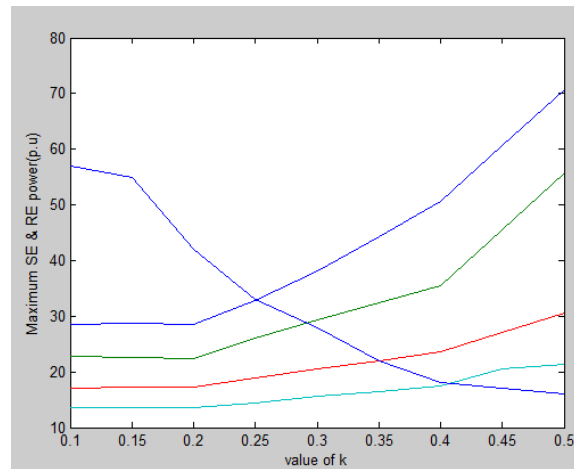


Figure 8: Variation in maximum RE power of section I and SE power of section II against k for different values of %c.

Figure (9) shows the variation in optimal off centre location of the shunt facts device against the degree of compensation level (%C) for the given R/X ratio of the line. It can be observed that the optimal off centre location increases linearly and reaches its highest value 55% for %c=45.

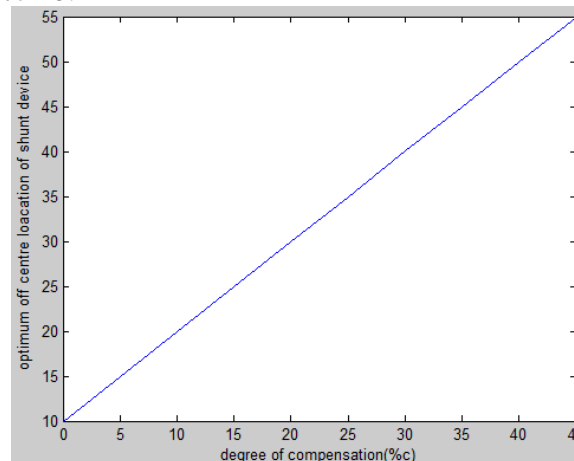


Figure 9: Variation in optimum off centre location of shunt facts device against %c

Optimal location using fuzzy control

The efficiency of methods prior to fuzzy logic, even though good, depends mainly on the goodness of data. Fuzzy logic provides a remedy for any lack of uncertainty in the data. Fuzzy logic has the advantage of including heuristics and representing engineering judgments into the optimal placement of shunt facts device. Further more, the solutions obtained from a fuzzy controller can be quickly assessed to determine their feasibility in being implement in the transmission systems.

Benefits of Fuzzy control

- Implementing expert knowledge for a higher degree of automation
- Robust non-linear control.
- Relates Input to Output in Linguistic terms, which are easily understood by lay persons.
- These are capable of handing complex Non-Linear, Dynamic systems using simple solutions.
- Reduction of development and maintenance time.
- In daily home appliances like washing machines self focusing cameras etc.

Development of Fuzzy logic system

Developing a fuzzy logic system desires the following steps to be carried out.

- Creating linguistic variables of the system. The linguistic variables are the “vocabulary” of the in which the rule work.
- Designating the structure of the system. The structure represents the information flow within the system; that is what input variables are combined with which other variables black and so on.
- Formulation the control strategy a fuzzy logic rules.
- Selecting the appropriate defuzzification method for the application.

The two main objectives are considered mainly

1. To improve power transfer capability
2. To improve stability

Power angle and value of k (value of fraction of line length) are modelled using fuzzy membership functions. A Fuzzy Inference (FIS) containing a set of rules is then used to determine where the maximum power transfer capability is obtained by placing shunt facts device in various series compensation levels. Now, a Fuzzy Inference System (FIS) is developed using MAT LAB 7.12 with two input and one output variables.

The inputs and outputs of FIS are modeled by fuzzy membership functions. Two inputs power angle δ^m and degree of compensation (%) and one output for value of k are designed. The membership functions

for (δ^m) are triangular and are denoted by L, LM, M, HM, H. The values of per unit ranges from [0-180⁰].

The membership functions for (%) are triangular and are denoted by , LM, M, HM, H, The values of per unit ranges from [0-0.45].

The membership functions for value of k are triangular and are denoted by L, LM, H, HM and H. The membership functions of the variables as shown in figures given below.

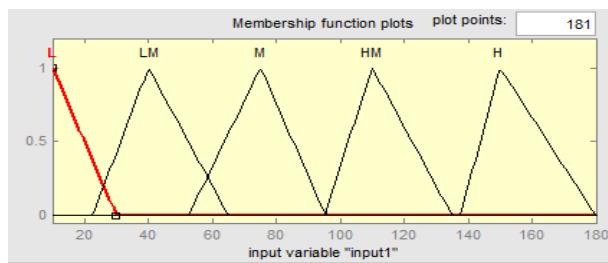


Figure 10: Membership functions for δ^m

The values of membership functions are given below.

L	LM	M	HM	H
10-30	22-65	55-95	95-135	135-180

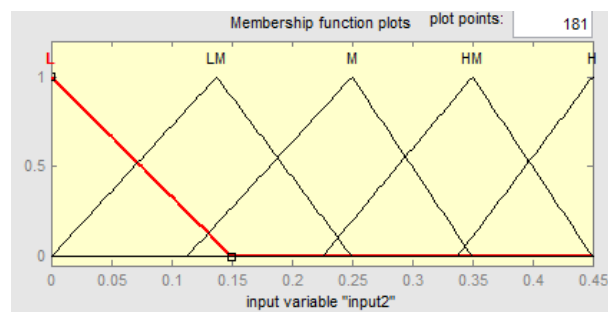


Figure 11: Membership functions for %c.

The values of membership function are given below

L	LM	M	HM	H
0-0.15	0-0.25	0.15-0.35	0.23-0.45	0.33-0.45

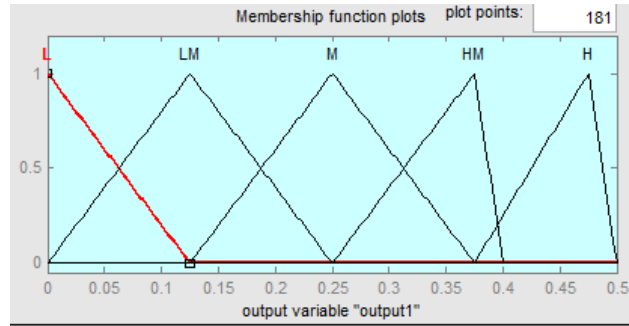


Figure 12: Membership functions for value of k

The values of membership function are given below

L	LM	M	HM	H
0-0.125	0-0.25	0.125-0.375	0.25-0.4	0.375-0.5

Rules are framed in the form “IF premise (or antecedent) THEN conclusion (or consequent)”. Are used to determine the suitability of a particular location of shunt facts device.

Rules are framed we using decision matrix

1. If (input 1 is L) and (input 2 is L) then (output 1) is H (1).
2. If (input 1 is LM) and (input 2 is H) then output is (M).

Like this the 25 rules are framed by using decision matrix.

AND		Degree of compensation(%S)				
		L	LM	M	HM	H
Transmission angle(δ_m)	L	H	H	HM	HM	HM
	LM	H	HM	HM	HM	M
	M	H	HM	HM	M	M
	HM	M	M	M	LM	LM
	H	LM	LM	LM	L	L

After receiving the inputs the FIS, based on the rules framed in the decision matrix, calculates the suitability membership function of each value. This is then defuzzified in order to determine the optimal placement of shunt facts device.

Optimal location (Value of k)	
Conventional Method	Fuzzy method
0.25	0.205

Conclusion :

This paper has presented a novel method to determine the optimal placement of shunt facts device in a long transmission line by using conventional method and fuzzy method.

It has been found by conventional method the shunt fact devices has to be placed slightly off centre to get the highest possible benefit when the power flows in a particular direction the optimal location from the centre depends upon the line resistance, and it increases almost linearly as the R/X ratio of the line is increased. Both the power transfer capability and stability of the system can be further improved if the shunt fact device is placed at the new optimal location instead of at the midpoint of a line having non zero resistance. This paper also verifies the optimal location of the shunt facts device by using fuzzy control method and found that the optimal placement is at $K = 0.205$ shifted towards the generator side and also improves the maximum power transfer capability of the transmission line

References

- [1] Zhang, B.M., Ding, Q.F “The development of Facts and its control”, Advances in power system control, operation and management, APSCOM-97, Fourth International Conference, Vol.1, Nov. 1997, pp:48-53.
- [2] Paserba, J.J.; “How facts controllers benefit AC transmission systems”, power engineering society general meeting, IEEE, Vol.2; June 2004, pp:1257-1262.
- [3] A.Edris, R. Adapa, M.H.Baker, L.Bohmann, K. Clark, K. Habashi, L. Gyugyi, J. Lemay, A. Mehraban, A.K. Myers, J. Reeve, F. Sener, D.R. Torgerson, R.R. Wood, Proposed terms and definitions for flexible AC transmission system [FACTS], IEEE Transactions on power delivery, vol.12, No. 4, October 1997 [DOI 10.1109/161.634216]
- [4] N.G. Hingorani, L. Gyugyi, understanding facts, Concepts and Technology of Flexible AC Transmission systems, IEEE press 2000.
- [5] M..H. Haque, 2000; “Optimal location of shunt facts device in long transmission line” IEE Proceedings on generation transmission & distribution, Vol. 147, No.4, pp.218-22, 2000 [Do 10.1049/ip – gtd: 20000412]
- [6] SAADA T, H: “Power system Analysis” (Mc Graw – Hill, 1999)
- [7] Xiao-Ping Zhang, Christian Rehtanz, Bikash Pal, 2006, *Flexible AC Transmission Systems: Modelling and Control*, Springer, March 2006.ISBN 978-3-540-30606-1
- [8] Giuseppe, Fusco / Mario, Russo, 2006, Adaptive Voltage Control in Power Systems: Modelling, Design and Applications (Advances in Industrial Control)? Springer | ISBN 184628564X | November 13, 2006 |
- [9] P. Kundur, 1994, Power system stability and control, EPRI Power System Engineering Series, New York, McGraw-Hill Inc., 1994. 328
- [10] Tate J.E and Thomas J.Overbye, 2005, “A Comparison of the Optimal Multiplier in Polar and Rectangular Coordinates” IEEE Transactions on Power systems, Vol.20,No 4, [DOI 10.1109/TPWRS. 2005. 857388]
- [11] M. Saravanan, S. M. R. Slochanal, P. Venkatesh, J. P. S. Abraham, 2007, “Application of particle swarm optimization technique for optimal location of FACTS devices considering cost of installation and system loadability”, *Electric Power Syst. Research*, vol. 77, pp. 276-283.

Hybridization of Neighbourhood Search Metaheuristic with Data Mining Technique to Solve p-median Problem

D.Srinivas Reddy¹, A.Govardhan², Ssvn Sarma³

¹Assoc.Professor, Dept of CSE, Vaageswari College of Engineering, Karimnagar, A.P., India.

²Professor, Department of CSE, JNTUH College of Engineering, Hyderabad, A.P., India.

³Professor, Department of CSE, Vaagdevi College of Engineering, Warangal, A.P., India.

Abstract:

Combinatorial optimization is the most panoptic area in current research paper. The p-median problem which is a combinatorial optimization problem is NP-Hard in nature that realizes facilitators which serves the maximum locations. The p-median problem will be practical in several applications areas such as escalating marketing strategies in the sphere of Management Sciences and in locating server positions in computer networks. In the proposed work the Metaheuristic based on Neighbourhood Search (NS) is hybridized with Data Mining Technique (HDMNS) with Frequent Mining to provide a solution to p-median problem. The resulting local optimal solution from NS method serves as a basis for identification of feasible solution space that holds different possible solutions of similar size and by the application of frequent mining technique on it results in identification of frequent items. Basing on the support count, most feasible solution is identified.

Keywords: Data Mining, Frequent item, GRASP, HDMNS procedure, Neighbourhood Search, NS Approach, USS

1. Introduction

The p-median problem can be represented with the mapping $d: C \times F \rightarrow R$, where F denotes the set of facilities, C represents the set of Customers and R the set of real numbers. The distance between the customer and the facility is represented by the mapping d , which is also termed as the distance function. The p-median problem ascertain a R facilities such that $R \subseteq F$ and $|R| = p$, for any positive integer p and number of facilities n , where $p \leq n$, such that the sum of the distances from each customer to its adjacent facility is minimized. Here every customer location is assumed as a facility i.e. $F = C$, and also for giving equal importance to each location it is considered that $w_i = 1$. The p-median problem can be represented mathematically as [24].

$$\text{Minimize } f(d, x) = \sum_{i=1}^n \sum_{j=1}^n w_i d_{ij} x_{ij} \quad (1)$$

$$\text{subject to } \sum_{j=1}^n x_{ij} = 1 \quad \forall i \quad (2)$$

$$x_{ij} \leq y_j \quad \forall i, j \quad (3)$$

$$\sum_{j=1}^n y_j = p \quad (4)$$

$$x_{ij} = 0 \text{ or } 1 \quad \forall i, j \quad (5)$$

$$y_j = 0 \text{ or } 1 \quad \forall j \quad (6)$$

Where,

n = number of locations

$x_{ij} = 1$ if a location i is assigned to facility located at j ,

$= 0$ other wise

$y_j = 1$ if j th location is a facility

$= 0$ other wise

d_{ij} = distance measured from location i to location j

p = preferred number of locations as facilities

The paper is structured as follows: In section 2 enlighten the existing GRASP and Neighbourhood Search based Metaheuristic approaches. Section 3 focuses on the proposed work, hybridization of Neighbourhood search method with data mining technique. Section 4 deals with experimental results and comparisons and Section 5 imparts the conclusions.

2. The Grasp And Neighbourhood Search Metaheuristics

Metaheuristics like genetic algorithms, GRASP, Neighbourhood Search Approach and others have been suggested and are functional to real-world problems in numerous areas of science [13] for p-median problem. GRASP's searching mechanism is iterative and each iteration consists of two phases: construction phase, to provide feasible solution and enhancement phase, to identify optimal solution [14][25][26]. The NS Approach mechanism is illustrated in Figure 1, Figure 2 and Figure 3. It is also having two phases- Then the construction phase and NB Search phase.

```

procedure NS Approach(list, p)
1. optml_sol  $\leftarrow \emptyset$ 
2. sol  $\leftarrow$  Construction(data points);
3. best_sol  $\leftarrow$  NBSearch(sol);
4. if cost(sol) > cost(optml_sol)
5.   optml_sol  $\leftarrow$  sol;
6. end if
7. until Termination criterion;
8. return optml_sol;
  
```

Figure 1. NS Approach procedure

```

procedure NBSearch(sol)
1. for each s in sol
2.   Compute neighbourhood of s;
3.   For each point x in neighbourhood
4.     new_sol  $\leftarrow$  swap(s,x);
5.     improved_sol  $\leftarrow$  Enhancement(sol);
6.   compare cost of new_sol and
       improved_sol and update best_sol
7. end for
8. end for
9. return best_sol
  
```

Figure 2: NB Search algorithm

The updation of the solution space is described in Figure 5. Basing on the updated solution space, the Frequent item set (FIS) are generated which consists the set of all distinct items that are present in the updated solution space. It is described in Figure 6. Support count is calculated and updated for each item in the FIS which is elucidated in Figure 7. After updating support count, sort the frequent items in the decreasing order of support count and then the mined solution is constructed by deliberating the items with high support count until the size of the solution or the number of items exactly equals to p. It is exemplified in Figure 8. The final phase is used to derive the optimal solution. The optimal solution is updated using Enhancement phase described in NS Approach which examines the global optimal solution that optimizes the objective function of the given p-median problem.

3. Proposed Work

The hybridized Data Mining Neighbourhood Search Approach (HDMNS()) procedure given in Figure 4 consists of three phases. The first phase NS Approach(), computes the initial solution using Neighbourhood Search approach by considering the given list and user specified p. It is described in detail in Figure 1, Figure 2 and Figure 3. The second phase is the core of the proposed work .i.e. application of data mining technique to the basic feasible solution. The obtained solution in first phase is input for the second phase which is used to generate the solution space (USS) that consists of all the probable solutions generated using the result obtained in the NSApproach().

```

procedure Enhancement( sol )
1. imp_sol  $\leftarrow$  sol;
2. imp_cost  $\leftarrow$  cost_eval(sol);
3. repeat
4.   no_improvements  $\leftarrow$  true;
5.   for i = 1 to p
6.     temp_best_sol  $\leftarrow \emptyset$ ;
7.     temp_best_cost  $\leftarrow \infty$ ;
8.     for each element e in Pi close to Pi
9.       t_sol  $\leftarrow$  swap(best_sol, e);
10.      t_cost  $\leftarrow$  appcosteval(t_sol);
11.     if appcost < approxbestcost then
12.       temp_best_sol  $\leftarrow$  t_sol;
13.       temp_best_cost  $\leftarrow$  t_cost;
14.     end if
15.   end for
16.   exactsolcost  $\leftarrow$  costeval(appbestsol);
17.   if exactsolcost < bestcost then
18.     imp_sol  $\leftarrow$  appbestsol;
19.     imp_cost  $\leftarrow$  exactsolcost;
20.   noimprovements  $\leftarrow$  false;
21.   end if
22. end for;
23. until noimprovements;
24. return imp_sol;
  
```

Figure 3. Enhancement phase NB Search

```

procedure HDMNS()
1. Initialize sol, optimal_sol, Mined_sol  $\leftarrow \emptyset$ 
2. Initialize sol_space  $\leftarrow \emptyset$ 
3. Initialize USS, FIS, UFIS  $\leftarrow \emptyset$ 
4. Read list, p
5. Sol  $\leftarrow$  NSApproach(list, p)
6. USS  $\leftarrow$  Update_sol_space(sol)
7. FIS  $\leftarrow$  Generate_frequent_items(USS)
8. UFIS  $\leftarrow$  Update_supportcount(FIS, USS)
9. Mined_sol  $\leftarrow$  Generate_mined_solution(UFIS)
10. Update optimal_sol
  
```

Figure 4. Hybridized data mining NS

procedure Generate_Frequent_items(USS)

1. Initialize $FIS \leftarrow \Phi$
2. Read all solutions in USS
3. For each solution in USS
Update FIS with distinct elements
4. End for
5. Return FIS

Figure 6. Generate frequent items algorithm

procedure Update_sol_space(sol)

1. Initialize $USS \leftarrow \Phi$
2. $Mod_list \leftarrow list - sol$
3. For each element in sol
Exchange element with element in
 mod_list to get new solution
Update USS
4. End for
4. Return USS

Figure 5. Update solution space algorithm

procedure Generate_Mined_solution(UFIS)

1. Initialize $Mined_sol \leftarrow \Phi$
2. Sort UFIS in decreasing order of support count
3. Update $Mined_sol$ with elements in UFIS with high support count
Until $Mined_sol$ size == p;
4. Return $Mined_sol$

Figure 8. Generate mined solution algorithm

procedure Update_Support_count(FIS, USS)

1. Initialize $UFIS \leftarrow \Phi$
2. Initialize each element support count to 0
3. For each element(x) in FIS
For each solution in USS
Update support count of x
End for
4. End for
5. Return UFIS

Figure 7. Update support count

4. Experimental Results

The experimental results obtained for GRASP, NS approach and Hybrid Data Mining Neighbourhood Search(HDMNS) are analyzed in this section, and the results are evaluated on the basis of quality of the solution against p. Experiments are carried out on data sets with 15, 25, 50 points. Results are tabularized and graphs are outlined. The origin of data sets under study is acquired from the web site of Professor Eric Taillard, Kent University of Applied Sciences of Western Switzerland. The associated website for p-median problem instances is <http://mistic.heig-vd.ch/taillard/problemes.dir/location.html>. In Figure 9 the optimal Objective function value i.e. cost for p-median problem is compared using algorithms GRASP, NS approach and HDMNS for the data set of size 50 with number of facility locations (p) incremented by 10. It is observed that HDMNS is working better than the other two techniques.

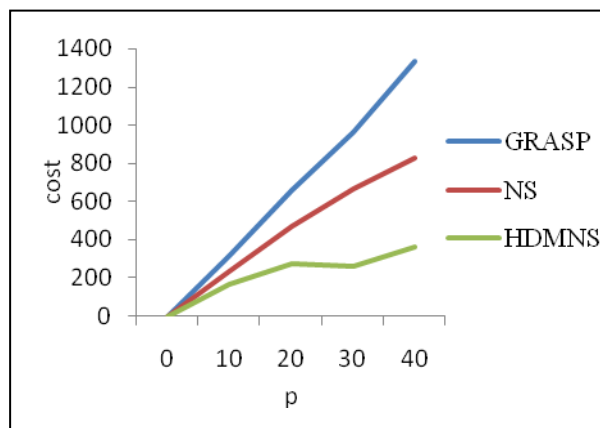


Figure 9. Cost comparison of GRASP, approach & HDMNS when N=50

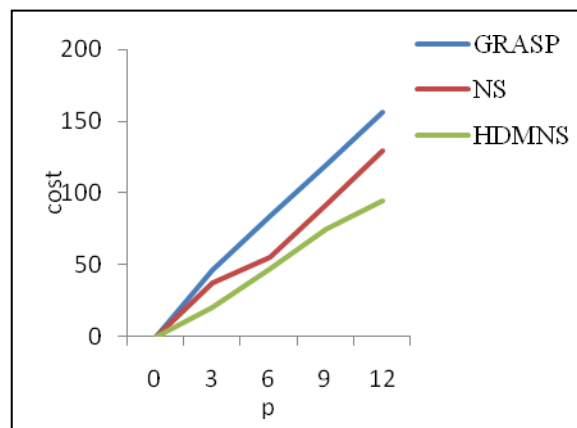


Figure 10. Cost comparison of GRASP, NS approach & HDMNS when N=15

NS

In Figure 10 the optimal Objective function value i.e. cost for p-median problem is evaluated using algorithms GRASP,

NS approach and HDMNS for the data set of size 15 with number of facility locations (p) raised by 3. It is perceived that HDMNS outperforms the other two techniques. Similarly Figure 11 is plotted with data set size 25 with p=5 and observed the same.

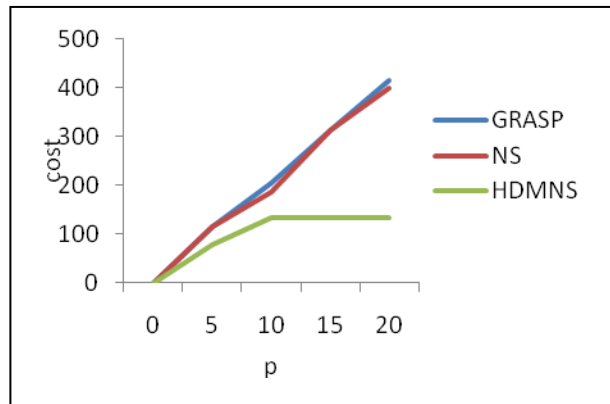


Figure 11. Cost comparison of GRASP, HDMNS when N=25

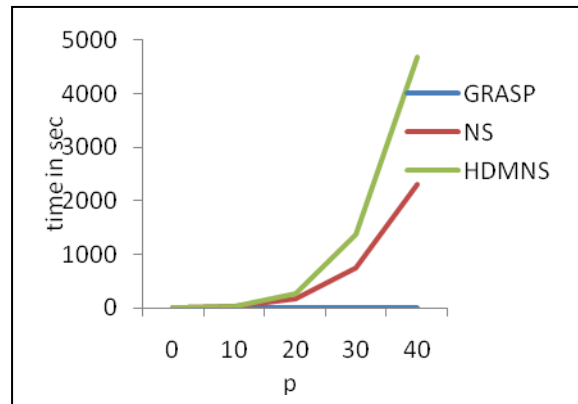


Figure 12. Execution time comparison of GRASP, NS approach & HDMNS when N=50

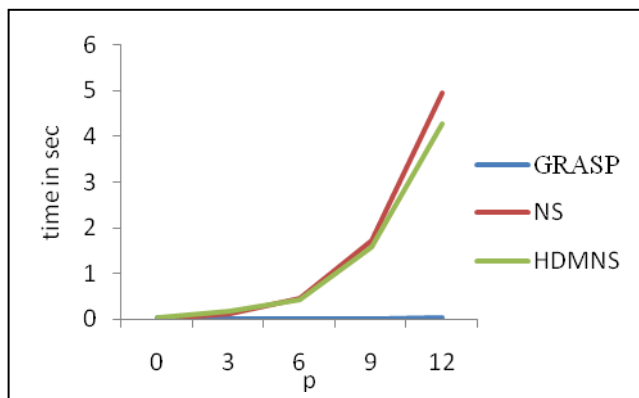


Figure 13. Execution time comparison of GRASP, HDMNS when N=15

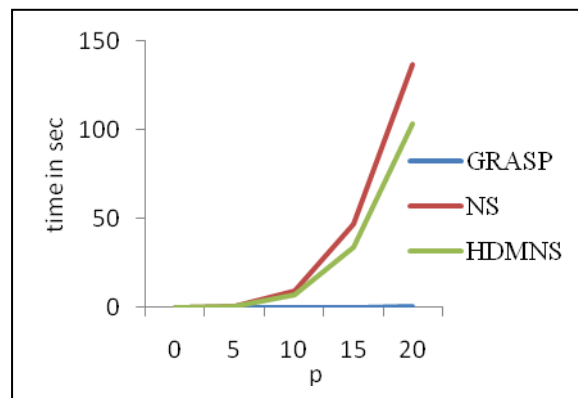


Figure 14. Execution time comparison NS approach & Vs GRASP, NS approach & HDMNS, N=5

Execution times are compared for all the three algorithms for N=50, 15 and 25 with p increments 10, 3 and 25 respectively and identified that HDMNS works better than other two. They are represented in Figure 12, Figure 13 and Figure 14.

5. Conclusions

It is observed that in all the test cases, Hybrid Data Mining Neighbourhood Search (HDMNS) Metaheuristic performs much better when compared with the efficient existing methods like GRASP and Neighbourhood Search Metaheuristic. It is also observed that in most of the cases the though the HDMNS includes Mining technique in addition with NS approach it takes almost same execution time as NS approach and produces much more better results than NS approach.

References

- [1] R. Agrwal and R. Srikanth. Fast algorithms for mining association rules, Proc. of the Very Large Data Bases Conference, pages 487-499, 1994.
- [2] T. A. Feo and M. G. C. Resende. A probabilistic heuristic for a computationally difficult set covering problem, Operational Research Letters, 8:67-71, 1989.
- [3] T. A. Feo and M. G. C. Resende. Greedy randomized adaptive search procedures, Journal of Global Optimization, 6:1609-1624, 1995.

- [4] T. A. Feo and M. G. C. Resende. GRASP: An annotated bibliography, Essays and Surveys in Metaheuristics, Kluwer Academic Publishers, 2002.
- [5] M. D. H. Gamal and Salhi. A cellular heuristic for the multisource Weber Problem, computers & Operations Research, 30:1609-1624, 2003.
- [6] B. Geothals and M. J. Zaki. Advances in Frequent Item set Mining Implementations: Introduction to FIMI03, Proc. of the IEEEICDM workshop on Frequent Item set Mining Implementations, 2003.
- [7] G. Grahne and J. Zhu. Efficiently using prefix-trees in mining frequent item-sets, Proc. of the IEEEICDM Workshop on Frequent Itemset Mining Implementations, 2003.
- [8] J. Han, J. Pei and Y. Yin. Mining frequent patterns without candidate generation, Proc. of the ACM SIGMOD Int. Conference on Management of Data, pages 1-12, 2000.
- [9] J. Han and M. Kamber. Data Mining: Concepts and Techniques, 2nd ed., Morgan Kaufman Publishers, 2006.
- [10] O. Kariv and L. Hakimi. An algorithmic approach to network location problems, part II: the p-medians, SIAM Journal of Applied Mathematics, 37:539-560, 1979.
- [11] N. Mladenovic, J. Brimberg, P. Hansen and Jose A. Moreno-Perez. The p-median problem: A survey of metaheuristic approaches, European Journal of Operational Research, 179:927-939, 2007..
- [12] S. Orlando, P. Palmerimi and R. Perego. Adaptive and resource- aware mining of frequent sets, Proc. of the IEEE In. conference on Data Mining, pages 338-345, 2002.
- [13] I. Osman and G. Laporte, Metaheuristics: A bibliography, Annals of Operations Research, 63:513-623, 1996.
- [14] M. G. C. Resende and C. C. Ribeiro. Greedy randomized adaptive search procedures, Handbook of Metaheuristics, Kulwer Academic Publishers, 2003.
- [15] M. H. F. Ribeiro, V. F. Trindade, A. Plastino and S. L. Martins. Hybridization of GRASP metaheuristic with data mining techniques, Proc. of the ECAI Workshop on Hybrid Metaheuristics, pages 69-78, 2004.
- [16] M. H. F. Ribeiro, V. F. Trindade, A. Plastino and S. L. Martins. Hybridization of GRASP Metaheuristic with data mining techniques, Journal of Mathematical Modeling and Algorithms, 5:23-41, 2006.
- [17] S. Salhi. Heuristic Search: The Science of Tomorrow, OR48 Keynote Papers, Operational Research Society, pages 38-58, 2006.
- [18] L. F. Santos, M. H.F. Ribeiro, A. Plastino and S. L. Martins. A hybrid GRASP with data mining for the maximum diversity problem, proc. of the Int. Workshop on Hybrid Metaheuristics, LNCS 3636, pages. 116-127, 2005.
- [19] L.F. Santos, C.V.Albuquerque, S. L. Martins and A. Plastino. A hybrid GRASP with data mining for efficient server replication for reliable multicast, Proc. of the IEEE GLOBECOM Conference, 2006.
- [20] L. F. Santos, S. L. Martins and A. Plastino. Applications of the DM-GRASP heuristic: A survey, In. Transactions in Operational Research, 15:387-416, 2008.
- [21] E. G. Talbi. A taxonomy of hybrid metaheuristics, Journal of Heuristics, 8:541-564, 2002.
- [22] B. C. Tansel, R. L. Francis, and T. J. Lowe. Location on networks: A survey, Management Science, 29:482-511, 1983.
- [23] I. H. Witten and E. Frank. Data Mining: Practical Machine Learning Tools and Techniques. 2nd ed., Morgan Kaufmann Publishers, 2005.
- [24] Moh'd Belal Al-Zoubi, Ahmed Sharieh, Nedal Al-Hanbali and Ali Al-Dahoud. A Hybrid Heuristic Algorithm for Solving the P-Median Problem. Journal of Computer Science (Special Issue) pages 80-83, Science Publications, 2005.
- [25] Alexandre Plastino, Eric R Fonseca, Richard Fuchshuber, Simone de L Martins, Alex.A.Freitas, Martino Luis and Said Salhi. A Hybrid Datamining Metaheuristic for the p-median problem. Proc. of SIAM Journal (Data Mining), 2009.
- [26] Sunil Nadella, Kiranmai M V S V, Dr Narsimha Gugulotu. A Hybrid K-Mean-Grasp For Partition Based Clustering of Two-Dimensional Data Space As An Application of P-Median Problem, In. Journal of Computer and Electronics Research 1:2278-5795, June 2012.

Key infrastructure elements for cloud computing

S.J.Mohana¹, M.Saroja², M.Venkatachalam³

^{1,2,3.} of Computer Applications, Erode Arts and Science college, Erode, India)

Abstract

Clouds consist of a collection of virtualized resources, which include both computational and storage facilities that can be provisioned on demand, depending on the users' needs. users are charged on a pay-per-use basis. This paper gives a quick overview of cloud and describes the key infrastructure elements for cloud computing. This paper is a brief survey based of readings on "cloud" computing and it tries to address, related research topics and challenges ahead.

Keywords – cloud computing, middleware, hypervisor, security, management, virtualization.

1. Introduction

Cloud computing has been the most prevalent technology in the past few years. Cloud computing is a model for enabling ubiquitous, convenient, on-demand network access to a shared pool of configurable computing resources (e.g., networks, servers, storage, applications, and services) that can be rapidly provisioned and released with minimal management effort or service provider interaction[1]. Cloud providers should satisfy customers' various workload requirements. When cost of operating cloud resource is considered, then the makespan also becomes an important issue. The Cloud is drawing the attention from the Information and Communication Technology community because of the set of services with common characteristics, provided by important industry players. However, existing technologies of cloud computing such as virtualization, utility computing and distributed computing are not new.

2. Types Of Cloud

Clouds can be classified as public, private, community or hybrid depending on the model of deployment. A private cloud is the cloud infrastructure owned or leased by a single organization and is operated solely for that organization. A public cloud is owned by an organization selling cloud services to the general public or to a large industry group. A Community cloud is shared by several organizations and supports a specific community that has shared concerns (e.g. mission, security requirements, policy, and compliance considerations). A hybrid cloud is a composition of two or more clouds (private, community, or public) that are bound together by standardized or proprietary technology that enables data and application portability (e.g. cloud bursting).

3. Key Characteristics

On-demand self-service: *Without human intervention, cloud user should be able to use computing capabilities, such as server time and network storage, as and when needed.*

Pay per use: cloud users are charged for what they use. The pricing model depends on the quality and quantity of services consumed [2]. Some of the factors considered for billing includes measuring storage, bandwidth and consumption of computing resources.

Ubiquitous network access : Ubiquitous network access allows all users to access any kind of information at anytime, and from anywhere.

Location independent resource pooling: The provider's computing resources are pooled to serve all consumers using a multi-tenant model, with different physical and virtual resources dynamically assigned and reassigned according to consumer demand[3]. Location of the cloud resources are abstracted from the consumers. Some of the cloud resources include storage, processing, memory, network bandwidth, and virtual machines.

Rapid elasticity: cloud computing has the ability to scale resources up and down as needed. For the consumers, the cloud resources available for rent appear to be infinite and can be purchased in any quantity at any time.

4. Architectural Blocks

The key infrastructural elements of cloud are hardware & networking, hypervisor, middleware, security & management

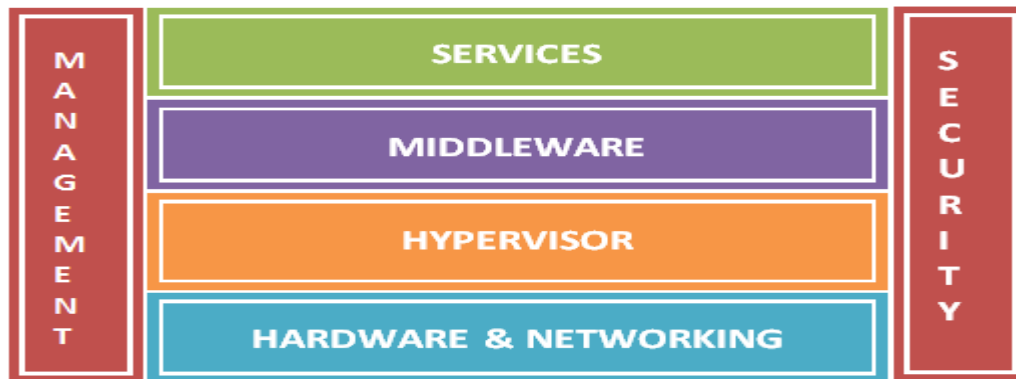


Figure 1: cloud architectural blocks

4.1 Hardware and Networking

The lower layer of cloud infrastructure has hardware and networking devices. It includes storage devices, servers, cooling units, power units, other hardware and networking components.

4.2 Hypervisor

A hypervisor can also be termed as virtual machine manager. It is a software that allows more than one operating systems to share a single hardware host. Each operating system appears to have the host machine's resources all to itself. However, the virtual machine manager is actually controlling and allocating the host machine's resources to each operating system. Hypervisor also makes sure that virtual machines cannot disrupt each other.



Figure 2: virtual machines

Basically, there are two kinds of server virtualization techniques: full virtualization and para virtualization. In full virtualization Virtual machine talks to hypervisor which communicates with the hardware platform. CPU understands the unmodified instructions generated by Virtualized OS. Advantages of full virtualization are complete decoupling of the software from the hardware and complete isolation of different applications. Disadvantages are VMM should provide additionally virtual bios, virtual memory space and virtual devices and also hypervisor creates and maintains data structures like shadow memory page table. VMware's virtualization products and Microsoft Virtual Server are examples of full virtualization. In para virtualization guest OS uses specialized API that talks to the VMM which sends the virtualization requests to the hardware. VMM does not need a resource intensive translation of instructions. Advantages of para virtualization are near native performance and migration. Disadvantage is that it is not applicable for Windows OS. Xen is a virtual machine monitor (hypervisor) for IA-32 (x86, x86-64), IA-64 architectures. It allows several guest operating systems to be executed on the same computer hardware concurrently.

4.3 Cloud Middleware

Software that integrates applications, services and content available on the cloud is called cloud middleware. Middleware is a software that glues various elements of cloud computing. Middleware is an important component of

cloud computing as it helps complex applications on a cloud to contact each other constantly to work in unison. Applications and web components hosted anywhere on the cloud can be re-used with this middleware technology. Some key characteristics possessed by Cloud Middleware are data management, user interfaces and portals, identity / security management, billing & metering and management & monitoring. Various Cloud Middleware's include Eucalyptus - University of California, Nimbus - Globus alliance, Open Nebula - DSA Research, Reservoir - European Union FP7 (associated with OpenNebula) and UEC - Ubuntu Enterprise Cloud- Ubuntu + Eucalyptus.

4.4 Cloud Services

Cloud computing provides three different kind of services :Platform as a Service(PaaS), Infrastructure as a Service (IaaS) and Software as a Service (SaaS). In PaaS, platform for developing and deploying an application is provided as a service to developers over the Web. Examples include Google AppEngine, Azure services and Amazon web services[4].In IaaS, hardware (server, storage and network), and associated software (operating systems virtualization technology, file system) are delivered as a service to cloud users. Examples include VMware, Amazon EC2. Software as a Service hosts and manages a given application in their own data center and makes it available to multiple tenants and users over the Web. Some SaaS providers use another cloud provider's PaaS or IaaS to offer their services. Some of SaaS providers include Oracle CRM On Demand, Salesforce.com, and Netsuite.

4.5 Security And Management

when cloud services are used security policies should be deployed to protect data, applications, and the associated infrastructure. Cloud users must trust the cloud providers with their environment and data. Identification & authentication: Priorities and permissions may be granted to specified users to access cloud resources. Every user must be verified and validated using various security mechanisms. Authorization : Authorization policy in cloud computing will determine the type of services, resources or activities the user is permitted. The cloud users must be authorized before performing certain activities. Confidentiality: Confidentiality plays an important role in cloud computing. Organization's data is distributed in cloud across multiple remote servers. Protecting data in cloud computing, allows for information security protocols to be enforced at various layers of cloud applications.

Integrity: Although outsourcing data into the cloud is economically attractive for the cost and complexity of long-term large-scale data storage, it's lacking of offering strong assurance of data integrity and availability may impede its wide adoption by both enterprise and individual cloud users [5]. Therefore cloud's data should be robustly imposed with ACID (atomicity, consistency, isolation and durability) properties.

Non-repudiation: A sender or receiver of a message cannot deny having sent or received the message. Using the traditional e-commerce security protocols and token provisioning to data transmission, cloud providers can assure non-repudiation in Cloud computing. Availability: Availability is one of the most critical information security requirements in Cloud computing because it is a key decision factor when deciding among private, public or hybrid cloud vendors as well as in the delivery models. The service level agreement is the most important document which highlights the trepidation of availability in cloud services and resources between the cloud provider and client.

5. Future of the Cloud

Industry analysts including Gartner expects 90 percent of organizations surveyed expect to grow with cloud citing cost-effectiveness and ease/speed of deployment as primary reasons for adoption. Organizations will make use of several trends such as shared, virtualized and automated IT architectures. Businesses of all sizes will adopt cloud due to the introduction of cloud-enabled application platforms.

6. Conclusion

Cloud computing model has immense potential as it offers significant performance gains as regards to response time and cost saving under dynamic workload scenarios[6]. This article discusses the concept of cloud computing, implementation mechanism, architecture and several forms and characteristics of cloud computing. There exists lot of opportunities in cloud computing to explore further for researchers as well as industrial developers.

Key open issues that needs further investigation includes Security, Privacy and Trust, Cloud Interoperability, Dynamic Pricing of Cloud Services, Dynamic Negotiation and SLA Management, Energy Efficient Resource Allocation and User QOS and Regulatory and Legal Issues.

References

- [1]. www.nist.gov > IITL > Computer Security Division
- [2]. 2.Cloud Computing PMO .Cloud Computing Initiative:May 6, 2009 Summit Briefing Book
- [3]. Information Systems and Technologies: 7th International Conference WEBIST 2011, Noordwijkerhout, The Netherlands, May 6-9, 2011, Revised Selected Papers
- [4]. Amazon simple storage service. Web Page
- [5]. <http://www.amazon.com/gp/browse.html?node=16427261>
- [6]. Cong Wang, Qian Wang, Kui Ren, Wenjing Lou, "Towards Secure and Dependable Storage Services in Cloud Computing," IEEE transactions on Services Computing, 06 May 2011
- [7]. Rajku mar Buyya, Anton Beloglazov, and Jemal Abawajy. "Energy-Efficient Management of Data Center Resources for Cloud Computing: A Vision, Architectural Elements, and Open Challenges".Elsevier journal, june 2009
- [8]. Sankaran Sivathanu, Ling Liu, Mei Yiduo, and Xing Pu." Storage Management in Virtualized Cloud Environment" cloud computing, 2010 IEEE international conference.
- [9]. <http://www.vmware.com/virtualization/>
- [10]. Toby Velte , Anthony Velte , Robert Elsenpeter . Cloud Computing, A Practical Approach. Edition 2010.
- [11].
- [12].
- [13].
- [14].
- [15].

Control Of Unstable Periodic Orbits Coexisted With The Strange Attractor

Dr. Nabajyoti Das

Assistant Professor, Department of Mathematics Jawaharlal Nehru College, Boko District: Kamrup (R), State: Assam, Country: India

Abstract

It is known that the frame of a chaotic attractor is given by infinitely many unstable periodic orbits, which coexist with the strange attractor and play an important role in the system dynamics. There are many methods available for controlling chaos. The periodic proportional pulses technique is interesting one. In this paper it is aimed to apply the periodic proportional pulses technique to stabilize unstable periodic orbits embedded in the chaotic attractor of the nonlinear dynamics: $f(x) = ax^2 - bx$, where $x \in [0,4]$, a and b and are tunable parameters, and obtain some illuminating results.

Key Words: Controlling chaos, periodic proportional pulse, unstable periodic orbits, chaotic attractor, discrete model.

2010 AMS Classification: 37 G 15, 37 G 35, 37 C 45

1. Introduction

In chaos theory, **control of chaos** is based on the fact that any chaotic attractor contains an infinite number of unstable periodic orbits. Chaotic dynamics then consists of a motion where the system state moves in the neighborhood of one of these orbits for a while, then falls close to a different unstable periodic orbit where it remains for a limited time, and so forth. This results in a complicated and unpredictable wandering over longer periods of time. Control of chaos is the stabilization, by means of small system perturbations, of one of the unstable periodic orbits. The result is to render an otherwise chaotic motion more stable and predictable, which is often an advantage. The perturbation must be tiny, to avoid significant modification of the system's natural dynamics. It is known that the frame of a chaotic attractor is given by infinitely many unstable periodic orbits, which coexist with the strange attractor and play an important role in the system dynamics. The task is to use the unstable periodic orbits to control chaos. The idea of controlling chaos consists of stabilizing some of these unstable orbits, thus leading to regular and predictable behavior. However, in many practical situations one does not have access to system equations and must deal directly with experimental data in the form of a **time series** [3, 10]. Publication of the seminal paper [1] entitled "Controlling chaos" by Ott, Grebogi and Yorke in 1990, has created powerful insight in the development of techniques for the control of chaotic phenomena in dynamical systems. There are many methods available [9] to control chaos on different models, but we take the advantage of the periodic proportional pulses technique [7], to control unstable periodic orbits in strange attractor by considering the one-dimensional nonlinear chaotic dynamics:

$$x_{n+1} = f(x_n) = ax_n^2 - bx_n, n = 0,1,2,\dots \quad (1.1)$$

We now highlight some useful concepts which are absolutely useful for our purpose.

1.1 Discrete dynamical systems

Any C^k ($k \geq 1$) map $E: U \rightarrow \mathfrak{R}^n$ on the open set $U \subset \mathfrak{R}^n$ defines an n -dimensional **discrete-time** (autonomous) smooth dynamical system by the state equation

$$\bar{x}_{t+1} = E(\bar{x}_t), t = 1,2,3,\dots$$

where $\bar{x}_t \in \mathfrak{R}^n$ is the state of the system at time t and E maps \bar{x}_t to the next state \bar{x}_{t+1} . Starting with an initial data \bar{x}_0 , repeated applications (iterates) of E generate a discrete set of points (the orbits) $\{E^t(\bar{x}_0) : t = 0,1,2,3,\dots\}$, where $E^t(\bar{x}) = \underbrace{E \circ E \circ \dots \circ E}_{t \text{ times}}(\bar{x})$ [6].

1.2 Definition: A point $\bar{x}^* \in \mathfrak{R}^n$ is called a **fixed point** of E if $E^m(\bar{x}^*) = \bar{x}^*$, for all $m \in \mathbf{C}^*$.

1.3 Definition: A point $\bar{x}^* \in \mathfrak{R}^n$ is called a **periodic point** of E if $E^q(\bar{x}^*) = \bar{x}^*$, for some integer $q \geq 1$.

1.4 Definition: The closed set $A \in \mathfrak{R}^n$ is called the **attractor** of the system $\bar{x}_{t+1} = E(\bar{x}_t)$, if (i) there exists an open set $A_0 \supset A$ such that all trajectories \bar{x}_t of system beginning in A_0 are definite for all $t \geq 0$ and tend to A for $t \rightarrow \infty$, that is, $\text{dist}(\bar{x}_t, A) \rightarrow 0$ for $t \rightarrow \infty$, if $\bar{x}_0 \in A_0$, where $\text{dist}(\bar{x}, A) = \inf_{\bar{y} \in A} \|\bar{x} - \bar{y}\|$ is the distance from the point \bar{x} to the set A , and (ii) no eigensubset of A has this property.

1.5 Definition: A system is called **chaotic** if it has at least one chaotic attractor.

Armed with all these ideas and concepts, we now proceed to concentrate to our main aim and objectives

2. Control of Chaos by periodic proportional pulses

In N. P. Chua's paper [7] it is shown that periodic proportional pulses,
 $x_i \rightarrow \lambda x_i$ (i is a multiple of q , where λ is a constant), (1.2)

applied once every q iterations to chaotic dynamics,
 $x_{n+1} = f(x_n)$, (1.3)

may stabilize the dynamics at a periodic orbit. We note that a fixed point of (1.3) is any solution x^* of the equation
 $x^* = f(x^*)$ (1.4)

and the fixed point is locally stable if

$$\left| \frac{df(x)}{dx} \right|_{x=x^*} < 1. \quad (1.5)$$

The composite function $g(x)$ is given by

$$g(x) = \lambda f^q(x). \quad (1.6)$$

where the dynamics is kicked by multiplying its value by the factor λ , once every q iterations. As above a fixed point of $g(x)$ is any solution x^* of

$$\lambda f^q(x^*) = x^* \quad (1.7)$$

and this fixed point is locally stable if

$$\left| \lambda \frac{df^q(x^*)}{dx} \right| < 1 \quad (1.8)$$

We note that a stable fixed point of g can be viewed as a stable periodic point of period q of the original dynamics f , kicked by the control procedure. Now the dynamics f is chaotic and wanted to control it so as to obtain stable periodic orbits of period q , by kicking once every q iterations, following equation (1.1).

To find a suitable point x^* and a factor λ satisfying (1.7) and (1.8), the function $Hq(x)$ is defined as

$$Hq(x) = \frac{x}{f^q(x)} \frac{df^q(x)}{dx} \quad (1.9)$$

Substituting from (1.7), equation (1.8) becomes

$$\left| Hq(x^*) \right| < 1. \quad (1.10)$$

Interestingly, if a point x^* satisfies the inequalities (1.10), then with the kicking factor λ defined by equation (1.6), the control procedure will stabilize the dynamics at a periodic orbit of period q , passing through the given point. It is important to note that, if the the impulse λ is too strong, it may kick the dynamics out of the basin of attraction, and in that case, the orbit may escape to infinity. In performing pulse control, one must have this precaution in mind.

3. Periodic proportional pulses on the concerned model

Periodic proportional pulses for stabilizing unstable periodic orbits embedded in a chaotic attractor can be well demonstrated by the nonlinear chaotic model (1.1), that is,

$$x_{n+1} = ax_n^2 - bx_n, n = 0,1,2,\dots$$

with the control parameter value $b = -3.9$. Here the parameter a is fixed as $a = 1$ and for this fixed value, it is observed that model (1.1) develops chaos via the period-doubling bifurcation route.

Period-doubling cascade for the model (1.1):

Table 1.1

Period	One of the Periodic points	Bifurcation Points.
1	$x_1 = 2.000000000000 \dots$	$b_1 = -3.000000000000 \dots$
2	$x_2 = 1.517638090205 \dots$	$b_2 = -3.449489742783 \dots$
4	$x_3 = 2.905392825125 \dots$	$b_3 = -3.544090359552 \dots$
8	$x_4 = 3.138826940664 \dots$	$b_4 = -3.564407266095 \dots$
16	$x_5 = 1.241736888630 \dots$	$b_5 = -3.568759419544 \dots$
32	$x_6 = 3.178136193507 \dots$	$b_6 = -3.569691609801 \dots$
64	$x_7 = 3.178152098553 \dots$	$b_7 = -3.569891259378 \dots$
128	$x_8 = 3.178158223315 \dots$	$b_8 = -3.569934018374 \dots$
256	$x_9 = 3.178160120824 \dots$	$b_9 = -3.569943176048 \dots$
512	$x_{10} = 1.696110052289 \dots$	$b_{10} = -3.569945137342 \dots$
1024	$x_{11} = 1.696240778303 \dots$	$b_{11} = -3.569945557391 \dots$
...

[Periodic points and period-doubling points are calculated using numerical mechanisms discussed in [8, 11] taking the fixed parameter value $a = 1$]

The period-doubling cascade accumulates at the accumulation point $b = -3.569945672\dots$, after which chaos arise. For the parameter $b = -3.9$ the system (1.1) is chaotic. The time series graph in the following figure (1.1) shows the chaotic behavior of the system:

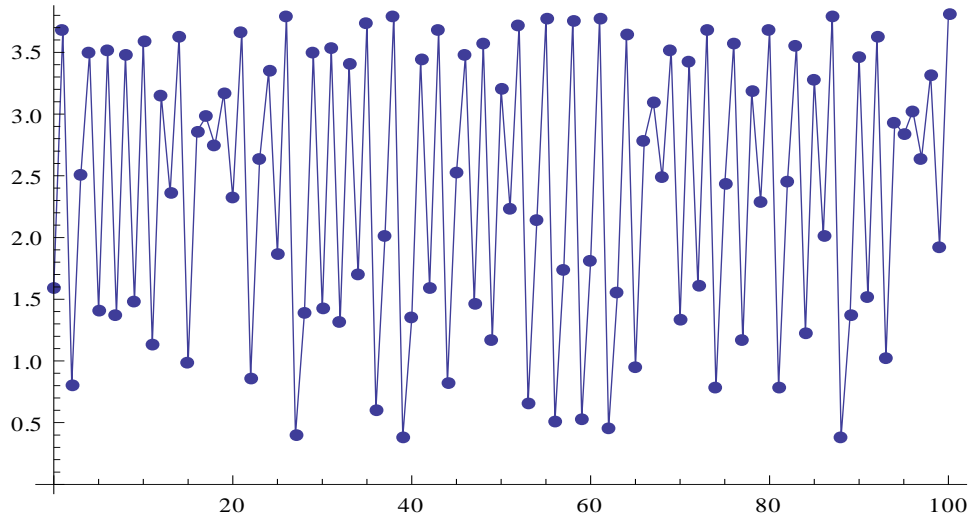


Fig. 1.1 Time series graph for parameter $b = -3.9$ and initial point $x_0 = 1.6$

For $q = 1$ and $b = -3.9$ the control curve $H1(x)$ is drawn in figure 1.2. The range is restricted to $-1 < Hq(x^*) < 1$, $q = 1$ and in this interval we can stabilize orbits of period one at every point x^* in the range about $(0, 2.6)$.

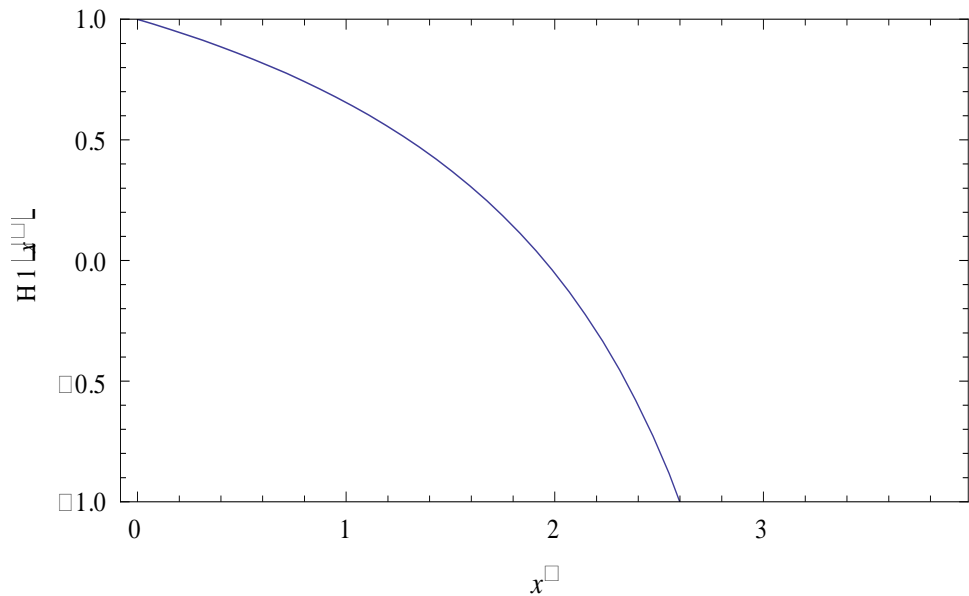


Fig. 1.2 Control curve for parameter $b = -3.9$

Taking $x^* = 1.9$ in the above stated range, the value of the kicking factor $\lambda = 0.5$ is calculated and the control procedure stabilizes the dynamics at a periodic orbit of period-one, passing through the given point as shown in the figure 1.3.

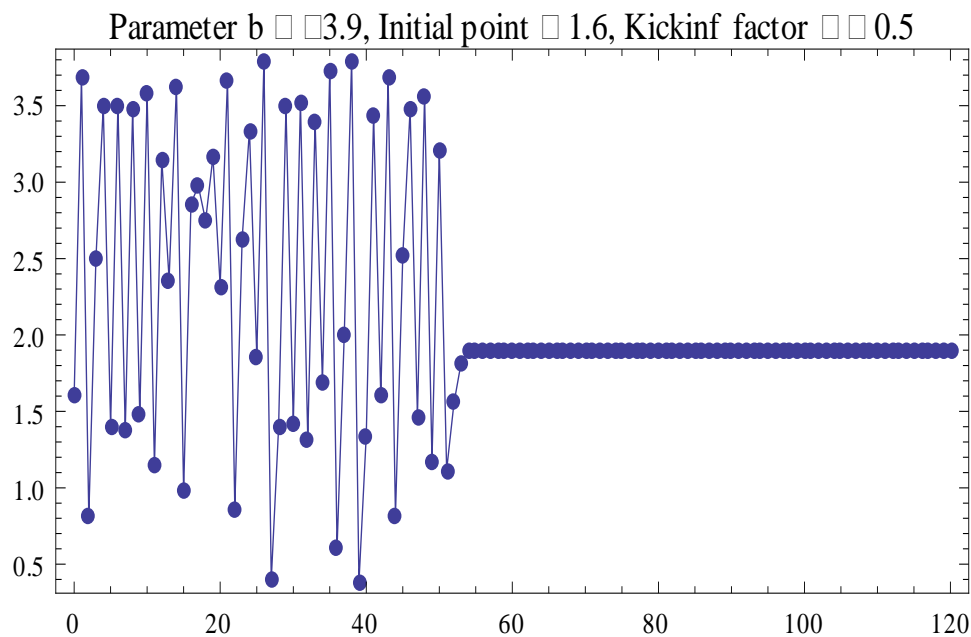


Fig. 1.3 Time series graph for parameter $b = -3.9$

Again for $q = 2$ and $b = -3.9$ the control curve $H_2(x)$ is drawn in figures 1.4. Here also the range is restricted to $-1 < Hq(x^*) < 1$, $q = 2$ and the figure 1.5 shows that we can stabilize orbits of period-two at point x^* only in three ranges. For this purpose the kicking factor is found as $\lambda \approx 0.868056$, taking the given point as $x^* = 3.3$.

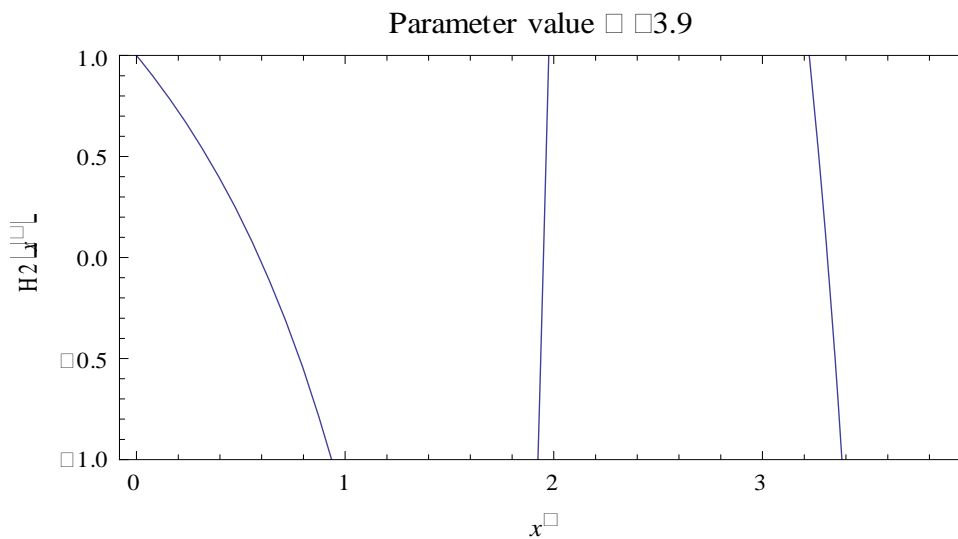


Fig. 1.4 Control curves for parameter $b = -3.9$

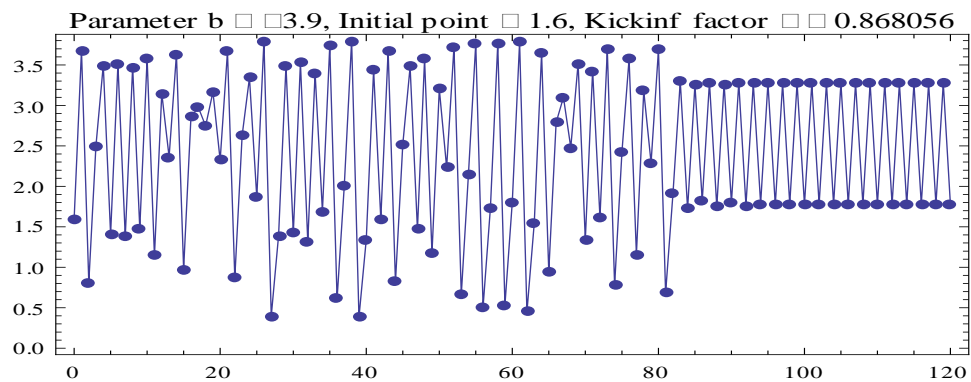


Fig. 1.5 Time series graph for parameter $b = -3.9$

Similarly for $q = 3,4$ and $m = 0.815$ the control curves $H3(x)$, $H4(x)$ are drawn in figures 1.6 and 1.7.

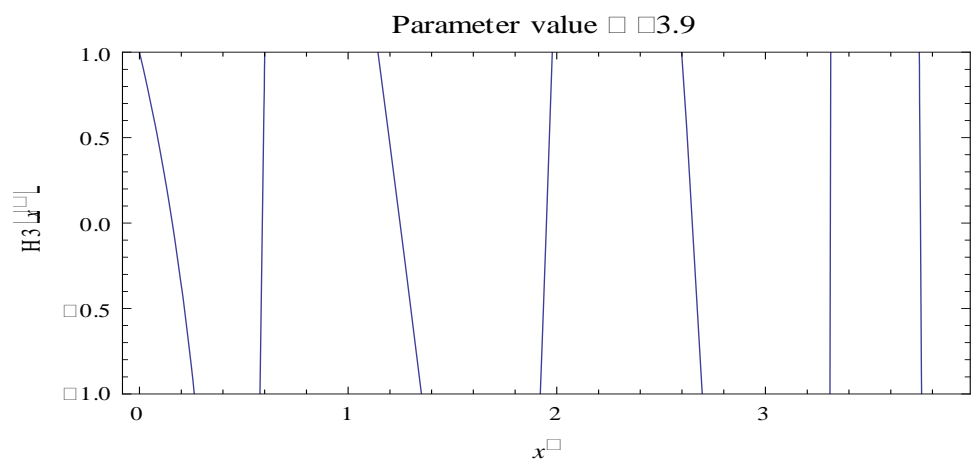


Fig. 1.6 Control curves for parameter $b = -3.9$

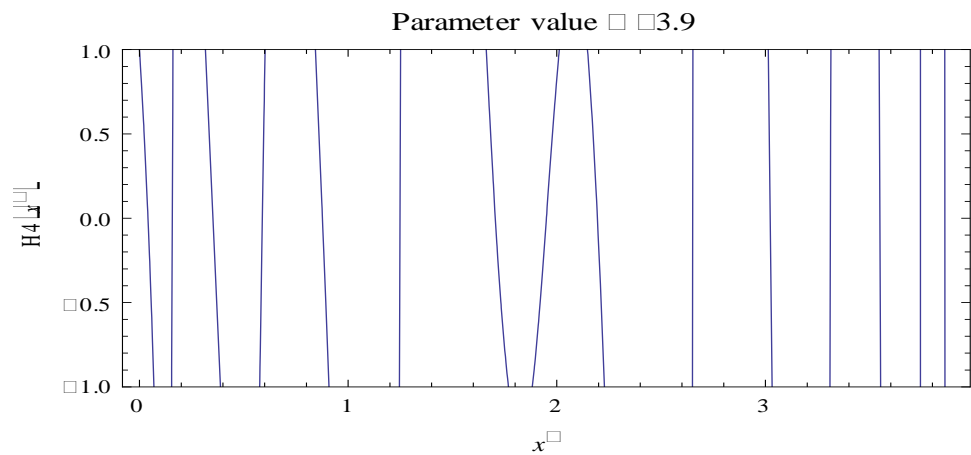


Fig. 8.7 Control curves for parameter $b = -3.9$

These figures indicate that there are 7 and 15 narrow ranges of x^* values of periods 3 and 4 respectively. We note that the control ranges are getting smaller and smaller as the periodicity increase. Lastly, $q = 4$ and $x^* = 1.11892$. stabilize orbits of period-4 with the kicking factor as shown in the figure 1.8.

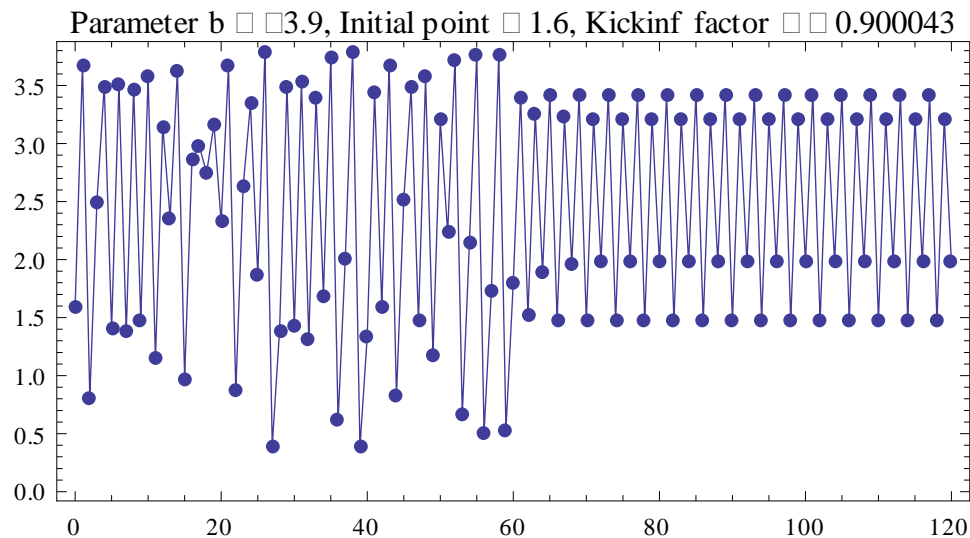


Fig. 1.8 Time series graph for parameter $b = -3.9$

4. Conclusion

By the above technique, we can conclude that an irregular orbit of any period can be controlled by the above technique. But in practice, chaos control always deals with periodic orbits of low periods, say $q = 1,2,3,4,5$.

5. Acknowledgements:

I am grateful to **Dr. Tarini Kumar Dutta**, Senior Professor of the Department of Mathematics, Gauhati University, Assam: India, for a valuable suggestion for the improvement of this research paper.

Bibliography

- [1] E. Ott, C. Grebogi, J. A. Yorke, Controlling Chaos, Phys. Rev. Lett. 64 (1990) 1196-1199
- [2] G. Chen and X. Dong, From Chaos to Order: Methodologies, Perspectives and Applications, World Scientific, 1998
- [3] J. M. Gutierrez and A. Iglesias, Mathematica package for analysis and control of chaos in nonlinear systems, American Institute of Physics, 1998
- [4] J. Güémez and M.A. Matias, Phys. Lett. A 181 (1993) 29
- [5] M.A. Matias and J. Güémez, Phys. Rev. Lett. 72 (1994) 1455
- [6] Marco Sandri, Numerical calculation of Lyapunov Exponents, University of Verona, Italy.
- [7] N.P. Chau, Controlling Chaos by period proportional pulses, Phys. Lett. A, 234 (1997), 193-197.
- [8] N. Das, R. Sharmah and N. Dutta, Period doubling bifurcation and associated universal properties in the Verhulst population odel, International J. of Math. Sci. & Engg. Appls. , Vol. 4 No. I (March 2010), pp. 1-14
- [9] T. Kapitaniak, Controlling Chaos – Theoretical and Practical Methods in Nonlinear Dynamics, Academic Press, New York, 1996.
- [10] T Basar “Systems & Control: Foundations & Applications “,University of Illinois at Urbana-Champaign.
- [11] T. K. Dutta and N. Das, Period Doubling Route to Chaos in a Two-Dimensional Discrete Map, Global Journal of Dynamical Systems and Applications, Vol.1, No. 1, pp. 61-72, 2001

A Distributed Canny Edge Detector and Its Implementation on FPGA

¹**Chandrashekar N.S.,² Dr. K.R. Nataraj**

¹Department of ECE, Don Bosco Institute of Technology, Bangalore.

² Department of ECE, SJB Institute of Technology, Bangalore.

Abstract

In this paper, we present a distributed Canny edge detection algorithm that results in significantly reduced memory requirements decreased latency and increased throughput with no loss in edge detection performance as compared to the original Canny algorithm. The new algorithm uses a low-complexity 8-bin non-uniform gradient magnitude histogram to compute block-based hysteresis thresholds that are used by the Canny edge detector. Furthermore, FPGA-based hardware architecture of our proposed algorithm is presented in this paper and the architecture is synthesized on the Xilinx Virtex 4 FPGA. The design development is done in VHDL and simulates the results in modelsim 6.3 using Xilinx 12.2.

Keywords: Canny Edge detector, Distributed Processing, Non-uniform quantization, FPGA.

1. Introduction

Edge detection is a very important first step in many algorithms used for segmentation, tracking and image/video coding. The Canny edge detector is predominantly used due to its ability to extract significant edges [1]. Edge detection, as a basic operation in image processing, has been researched extensively. A lot of edge detection algorithms, such as Robert detector, Prewitt detector, Kirsch detector, Gauss-Laplace detector and Canny detector have been proposed. Among these algorithms, Canny algorithm has been used widely in the field of image processing because of its good performance [2]. The Canny edge detector is predominantly used in many real-world applications due to its ability to extract significant edges with good detection and good localization performance. Unfortunately, the Canny edge detection algorithm contains extensive pre-processing and post-processing steps and is more computationally complex than other edge detection algorithms. Furthermore, it performs hysteresis thresholding which requires computing high and low thresholds based on the entire image statistics. This places heavy requirements on memory and results in large latency, hindering real-time implementation of the Canny edge detection algorithm [3]. Implementing image processing algorithms on reconfigurable hardware minimizes the time-to-market cost, enables rapid prototyping of complex algorithms and simplifies debugging and verification [4]. Edge detectors based on the first derivative do not guarantee to produce edge maps with continuous edge contours nor unwanted branches. Edge detectors based on the second derivatives, such as zero crossing; suffer from generating erroneous edges in textured images because of its high sensitivity to noise. Being an effective edge detector with single-pixel response, Canny operator has been widely used in accurately abstracting the edge information in image processing. However, taking its 4-step process into account, its real-time implementation based on CPU has become a significant problem, especially for the part of the edge tracing, which consumes a large amount of computing time. To solve the problem, GPU will be used for sake of its powerful ability of parallel processing while a new Canny operator is proposed with the introduction of parallel breakpoints detection and edge tracing without recursive operations [5]. The original Canny algorithm computes the higher and lower thresholds for edge detection based on the entire image statistics, which prevents the processing of blocks independent of each other [1]. In order to reduce memory requirements, decreased latency and increased throughput, a distributed canny edge detection algorithm is proposed in [1]. The hysteresis threshold calculation is a key element that greatly affects the edge detection results. In [3], it is proposed a new threshold selection algorithm based on the distribution of pixel gradients in a block of pixels to overcome the dependency between the blocks. However, in [1], the hysteresis thresholds calculation is based on a very finely and uniformly quantized 64-bin gradient magnitude histogram, which is computationally expensive and thereby, hinders the real-time implementation. In this paper, a method based on non-uniform and coarse quantization of the gradient magnitude histogram is proposed. In addition, the proposed algorithm is mapped onto reconfigurable hardware architecture. The threshold is calculated using the data of the histogram of gradient magnitude rather than is set manually in a failure-and-try fashion and can give quite good edge detection results without the intervening of an operator [6]. This improved new Canny algorithm is also implemented on FPGA (field programmable gate array) to meet the needs of real time processing.

This paper is organized as follows: Section 2 gives a brief overview of the original Canny edge detector algorithm. Section 3 presents the proposed distributed Canny edge detection algorithm which includes a novel method for the hysteresis thresholds computation based on a non-uniform quantized gradient magnitude histogram. The proposed hardware architecture and FPGA implementation algorithm are described in Section 4. Simulation results are presented in Section 5. A conclusion is given in Section 6.

2. Canny Edge Detector

The popular Canny edge detector uses the following steps to find contours presents in the image. The first stage is achieved using Gaussian smoothing. The resulting image is sent to the PC that sends it back to the gradient filter, but here we modified our gradient filter a bit because this time we don't only need the gradient magnitude that is given by our previous operator, but we need separately G_x and G_y . We also need the phase or orientation of our gradient which is obtained using the following formula:

$$\theta = \arctan \left[\frac{G_y}{G_x} \right]$$

As we can see, this equation contains an arctan and a division. These operators are very difficult to implement using hardware. We also don't need a high precision. The final θ has to give only one of the four following possible directions, as we can see in Figure 1. The fourth direction is the horizontal direction with zero degrees, not indicated in the figure.

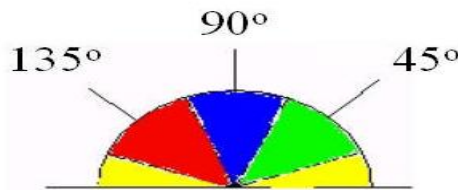


Figure 1: Possible Directions for the Gradient Phase

Arctan and the division can be eliminated by simply comparing G_x and G_y values. If they are of similar length, we will obtain a diagonal direction, if one is at least 2.5 times longer than the other, we will obtain a horizontal or vertical direction. After the edge directions are known, non-maximum suppression is applied. Nonmaximum suppression is used to trace pixels along the gradient in the edge direction and compare the values perpendicular to the gradient. Two perpendicular pixel values are compared with the value in the edge direction. If their value is lower than the pixel on the edge, then they are suppressed i.e. their pixel value is changed to 0, else the higher pixel value is set as the edge and the other two are suppressed with a pixel value of 0. Finally, hysteresis is used as a means of eliminating streaking. Streaking is the breaking up of an edge contour caused by the operator output fluctuating above and below the threshold. If a single threshold, T_1 is applied to an image, and an edge has an average strength equal to T_1 , then due to noise, there will be instances where the edge dips below the threshold. Equally it will also extend above the threshold making an edge look like a dashed line. To avoid this, hysteresis uses 2 thresholds, a high and a low. Any pixel in the image that has a value greater than T_1 is presumed to be an edge pixel, and is marked as such immediately. Then, any pixels that are connected to this edge pixel and that have a value greater than T_2 are also selected as edge pixels. If you think of following an edge, you need a gradient of T_2 to start but you don't stop till you hit a gradient below T_1 [7].

The original Canny algorithm [3] shown in Fig 2, consists of the following steps executed sequentially:

- Low pass filtering the image with a Gaussian mask.
- Computing horizontal and vertical gradients at each pixel location.
- Computing the gradient magnitude at each pixel location.
- Computing a higher and lower threshold based on the histogram of the gradients of the entire image.
- Suppressing non-maximal strong (NMS) edges.
- Computing the hysteresis high and low thresholds based on the histogram of the magnitudes of the gradients of the entire image.
- Performing hysteresis thresholding to determine the edge map.

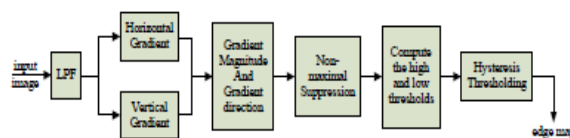


Figure 2: Block Diagram of the Canny Edge Detection

In our implementation, the architecture is synthesized on the Xilinx VIRTEX 4 FPGA. The results show that a 16-core architecture (3 X 3 block size for 256 X 256 image) leads to 16 times decrease in running time without performance degradation when compared with the original frame-based Canny algorithm.

3. Proposed Distributed Canny Edge Detection Algorithm

The superior performance of the frame-based Canny algorithm is due to the fact that it computes the gradient thresholds by analyzing the histogram of the gradients at all the pixel locations of an image. Though it is purely based on the statistical distribution of the gradient values, it works well on natural images which consist of a mix of smooth regions, texture regions and high-detailed regions [1]. Directly applying the frame-based Canny at a block-level would fail because such a mix of regions may not be available locally in every block of the frame. This would lead to excessive edges in texture regions and loss of significant edges in high detailed regions. The Canny edge detection algorithm operates on the whole image and has a latency that is proportional to the size of the image. While performing the original canny algorithm at the block-level would speed up the operations, it would result in loss of significant edges in high-detailed regions and excessive edges in texture regions. Natural images consist of a mix of smooth regions, texture regions and high-detailed regions and such a mix of regions may not be available locally in every block of the entire image. In [1], it is proposed a distributed Canny edge detection algorithm, which removes the inherent dependency between the various blocks so that the image can be divided into blocks and each block can be processed in parallel. The input image is divided into $m \times m$ overlapping blocks. The adjacent blocks overlap by $(L - 1)/2$ pixels for a $L \times L$ gradient mask. However, for each block, only edges in the central $n \times n$ (where $n = m + L - 1$) non-overlapping region are included in the final edge map. Steps 1 to 4 and Step 6 of the distributed Canny algorithm are the same as in the original Canny algorithm except that these are now applied at the block level. Step 5, which is the hysteresis high and low thresholds calculation, is modified to enable parallel processing. In [1], a parallel hysteresis thresholding algorithm was proposed based on the observation that a pixel with a gradient magnitude of 2, 4 and 6 corresponds to blurred edges, psycho visually significant edges and very sharp edges, respectively. In order to compute the high and low hysteresis thresholds, very finely and uniformly quantized 64-bin gradient magnitude histograms are computed over overlapped blocks. If the 64-bin uniform discrete histogram is used for the high threshold calculation, this entails performing 64 multiplications and $64 \times N_p$ comparisons, where N_p is the total number of pixels in an image. Therefore, it is necessary to find a good way to reduce the complexity of the histogram computation. As in [6], it was observed that the largest peak in the gradient magnitude histograms after NMS of the Gaussian smoothed natural images occurs near the origin and corresponds to low-frequency content, while edge pixels form a series of smaller peaks where each peak corresponds to a class of edges having similar gradient magnitudes. The proposed distributed thresholds selection algorithm is shown in Fig.3. Let G_t be the set of pixels with gradient magnitudes greater than a threshold t , and let N_{G_t} for $t = 2, 4, 6$, be the number of corresponding gradient elements in the set G_t . Using N_{G_t} , an intermediate classification threshold C is calculated to indicate whether the considered block is high-detailed, moderately edged, blurred or textured, as shown in Fig. 3. Consequently, the set $G_c = G_{t=C}$ can be selected for computing the high and low thresholds. The high threshold is calculated based on the histogram of the set G_c such that 20% of the total pixels of the block would be identified as strong edges. The lower threshold is the 40% percentage of the higher threshold as in the original Canny algorithm.

```

Let  $G_t$ : set of pixels with gradient magnitudes greater
        than a threshold  $t$ 
 $N_{G_t}$ : the number of elements in the set  $G_t$ 

Step 1: Determine  $G_t$  for  $t = 2, 4,$  and  $6$  and  $N_{G_t}$  for  $t = 2, 4, 6$ 
Step 2: If ( $N_{G_6} > 0.25 * \text{Total\_block\_pels}$ )
         $C = 6$  /*High-detailed*/
    else If ( $N_{G_4} > 0.05 * \text{Total\_block\_pels}$ )
         $C = 4$  /*moderately-edged*/
    else If ( $N_{G_2} < 0.25 * \text{Total\_block\_pels}$ )
         $C = 2$  /*blurred*/
    Else
        Exit; /*textured*/
Step 3: Compute the 8-bin non-uniform gradient magnitude
        histogram of  $G_c$  and the corresponding cumulative
        distribution function  $F(G_c)$ .
Step 4: Compute High_threshold as  $F(\text{High\_threshold}) = 0.8$ 
Step 5: Compute Low_threshold =  $0.4 * \text{High\_threshold}$ 
    
```

Figure 3: Pseudo-code of the proposed Distributed threshold Selection Scheme

We compared the high threshold value that is calculated using the proposed distributed algorithm based on an 8-bin non-uniform gradient magnitude histogram with the value obtained when using a 16-bin non-uniform gradient magnitude histogram. These two high thresholds have similar values. Therefore, we use the 8-bin non-uniform gradient magnitude histogram in our implementation.

4. Implementation Of The Proposed Distributed Canny Algorithm

In this section, we describe the hardware implementation of our proposed distributed canny edge detection algorithm on the Xilinx VIRTEX 4 FPGA . We provide a high-level architecture diagram as follows.

Architecture: Depending on the available FPGA resources, the image needs to be partitioned into q sub-images and each sub-image is further divided into $p \times m \times m$ blocks. The proposed architecture, shown in Fig. 4, consists of q processing units in the FPGA and some Static RAMs (SRAM) organized into q memory banks to store the image data, where q equals to the image size divided by the SRAM size.

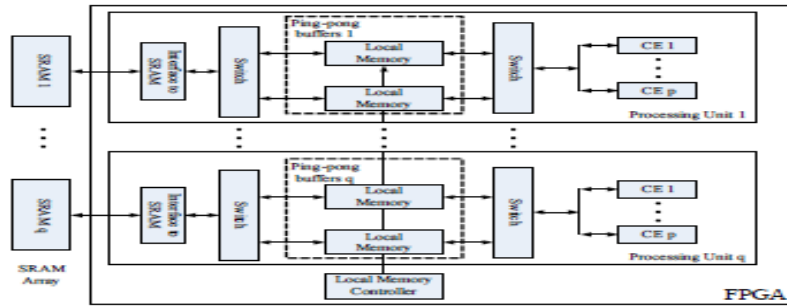


Figure 4: The Architecture of the proposed Distributed Canny Algorithm

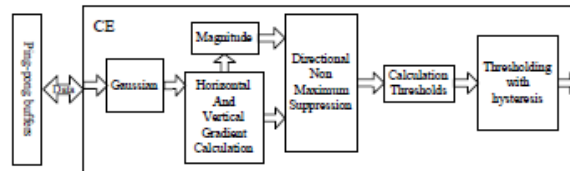


Figure 5: Block diagram of the CE (compute engine) for the proposed Distributed Canny edge Detection

Each processing unit processes a sub-image and reads/writes data from/to the SRAM through ping-pong buffers, which are implemented with dualport Block RAMs (BRAM) on the FPGA. As shown in Fig.4, each processing unit (PU) consists of p computing engines (CE), where each CE detects the edge map of an $m \times m$ block image. Thus, $p \times q$ blocks can be processed at the same time and the processing time for an $N \times N$ image is reduced, in the best case, by a factor of $p \times q$. The specific values of p and q depend on the processing time of each PE, the data loading time from the SRAM to the local memory and the interface between FPGA and SRAM, such as total pins on the FPGA, the data bus width, the address bus width and the maximum system clock of the SRAM. In our application, we choose $p = 2$ and $q = 8$. In the proposed architecture, each CE consists of the following 6 units, as shown in Fig.5:

1. Smoothing unit using Gaussian filter.
2. Vertical and horizontal gradient calculation unit.
3. Magnitude calculation unit.
4. Directional non-maximum suppression unit.
5. High and low threshold Calculation unit.
6. Thresholding with hysteresis unit.

5. Simulation Results And Analysis

Figure 6.shows the implementation software result and the FPGA implementation generated result. For the 256 X 256 camaramen image using the proposed distributed Canny edge detector with block size of 3 X 3 and a 3×3 gradient mask. The FPGA result is obtained using ModelSim.

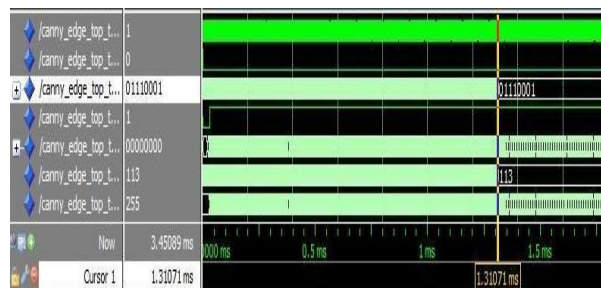


Figure 6: Simulation waveform for canny Edge Detection system



Figure 7: Comparison results of 256 X 256 camaramen image (a) Original image (b) Bluring image

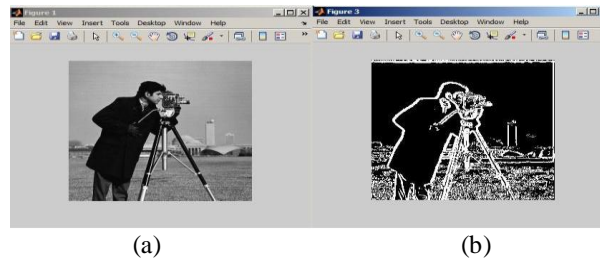


Figure 8: Comparison results of 256 X 256 camaramen image (a) original image and (b) Edge map image

6. Conclusion

We proposed a novel nonuniform quantized histogram calculation method in order to reduce the computational cost of the hysteresis threshold selection. As a result, the computational cost of the proposed algorithm is very low compared to the original Canny edge detection algorithm. The algorithm is mapped to onto a Xilinx Virtex-4 FPGA platform and tested using ModelSim. It is capable of supporting fast real-time edge detection for images and videos with various spatial and temporal resolutions including full-HD content. For a 100 MHz clock rate, the total processing running time using the FPGA implementation is 0.655 ms for a 256 X 256 image.

References

- [1] S. Varadarajan, C. Chakrabarti, L. J. Karam, and J. M. Bauza, "A Distributed psycho-visually motivated canny edge detector," IEEE ICASSP, pp. 822–825, Mar. 2010.
- [2] L. Torres, M. Robert, E. Bourennane, and M. Paindavoine, "Implementation of a recursive real time edge detector using Retiming techniques," VLSI, pp. 811–816, Aug. 1995.
- [3] Qian Xu, Chaitali Chakrabarti and Lina J. Karam, "A Distributed Canny Edge Detector and Its Implementation On FPGA", Tempe, AZ.
- [4] D. V. Rao and M. Venkatesan, "An efficient reconfigurable Architecture and implementation of edge detection algorithm Using Handle-C," ITCC, vol. 2, pp. 843–847, Apr. 2004.
- [5] Shengxiao Niu, Jingjing Yang, Sheng Wang, Gengsheng Chen, "Improvement and Parallel Implementation of Canny Edge Detection Algorithm Based on GPU".
- [6] W. He and K. Yuan, "An improved Canny edge detector and its Realization on FPGA," WCICA, pp. 6561–6564, Jun. 2008.
- [7] J. Canny, "A computational approach to edge detection," IEEE Trans. PAMI, vol. 8, no. 6, pp. 679–698, Nov. 1986.

Analytic Hierarchy Process for Evaluation Of Environmental Factors For Residential Land Use Suitability

V.D.Patil¹, R.N.Sankhua², R.K.Jain³

¹Research Scholar, Civil Engg Dept, Sinhgad College of Engg, Univ of Pune(India)

²Director, NWA,Pune,India

³Professor, Pad.Dr D.Y Patil Institute of Tech. and Engg, Pune, India

Abstract

An attempt has been endeavored in the Analytical Hierarchical Process of land use suitability for residential land uses of in conjunction with environmental factors Response using spatial technique for Pimpri-Chinchwad-Municipal Corporation (PCMC) area. This is just an amalgamation of a heuristic algorithm that provides good approximate, but not necessarily optimal solution to a given model in the area under consideration. To derive ratio scales from paired comparisons in employing such an algorithm, one may be able to precisely measure the 'goodness' of the approximation. In the present envisaged study, the environmental elements factors like Water availability, Flood line distance, Air pollution data, Water Quality Index and Distance of Waste disposal site affecting in the process are analytically and logically encompassed to make a gainful research through a scientifically proven method, which has been depicted in this present paper in a sequential manner.

KeyWords: Multi Criteria Decision Analysis (MCDA), Analytical Hierarchy Process (AHP), land-use suitability, environmental factors, Consistency Index(CI), Random Index (RI) , Consistency Ratio (CR)

1. Introduction

Land suitability assessment through environmental factors is an intrinsically complex multi-dimensional process, involving multiple criteria and multiple factors. Multi-criteria methods can serve as useful decision aids for carrying out the case. AHP has the flexibility to combine quantitative and qualitative factors, to handle different environmental groups of actors. Finally, the use of AHP is illustrated for a case study involving environmental impact. This is similar to choosing an appropriate location and the goal is to map a suitability index for the entire study area. It is the fundamental work and an important content of overall land use planning, which requires a scientific approach to guide development, avoid errors in decision-making and over-investment, for sustainable utilization of land resources [3],[15]it used map overlays to define homogeneous zones, and then they applied classification techniques to assess the residential land suitability level of each zone. These classification techniques have been based on Boolean and fuzzy theory or artificial neural networks. The processes of land use involve evaluation and grouping of specific areas of land in terms of their suitability for a defined use. The principles of sustainable development make land-use suitability analysis become increasingly complex due to consideration of different requirements/criteria [2].

2. STUDY AREA

As emerged from the defined objectives of the research, the study area has been chosen which encompasses the extent of latitude from 18°34'3.417"N to 18°43'22.033"N latitude and longitude 73°42'38.595" E to 73°56'2.726" E . The area lies within the domain of Pimpri-Chinchwad area of Maharashtra, India, as depicted in Figure 1. The area is situated in the climate zone of hills and plain, it is influenced by common effects of tropical monsoon climatic belt with the three distinct seasons. The annual average temperature is about 25°C. The average annual rainfall is about 600-700 mm, but is irregularly distributed. The maximum rainfall is observed in June-September. Pimpri-Chinchwad city, one of the fast growing medium size cities of Maharashtra with a population of about 1.7 million in 2011 (projected) and sprawling over an area of 174 sq. km.

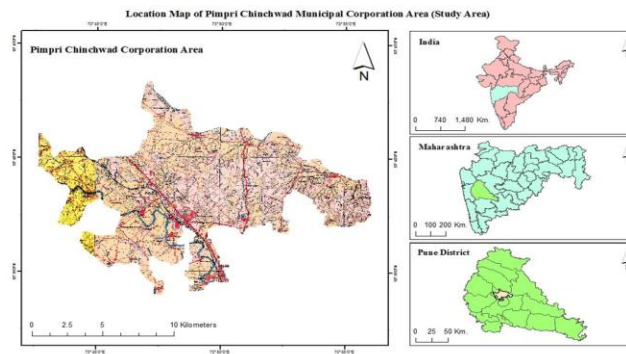


Fig.1. Study area.

3. EARLIER RESEARCH

The Analytic Hierarchical Process (AHP) is one of the methodological approaches that may be applied to resolve highly complex decision making problems involving multiple scenarios, criteria and factors [14]. Proposed in the 1970s by Thomas L. Saaty, it constructs a ratio scale associated with the priorities for the various items compared. In his initial formulation, conventional AHP, Saaty proposed a four-step methodology comprising modeling, valuation, prioritization and synthesis. At the modeling stage, a hierarchy representing relevant aspects of the problem (criteria, sub-criteria, attributes and alternatives) is constructed. The goal or mission concerned in the problem is placed at the top of this hierarchy. Other relevant aspects (criteria, sub-criteria, attributes, etc.) are placed in the remaining levels [1]. In the AHP method, obtaining the weights or priority vector of the alternatives or the criteria is required. For this purpose Saaty (1980) has used and developed the Comparison Method (PCM), which is explained in detail in next part of the work [5]. This study focuses on the utility of the AHP as a model for capturing expert knowledge on environmental systems where data may be lacking. The AHP method commonly used in multi-criteria decision making exercises was found to be a useful method to determine the weights, compared with other methods used for determining weights. When applying AHP, constraints are compared with each other to determine the relative importance of each variable in accomplishing the overall goal.

4. DATA USED AND METHODOLOGY

AHP is a comprehensive intuitive method for formulating and analyzing decisions. AHP has been applied to numerous practical problems in the last few decades [17]. Because of its intuitive appeal and flexibility, many corporations and governments routinely use AHP for making major policy decisions [3]. A brief discussion of AHP for environmental evaluation is provided in this text. More detailed description of AHP and application issues can be found elsewhere [14]. The Linear Imaging Self Scanner (LISS III) digital data of having spatial resolution of 23.5 m for April, 2008 and May, 2008 have been taken in conjunction with Aster Digital Elevation Model (DEM) data of 30 m resolution downloaded from Aster GDEM website. Analog and other ancillary data were collected from Survey of India Toposheets 47/F/14 and 47/F/10 of 1:50000 scales for Pimpri-Chinchwad-Municipal Corporation area and PCMC office.

Application of AHP to a decision problem involves four steps:

- i. Structuring of the decision problem into a hierarchical model.
- ii. Making pair-wise comparisons and obtaining the judgmental matrix.
- iii. Local priorities and consistency of comparisons.
- iv. Aggregation of local priorities

The entire methodology of the present work is focused on the application of AHP and GIS for land use suitability analysis for residential land use has been given below. The principal steps involved in the methodology are as follows:

- Raster map creation
- Geo-referencing
- Extraction of study area
- Preparation of various raster layers
- AHP and GIS analysis

TABLE 1: NINE-POINT WEIGHING SCALE FOR PAIR-WISE COMPARISON

Descriptions of preference	Scale
Equally	1
Equally to moderately	2
Moderately	3
Moderately to strongly	4
Strongly	5
Strongly to very Strongly	6
Very Strongly	7
Very Strongly to extremely	8
Extremely	9

After standardization all criteria and sub criteria were weighted using pair wise comparison method. An example of main criteria weighing is given in Table 2.

TABLE 2: WEIGHING MATRIX FOR MAIN CRITERIA

Criteria	Sub Criteria	Standards Adopted	Weight
Environmental Elements	Water Availability	> 4000	9
		3000 – 4000	6
		2000 – 3000	3
		1000 – 2000	2
		0 – 1000	1
	Flood Line Distance	> 400	9
		300 – 400	5
		200 – 300	2
		100 – 200	1
		0 – 100	Restrict ed
	Air Pollution Data	1	9
		2	5
		3	3
		4	2
		5	1
WQI	> 55.5	9	
	53.5 - 55.5	6	
	51.5 - 53.5	3	
	< 51.5	2	
	Distance From Waste Disposal Site	> 4000	9
	3000 – 4000	5	
	2000 – 3000	3	
	1000 – 2000	1	
	< 1000	1	

The three main AHP criteria such as selection, weighing and overly are described below.

A. Selecting Criteria

In this study criteria were selected using the literature reviews of internal and external references, interviewing the stakeholders.

B. Weighing of Criteria (Scale for pair wise comparison)

For determining the relative importance of criteria the pair-wise comparison matrix using Saaty's nine-point weighing scale were applied. In AHP, all identified factors are compared against each other in a pair wise comparison matrix which is a measure of relative importance/preference among the factors. Therefore, numerical

values expressing the relative preference of a factor against another. Saaty (1977) notes that suggested a scale for comparison consisting of values ranging from 1 to 9 which describe the intensity of importance, by which a value of 1 expresses equal importance and a value of 9 is given to those factors having an extreme importance over another factor as shown in Table 1 [7]. Then by using the information from table 1, the factors were pair wise compared. In order to compare criteria with each other, all values need to be transformed to the same unit of measurement scale (from 0 to 1), whereas the various input maps have different measurement units (e.g. distance maps, temperature etc.).

TABLE 3 :WEIGHING MATRIX FOR SUB CRITERIA OF AIR POLLUTION

Criteria	Sub Criteria	Standards Adopted	Weight
Air Pollution	SOx(%)	>70	9
		63-70	5
		55-63	3
		47-55	2
		<47	1
		>600	9
	SPM	472-600	5
		344-472	3
		216-344	2
		<216	1
		>67	9
		61-67	5
		55-61	3
		49-55	1
NOx	<49	1	

TABLE 4: NORMALIZED MATRIX FOR SUB CRITERIA OF AIR POLLUTION (NOX)

TABLE 8: FINAL SUITABILITY

Sr No	Level	Rank
1	Highly Suitable	5
2	Suitable	4
3	Moderately suitable	3
4	Slightly suitable	2
5	Unsuitable	1

It could be seen that for preventing bias thought criteriaweighting the Consistency Ratio was used.

$$C.I = \frac{\lambda_{max} - n}{n - 2} \quad (1)$$

$$C.R. = \frac{C.I.}{R.I.} \quad (2)$$

Where,

n= Number of items being compared in the matrix,

λ_{max} = Largest Eigen Value,

RI = Random Consistency Index

C. Overlaying

After weighing of criteria regarding their importance for land suitability analysis, all criteria maps were overlaid using suitability index.

Suitability Index, $SI = (RI * A1 * \Sigma RI.Bi * RI .KBi)$

$$+ (RI * A2 * \sum RI.Cy * RI.KCy) + (RI * AN * \sum RI.Dz * RI.KDz)$$

Where,

SI is the Suitability Index of each cells; N is the number of main criteria; RI, A1, RI, A2 ... R_N, A_N are the relative importance of the main criteria A1, A2 ... A_N, respectively; m, i and j are the number of sub criteria directly connected to the main criteria A1, A2 ... A_N, respectively. RIB, RIC and RID are the relative importance of sub criteria B, C and D directly connected to the main criteria A1, A2 ... A_N, respectively. RIKB, RIKC and RIKD are the relative importance of indicators category k of sub criteria B, C and D and main criteria A1, A2 ... A_N, respectively.

D. Calculation of score value for each criterion

The suitability value for water availability, flood hazards, air pollution, water quality index, waste disposal in Pimpri-Chinchwad area and the criterion for each land mapping unit is determined through the maximum limitation method that affects the land use. The above five representative natural physical characteristics are used in Environment response model and constitute the sub-criteria under Environment criteria. Before applying weighted linear combination equation to calculated suitability index, these calculated scores are standardized to the measured scale 9 (very high suitability), 7 (High), 5 (medium), and 1 (Low). All of the classifications and ranking values in spatial analysis are obtained according to some studies of Al-Shalabi et al. (2006), Kordi (2008) and based on visiting the study area.

E. Preparing of residential land suitability maps

After weighting the criteria, as regards the relative importance of each criterion as well as suitability index, all the criterion maps were overlaid and final residential land suitability map was prepared.

TABLE 5: SUITABILITY ACCORDING TO WATER AVAILABILITY (NORMALIZED MATRIX)

Class	< 200	200 - 400	400 - 600	600 - 800	> 800	Sum	PV	Score
<200	0.46	0.53	0.40	0.38	0.35	2.11	0.42	9.00
200 - 400	0.23	0.26	0.40	0.30	0.25	1.44	0.29	6.14
400 - 600	0.15	0.09	0.13	0.23	0.20	0.80	0.16	3.41
600 - 800	0.09	0.07	0.04	0.08	0.15	0.43	0.09	1.82
> 800	0.07	0.05	0.03	0.03	0.05	0.23	0.05	0.97

TABLE 6: SUITABILITY ACCORDING TO FLOOD LINE DISTANCE (NORMALIZED MATRIX)

Class	>400	300-400	200-300	100-200	0-100	Sum	PV	Score
>400	0.56	0.64	0.52	0.43	0.36	2.51	0.50	9.00
300-400	0.19	0.21	0.31	0.31	0.28	1.30	0.26	4.66
200-300	0.11	0.07	0.10	0.18	0.20	0.67	0.13	2.40
100-200	0.08	0.04	0.03	0.06	0.12	0.34	0.07	1.21
0 - 100	0.06	0.03	0.02	0.02	0.04	0.17	0.03	0.62

Suitability maps resulting from multi-criteria evaluation (MCE) and multi-objective land allocation have shown different classes for which the degree of sensitivity to accept new building for example residential estates and urban settlements vary from extremely prone areas to weakly prone. Based on relative weights of the suitability factors for development, suitability ranges were identified as shown in Table 8. Figure 2 depicts the final map (suitability map), which divided to 5 best areas in increasing order are : 1, 2, 3, 4 and 5 and are shown in different colours.

TABLE 7: SUITABILITY ACCORDING TO AIR POLLUTION ZONE (NORMALIZED MATRIX)

Class	5	4	3	2	1	Sum	Priority Factor	Score
5	0.51	0.63	0.47	0.38	0.32	2.30	0.46	9.00
4	0.17	0.21	0.35	0.30	0.26	1.29	0.26	5.00
3	0.13	0.07	0.12	0.23	0.21	0.75	0.15	3.00
2	0.10	0.05	0.04	0.08	0.16	0.43	0.09	2.00
1	0.09	0.04	0.03	0.03	0.05	0.23	0.05	1.00

TABLE 8 : SUITABILITY ACCORDING TO WATER QUALITY INDEX – (NORMALIZED MATRIX)

Class	>56.5	55.5-56.5	54.75-55.75	52.75-54.75	< 52.75	Sum	PV	Score
>56.5	0.56	0.64	0.52	0.43	0.36	2.51	0.50	9.00
55.5-56.5	0.19	0.21	0.31	0.31	0.28	1.30	0.26	5.00
54.75-55.75	0.11	0.07	0.10	0.18	0.20	0.67	0.13	3.00
52.75-54.75	0.08	0.04	0.03	0.06	0.12	0.34	0.07	1.00
< 52.75	0.06	0.03	0.02	0.02	0.04	0.17	0.03	1.00

TABLE 9 : SUITABILITY ACCORDING TO WASTE DISPOSAL (NORMALIZED MATRIX)

Class	>4000	3000-4000	2000-3000	1000-2000	0-1000	Sum	PV	Score
> 4000	0.56	0.64	0.52	0.43	0.36	2.51	0.50	9.00
3000 - 4000	0.19	0.21	0.31	0.31	0.28	1.30	0.26	4.66
2000 - 3000	0.11	0.07	0.10	0.18	0.20	0.67	0.13	2.40
1000 - 2000	0.08	0.04	0.03	0.06	0.12	0.34	0.07	1.21
0 - 1000	0.06	0.03	0.02	0.02	0.04	0.17	0.04	0.62

TABLE 10: FINAL SUITABILITY ACCORDING TO ENVIRONMENTAL FACTORS (RECIPROCAL MATRIX)

Class	W	F	A	WQ	WD	Sum	Priority Vector	Score
Water Avail	0.54	0.64	0.47	0.43	0.36	2.44	0.49	9.00
Flood	0.18	0.21	0.35	0.31	0.28	1.33	0.27	4.91
Air Pollu.	0.14	0.07	0.12	0.18	0.20	0.71	0.14	2.61
WQI	0.08	0.04	0.04	0.06	0.12	0.34	0.07	1.26
Waste Disp.	0.06	0.03	0.02	0.02	0.04	0.17	0.03	0.64

The following results emerged out of the present study:

- The area of interest has been classified in to nine using supervised algorithm and different suitability classes are obtained.
- The criteria used are water availability, flood line distance, air pollution data, water quality index and distance of waste disposal site (5classes each) and their combined effect map is shown in figure no 2 illustrating the suitability of the area. These results are based on the data received and accordingly results are drawn .
- AHP used hierarchical structures for nine scales with the Environmental criteria, and were devised for the designof AHP applicability for residential land use suitability .

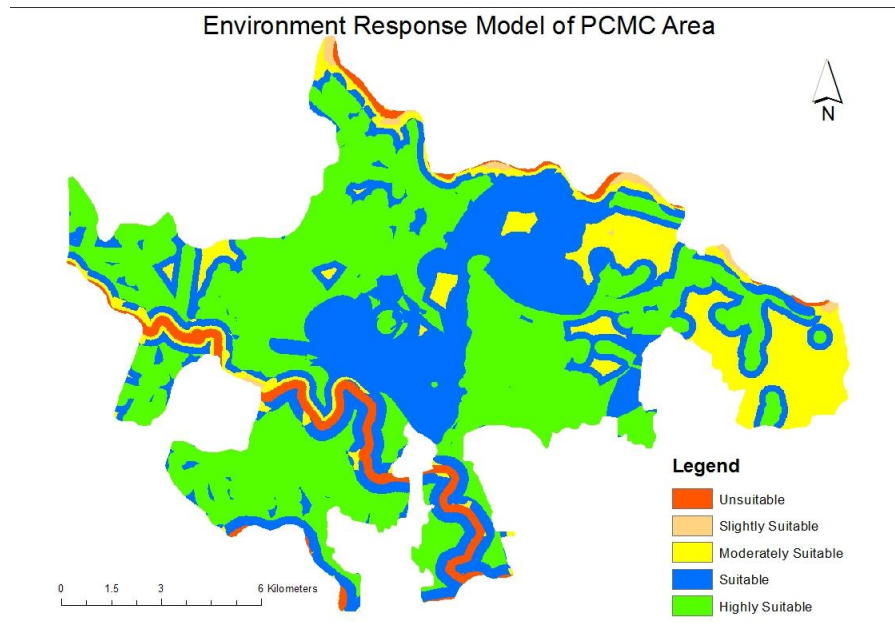


Fig.2 Final suitability map

The AHP was devised for all the sub criteria, evaluating their relative scores for attribute classes together with the environment response model and residential land use suitability for PCMC area.

5. CONCLUSIONS

The analysis of this study mainly focused on highly suitable areas as these areas have the highest potential for construction purposes, i.e. residential land use. We applied the AHP model to land use suitability analysis based on five criteria layers. The Analytic Hierarchy Process (AHP) method was found to be a useful method to determine the weights, compared with other methods used for determining weights. The sensitivity utility of the model helped to analyze the decision before making the final choice. The AHP method could deal with inconsistent judgments and provided a measure of the inconsistency of the judgment of the respondents, so it is superior. This assessment is useful for land use decision-making and urban development of the PCMC area. This is very important for planners to decide whether land should be developed or conserved. This application can also help to consider the strategic urban land development framework and the short-term land use policies can also be formulated. The approach, therefore, would help to monitor urban land development for the planners and policy makers for formulating urban growth policies and strategies of the city.

REFERENCES

- [1] Altuzarra, A., María, J. & Jiménez, M. Salvador, M. (2007). A Bayesian prioritization procedure for AHP-group decision making. *EurJOper Res.*, v.182, No(1), pp. 367-382.
- [2] Duc, T.T. (2006). Using GIS and AHP technique for land-use suitability analysis. *International Symposium on Geoinformatics for Spatial Infrastructure Development in Earth and Allied Sciences.*
- [3] Elkarni, F. and Mustafa, I. (1993). Increasing the utilization of solar energy technologies (SET) in Jordan: Analytic Hierarchy Process. *Energy Policy* **21**, 978–984.
- [4] Hall, G.B. Wang, F. Subaryono. (1992). Comparison of Boolean and fuzzy classification methods in land suitability analysis by using geographical information systems. *J. Environ. Planning.*, V.4, No. 24, pp. 497–516.
- [5] J. Chen, Y. & Wu, J.P. (2009). Cellular automata and GIS based land use suitability simulation for irrigated agriculture. *18th World IMACS / MODSIM Congress, Cairns, Australia* 13.
- [6] Kordi, M. (2008). Comparison of fuzzy and crisp analytic hierarchy process (AHP) methods for spatial multicriteria decision analysis in GIS. Master. Thesis, University of Gavle.

- [7] M. Bagheri, Z. Z. Ibrahim, W. N. A. Sulaiman and N. Vaghefi (2011) Integration of Analytical Hierarchy Process and Spatial Suitability Analysis for Land Use Planning in Coastal Area, published in, "The proceedings of the first Iranian Students Scientific Conference in Malaysia.
- [8] Marinoni, O., (2004). Implementation of the analytical hierarchy process with VBA in ArcGIS, *J Comput Geosci*, 30(6): 637–646
- [9] Saaty, T. L. (1980). The analytic hierarchy process. Polytechnic University of Hochiminh city, Vietnam McGraw-Hill, New York.
- [10] Saaty, T. L. (1988). Multi criteria Decision Making: The Analytical Hierarchy Process. RWS Publications, Pittsburgh, PA.
- [11] Saaty, T. L. (1990). An exposition on the AHP in reply to the paper 'remarks on the analytic hierarchy process. *Manag. Sci.*, 36, 259–268,
- [12] Saaty, T. L. (1994). Highlights and critical points in the theory an application of the analytic hierarchy process. *Eur. J. Oper. Res.*, 74, 426–447.
- [13] Saaty, T. L. (1995). Decision Making for Leaders: The Analytic Hierarchy Process for Decisions in a Complex World. 3d ed. RWS Publications, Pittsburgh, PA.
- [14] Saaty, T. L. (2000). Fundamentals of Decision Making and Priority Theory with the Analytic Hierarchy Process. Pittsburg: RWS Publications.
- [15] Saaty, T.L., (1977). A scaling method for priorities in hierarchical structures. *J. Math Psycho.*, 15: 231-281.
- [16] Saaty, T.L., (1980). The Analytic Hierarchy Process. McGraw-Hill, New York., pp. 20-25.
- [17] Shim, J. P. (1989). Bibliographical research on the analytic hierarchy process (AHP). *Socio-Economic Planning Sciences* 23, 161–167.
- [18] Wang, F. (1994). The use of artificial neural networks in a geographical information system for agricultural land-suitability assessment. *Environment and planning A.*, No.26, pp. 265–284.

Steganography With Data Integrity

Deepali

Department of Computer Science and Engineering
PEC University of Technology
, Chandigarh

Abstract

Steganography is the technique of hiding private or sensitive information within something that appears to be nothing out of the usual. Steganography is often confused with cryptology because the two are similar in the way that they both are used to protect important information. The difference between the two is that Steganography involves hiding information so it appears that no information is hidden at all. In this paper, we describe method of Steganography based on embedding encrypted message bits using RSA Algorithm in the 1st least significant (LSB Technique) and last 4 significant bits (Modulus 4 bit technique) of the pixel of image. Here we also provide integrity using MD5 hash algorithm. The analysis shows that the PSNR is improved in the case of LSB technique. Use of hash algorithm provides data integrity.

Keywords:Data integrity, LSB technique, MD5 Hash Algorithm, Modulus 4 bit algorithm, PSNR, RSA Algorithm, Steganography

1. Introduction:

Steganography is the technique of writing hidden messages in such a way that no one apart from the intended recipient knows of the existence of the hidden message. It is taken from Greek word “STEGANOS” which means “Covered” and “GRAPHIE” which mean “Writing”. So, Steganography is a method of covering important information behind an image. Steganography ancient origins can be traced back to 440 BC, from the Histories of Herodotus. Demeratus sent a warning about a forthcoming attack to Greece by writing it on a wooden panel and covering it in wax. During World War 2 invisible ink was used to write information on pieces of paper so that the paper appeared to the average person as just being blank pieces of paper. Liquids such as milk, vinegar and fruit juices were used, because when each one of these substances are heated they darken and become visible to the human eye. It is not a rule that we must hide data in image files only; we can also hide data in MP3 and Video files too. When hiding information inside images the LSB (Least Significant Byte) method is usually used. When hiding information inside Audio files the technique usually used is low bit encoding which is somewhat similar to LSB that is generally used in Images. The problem with low bit encoding is that it is usually noticeable to the human ear, so it is a rather risky method for someone to use if they are trying to mask information inside of an audio file. Spread Spectrum is another method used to conceal information inside of an audio file. This method works by adding random noises to the signal, the information is concealed inside a carrier and spread across the frequency spectrum. When information is hidden inside video the program or person hiding the information will usually use the DCT (Discrete Cosine Transform) method. Steganography in Videos is similar to that of Steganography in Images, apart from information is hidden in each frame of video. When only a small amount of information is hidden inside of video it generally isn't noticeable at all, however the more information that is hidden the more noticeable it becomes. So Steganography in Images is preferred.

2. Related Work:

2.1 Ls b Insertion Method

The least significant bit insertion method is probably the most well known image Steganography technique. It is a common, simple approach to embed information in a graphical image file. Unfortunately, it is extremely vulnerable to attacks, such as image manipulation. A simple conversion from a GIF or BMP format to a lossy compression format such as JPEG can destroy the hidden information in the image. When applying 4LSB techniques to each bytes of a 8-bit image, one bit can be encoded to each pixel. Any changes in the pixel bits will be indiscernible to the human eye. The main advantage of 4LSB insertion is that data can be hidden in the last four least significant bits of pixel and still the human eye would be unable to notice it. Care needs to be taken in the selection of the cover image, so that changes to the data will not be visible in the stego-image.

2.2 RSA Algorithm:

Encrypting using RSA, we encrypt our data that is hidden in an image. Hackers can not identify hidden data in images easily and at most they can get encrypted data from images which will not reveal any confidential information.. Care should be taken during the selection of prime numbers, so that hacker will not able to reveal key to decrypt.

2.3 MD5 Algorithm:

MD5 algorithm provides data integrity. Message digest is sent along encrypted data which is hidden in image. At receiver side, receiver first get data from image, decrypt it and then find message digest using same algorithm and compare it with original message digest. If they are same, data isn't tempered. Hence data integrity is maintained.

3. Implementation:

The proposed work provides data integrity using hash algorithm MD5. We create message digest that is sent along encrypted data. This digest is hidden in image. At receiver side, receiver first get data from image, decrypt it and then find message digest using same algorithm and match with original message digest. The challenge in this work was to find a way to camouflage a secret message in an image without perceptible degrading the image quality and to provide confidentiality and data integrity that make man-in-middle attack difficult. Therefore, we applied a encryption using RSA algorithm and MD5 hash algorithm. The main idea of this method is to utilize least significant bit or modulus 4 significant bits of a cover image to hide message bits. This approach is illustrated in details in the following four steps (algorithm):

- Step 1: Applying RSA encryption using sender's private key

Here sender and receiver generate their public and private keys using RSA algorithm and save in file. Then message bits are encrypted with sender's private key using RSA encryption $c = m^c \pmod{n}$. We do this encryption to provide authentication that data is sent by intended user because intended user know his private key.

- Step 2: Applying RSA encryption using receiver's public key

Here encrypted message is again encrypted with receiver's public key using RSA encryption

$c = m^c \pmod{n}$. We do this encryption to provide confidentiality that data is not read by any intruder without knowing private key.

- Step 3: Applying hash algorithm

Here original message is hashed with MD5 algorithm to create message digest that is sent along encrypted message to provide data integrity.

- Step 4: Embedding encrypted message bits and message digest

In this step, encrypted message bits are embedded one by one in image either at least significant bit or last four bits. In the first row of image we hide the size of our message that has to hide so, that we receiver can easily recover the message by knowing his private key. And from 2nd row data is hidden and a stego image is produced.

At receiver end data is extracted from stego image and decrypted by receiver's private key and then with sender's public key and after that message digest is created. If message digest matches with original message digest then data is not tempered and accepted.

4. Analysis

The obtained results of the experiments are summarized in the following Table 1.1 which shows PSNR of the different image categories (mountains, pokemon, dog, monkey, laptop, tree) that conceal same message. Table shows that for all type of images LSB technique has high PSNR value than modulus 4 bit technique. It means LSB causes less degradation in cover image than modulus 4 bit. From images shown below original and stego images cant be differentiated but magnified histogram of images shows that LSB is more closer to original image than modulus 4 bit and it ensures data integrity.

TABLE 1.1

IMAGE TYPE	LSB (PSNR Value)	MODULUS 4 BIT (PSNR Value)
Mountain	78.5481	64.0353
Pokemon	66.5931	52.0803
Dog	66.7186	52.0888
Monkey	66.7001	52.5743
Laptop	66.7514	50.3696
Tree	73.8528	58.8528



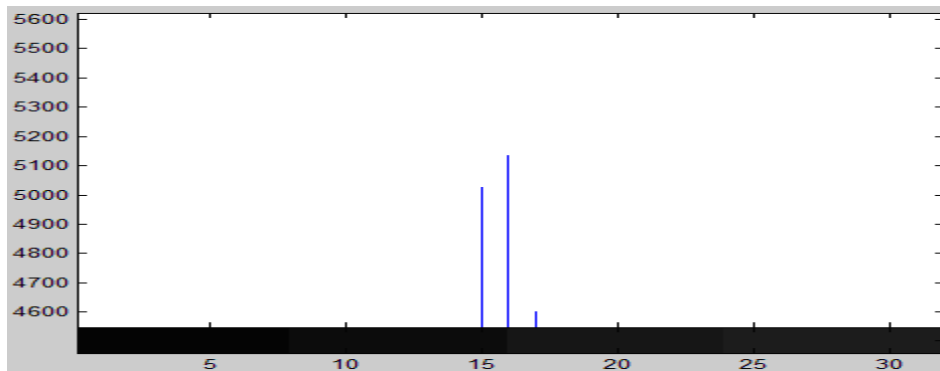
LSB Image



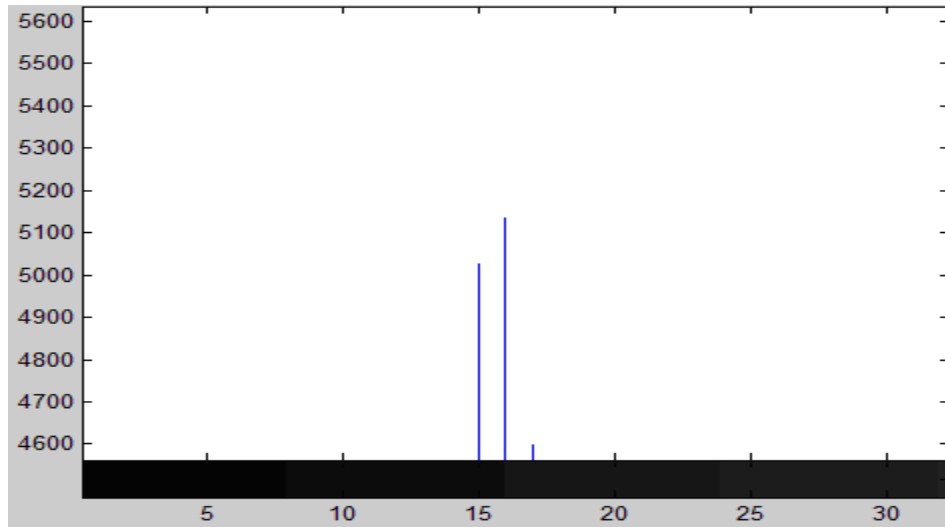
Modulus 4 Image



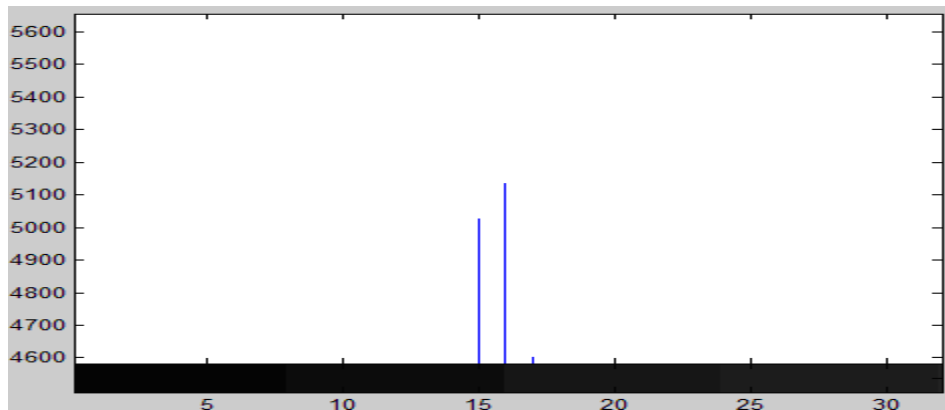
Original Image



Modulus 4 Histogram



LSB Histogram



Original Histogram

References

- [1] Beenish Mehboob and Rashid Aziz Faruqi "A Steganography Implementation" in 2008 IEEE
- [2] Nedal M. S. Kafri¹ and Hani Y. Suleiman Bit-4 of Frequency Domain-DCT Steganography Technique in 2009 IEEE
- [3] Ismail Avcibas N.M. and B. Sankur, "Steganalysis using image quality metrics", In *IEEE Transactions on Image Processing*, vol. 12, No. 2., February 2003.
- [4] M. S. Sutaone, M.V. Khandare "Image Based Steganography Using LSB Insertion Technique"
- [5] Swati Tiwari¹, R. P. Mahajan² "A Secure Image Based Steganographic Model Using RSA Algorithm and LSB Insertion" in *International Journal of Electronics Communication and Computer Engineering* Volume 3, Issue 1, ISSN 2249 –071X

Estimation of Word Recognition by Using Back-Propagation Neural Network

Pin-Chang Chen¹, Hung-Teng Chang², Li-Chi Lai³

¹ Assistant Professor, Department of Information Management, Yu Da University, Miaoli, Taiwan, R.O.C.

² Assistant Professor, Department of Information Management, Yu Da University, Miaoli, Taiwan, R.O.C.

³ Teacher, Linsenes Elementary School, Miaoli, Taiwan, R.O.C.

Abstract:

In recent years, the studies on literacy and reading have been taken seriously. A lot of researchers mention that the key factor to improve the students' reading ability is word recognition. If teachers realize the ability of students' vocabulary, they can use remedial teaching to help the sub-standard students. This study uses the back-propagation neural network to establish an experimental model. The comparison of the literacy estimated results between the back-propagation neural network and the traditional statistical method is verified. This study proves that the back-propagation neural network has good credibility and extension, as well as the estimated results can be taken as the classified basis on students' literacy.

Keywords: Word Recognition, Reading Ability, Back-Propagation, Neural Network, Vocabulary Volume.

1. Introduction

Literacy is the foundation of reading and writing. If learners lack literacy skills or have a literacy problem, their future reading and learning may be both affected. They may waste a lot of time during reading and thus fail to engage in effective learning or affect their learning achievement [1]. Consequently, if the literacy skills children should possess can be understood, it is possible to provide the children who fail to meet the standard with remedial teaching. As a result, the test on vocabulary volume is particularly important. At present, there is no consistent estimation method used for assessing vocabulary volume in Taiwan. The difference in the chosen tools tends to lead to significant difference in estimation results. Therefore, it is a necessary procedure to use a standardized test for data identification or diagnosis [2]. However, a formal assessment is required for performing screening or growth monitoring. Taking vocabulary volume for example, if there is a test on vocabulary volume for a teacher can perform, calculate the score and perform several assessments within a year without spending too much time or disclosing its content, the objective of performing screening and growth monitoring can be achieved [3]. The studies concerning vocabulary volume in Taiwan are mainly qualitative studies which seldom investigate statistical method for estimating vocabulary volume [4]. Artificial neural network is capable of learning and memorizing the inputs to the outputs, and back-propagation neural network is the most representative model commonly in practice. It is a supervisory learning network and is thus applicable to the application of diagnosis and prediction. Back-propagation neural network has been comprehensively applied to various fields. In recent years, it has frequently been applied to the financial prediction of stocks and futures. The purpose of this study was to use artificial neural network to predict vocabulary volume and to compare the result to the prediction result of vocabulary volume using traditional statistical method, as well as to verify that artificial neural network can be comprehensively promoted. Moreover, because artificial neural network possesses good learning and memory models, as the variables input in the network are increased or decreased, the target value can be calculated through the training of artificial neural network model. Therefore, it can be provided as an alternative estimation tool.

2. Problem Statement

The subjects of this study were elementary school students in a remote area in Miaoli County, Taiwan. Because grade 1 and 2 students are still at the stage of word decoding and recognition, this study selected grade 3 to 6 students as the subjects. To obtain more data, the first vocabulary volume test was performed on 46 grade 3 to 6 students in the second semester of 2010 academic year where the total sample size was 46. The second vocabulary volume test was performed on 37 grade 3 to 6 students in the first semester of 2011 academic year where the total sample size was 37. That is, the total sample size in this study was 83. The main purpose of this study was to investigate and compare the difference in the estimated vocabulary volume using artificial neural network and that using traditional statistical method. This study used the Self-edited Vocabulary Estimation Test compiled by Professor Jun-Ren Li [5] as the traditional statistical method to perform a test on vocabulary volume. The test results were input into the calculation template of Excel, and formula were used to calculate the estimated vocabulary volume. As for the application of artificial neural network, back-propagation neural network software Alyuda NeuroIntelligence was used to input the aforesaid result of vocabulary volume as the input value. The experimental model was established based on data training and

the output target value was the estimated vocabulary volume. This study compared the results of vocabulary volumes obtained from these two methods to verify that the neural network can be comprehensively applied.

3. Self-Edited Vocabulary Estimation Test

In 2010, Professor Jun-Ren Li at Department of Educational Psychology and Counseling, National Taiwan Normal University edited a test based on 5,021 word bank of Survey Report on Commonly Used Words by Elementary School Students issued by National Languages Committee (2002), classified words into three groups for random selection according to word frequency, and selected a total of 60 words as the test content. The test method was explained as follows:

3.1. Method for performing the test:

The test was performed on individuals one-on-one where the researcher read the test questions and the students verbally answered questions.

3.2. Time of the test:

The time of the test was not restricted, and there was no need to count the time. In general, it was estimated that each student could complete the test within 15 minutes.

3.3. Test method:

The students were requested to look at the test questions from the left to the left and from the top to the bottom and to make phrases for the words they knew in order. The students were all requested to answer the questions on the target words in the form of "X of XX." For example, for target word "affection," students should answer "affection of emotional affection." The students would be provided with examples before the initiation of the test to enable them to fully understand how to answer questions.

3.4. Scoring Principles:

- (1) When a student makes a phrase or is able to point out the correlation, the answer will be deemed right.
- (2) When a student fails to make a phrase or sentence, the answer will be deemed wrong and no score will be given.
- (3) Two-word phrases, three-word phrases or proverbs are all acceptable. For example, dragon boat "racing."
- (4) Names of people, such as Yat-Sen "Sun" will be deemed right.
- (5) Buzzwords, such as having had "enough," will be deemed right as long as they are used correctly.
- (6) Misidentification of target words will be deemed wrong. For example, for the target word "special," students answering "very of very special;" for the target word "health," students answering "very of very health." Such confusion will be deemed wrong.

3.5. Scoring method:

60 target words in the test were classified into three groups with the marks of ○, Δ, and □ at the bottom of Chinese letters. The number of correct phrases made would be in each group would be recorded in the score field at the bottom of record form.

3.6. Calculation of results:

The test results were input into the calculation template of Excel, and a formula was used to calculate the estimated vocabulary volume. The calculation formula was as follows:

$$(\circ \text{ Number of correct answers} \times 1500 \div 24) + (\Delta \text{ Number of correct answers} \times 1500 \div 24) + (\square \text{ Number of correct answers} \times 2000 \div 12) = \text{Estimated vocabulary volume} \quad (1)$$

4. Back-propagation Neural Network

Back-propagation neural network is the most representative model of comprehensive application among current artificial neural networks. Data training was used to establish the system model, and the system model could be applied to estimation, prediction, or diagnosis [6]. This study used back-propagation neural network to establish the experimental model and used the artificial neural network software Alyuda Neuro Intelligence to conduct the experiment. The procedures for establishing the model of artificial neural network were as follows [7]:

4.1. Data analysis:

This study collected data and transformed them into matrices to facilitate the input into the artificial neural network. In addition, the factors affecting estimation results were analyzed to determine the input value. The number of correct answers of the three groups ○, Δ, and □ (test results of vocabulary volume) were used as input variables.

4.2. Data pre-processing:

The analyzed data were processed. The data of input layer were reflected to $[-1, 1]$, and that of output layer were reflected to $[0, 1]$.

4.3. Designing the framework of artificial neural network:

It was very important to set up various parameters in the model of artificial neural network. The use of inadequate settings would lead to difficulty in convergence and early termination of network. The parameters required to be set up in the back-propagation neural network were as follows [8]:

- (1) Number of hidden layers: in general, the convergence effect of one or two layers would be better. The excessive number of layers would lead to poor convergence effect. The lack of hidden layer would lead to the failure to reflect how units interact and affect one another, leading to larger error.
- (2) Number of hidden layer processing units: there was no specific criterion on the number.
- (3) Other parameters: e.g. learning rate, convergence target value, number of training cycles, etc. It was extremely hard to find out a universal principle for setting up artificial neural network under different circumstances. Therefore, this study used trial-and-error approach to test various parameters in an attempt to find out the optimal parameter combination.

4.4. Training artificial neural network:

The artificial neural network was operated by constantly adjusting weight values and threshold values through training. The optimal solution calculated by network would be used as target output.

4.5. Testing and analyzing performance:

This procedure made it possible to compare the difference between estimated value and actual value. Moreover, the accuracy could be understood based on correlation graphs. If the difference between training results was too large, procedures 1 to 4 should be repeated for training.

4.6. Assessment and verification:

The artificial neural network completing the training could be used to predict new cases. This study used the results of 20 vocabulary volume at other schools as test data to verify the accuracy of network and to amend it again.

5. Simulation Results

This study obtained a total of 83 effective sample data from Self-edited Vocabulary Estimation Test, and used the artificial neural network software Alyuda NeuroIntelligence to conduct the experiment.

5.1. Data analysis:

Vocabulary volume \circ , vocabulary volume Δ , and vocabulary volume \square were used as dependent variables of input layer, while estimated vocabulary volume was used as the independent variable of output layer. After 83 data were arranged in order, the first 57 data were the training data for training the artificial neural model, 13 data were used as verification data, and 13 data were used as testing data.

5.2. Data pre-processing:

The input and output data used in this model were processed. The data of the input layer were reflected to $[-1, 1]$, and that of the output layer were reflected to $[0, 1]$.

5.3. Designing the framework of artificial neural network:

The parameters were different under different circumstances. After the testing, this study found that the optimal number of neurons of input layer was 3, the optimal number of neurons of hidden layer was 5, and the optimal number of hidden layers was 1, as shown in Figure 1.

5.4. Simulation training:

Seven algorithms could be used in the training model, and there was no significant difference among them. The users could choose the proper one according to the characteristics of the questions. After the testing, this study chose Limited Memory Quasi-Newton, the most effective one, and set up the number of training cycling as 500 times. After the simulation training was completed, the optimal convergence effect was achieved, as shown in Figure 2.

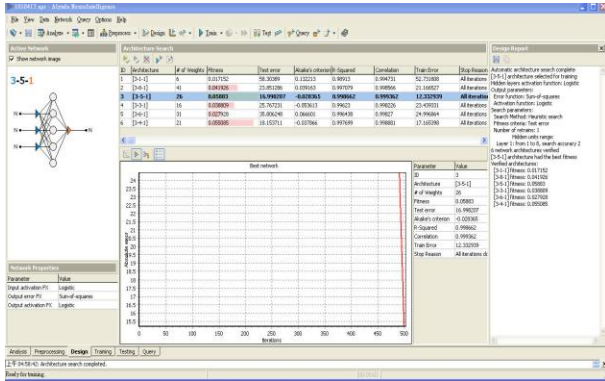


Fig. 1. Neural Network Architecture

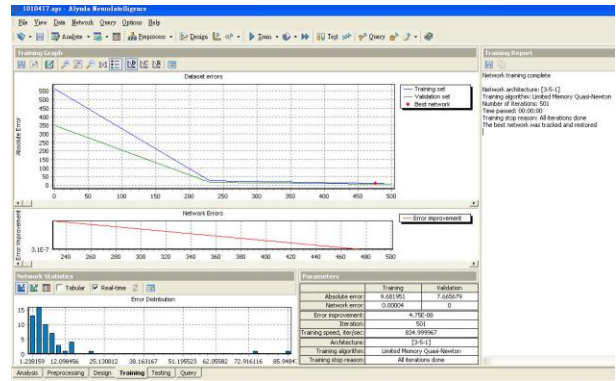


Fig. 2. Simulation Training

5.5. Testing and analyzing performance :

After the testing was completed, the comparison between the estimated values and actual values and result assessment were shown in Figure 3. According to the results, the comparison between the estimated value and actual value showed that the correlation was 0.999484, R-squared was 0.99845, and the error was small. The correlation was highly positive, suggesting that the vocabulary volume estimation model established in this study was feasible and accurate.

5.6. Assessment and verification:

This study obtained 20 vocabulary volume test results from other school as the testing data to verify the artificial neural network which completes the verification training can be used to predict new cases. The verification results showed that its predication was accurate and could be used for estimation of vocabulary volume, as shown in Figure 4.

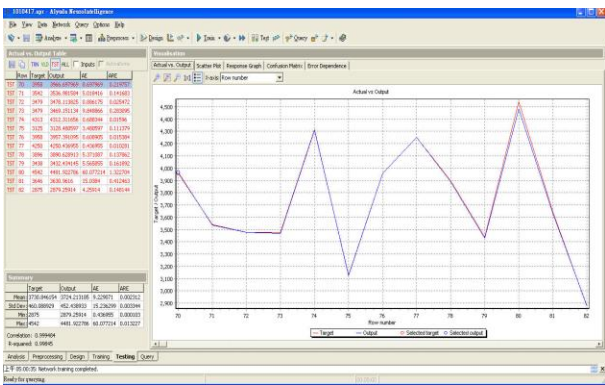


Fig. 3. Estimated Values and Actual Values

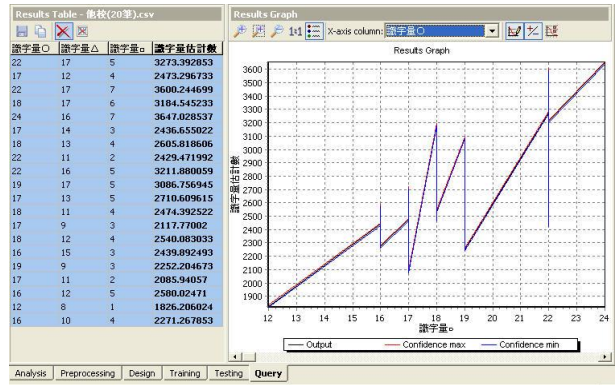


Fig. 4. Assessment and Verification

6. Conclusion

According to the simulation results of this study, 83 test results of vocabulary volume estimation of grade 3 to 6 students at Linsenes elementary school in Miaoli County were used as input values. With the training and learning of artificial neural network, the experimental model was established. Through simulation training, 20 data obtained from other elementary schools were used for verification to prove that the estimated results of artificial neural network were reliable. Comparing to the calculation template established by vocabulary volume estimation test using traditional statistical method, the error of output value from the model established by back-propagation neural network was extremely small, verifying that artificial neural network could be comprehensively applied to various estimations and predictions and be provided as an alternative as estimation tool. Moreover, artificial neural network possessed good learning and memory models. As other variables were decreased or increased, artificial neural network could replace the original statistical method to achieve great prediction effect.

References

- [1] H. Catts, S. Adlof and S.E. Weismer. Language Deficits in Poor Comprehenders: A Case for the Simple View of Reading, *JSLHR*, Volume 49, pp. 278-293, 2006.
- [2] R.P. Carver. Predicting Reading Levels in Grades 1 to 6 From Listening Level and Decoding Level: Testing Theory Relevant to the Simple View of Reading, *Reading and Writing: An Interdisciplinary Journal*, Volume 10, pp. 121-154, 1997.
- [3] A. Lin, D.M. Podell and N. Rein. The Effects of CAI on Word Recognition in Mildly Mentally Handicapped and Nonhandicapped Learner, *Journal of Special Education Technology*, Volume 11, Issue 1, pp. 16-25, 1991.
- [4] I. Mullis, M.O. Martin, A.M. Kennedy and F. Pierre. PIRLS 2006 International Report: IEA's Progress in International Reading Literacy Study in Primary Schools in 40 Countries, *TIMSS & PIRLS*, International Study Center, Chestnut Hill, MA: Boston College, 2007.
- [5] J.R. Li. Phonological Awareness and Chinese Character Acquisition in Taiwan Children: A Reading Ability Control Design Research, Paper presented at the International Symposium on Cognitive Processes of Chinese Language, University of Hong Kong, Hong Kong, 1997.
- [6] L. Fu and L.B. Kara. Neural Network-Based Symbol Recognition Using a Few Labeled Samples, *Computers & Graphics*, Volume 35, Issue 5, pp. 955-966, 2011.
- [7] N.K. Kasabov, R.I. Kilgour and, S.J. Sinclair. From Hybrid Adjustable Neuro-Fuzzy Systems to Adaptive Connectionist-Based Systems for Phoneme and Word Recognition, *Fuzzy Sets and Systems*, Volume 103, Issue 2, pp. 349-367, 1999.
- [8] J.H. Chiang. A Hybrid Neural Network Model in Handwritten Word Recognition, *Neural Networks*, Volume 11, Issue 2, pp. 337-346, 1998.

PERSPECTIVE OF WATERSHED MANAGEMENT IN OUR MODERN SOCIETY

¹**Biplab Das,** ²**Dr.AdityaBandyopadhyay**

¹ Research Scholar (PhD), Indian Institute of Engineering, Science and Technology, Kolkata

² Professor, Indian Institute of Engineering, Science and Technology, Kolkata

Abstract: Watershed management is very important in our modern society. Basically watershed is a region delineated with a well-defined topographic boundary and water outlet. It is a geographic region within which hydrological conditions are such that water becomes concentrated within a particular location. The terms watershed, catchment, and basins are often used interchangeably. They have long been recognized as desirable units for planning and implementing developmental programmes. A watershed, also called a "drainage basin" in North America, is an area in which all water flowing into it goes to a common outlet, such as the same estuary or reservoir. Watersheds themselves consist of all surface water and include lakes, streams, reservoirs and wetlands, as well as all groundwater and aquifers.

1. Significance Of The Study:

Watershed management encompasses the simultaneous consideration of hydrological, pedological, and biological resources, necessitating the need for making better use of analytical tools and approaches, which address spatial and temporal variability, is critical. The cumulative impacts of human activities, which threaten the ecological, economic, and aesthetic integrity of many drainage systems and the strategies to mitigate these impacts, have explicit spatial dimensions. Watershed approaches in resource planning require timely and accurate data with spatial as well as statistical aspects. In this regard, GIS holds great promise with a provision to handle spatial and temporal data and aid as an integrative planning tool for watershed management.

2. OBJECTIVES:

To understand main importances of watershed management in our modern society.
Maintaining an adequate supply of water to meet demands for irrigation, agriculture, as well as domestic and industrial uses at acceptable levels of assurance.
Reducing vulnerability to natural disasters such as floods, droughts and landslides.
Improving the economic and social condition of the disadvantaged and those deficient in resources.
Distributing the benefits of land and water resources development more equally amongst the stakeholder.

3. METHODOLOGY

The research work prepared in three stages which are as follows –

Pre-field work:

This stage includes - i) collection of districts map ii) collection of secondary information from district handbook, census report, others books and journals etc. iii) preparation of questionnaire statistical schedule for collection of primary data which are closely related with the research work.

Field work:

By questionnaire schedule primary data will be collected from the study area. Observation schedule also help to collect the information.

Post field work:

Collected data will be classified in a master table and various cartographic and statistical techniques will be made in support of the theoretical discussion.

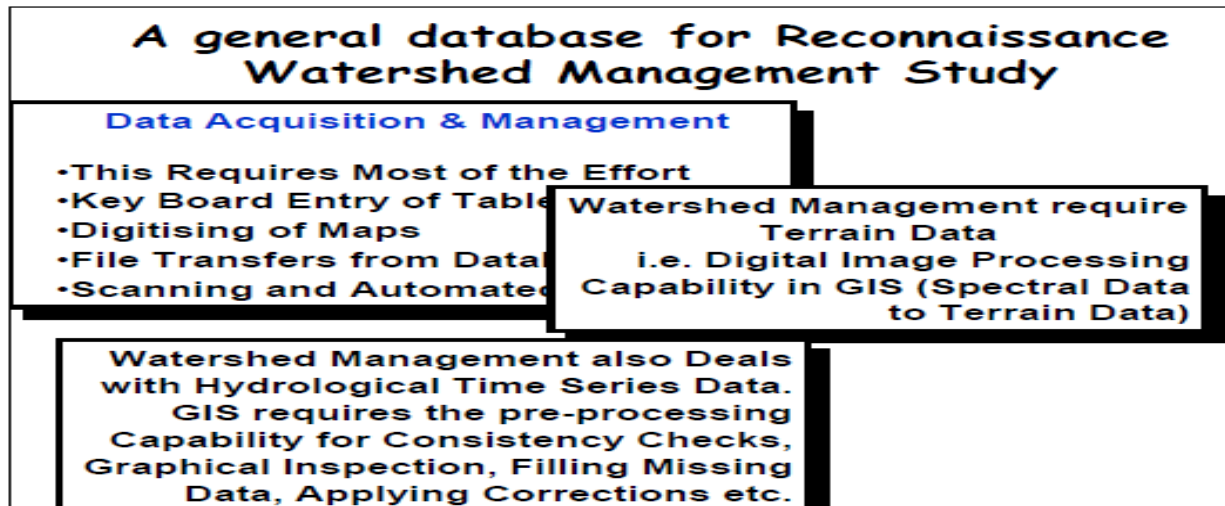


Fig- 1: A Model of Research Methodology

4. RESULTS:

MAIN PERSPECTIVE OF WATERSHED MANAGEMENT:

The degree to which people and civil society actively participate in conservation and resource management is one of the most critical factors that determines the success or failure of the process. Participation enables stakeholders to formulate their interests and concerns and integrate them into decision making, planning and policy development. Participation can take on a more passive form with a relatively low level of involvement as in the ‘top-down’ consultative model. Alternatively, the ‘bottom up’ approach promotes much higher levels of public and institutional involvement and can lead towards civil empowerment and self-mobilization. Modern watershed management attempts to combine both the ‘bottom up’ and ‘top down’ approaches through negotiation and dialogue. Watershed management facilitates the multi-sectoral and multi-stakeholder negotiation processes by providing the necessary platform to examine the interests of the different parties from the overall watershed perspective. This results in the formulation of guidelines or plans for the maintenance of watershed functions, as shown in the following model-

Problems and Possible Interaction

<i>Flooding</i>	Flood Control Reservoirs, Construction of Levees Flood Plain Management Re-vegetation(Denuded Areas)
<i>Unstable Slopes / Land Slides</i>	Slope Protection & Drainage Structures
<i>Erosion</i>	Erosion Control Structures Contour Terracing Re-Vegetation
<i>Deficient Water Supplies</i>	Storage Reservoirs Water Harvesting Vegetation Manipulation Pumping of Deep Groundwater

<i>Energy Shortage</i>	Fuel Wood Harvesting Hydro-Power Development
<i>Food Shortage</i>	Develop Agricultural Areas Develop Agricultural Practices Increase Livestock
<i>Poor Quality Drinking Water</i>	Develop Wells and Springs Treat Water
<i>Polluted Streams / Reduced Fishery</i>	Control Pollutant Entry Treat Wastewater
<i>Sedimentation of Navigation Tracks</i>	Erosion Control Structures Dredging and Mining
<i>Timber Shortage - Timber Harvesting</i>	

The water allocation amongst the basin states should be guided by a national perspective with due regard to water resources availability and requirement within each state and the river basin. Necessary guidelines should be formulated accordingly for allocation of water amongst the basin states. In planning operation systems, water allocation priorities should broadly be as below,

1. Drinking and domestic use
2. Sustaining livelihoods
3. Sustaining environment, maintaining river systems and aquatic conservation
4. Irrigation and hydro-power
5. Thermal power and industries
6. Recreation and religious uses
7. Navigation

The first three uses have the highest priority but within these, the allocation of water should be decided by the people at the watershed level. For allocation to other uses where bulk supplies are required and where supply to the first three categories is affected, people's agreement would be necessary.

4.1. Drinking and Domestic Use:

Adequate drinking water facilities should be provided to the entire population both in urban and in rural areas. Irrigation and multipurpose projects should invariably include a drinking water component, but these should only supplement locally developed sources of drinking water. Drinking water needs of human beings and animals should be the first charge on any available water. The community should have the first right to use rainfall directly, store and recharge groundwater wherever possible. The rights over water should not be restricted to only those who own land. Water should be allocated on per head basis and not on the basis of land area and heavy water consuming crops should not be allowed by consensus/agreement.

4.2. Sustaining Livelihoods:

There is a specific geographical concentration of backwardness and poverty in drought-prone areas. Continuous degradation of natural resources, severe erosion, depletion of ground-water reserves, low productivity, low wage rate etc. are some of the endemic problem in these areas. Any livelihood strategy meant for this region should encompass the

programme of arresting the process of degradation of natural resources, restoring ecological balance and, at the same time directly address poverty. One needs to understand poverty not only as a scarcity of cash or lack of purchasing power, but also as a lack of access to natural resources and its management because it is the biomass-based subsistence economy within which majority of people live.

4.3. Sustaining Environment, Maintaining River Systems and Aquatic:

A minimum good quality water flow should be ensured at all times as required for the life of the river and for sustaining livelihoods. This should include the allocation of water for various purposes including conserving the environment, preventing groundwater salinity and sea water intrusion, supporting livelihood based on aquatic life and other uses of water, recreation, and cultural activities like bathing and festivities. The requirement of water for these various purposes should be calculated scientifically. To begin with at least 50 per cent of the lean period flow before the structure was built (average of 1-2 months) over and above the committed use should be allowed to go downstream of all existing and new structures. Implementation of this would be possible only with the help of all communities involved with proper monitoring and also by allocating this quantity on a priority from new reservoirs. Traditional and natural wetlands and water bodies like tanks, jheels, chores and village ponds, etc. have been badly neglected in the last few decades. These structures should be restored, maintained and used properly and these water bodies should not be allowed to be encroached upon for any other land use.

4.4. Irrigation And Hydro-Power:

Irrigation planning either in an individual project or in a basin, as a whole should take into account the irritability of land, cost effective irrigation options possible from all available sources (including traditional ones). Wherever water is scarce, if economically advantageous, deficit irrigation may be practiced.



Fig-2: A Process of Irrigation

The irrigation intensity should be such as to extend the benefits of irrigation to as large a number of farm families as possible, keeping in view the need to maximize production and providing minimum sustainable income above the poverty level. Water intensive crops such as sugar cane and paddy should be strongly discous the areas of water scarcity. Irrigation efficiency in irrigation projects should be improved from the present average of 35 per cent to the maximum achievable, which is approximately 60 percent. Water allocation in an irrigation system should be done with due regard to equity and social justice. Disparities in the availability of water between head-reach and tail-end farms and between large and small farms should be obviated by adoption of a rotational water distribution system and supply of water on a volumetric basis to WUAs subject to certain ceilings. WUAs should have an important role to play in managing distribution, maintenance and recovery of service charges.

Canal irrigated areas have created some water-logged areas which need to be drained out to make the land fit for agriculture and other purposes. First attempt should be to avoid the supply of excess water and then wherever possible, bio-drainage, and vertical drainage should be preferred rather than surface drainage. The quality of surface drainage water should be improved so as to make it reusable for various purposes. The basic idea should be to store the water after proper treatment, so that water can be reused usefully rather than flow to the sea during the monsoon without use. A combination of drainage arrangements should be adopted to use the least amount of land and which can also be properly maintained at least cost on a regular basis.

4.5. Thermal Power And Industries:

Most of the thermal power houses and industries with heavy use of water should be located on the coast. They should be encouraged to use sea water/desalinated water, adopt processes with minimum use of water, recycle and reuse and discharge only treated and cooled water into the sea to maintain its ecology.

4.6. Navigation

In order to save energy and reduce our dependence on petroleum products, the major portion of which are imported, navigational transport in rivers is essential. This will require that minimum flow and depth in specific reaches of the river is assured.

5. Conclusion:

The people of these areas face a rapid decline in their standard of living as natural resource base become degraded and loses its ability to recover. Increasing number of environmental refugees migrate to other lands, which are then also endangered by over use. The programme should be such that first, they focus on the positive synergies between poverty reduction, economic efficiency, and environmental protection. Second, the projects are developed with the beneficiaries rather than for them. Third, they are based on an integrated approach to natural resource planning and management in consonance with an Environment Action Plan.

References:

- [1] Balasubramanian, R and K.N.Selvaraj (2003). Poverty, Private Property and Common Pool.
- [2] Resources Management: The Case of irrigation Tanks in South India, SANDEE Working Paper No.2-03, South Asian Network for development and Environmental Economics.
- [3] Bardhan, Pranab (1993), "Analytics of the Institutions of Informal Co-operation in Rural Development," World Development, 21 (4): 633-639.
- [4] s.B and Bandyopadhyay.A.(2012). 'Causes of Flood by Indian River' A Case Study of Transboundary River Icchamati in Gangetic Delta, International Journal of Advanced Research in Computer Science and Electronics Engineering, Volume 1, Issue 7, September 2012,277-292, ISSN: 2277 – 9043.
- [5] *Das.B(2011).Flood Risk Management by Transboundary River of Gangetic Delta ,Lap Lambert Academic Publishing ,Saarbrücken, Germany,65-79.
- [6] Giri.P, Barua.P and Das.B(2012). 'Sundarban Delta: Perspective for the Long Term Future', Lap Lambert Academic Publishing ,Saarbrücken, Germany,84-143.
- [7] Kerr, John, G Pangre, Vasudha LPangre and P I George (2002), "An Evaluation of Dryland Watershed Development Projects in India," EPTD Discussion Paper, No.68, Washington D C: International Food Policy Research Institute.
- [8] Meinzen-Dick, Ruth, K V Raju and A Gulati (2002), "What Affects Organisation and Collective Action for Managing Resources? Evidence from Canal Irrigation Systems in India," World
- [9] Meinzen-Dick, Ruth, Monica Di Gregorio and Nancy McCarthy (2004), "Methods for Studying Collective Action in Rural Development," Agricultural Systems, 82: 197-214.
- [10] Palanisami, K, D Suresh Kumar and B Chandrasekaran (2002), "Watershed Development: Concept and Issues," Watershed Management: Issues and Policies for the 21st Century,

Formation of Knowledge Sharing System for Asia-Pacific Countries by Using Modern Information Techniques

¹Nalin Warnajith, ²Sarkar Barbaq Quarmal, ³Masanori Itaba, ⁴Atsushi Minato
⁵Satoru Ozawa

1,2,3,4,5, Graduate School of Science & Engineering, Ibaraki University, Hitachi 316-8511, Japan

Abstract: This paper describes the establishment of an e-Learning platform for Asia-Pacific countries where teachers and researchers of this region can share their knowledge and collaborate in education and research activities in order to face the challenges of the rapidly changing world. In the first part of the paper, the present e-Learning status, scopes and constraints in the Asia-Pacific region have been briefly discussed. In the later part, the technical issues regarding the development and implementation of the knowledge sharing system (Knowledge Integration Servers System for E-Learning: KISSEL) is explained. From the test results and feedbacks from the teachers' communities in the project member countries, it has been found that the KISSEL is useful for the improvement of education and research activities in Asia-Pacific countries.

Keywords: e-Learning, Knowledge-sharing, KISSEL, Data Synchronization

1. Introduction

The term e-Learning caught the attention of the educators for the first time in the 1990's when the Internet started to spread very quickly. Although it has a relatively short history of about two decades, it has become an important issue in universities, research organizations, high schools etc. In relation to e-learning/education, there are some commonly used terms, i.e., online learning/education, distance learning/education, web based learning/training, computer based training/learning/education. There are quite a few definitions of e-Learning. Hence, it is difficult to find a concrete definition of e-Learning. In this paper, let us consider that e-Learning is "The use of new multimedia technologies and the Internet to improve the quality of learning by facilitating access to resources and services as well as remote exchanges and collaboration" [1]. So an important characteristic of e-Learning is the interactivity with the learners. Interactive multimedia technologies are engrossing. It provides the opportunity for deep involvement, which captures and holds learner interest. As far as the level of e-Learning in Asia-Pacific countries is concerned, they are still backward compared to developed countries. The KISSEL project, which was started by a research group of Ibaraki University, Japan, is a new approach for the improvement of e-Learning in these countries. The term KISSEL stands for "Knowledge Integration Servers System for **E-Learning**" and it is a knowledge sharing system which is designed to cater to teachers' communities in Asia-Pacific countries [2]. The reason why the target area is restricted to Asia-Pacific countries is that the degree of the development of ICT infrastructure and also the e-learning environment is similar in these countries and the knowledge to be shared is similar in character. KISSEL is developed to provide resources (especially in the form of multimedia e-Learning contents), tools and techniques needed for student-teacher communication and self-learning. The aim of this paper is to report technical aspects of the development of KISSEL project and its functionalities.

2. KISSEL : Knowledge Integration Servers System For E-Learning

2.1. Present e-Learning status in Asia-Pacific region

The e-Learning is still at the beginning phase in developing Asia-Pacific countries. Due to the underdeveloped economy, these countries could not yet establish a reliable ICT infrastructure which is one of the basic requirements for an effective e-learning system. Hence, most of the learners in these countries are not yet familiar with the term "e-Learning". There are a few major issues like national strategy, connectivity, accreditation, acceptability, quality_of the learning materials, and relevant contents that have to be considered for any e-learning program [3]. Another critical concern raised on the e-Learning activities is the cost perspective. Learners of the developing countries have financial constraints to participate in the program which is too costly for them. They have limited scopes to get the learning facilities as it relates with high-tech equipment, in many cases. So, for the developing countries, they need to reframe the strategy of e-Learning to make it familiar in the communities more effectively. The aim of the KISSEL project is to encourage teachers in Asia-Pacific countries to set up communities of e-Learning among themselves and to share knowledge in the form of e-learning

materials. Even though, e-Learning has not yet been properly introduced to the people in this region, the majority of the teachers in these countries believe that the e-learning method will contribute in realizing better education systems in their countries. In recent years, all the governments in this region are investing in ICT to improve the quality of works in all sectors, especially in the education and training sectors. Schoolnet, skool and e-Village projects in Sri Lanka [4, 5], e-book project for school students in Bangladesh [6] etc., are examples of such efforts.

2.2. Overview of KISSEL

The basic idea of KISSEL is to set up a server system, which works as a web portal, where teachers can have the opportunity to have their own network among themselves. The point is that the server works as a platform not only for exchanging their idea but also for sharing their modern techniques and useful teaching materials for e-Learning. One of the reasons why this system concerns about teachers is that they are always keeping contact with students. Therefore, they can become the best interface to transfer ICT to the young generation. Teachers should first gain or have interest in the use of ICT. The teachers should help each other to promote their skills for ICT. In order to do this, we note the role of teachers' community.



Figure 1. Basic structure of KISSEL

KISSEL is composed of several server machines which are settled in different countries in the Asia-Pacific region. They work cooperatively. Figure 1 illustrates how KISSEL works. There are two parts in each of the KISSEL servers, i.e. the international sector and the local sector. The local sector is designed and developed by the hosting country in their native language or in English. The local sector is freely used for domestic proposes. The contents of the local sector which are worth sharing in the other countries are translated into English and are put in the international sector [7]. We believe that the native language is best suited in education because it can teach or reaches the students more closely rather than a foreign language such as English. But in order to share knowledge internationally, there should be a common language. Hence, English has been chosen as the language of the international sector, because it is taught as the second language in most of these countries. The contents of the international sector of each KISSEL servers is being copied automatically (see Section 3.4). The content newly uploaded to an international sector of one KISSEL server is reflected to all KISSEL servers by the mirroring function of KISSEL. In such a way, data sharing is being carried out between teachers' communities in Asia-Pacific countries.

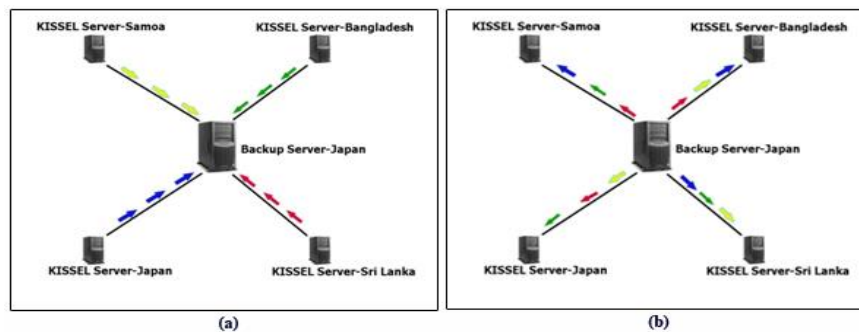


Figure 2. Synchronization process between servers (a) From local servers to Backup server, (b) backup server to local servers

Presently, KISSEL servers are settled in Japan, Sri Lanka, Bangladesh and Vietnam. In near future, KISSEL servers will be installed in some other countries in Asia-Pacific region. Multimedia learning materials such as videos, audios, animations etc., are mainly focused in the KISSEL project. Dealing with the heavy e-Learning materials in the KISSEL system, the available Internet bandwidth and the ICT infrastructure in these countries are main things to be considered in this study.

2.3. Why a new system is needed?

By character, KISSEL is similar to the so called “Content Management Systems, CMS” as well as the “Social Networking Services, SNS”. Therefore, a question may arise here, “why a new different system is needed? ...why don’t we use a platform that is already established?” The answers are the followings:

- (1) The aim of KISSEL is not to produce uncertain relationships between many and unspecified people directly over the Internet but to produce connections between certain teacher's communities which already exist in Asia-Pacific countries,
- (2) One of the visions of KISSEL project is to share knowledge and experiences in education which are already accumulated in these countries in the forms of their native languages,

Therefore, a special device and mechanism is needed which enables cooperation of teachers' communities in different countries. Alongside (1) and (2), the following factors are also noted. Firstly, the visionary group of KISSEL aims at establishing a user-friendly system so that even the people who lack in ICT capabilities can use the system without difficulties. Secondly, the system should be secure from any Internet attacks. Thirdly, it should be failsafe designed. There are several cooperative KISSEL servers in different countries that if one or more of those get in problem, the others can work as back-ups.

2.4. Management of KISSEL servers

As KISSEL is operating internationally, several levels of user categories were introduced depending on their accessibilities (Fig. 3).

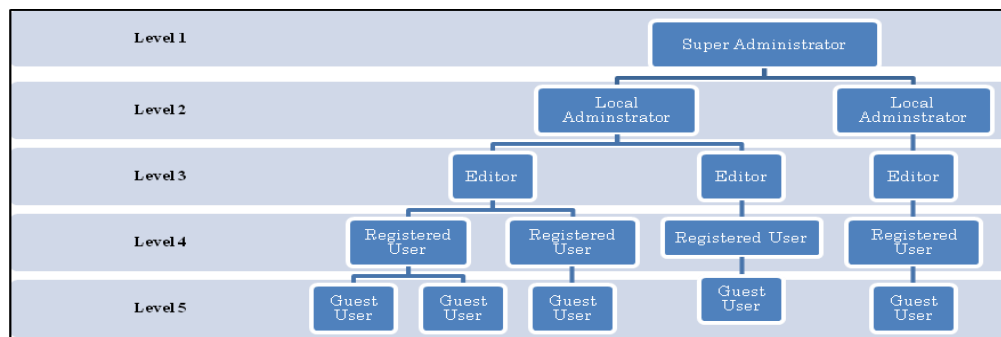


Figure 3. User levels in KISSEL

- a). Super Administrator
This user is in charge of the backup server (master server) in Japan (see Section 3.3) and hence the overall system. Super administrator (Level 1) is capable of performing all the functionalities of the system including server management, backup management and so on. Also, he is responsible for the maintenance of the operational level.
- b). Local Administrator
The local administrators are in charge of the administration of the servers in their countries. The local administrators are capable of performing tasks such as user management, content category management, learning materials management in the local servers etc. Also they are responsible to carry out system updates and to communicate with editors (Level 3) according to the instructions given by the super administrator.
- c). Editor
Editor (Level 3) can upload learning materials and modify own materials.
- d). Registered User
The user of this level can view the contents of the system and download them. Also they can put comments, feedbacks and rate the content.
- e). Guest
The guests can only view abstracts of contents.

3. Development And Implementation of KISSEL

For implementation of the KISSEL system, the evolutionary development model [8] was adopted, which can realize incremental product releases, frequently delivery dynamic plans and processes to users.

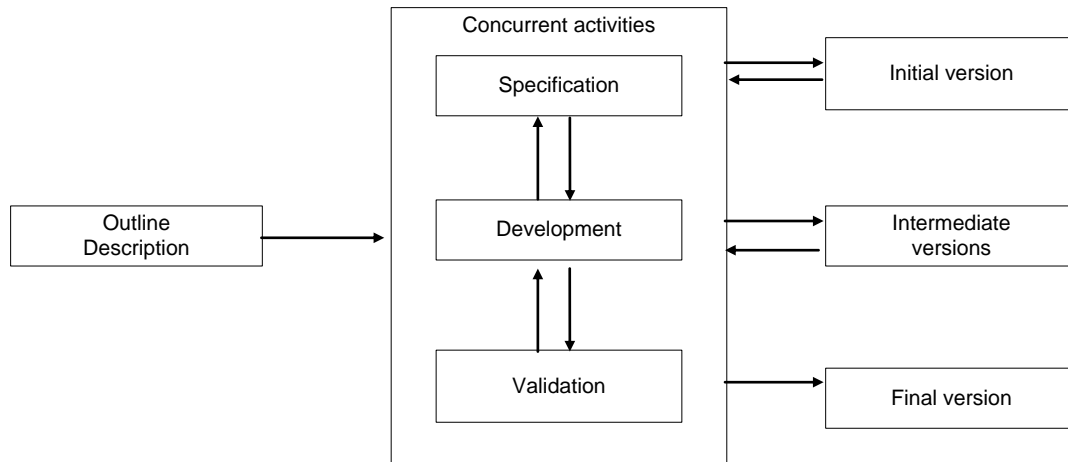


Figure 4. Data flow of the evolutionary model

Look at the Figure 4. The objective is to evolve a final system from an initial outline specification starting with well understood requirements and adding new features as proposed by the end users. Initial version of the system acts as a prototype to help to elicit requirements for the intermediate versions. This process will be repeated until a final system has been delivered.

3.1. Three-Tier Architecture

In order to realize aimed functionalities of KISSEL, the three-tier architecture [9] is used.

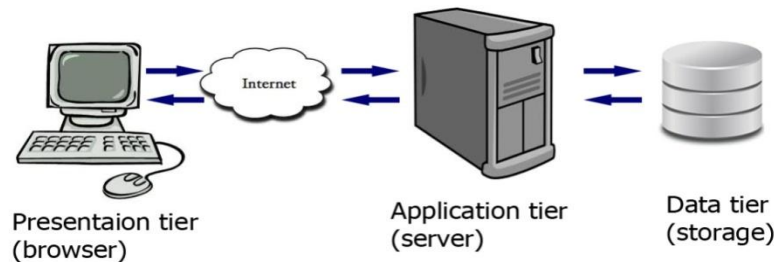


Figure 5 Three tier architecture of the KISSEL

The three tier architecture is composed of presentation tier, application tier and data tier. In the presentation tier, the user interface has to be built to display information to the user and to get input from the user. In this tier, the main concepts of the web application design facilities in the KISSEL system are adopted. The following tools and techniques are used for this purpose: HTML, JavaScript, Adobe Photoshop CS3, AJAX and CSS. Application tier works as an intermediary for data exchange between the presentation and data tiers. The KISSEL was designed to run on Linux based Apache web server with PHP (Personal Home Pages) as the general-purpose server-side scripting language. PHP 5.2 is used in KISSEL system and CentOS 5.6 is used as the server OS. Function of the data tier is to set the database back and forth. Written database queries and stored procedures are used to access the database or to perform any operation to the database. It will get the data from the application tier and send it to database or get the data from the database and send that to the application tier. In KISSEL, MySQL is used as the back-end database which is one of the most popular open source databases because of its high performance, high reliability and ease of use. Many of the world's largest and fastest-growing organizations including Facebook, Google, Adobe rely on MySQL to save time and money powering their high-volume websites, business-critical systems and packaged software [10].

3.2. One KISSEL Server Per Country

To overcome the bandwidth problem [11], the method "one server per country" has been adopted in the KISSEL project. Note that the local server work as a "cash sever". For example, the average bandwidth for international connection in Sri Lanka is nearly 963Kpbs. But within the university system inside the country optical-fiber links, it is ranging from 10 Mbps to 34Mbps, and it is 2 Mbps for links to universities at distant locations where optical fiber is not available [12]. So even large multimedia resources can be accessed very easily inside the country by using KISSEL server located in their own country.

3.3. KISSEL backup server (master server) in Japan

One backup server for KISSEL system has installed in Japan in addition to the Japanese local KISSEL servers. The aim of this backup server is

- (1) To make the synchronization process more efficient,
- (2) To act as an emergency restoration resource when a server fails in the system,
- (3) To make it easy to add more KISSEL local server to the system.

3.4. Data Sharing Process

Data sharing of the KISSEL contents is done in following steps:

- I. Contents are uploaded in native language/English in the local sector of the KISSEL local server.
- II. The contents worth sharing internationally are uploaded to the international sector of the local server. This process is carried out by local administrator.
- III. The newly added data of international sector of each local server is synchronized to the backup server (master server).

3.5. Optimized bandwidth usage

In order to select the best suited time period for the synchronization of KISSEL contents, daily bandwidth usage has to be investigated. Firstly, synchronization performance was analyzed between one local server in Japan and the backup server located in Ibaraki University, Japan. A video file (~35 MB) was used as the test data for this analysis. The synchronization process between these two servers was repeated once in every 30 minutes, and the speed acquired for this process was recorded (Fig. 6). As the servers were located in the same subnet of the campus LAN, this synchronization process affected the internal web traffic only. In the synchronization experiment, both download (from the backup server to the local server) and upload (from the local server to the backup server) speed were examined. The time was recorded in GMT in order to avoid the local time differences in similar synchronization experiments between the local servers in different countries and the backup sever in Japan. From Fig 6, it is clearly seen that there are no significant changes in both upload and download speeds. The average download speed was about 4.5 Mbps and the average upload speed was about 6 Mbps, which are very healthy for synchronization process. It has been found from the experiment that the synchronization can be carried out at any time of the day for two servers located in Japan.

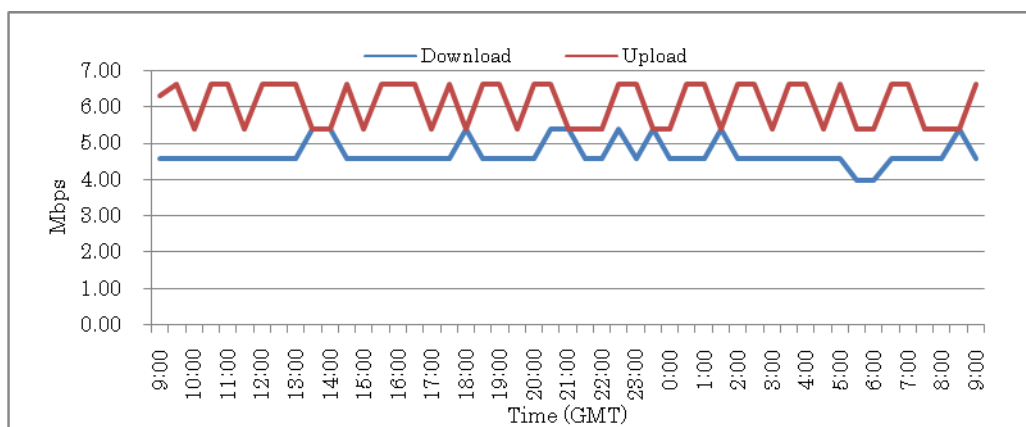


Figure 6. Synchronization speeds between the local server and the backup server in Japan

The similar experiment was carried out between a Sri Lankan local server which is located in the Open University, Sri Lanka and the backup server located in Ibaraki University, Japan. Theoretically maximum speed of 10Mbps is allocated

to the Open University [12]. But, due to the internal demand for the Internet and the network infrastructure, this amount of speed is not available. The same video file was used in this synchronization experiment. Figure 7 shows the results.

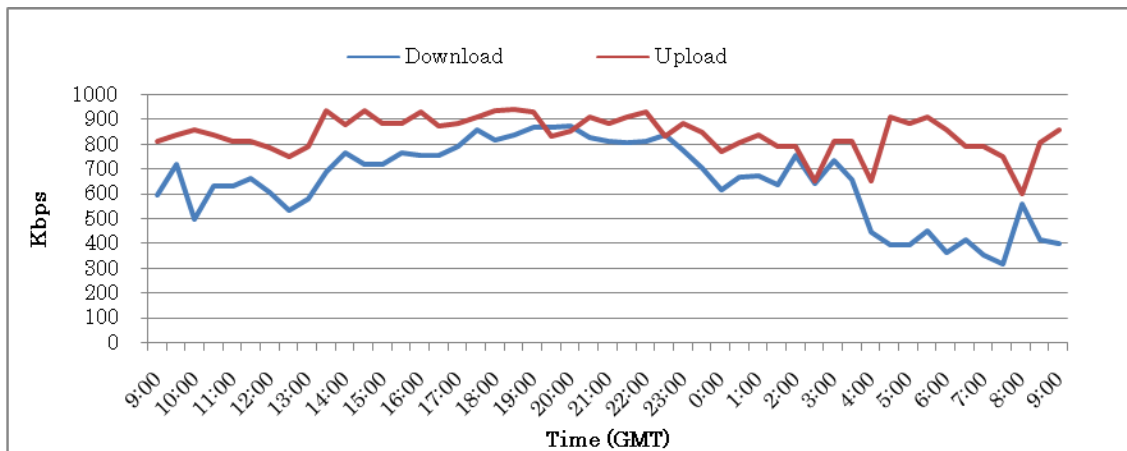


Figure 7. Synchronization speeds between Sri Lankan local server and the backup server in Japan

It is seen from Fig.7 that the maximum download speed is 850 Kbps and the maximum upload speed is 935 Kbps. These values are about one fifth of the data transfer speed between the two KISSEL servers in Japan. Fig 7 shows that the download speed is comparably low between 04:00 to 14:00 GMT (10:30 to 20:30 in Sri Lankan local time) due to the heavy usage of the bandwidth for the university activities. The highest speed of synchronization was recorded between 18:00 to 23:00 GMT (00:30 to 05:30 in Sri Lankan local time). This can be understood that in Sri Lanka, the number of users (mostly students) in the university network in this period is very small and accordingly the download speed is relatively high. Regarding the upload speed, there were no significant differences in time. This is because most of the users only view and download contents and there are very few users who upload contents. Between 14:00 to 23:00 GMT (20:30 to 05:30 in Sri Lankan local time), the upload speed is slightly higher. So the best time period for data synchronization between Sri Lankan local server and the master server is 18:00 to 23:00 GMT. Using the same method, the band width optimized time slot was identified for each country. The Fig 8 and Fig 9 show results of synchronization experiments between local servers in Bangladesh (located at Rajshahi University of Engineering and Technology, Rajshahi, Bangladesh) and Vietnam (located at the University of Science, Ho Chi Minh City, Vietnam) and the master server respectively.

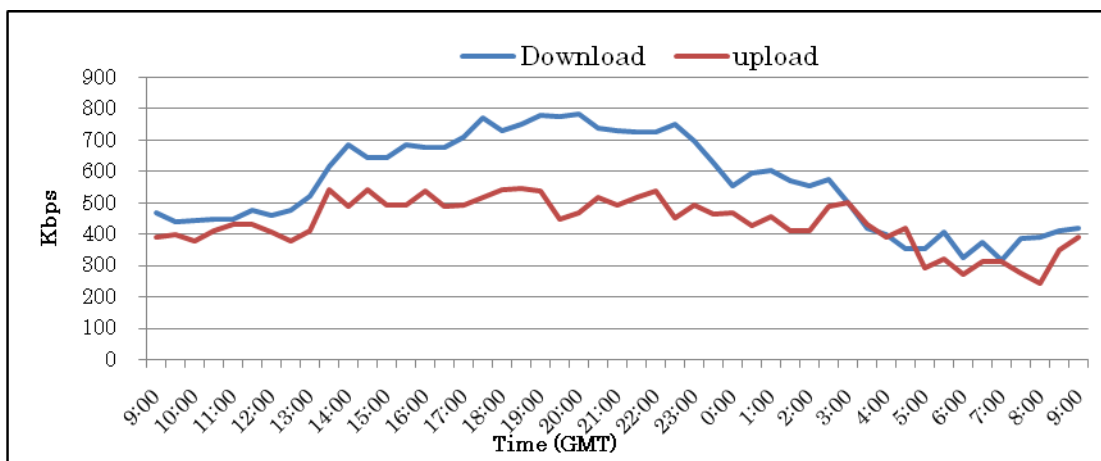


Figure 8. Synchronization speeds between Bangladeshi KISSEL server and master server

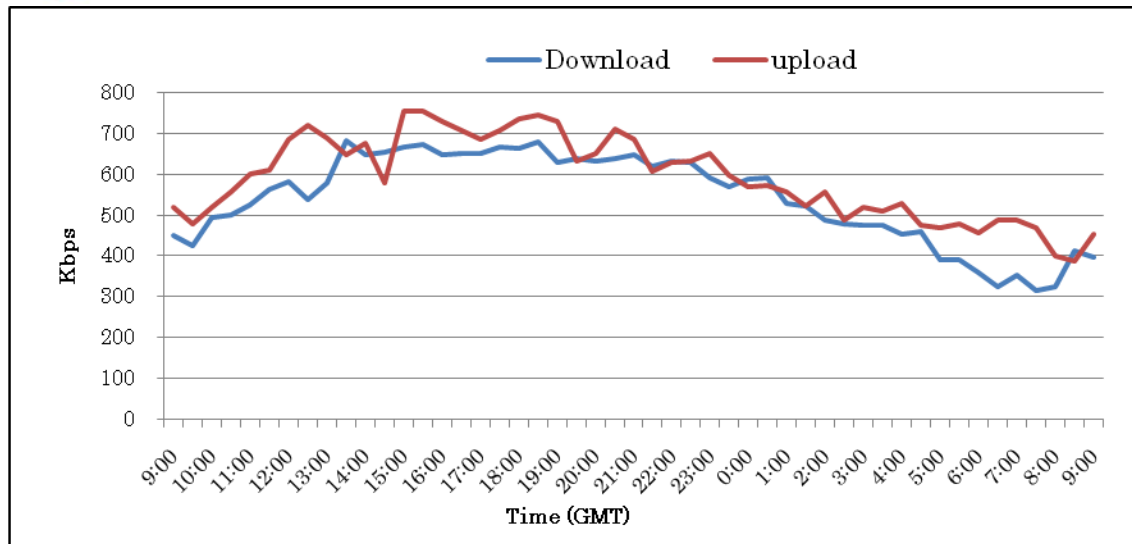


Figure 9. Synchronization speeds between Vietnamese KISSEL server and master server

3.6. Using rsync for synchronization

The *rsync* is a fast and versatile file copying tool available for *Linux* systems [13]. It can copy local contents, to/from another host over the remote shell, or by a remote *rsync* daemon. It contains a large number of options that control every aspects of its behavior and allows very flexible specification of files to be copied [13]. The *rsync* starts working just like other remote file copying methods. But later, *rsync* controls copying of only newly updated part of the file. This makes updates faster, especially over slower links like modems. The other file transfer methods, e.g. FTP, transfers the entire file even if only one byte is changed. Also *rsync* offers a lot of useful functionalities that FTP and other tools don't offer easily. Synchronization between KISSEL server in Sri Lanka (IP: 192.248.73.246) and backup server in Japan (IP: 157.80.97.117) can be carried out by installing the following shell command from 157.80.97.117. `rsync -avz -e ssh rsyncuser@192.248.73.246:/home/content/ /home/content` But, *rsync* is a secure shell command so it needs authentication for executing. This issue can be addressed by using the method of *public-key* [14] because the synchronization process between servers must be carried out periodically without human interaction. The automation of synchronization process was carried out by the combined use of *rsync* and *crontab* [15], where the values determined by the method (see Section 3.5) was used as the synchronization time parameter. Thus, each server is synchronized with master server once a day.

3.7. Synchronization of KISSEL web interface

Although by the *rsync* method all the contents can be synchronized, a separate method must be carried out to replicate the *MySQL* back-end database that is used for KISSEL web-based interface [16], i.e., user management, server management, category managements etc. In this replication algorithm, the two databases in the two servers were compared to each other considering the Added, Modified and Deleted database entries. Firstly, these examinations are done in KISSEL master server, and a daily backup file for future usage is produced. Then, the fresh database from the KISSEL master server is replicated to the other local servers. In this replications, the amount of transferring data are much smaller than the total contents of KISSEL system. Therefore, the bandwidth problem does not occur in this process.

4. Conclusion

The test of KISSEL system performance was successfully carried out in Japan, Sri Lanka, Bangladesh and Vietnam. Also, introductory seminars and workshops on KISSEL have been carried out in the member countries by the members of the KISSEL group working in Japan and it has been found that KISSEL system is completed up to a satisfactory level for the users.

5. Acknowledgement

This work was supported by the Grants in Aid 20500825, the Grand in Aid 24650124 and the Grants in Aid 24300278, Ministry of Education, Culture Sports, Science and Technology, Japan

6. References

- [1]. "elearningeuropa.info-elearning", <<http://www.elearningeuropa.info/glossary/>>, (Accessed 30-08-2012)
- [2]. G Dassanayaka, V. Patu, Atsushi Minato, Satoru Ozawa, S.Wijayawickrama, Nalin Warnajith, "Identify security issue when implementing knowledge Integrate Servers System for E-Learning", Proc ISCIU5, pp79-80, Nov 2009
- [3]. Survey of ICTs for Education in India and South Asia, Extended Summary, 2010, infoDev , PricewaterhouseCoopers
- [4]. S.P.I.P. Kumara, Nalin Warnajith, ICT for Sri Lankan secondary school level, The 7th International Student Conference at Ibaraki University, Ibaraki, Japan, December 3-4, 2011: O-220.
- [5]. Nalin Warnajith, Gamunu Dassanayake, D.D.G.L. Dahanayaka, Hideyuki Tonooka, Atsushi Minato, Satoru Ozawa and Meepagalage P. M. Perera (2012) Prototype of E-Learning Management System for Secondary School in Sri Lanka, 11th International conference on Information Technology Based Higher Education and Training (ITHET 2012), Istanbul, Turkey, pp. 10
- [6]. "e-Book project", <<http://www.ebook.gov.bd/>>, (Accessed 26-10-2012)
- [7]. Gamunu Dassanayake, Nalin Warnajith, D.D.G.L. Dahanayaka, Hideyuki Tonooka, Atsushi Minato, Satoru Ozawa and Meepagalage P. M. Perera (2012) The Planning, Implementation and Economics of the Knowledge Integration Server System for E-Learning (KISSEL), 11th International conference on Information Technology Based Higher Education and Training (ITHET 2012), Istanbul, Turkey, pp.9-10
- [8]. Krzanowski R., Raper J., 2000-- Krzanowski R., Raper J., Spatial evolutionary modeling, Oxford University Press, New York, 2000, pp3-6
- [9]. Gary B. Shally, Hary J. Rasenblatt, "Systems Analysis and Design", 9th Ed. Course Technology, Canada, 2012, pp464
- [10]. "Why MySQL?",<<http://www.mysql.com/why-mysql/>>,(Accessed 30.08.12).
- [11]. Giuseppe Aceto a, AlessioBotta a, AntonioPescapè a,n, MaurizioD'Arienzo, Unified architecture for network measurement: The case of available bandwidth, Journal of Network and Computer Applications 35 , 2012
- [12]. "Status of the Internet in Sri Lankan Universities " <<http://www.ac.lk>> (Accessed 30.08.12).
- [13]. "A Tutorial on Using RSYNC" <http://everythinglinux.org/rsync/>> (Accessed 25.08.12).
- [14]. Severn Tsui , " SSH Public Key Authentication" https://cs.uwaterloo.ca/cscf/howto/ssh/public_key/ , (Accessed 2012-09-20)
- [15]. Pantz , "Crontab Information", 2007, <http://www.pantz.org/software/cron/croninfo.html> (Accessed 2012-09-22)
- [16]. Nalin Warnajith, G Dassanayaka, D.D.G.L. Dahanayaka, A. Minato, S.Ozawa, "Development of Data Managing System in Common with Moodle and Xoops", Proc ISCIU6, pp 57-58, Nov 2010

Location Of The Zeros Of Polynomials

M.H. Gulzar

Department of Mathematics
University of Kashmir, Srinagar 190006.

Abstract: In this paper we prove some results on the location of zeros of a certain class of polynomials which among other things generalize some known results in the theory of the distribution of zeros of polynomials.

Mathematics Subject Classification: 30C10, 30C15

Keywords and Phrases: Polynomial, Zeros, Bounds

1. Introduction And Statement Of Results

A celebrated result on the bounds for the zeros of a polynomial with real coefficients is the following theorem, known as Enestrom–Kakeya Theorem [1, p.106]

Theorem A: If $0 < a_0 \leq a_1 \leq \dots \leq a_n$, then all the zeros of the polynomial

$$P(z) = a_0 + a_1z + a_2z^2 + \dots + a_{n-1}z^{n-1} + a_nz^n$$

lie in $|z| \leq 1$.

Regarding the bounds for the zeros of a polynomial with leading coefficient unity, Montel and Marty [1, p.107] proved the following theorem:

Theorem B: All the zeros of the polynomial

$$P(z) = a_0 + a_1z + a_2z^2 + \dots + a_{n-1}z^{n-1} + z^n$$

lie in $|z| \leq \max(L, L^n)$ where L is the length of the polygonal line joining in succession the points $0, a_0, a_1, \dots, a_{n-1}; i.e.$

$$L = |a_0| + |a_1 - a_0| + \dots + |a_{n-1} - a_{n-2}| + |1 - a_{n-1}|.$$

Q.G. Mohammad [2] proved the following generalization of Theorem B:

Theorem C: All the zeros of the polynomial Of Theorem A lie in

$$|z| \leq R = \max(L_p, L_p^{\frac{1}{n}})$$

where

$$L_p = n^{\frac{1}{q}} \left(\sum_{j=0}^{n-1} |a_j|^p \right)^{\frac{1}{p}}, p^{-1} + q^{-1} = 1.$$

The bound in Theorem C is sharp and the limit is attained by

$$P(z) = z^n - \frac{1}{n}(z^{n-1} + z^{n-2} + \dots + z + 1).$$

Letting $q \rightarrow \infty$ in Theorem C, we get the following result:

Theorem D: All the zeros of $P(z)$ Of Theorem A lie in $|z| \leq \max(L_1, L_1^{\frac{1}{n}})$ where

$$L_1 = \sum_{i=0}^{n-1} |a_i| .$$

Applying Theorem D to the polynomial $(1-z)P(z)$, we get Theorem B.

Q.G. Mohammad, in the same paper, applied Theorem D to prove the following result:

Theorem E: If $0 < a_{j-1} \leq ka_j, k > 0$, then all the zeros of

$$P(z) = a_0 + a_1z + a_2z^2 + \dots + a_{n-1}z^{n-1} + a_nz^n$$

lie in $|z| \leq \max(M, M^{\frac{1}{n}})$ where

$$M = \frac{(a_0 + a_1 + \dots + a_{n-1})}{a_n} (k-1) + k .$$

The aim of this paper is to give generalizations of Theorems C and E. In fact, we are going to prove the following results:

Theorem 1: All the zeros of the polynomial

$$P(z) = a_0 + a_1z + a_2z^2 + \dots + a_\mu z^\mu + z^n, 0 \leq \mu \leq n-1$$

lie in

$$|z| \leq R = \max(L_p, L_p^{\frac{1}{n}})$$

where

$$L_p = n^{\frac{1}{q}} \left(\sum_{j=0}^{\mu} |a_j|^p \right)^{\frac{1}{p}}, p^{-1} + q^{-1} = 1.$$

Remark 1: Taking $\mu = n-1$, Theorem 1 reduces to Theorem C.

Theorem 2: If $0 < a_{j-1} \leq ka_j, k > 0$, then all the zeros of

$$P(z) = a_0 + a_1z + a_2z^2 + \dots + a_\mu z^\mu + a_n z^n, 0 \leq \mu \leq n-1,$$

lie in $|z| \leq \max(M, M^{\frac{1}{n}})$ where

$$M = \frac{(a_0 + a_1 + \dots + a_\mu)}{a_n} (k-1) + k .$$

Remark 2: Taking $\mu = n-1$, Theorem 2 reduces to Theorem E and taking $\mu = n-1, k=1$, Theorem 2 reduces to Theorem A due to Enestrom and Kakeya..

2. Proofs Of Theorems

Proof of Theorem 1. Applying Holder's inequality, we have

$$\begin{aligned} |P(z)| &= |a_0 + a_1z + a_2z^2 + \dots + a_\mu z^\mu + z^n| \\ &\geq |z|^n \left[1 - \sum_{j=1}^{\mu+1} |a_{j-1}| \frac{1}{|z|^{n-j+1}} \right] \\ &\geq |z|^n \left[1 - n^{\frac{1}{q}} \left(\sum_{j=1}^{\mu+1} |a_{j-1}|^p \frac{1}{|z|^{(n-j+1)p}} \right)^{\frac{1}{p}} \right]. \end{aligned}$$

If $L_p \geq 1, \max(L_p, L_p^{\frac{1}{n}}) = L_p$. Let $|z| \geq 1$. Then $\frac{1}{|z|^{(n-j+1)p}} \leq \frac{1}{|z|^p}, j = 1, 2, \dots, \mu + 1$.

Hence it follows that for $|z| > L_p$,

$$|P(z)| \geq |z|^n \left[1 - \frac{n^q}{|z|^n} \left(\sum_{j=0}^{\mu} |a_j|^p \right)^{\frac{1}{p}} \right] = |z|^n \left[1 - \frac{L_p}{|z|} \right] > 0.$$

Again if $L_p \leq 1$, $\max(L_p, L_p^{\frac{1}{n}}) = L_p^{\frac{1}{n}}$. Let $|z| \leq 1$. Then

$$\frac{1}{|z|^{(n-j+1)p}} \leq \frac{1}{|z|^{np}}, j = 1, 2, \dots, \mu + 1.$$

Hence it follows that for $|z| > L_p^{\frac{1}{n}}$,

$$|P(z)| \geq |z|^n \left[1 - \frac{n^q}{|z|^n} \left(\sum_{j=0}^{\mu} |a_j|^p \right)^{\frac{1}{p}} \right] = |z|^n \left[1 - \frac{L_p}{|z|^n} \right] > 0.$$

Thus $P(z)$ does not vanish for $|z| > \max(L_p, L_p^{\frac{1}{n}})$ and hence the theorem follows.

Proof of Theorem 2. Consider the polynomial

$$\begin{aligned} F(z) &= (k - z)P(z) = (k - z)(a_0 + a_1 z + \dots + a_{\mu} z^{\mu} + a_n z^n) \\ &= ka_0 + (ka_1 - a_0)z + (ka_2 - a_1)z^2 + \dots + (ka_{\mu} - a_{\mu-1})z^{\mu} - a_{\mu} z^{\mu+1} \\ &\quad + ka_n z^n - a_n z^{n+1} \end{aligned}$$

Applying Theorem C to the polynomial $\frac{F(z)}{a_n}$, we find that

$$\begin{aligned} L_1 &= \frac{k(a_0 + a_1 + \dots + a_{\mu}) - (a_0 + a_1 + \dots + a_{\mu-1} + a_{\mu}) + ka_n}{a_n} \\ &= \frac{(k-1)(a_0 + a_1 + \dots + a_{\mu})}{a_n} + k \end{aligned}$$

=M

and the theorem follows.

References

- [1] M. Marden, The Geometry of Zeros., Amer.Math.Soc.Math.Surveys ,No.3 ,New York 1949.
- [2] Q.G. Mohammad , Location of the Zeros of Polynomials , Amer. Math. Monthly , vol.74,No.3, March 1967.